DOCTORAL DISSERTATION

Accelerated methanogens' decay in the acidic environment and its mathematical modelling

Meng SUN

March 2023

THE UNIVERSITY OF KITAKYUSHU

GRADUATE SCHOOL OF ENVIRONMENTAL ENGINEERING

Accelerated methanogens' decay in the acidic environment and its mathematical modelling

by

Meng SUN

March 2023

This dissertation is submitted for the degree of Doctor of Engineering

DECLARATION

I hereby declare that this dissertation has been composed solely by myself and the data presented in it are my own work. It contains no material previously published or written by another person, except where due reference has been made in the text. This dissertation has not been previously submitted, in whole or in part, to any university or other tertiary institution for any degree, diploma, or the other qualification.

March 2023, Kitakyushu, Japan

Author   Supervisor

Meng SUN   Professor Hidenari Yasui

ACKNOWLEDGEMENT

ABSTRACT

In an effort to increase the sources of renewable energy, numerous AD plants are being constructed around the world to convert organic waste into biogas. These plants typically use chemostat reactors fed with food waste, animal manure, and/or municipal solid waste. Organic food waste is an ideal source for biogas recovery due to its high biodegradability. To reduce the cost and space required for construction, these biogas recovery systems are often designed as high-loaded plants. However, these high-loaded plants are prone to encountering acidic failure when unexpected high loads of biodegradable material are fed into the reactor. This imbalance in reaction rates between the fermentative microorganisms (such as acidogens and fast-growing bacteria) and the slow-growing methanogens leads to an accumulation of organic acids, particularly volatile fatty acids (VFAs), which decreases the pH in the reactor. The resulting decrease in pH inhibits the growth of the methanogens, further deteriorating the removal rate of the accumulated VFAs. This downward spiral can eventually lead to a complete collapse of the system, resulting in acidic failure.

The concentrations of VFAs and pH levels in the event of system overload can vary significantly, as shown in various studies [1,2,3]. The appropriate remedial strategy depends on the nature of the inhibition - biocidal or biostatic. In the case of biocidal inhibition, it is necessary to eliminate the inhibitory substances as soon as possible to prevent biomass loss. On the other hand, if biostatic inhibition is prominent, it may be possible to simply reduce the influent load and wait for the process to recover. Despite the practical applications of these inhibition phenomena, the target pH and/or target VFA concentrations (including VFA species) for mitigating biocidal effects have not been well documented in the literature, except for long-chain fatty acid inhibition. This is likely due to the recent discovery of the biocidal effects of VFAs and pH in methane (CH_4) fermentation systems. Nevertheless, the inhibition phenomena are being utilized to develop material-recovery processes, such as VFA recovery, which is a current hot topic in anaerobic systems. Therefore, clarifying the biocidal effect of VFAs and pH would help in the development of new processes and in selecting remedial strategies against acidic failure.

Intermediate product inhibition is a widespread phenomenon that can impact the performance of biological treatment processes, particularly in CH_4 fermentation systems. These systems involve sequential microbial reactions that are mediated by acidogens, acetogens, and methanogens. When the systems are highly overloaded, the rate of acidogenic reaction is often

greater than those of acetogens and methanogens, leading to the accumulation of intermediate products, such as VFAs and protons, in the reactors. The conventional Anaerobic Digestion Model No.1 (ADM1) assumes that high VFA environments, characterized by high concentrations of undissociated VFAs and low pH, inhibit the microbial substrate conversion rates and microbial growth. This type of inhibition is referred to as biostatic inhibition, where microorganisms are not killed but their growth rates are inhibited. The reaction rates can be recovered once the inhibitory substance concentration is reduced or removed. However, recent studies have shown that high VFA concentrations and/or low pH can also have biocidal effects on the methanogens. Lins et al. (2014) found that a high concentration of acetate (150 mM) can enhance methanogens' decay, even at a circum-neutral pH of 7.5, in thermophilic anaerobic reactors [4]. Sun et al. (2020) also found that low pH, induced by phosphoric acid, can accelerate methanogens' death [5].

The biostatic inhibition of microorganisms can be mathematically represented as the product of factors that limit the specific reaction rate of the microbes. This is achieved by using a product of switching functions for hydrogen inhibition and ammonia inhibition in the Monod-type equation. In contrast, biocidal inhibition leads to irreversible loss of microbial activity and is correlated with biomass loss. It can be expressed as a stochastic summation of inactivation probabilities caused by biocidal substances over time. This is represented by the summation of first-order coefficients for inherent biomass decay, decay caused by inhibitory substance A and decay caused by inhibitory substance B, and so on [6]. The VFA (and proton) inhibition can therefore be theoretically mapped to either a biostatic or biocidal process, or a combination of both. However, compared to the studies of biostatic phenomena, research on biocidal inhibition and its effect on product inhibition is limited.

To investigate the biocidal effect of low pH, a series of batch experiments were conducted. The results showed that the failure of the digester under low pH conditions is due to the accelerated decay of the methanogenic biomass. Lab-scale reactors were used to prepare two types of methanogen-enriched cultures using acetate and formate as substrate. The impact of the VFA species and low pH on the biomass decay were analyzed through statistical analysis of the experimental results. The results showed that when enriched acetate-degrading methanogens were exposed to low pH (pH = 5.1 with phosphoric acid) in a batch experiment, the specific decay rate increased as much as ten times compared to the rate at pH 7.0. Similarly, the specific decay rate for formate degraders also increased under low pH conditions while the

fermentative microorganisms appeared to be tolerant.

A Propidium Mono-Azide-quantitative Polymerase Chain Reaction (PMA-qPCR) analysis revealed that the archaeal biomass dominated by methanogens dropped by 71-79% after 6 days of the acidic batch experiment, while the bacterial biomass dominated by acidogens decreased by only 25%. The decrease in the number of living cells at different pH was monitored to determine the correlation between decay rate and incubation pH. In another set of batch experiments, the cultures were incubated in lab-scale vessels under different pH conditions with formate, acetate, propionate, butyrate, valerate or phosphate buffer solution. The results showed that the methanogenic archaea were highly sensitive to acidic environments, with the decay rate accelerated at pH below 6.5 leading to inactivation. At pH 4.0, the archaeal specific decay rates were elevated more than 40 times compared to the rate at pH 7.0. These observations suggest that the methanogen decay is caused by low pH rather than elevated concentrations of VFA compounds during the acidic failure of anaerobic digester. The decay rate was comparable between the batch test with VFA and without VFA, providing strong evidence that low pH, rather than the elevated VFA concentrations, is the primary cause of the methanogen decay.

In a long-term experimental cultivation process, six datasets were collected to monitor the changes in acetate and volatile suspended solids (VSS) concentrations, pH, and CH_4 production rate over a 400-day period. The ADM1 model, which included either a pH sub-model or an undissociated acetate sub-model, was able to accurately predict the decline in reactor performance during acidic failure, but it failed to simulate the subsequent recovery following a reduction in influent loading. A statistical analysis showed that the correlation coefficient (Nash-Sutcliffe model efficiency coefficient, NSE) was relatively low, ranging from 0.31 to 0.38, despite being improved from the original NSE value of -0.04. To address this mismatch, a lag-phase sub-model was introduced. This sub-model comprised of the remaining relative activity of the microorganisms at the peak of inhibition and a half-saturation coefficient to represent the specific length of the lag phase. With the addition of this sub-model, the NSE was significantly improved to 0.49 to 0.53 in the calibrated ADM1 model.

The developed biocidal model in this study can provide valuable technical information for understanding and resolving issues in malfunctioned anaerobic plants experiencing acidic failure or for maintaining intentional acidification for VFA recovery. The empirical formula was used to model the biocidal effect at low pH based on the obtained low-pH inhibition

kinetics. Additionally, the parameter set was provided to calculate the potential risks of acidic failure in the design and operation of anaerobic reactors and to determine optimal operating conditions for VFA recovery reactors. The lag-phase sub-model, which consisted of the relative remaining activity of biomass at maximum acidic inhibition and the empirical delay coefficient, was included to improve the prediction accuracy of the modified ADM1 model. The NSE was improved by 37% to 0.53, demonstrating the effectiveness of the lag-phase sub-model.

ABBREVIATIONS

AD	Anaerobic Digestion
ADM1	Anaerobic Digestion Model No.1
COD	Chemical Oxygen Demand
CSTR	Continuous Stirred Tank Reactor
HRT	Hydraulic Retention Time
IWA	International Water Association
LCFA	Long chain fatty acids
NSE	Nash-Sutcliffe model Efficiency coefficient
OLR	Organic Loading Rate
PMA-qPCR	Propidium Mono-Azide-quantitative Polymerase Chain Reaction
SRT	Solids Retention Time
unVFA	undissociated VFA
VFA	Volatile Fatty Acid
WWTP	Wastewater Treatment Plant
$\mu_{\text{max,ace}}$	Maximum specific growth rate from acetate
$K_{\text{s,ace}}$	Half-saturation coefficient on acetate
$\mu_{\text{max,for}}$	Maximum specific growth rate from formate
$K_{\text{s,for}}$	Half-saturation coefficient on formate
b_{ace}	Decay rate of acetate utilizer
b_{for}	Decay rate of hydrogen utilizer
Y_{ace}	Yield of biomass on acetate
Y_{for}	Yield of biomass on formate
n	Power factor of pH inhibition
I_{pH}	pH inhibition function on methanogen
pH_{LL}	Lower level pH where methanogen is completely inhibited
pH_{UL}	Upper level pH where low-pH inhibition is initiated
X_{APO}	Total acidogenic bacteria
X_{MPO}	Total methanogenic archaea
X_{ac}	Acetoclastic methanogenic archaea
X_{h2}	Hydrogenotrophic methanogenic archaea
X_{U}	The inert fraction

TABLE OF CONTENTS

LIST OF TABLES

LIST OF FIGURES

CHAPTER 1. INTRODUCTION

1.1. Anaerobic fermentation used in organic wastes treatment

Anaerobic digestion (AD) is a dynamic process where bacteria and archaea collaborate to break down different organic substances, such as food waste, wastewater biosolids, and animal manure, in the absence of oxygen. This process is commonly used for waste treatment with a focus on producing biogas. The AD process takes place in specialized, airtight containers known as digesters. These digesters come in a range of shapes and sizes, tailored to the specific conditions of the feedstock. The complex microbial communities within these digesters break down the organic matter into biogas and digestate, which is then expelled from the digester.

AD has been utilized for decades as a means of waste treatment and bioenergy production, with the first recorded anaerobic digester dating back to 1859 [7]. The energy crisis of the 1970s brought about increased interest in renewable energy and sparked a significant growth in the application of AD for treating biodegradable waste and industrial wastewater. Today, AD is a well-established waste-to-energy technology, particularly for the treatment of biodegradable waste and sewage sludge. Unlike other waste treatment methods, AD does not require any pretreatment for high water content waste [8].

During the AD process, the properties of the biodegradable waste undergo significant changes. This not only results in the production of biogas, but also has positive impacts on the management of the residual sludge. AD stabilizes the digested sludge, reducing pathogen and odor emissions, and decreasing sludge dry matter, leading to a significant reduction in final sludge volume. This makes it easier to dispose of the sludge through landfill, incineration, or use it as an organic fertilizer. These benefits of AD have been widely acknowledged, and the technology is widely used in many countries.

1

Table 1.1 Biogas production in several countries and biogas production from WWTPs

Country	Year	Number of biogas plants	Biogas production (GWh/year)
Australia	2021	247	1587
Austria	2020	283	561
Brazil	2021	638	11700
China	2018	108100	72000000
Finland	2020	109	877
Germany	2020	10551	120000
Ireland	2019	59	752
Japan	2018	104	360[*1]
Norway	2019	162	782
Sweden	2020	282	2161
Switzerland	2019	434	1519
UK	2020	685	26000
USA	2018	2300	28800[*2]

[*1] Ministry of Land, Infrastructure, Transport and Tourism. http://www.mlit.go.jp/common/000233247.

[*2] Energy Information Administration (EIA), https://www.fortunebusinessinsights.com/industry-reports/biogas-market-100910.

The statistics of the International Energy Agency (IEA Bioenergy Task 37, 2022) show the number of biogas plants and biogas production in different countries [9], as presented in **Table 1.1**. Among the 37 countries in the IEA Bioenergy Task, China has the largest number of biogas plants with over 108,000, far surpassing the second largest country, Germany, with over 10,000 biogas plants. Meanwhile, the United States has over 2,300 biogas-producing sites across its 50 states. Of the 1,200 wastewater treatment facilities with anaerobic digesters, around 860 are using their own biogas [10]. While European countries have a long history of using anaerobic technology, none of them has more than 700 biogas plants. In Japan, policies such as SPIRIT21 and Sewerage Vision 2100 have been implemented to improve the utilization of wastewater and sewage sludge, resulting in active use of sewage sludge for energy recovery through the AD process. According to the Japan Sewage Works Agency (JSWA), 280 out of 2,150 wastewater treatment plants are operating AD systems, producing an average of 0.5 m3 CH_4/kg-VS of biogas, equivalent to nearly half of the total

energy consumption of the plant itself [11].

Meanwhile, China has the highest annual biogas production at 72,000 TWh, followed by Germany with 120 TWh/year. Other countries produce less than 30 TWh per year. Some countries' biogas production is estimated based on heat and electricity production with an assumed efficiency of 35%. The use of biogas varies among countries with most using it for heat and electricity generation. Sweden is an exception, using more than half of its biogas production as vehicle fuel. Policy support has increased the use of biogas in the natural gas network in some countries. There are ongoing biogas projects in member countries, focused on improving digestion processes, utilization and resource allocation.

1.2. Reaction process and challenges to maintain the system stability

1.2.1. Conversion processes in anaerobic digestion

AD is a process of breaking down complex organic material through the action of a group of microorganisms. The process involves four stages: hydrolysis, acidogenesis, acetogenesis, and methanogenesis. These stages are depicted in **Figure 1.1** [12].
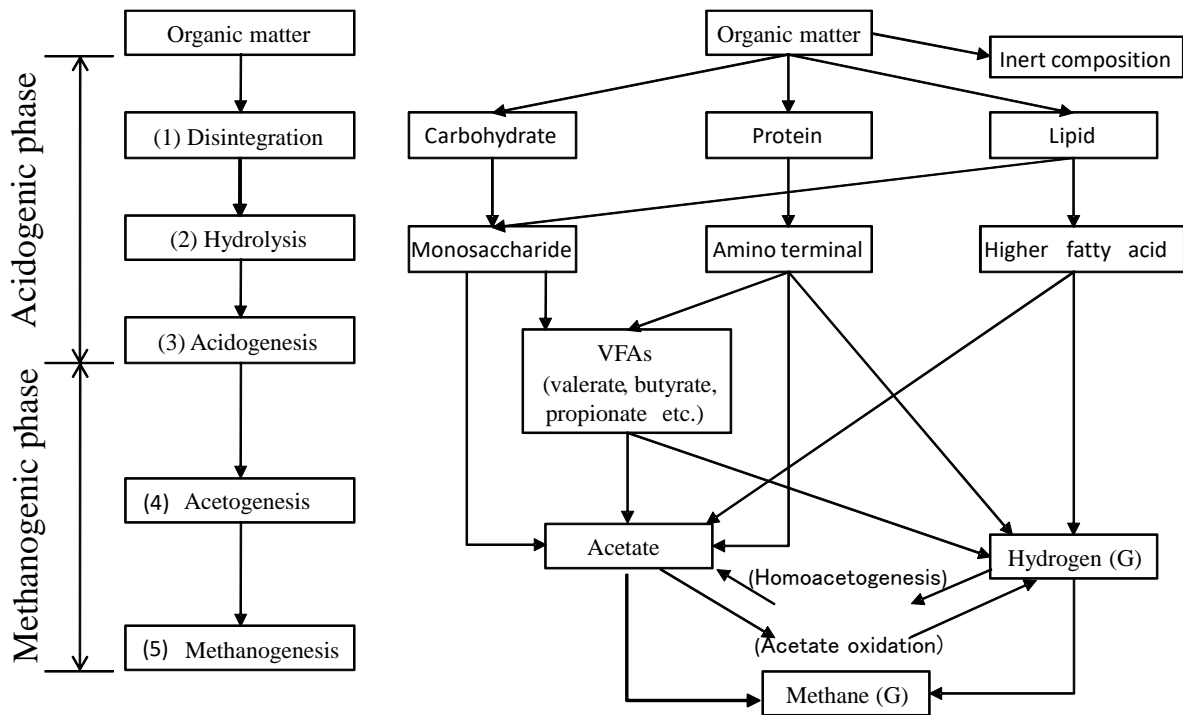
Figure 1.1 Organic COD compositions biodegradation in anaerobic fermentation process

Hydrolysis is the first and crucial step in the AD process. It is also known as enzymatic hydrolysis, as it relies on the activity of extracellular enzymes produced by microorganisms. These enzymes break down complex organic waste into simple and soluble forms (monomers and oligomers). The success of AD largely depends on the efficiency of hydrolysis. The microorganisms involved in this stage include *Clostridium*, *Bacillus*, *Acetovibrio*, *Micrococcus*, and *Staphylococcus*. A list of typical microorganisms involved in the AD process can be found in **Table 1.2** [13,14].

Table 1.2 Typical microorganisms involved in anaerobic digestion.

Type of Organisms	Microorganism involved in the conversion
Hydrolytic bacteria (hydrolysis)	*Acetovibrio, Cellulomonas, Clostridium, Staphylococcus, Bacillus, Bacterium, Bacteriodes, Peptococcus, Micrococcus*
Acidogenic bacteria (acidogenesis)	*Clostridium, Eubacterium, Streptococcus, Zymomonas*
Acetogenic bacteria (acetogenesis)	*Bacillus, Sarcina, Syntrophospora, Syntrophomonas, Clostridium, Desulfobacter, Desulfuromonas, Desulfovibrio, Escherichia, Lactobacillus, Micrococcus, Pseudomonas, Streptococcus, Selenomonas,Staphylococcus,Veillonella*
Methanogenic archaea (methanogenesis)	*Methanosaeta, Methanosarcina, Methanobacterium, Methanobrevibacterium, Methanococcus, Methanospirillum*

Acidogenesis, also known as the acidification phase, is the second step in the AD process. In this stage, simple organic compounds produced during hydrolysis are converted into various organic acids, such as VFAs (acetic, propionic, butyric), alcohols (methanol, ethanol), aldehydes, carbon dioxide (CO_2), and hydrogen (H_2). The microorganisms responsible for this process include *Clostridium*, *Eubacterium*, *Streptococcus* and *Zymomonas*.

During acetogenesis, the acetogenic bacteria transform organic acids into compounds such as acetate, CO_2, and H_2. These compounds serve as the substrate for CH_4 production by methanogenic archaea in the final stage of AD, methanogenesis. However, the produced hydrogen can be toxic to microorganisms. To overcome this, a symbiotic relationship occurs between acetogens and autotrophic methanogens, where hydrogen is used as a substrate for CH_4 production. This relationship is referred to as syntrophy.

The final stage of AD is methanogenesis, where CH_4 is produced from the substrates generated in the previous stages, including acetic acid, H_2, CO_2, formate, methanol, methylamine, or dimethyl

sulfide. The methanogenic microbes are sensitive to low pH levels, with an optimum range of 6.5-8.0. Only 30% of the CH_4 generated during this stage is produced from the reduction of CO_2 by autotrophic methanogens. During the acidification phase, acidic bacteria generate organic acids using hydrogen gas, while little hydrogen gas is produced during the acetogenic phase [13].

The conversion of complex organic compounds into CH_4 and CO_2 in AD is made possible through the collaboration of four groups of microorganisms, as presented in **Table 1.3** [15]. These microorganisms include primary fermentation bacteria, secondary fermentation bacteria (syntrophic and acetogenic bacteria), and two types of methanogens belonging to the archaea domain. These microbes exist in the natural environment and play various roles in the anaerobic degradation of waste.

Table 1.3 Microbial cooperation in organic matter degradation

Microorganisms	Electron donor	Electron acceptor	Product	Reaction type
Fermentative bacteria	Organic carbon	Organic carbon	CO_2	Hydrolysis
Syntrophic bacteria	Organic carbon	Organic carbon	H_2	Acidogenesis
Acetogenic bacteria	Organic carbon/H_2	CO_2	CH_3COOH	Acetogenesis
Methogenic archaea	Organic carbon/H_2	CO_2	CH_4	Methanogenesis

In AD, each step has specific operational requirements, particularly for methanogenesis where the methanogenic archaea convert acetate into CH_4 and CO_2. The microorganisms that drive AD are divided into two groups: acid producers and CH_4 producers. Acid producers break down organic matter in the feed into small, simple molecules (acidogens and acetogens), while CH_4 producers convert these molecules into CH_4 and CO_2. These two groups of microorganisms have different physiological characteristics, growth rates, and sensitivities to operational conditions [16]. The inability to maintain a balance between these two groups often leads to AD process failure. Operating conditions such as temperature, as well as metabolic intermediates of the substrate (e.g., VFAs) can

disrupt the stability of the AD system and cause over-acidification [17]. This is a common issue in single-tank systems, where maintaining a neutral pH level is necessary to sustain the biochemical reaction.

Over-acidification is often caused by insufficient control and, in particular, fluctuating and/or excessive loading of the organic substrate. Bicarbonate acts as a chemical buffer to regulate the pH at neutral levels, which is the optimal pH range for a single-tank AD process. Each step of the AD process has its own preferred pH range, with the first step favored at low pH values and the second at higher values. If the pH drops substantially below 6.5 during the first step, the methanogenic organisms will not be able to survive, resulting in the cessation of CH_4 production [18]. This situation is described as inhibition and, in extreme cases, it can take several months to restore the process to full operational levels [19].

1.2.2. Inhibition factors in anaerobic digestion

Inhibition in AD systems refers to any factor that impairs the microbial activity or reduces the biomass within the system. It can be caused by a variety of factors including, but not limited to, overloading of organic substrate, fluctuations in pH, high levels of toxic compounds, and high concentrations of metabolic intermediates such as VFAs. When inhibition occurs, the steady-state rate of CH_4 production is reduced and the accumulation of organic acids becomes evident [20]. Overloading of the substrate can result in an excessive production of VFAs and protons, leading to over-acidification and, ultimately, the inhibition of methanogenic reactions. This can result in a failure of the AD process, which can take several months to recover to its fully operational levels [21]. Therefore, it is crucial to monitor and control the operational conditions of AD systems to avoid any inhibitory factors and maintain efficient biodegradation of organic matter.

In the past, extensive research has been conducted on the mechanism of product inhibition in AD. Inhibitors of CH_4 fermentation can be broadly categorized as either specific or nonspecific [22]. Specific inhibitors impact only the group of methanogenic microorganisms active in the final stage of fermentation, while nonspecific inhibitors affect both methanogens and other microorganisms. There have been numerous studies that have documented the effects of various chemical substances on CH_4 production by archaea, under different conditions and at varying concentrations of inhibitors [23]. According to these studies, there are two main forms of inhibition: biostatic and biocidal [24]. Biostatic inhibition temporarily reduces the growth rate of microorganisms but does not kill them, and the reaction rate can be quickly restored to previous levels by lowering the concentration of the inhibitory substance [20]. On the other hand, biocidal inhibition leads to the irreversible inactivation of microorganisms and decay of biomass, resulting in a permanent loss of activity. The biocidal inhibition can be expressed as a probabilistic sum of the inactivation probabilities of the microorganisms over time due to biocidal substances [6]. Some inhibitory factors can be mitigated or avoided by reducing the OLR or by pretreating the substrate [25].

As an efficient waste treatment technology that harnesses natural anaerobic decomposition to reduce waste volume and generate biogas, anaerobic digestion has been widely adopted as a source of renewable energy. However, it can be inhibited by toxic materials present in the system, either as components of the waste stream or as byproducts of the metabolic activities of the digester bacteria. These toxic compounds hinder the activities of the sensitive hydrogen-producing acetogens and methanogenic bacteria and may cause a decrease in CH_4 formation, a reduction in the CH_4 content of biogas, or even complete failure of methanogenesis. The following chapters will provide a comprehensive comparative summary of research on the inhibition of anaerobic processes by operational conditions such as temperature and pH, specific organic toxicants like long-chain fatty acids (LCFAs), and inorganic toxicants like ammonia and sulfide. The inhibition mechanism of some

factors is also analyzed and estimated [22].

Long chain fatty acids. The CH_4 fermentation of substrates with a high content of fatty fractions is often hindered by LCFAs. These compounds are toxic to CH_4 fermentation microorganisms, slowing their growth and causing cell membrane damage. The extent of inhibition caused by LCFAs depends on various factors, including the type of LCFA, microorganism population, and temperature [26]. Research has shown that thermophilic microorganisms involved in CH_4 fermentation are more susceptible to LCFAs compared to mesophilic microorganisms, due to differences in cell membrane composition [27]. It is believed that the inhibition of anaerobic metabolism by LCFAs is a result of the adsorption of these fatty acids onto the cell wall and membrane, affecting metabolic transport [22, 28]. The detergent properties of LCFAs result in solubilization of the lipid bilayer or membrane proteins, causing inhibition of enzyme activity [29], disruption of the electron transport chain [30], or even cell lysis [31]. The structure of LCFAs influences its inhibitory effect, with LCFAs having longer carbon chains having a more significant impact on microbial activity than those with shorter chains [32]. Additionally, the inhibitory effect of LCFAs is positively correlated with the number of double bonds in the LCFAs [33].

Ammonia nitrogen. High concentrations of ammonia, which are produced from the degradation of nitrogen-based compounds such as proteins, can have toxic and inhibitory effects on microorganisms [34]. The balance between ammonia and ammonium ion concentrations depends on the pH value and the temperature of the digester, and increases with an increase in these values. Free ammonia is more toxic to methanogens than ionized ammonium (NH_4^+) due to its faster diffusion through the cell membrane, leading to proton imbalance and/or potassium deficiency [35]. On the other hand, ionized ammonium directly inhibits the CH_4 synthesizing enzyme [36]. When free ammonia passively diffuses into methanogens, the resulting difference in intracellular pH causes some of them to convert to ammonium, which absorbs protons (H^+) in the process. To balance the

9

protons, the cells expend energy by using a potassium antiporter [37].

Hydrogen sulfide. Hydrogen sulfide (H_2S), which is produced from the degradation of proteins, has the ability to inhibit microbial activity at even low concentrations [38]. The presence of H_2S in biogas not only reduces the bioavailability of microelements but also causes corrosion to equipment and cogeneration units [39]. The process of reducing sulfate to sulfide is theorized to yield more energy than methanogenesis, which could make the latter process noncompetitive and decrease the rate of methanogenesis and CH_4 production [40]. H_2S can also denature proteins by forming cross-links among polypeptide chains, interfering with key metabolic enzymes, and affecting the assimilation of sulfur and intracellular pH [41]. The uncoupling of growth from energy production and cell maintenance also requires more energy [42]. The toxicity of sulfide is often associated with its undissociated form, which can easily pass across cell membranes due to its neutral molecular form and high reactivity with cellular components [43]. The chemical equilibrium of sulfide species is dependent on pH, with most of the total sulfide in the HS^- form at pH 8.0, and most in the H_2S form at pH 6.0.

Temperature. The operating temperature is a critical factor that affects the performance of AD reactors, as it determines the ideal conditions for the survival and optimal growth of the microbial community [44]. Methanogens have two temperature ranges in which they perform optimally, known as mesophilic and thermophilic temperature ranges. Mesophilic digesters exhibit high efficiency when operated within a temperature range of 25-40 ℃, while thermophilic digesters have an optimum temperature range of 50-65 ℃ [45]. A sudden change in temperature in the digester can cause thermal shock to the process, particularly in thermophilic digestion where microbes are more sensitive to temperature fluctuations [46]. This can affect other process parameters, such as increasing the concentrations of ammonia and hydrogen sulfide, which can inhibit fermentation [34,38].

pH value. Although the detrimental impact of low pH on methane production is well-established, its influence is interrelated with numerous other factors, and the precise mechanisms behind the pH inhibition remain ambiguous [47]. Most microorganisms thrive in a neutral pH range. Methanogens are highly sensitive to pH and perform optimally at a pH of 7.0. On the contrary, acidogenic bacteria are able to tolerate a wider pH range [48]. Hydrolytic and acidogenic bacteria function best within a pH range of 5.5 to 6.5 [49]. Maintaining an optimal pH for all microorganisms in the single digester can be difficult, especially for substrates with diverse compositions.

The sensitivity of methanogenic archaea to pH-dependent inhibition poses a significant challenge in anaerobic digestion, as it can significantly impede the production of biogas. The buildup of intermediate VFAs resulting from this inhibition can reach levels that can cause system failure [5]. This is a vital area of investigation, as there is a noticeable lack of information and understanding in the current studies [50].

1.2.3. Effect of low-pH values on methane fermentation

The pH level is main factor that affects the fermentation process [8,51]. Optimal biogas production in AD occurs in a pH range of 6.8 to 7.5 as depicted in **Figure 1.2** [52,53]. Methane-producing bacteria are highly sensitive to changes in pH and prefer a neutral environment around 7.0, as their growth rate slows down below pH 6.6. It is crucial to maintain the pH within this range as biogas yields drop significantly outside of it. Meanwhile, acid-forming bacteria are less sensitive and can tolerate a pH range of 4.0 to 8.5, with optimal conditions for hydrolysis and acidogenesis being between 5.5 and 6.5. As a result, some designers separate the hydrolysis/acidification stage from the acetogenesis/methanogenesis stage. A decrease in pH leads to an increase in the population of bacteria in the acidogenesis phase, which exacerbates the acidification of the environment through the

production of short-chain fatty acids. VFAs are intermediate products that are produced during the degradation of organic matter in the AD process. While VFAs are necessary for the production of methane in AD, high concentrations of VFAs can inhibit or slow down the process, reducing the efficiency of biogas production [24].

The inhibition of methane fermentation by high levels of VFAs can occur through several mechanisms, including changes in pH, osmotic pressure, and toxicity to the microorganisms responsible for the process. An acidic environment also inhibits the roles of acetogenesis and methanogenesis phase microorganisms, leading to a severe decrease in biogas production. At the start of fermentation, acidogens and acetogens produce acids and CO_2, causing the pH to decrease. The methane-producing archaea then consume the acids, leading to an increase in pH and eventual stabilization. This factor is significant because it affects the concentration of ionized and non-ionized forms of methanogenesis inhibitors such as excessive fatty acids, hydrogen sulfide, and ammonia, which are toxic only in their non-ionized forms [25].
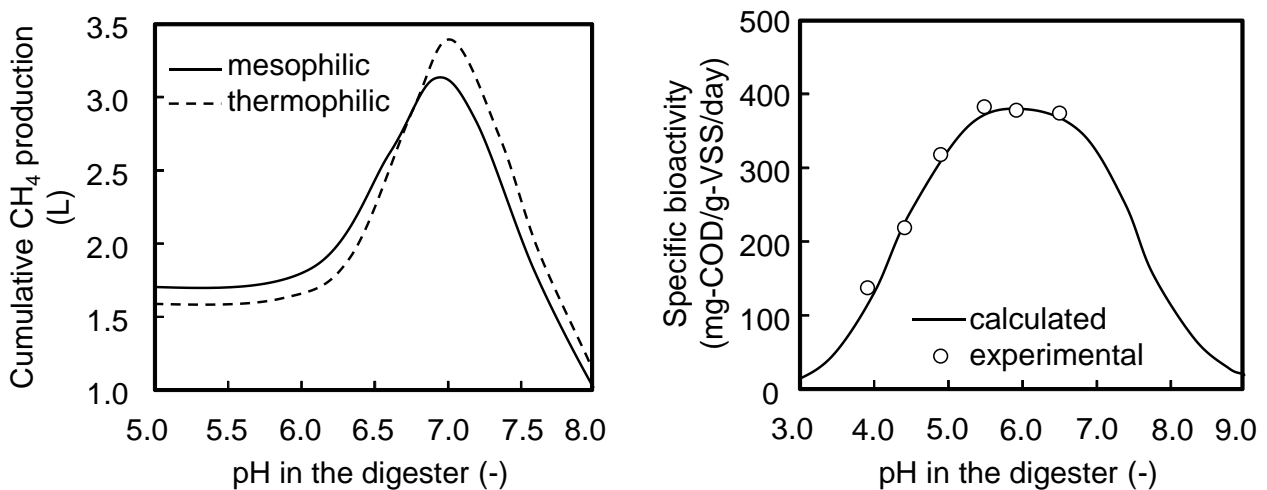
Figure 1.2 The effect of pH on methane production on mesophilic and thermophilic conditions over the pH ranging from 5.0 to 8.0 (left) and specific activity of acidogenesis (right)

The challenges of operating at a low pH level in anaerobic digestion processes include increased acid requirements, buildup of volatile fatty acids, decreased methane production, and inhibition of methanogenesis and hydrolysis. While continuous operation has not been thoroughly studied, particularly in relation to inhibition recovery, acclimation of the microbial community may lead to different outcomes [5,20]. Batch testing, on the other hand, fails to account for the acclimation process and the regular dosing of acid leads to fluctuations in pH, particularly in batch reactors operating at low pH levels (< 5.5). Additionally, batch testing does not accurately reflect the continuous operation of full-scale reactors. Further research is necessary to expand previous batch studies to full-scale analysis.

1.3. Research objectives and thesis structure

The dissertation is comprised of seven chapters, each focusing on a specific aspect of the research topic:

Chapter 1, provides an overview of the development of anaerobic biological fermentation in wastewater treatment and highlights the typical characteristics and challenges of this process.

Chapter 2, delves into the various parameters that inhibit the microorganisms, particularly acetoclastic and hydrogen-utilizing methanogens, in anaerobic digesters. It also explains how activity is affected by VFAs accumulation and pH drop, and outlines the challenges posed by low pH conditions.

Chapter 3, introduces the biochemical and statistical methods used to determine the concentration of living methanogens in anaerobic incubators using the IWA-Anaerobic Digestion Model No.1 as a mathematical framework. The necessary laboratory analyses and materials

required for this method are also discussed.

Chapter 4, describes the incubation method used to create a methanogen-enriched culture using municipal digestate as the inoculum and feeding a synthetic substrate in a chemostat over several months. The comparative analysis of the enriched cultures for further batch experiments is also presented.

Chapter 5, demonstrates the dynamic estimation of low pH inhibition on the decay of methanogenic biomass in enriched cultures using phosphate buffer solution. The irreversible inhibition of the accelerated decay of methanogens in acidic pH environments is explored, and the pH inhibition function in the ADM1 model is modified to reflect this phenomenon. The primary cause of pH inhibition is determined to be high hydrogen ion concentration, rather than undissociated VFAs.

Chapter 6, presents a mathematical analysis of the pH inhibition phenomenon during long-term acclimatization and calibrates the kinetic parameters contrastively for methanogenesis in the ADM1 model. The discussion in this chapter focuses on the potential consequences of low pH conditions on biomass decay and activity hysteresis, and a new auxiliary model, known as the pH-lag model, is introduced to provide further insights.

Chapter 7, summarizes the key findings of the research, speculates the mechanisms behind the inhibition of methanogenesis, and provides recommendations for future studies.

CHAPTER 2. EXISTING RESEARCH

2.1. Structure of the biochemical reactions in anaerobic fermentation

2.1.1. Disintegration and hydrolysis of complex organic material

The process of disintegration and hydrolysis is a crucial aspect of the breakdown of complex organic matter into soluble substrates. Disintegration is a combination of biological and non-biological processes that break down composite particulates, including particulate carbohydrates, proteins, and lipids, into simpler substances. The non-biological step allows for the versatility of the process and enables the lysis of biological sludge and complex organic material.

The three parallel enzymatic steps represent the differences in the hydrolysis rates of carbohydrates, proteins, and lipids, which are the main substrates. The inclusion of the composite organic material allows for the effective recycling of dead anaerobic biomass [54]. Hydrolysis, in this context, refers to the degradation of particulate or macromolecular substrates into their soluble monomers, catalysed by enzymes produced by organisms that directly benefit from the soluble products. The main particulate substrates undergoing hydrolysis are carbohydrates, proteins, and lipids. This process is a formal chemical definition of hydrolysis and is crucial for waste-activated and primary sludge digestion [12].

2.1.2. Acid-producing microbial process of acidogenesis and acetogenesis

Acidogenesis is a process of acid-producing fermentation that occurs in the absence of an additional electron acceptor or donor [55]. It involves the degradation of soluble sugars and amino acids into simpler products, such as alcohols, aldehydes, and VFAs, as well as acetate, H_2, and CO_2 [56]. The degradation of amino acids also results in the production of ammonia (NH_3).

15

Acidogenic bacteria can be either facultative anaerobes or strict anaerobes, with species belonging to the family *Enterobacteriaceae* being commonly identified as active fermenters [57]. Other species commonly found in anaerobic digesters include *Lactobacillus*, *Escherichia*, *Staphylococcus*, *Pseudomonas*, *Sarcina*, *Streptococcus*, *Desulfobacter*, and *Desulforomonas*. These bacteria transform sugars and amino acids into fatty acids, acetate, and NH_3 [58]. The acidogenic stage can be represented by the following equations: **Equation 2.1, Equation 2.2** and **Equation 2.3** [59].

$$C_6H_{12}O_6 \leftrightarrow 2CH_3CH_2OH + 2CO_2 \qquad\qquad \text{Equation 2.1}$$

$$C_6H_{12}O_6 + 2H_2 \leftrightarrow 2CH_3CH_2COOH + 2H_2O \qquad\qquad \text{Equation 2.2}$$

$$C_6H_{12}O_6 \leftrightarrow 3CH_3COOH \qquad\qquad \text{Equation 2.3}$$
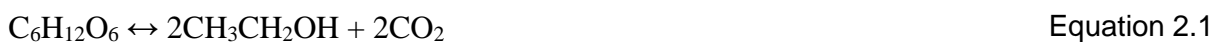
2.1.3. Aceticlastic methanogenesis and hydrogen-utilising methanogenesis

Aceticlastic methanogenesis and hydrogen-utilizing methanogenesis are two major processes involved in the production of methane. Aceticlastic methanogenesis is a process in which methane is produced through the anaerobic degradation of acetate, a short-chain fatty acid commonly produced by the fermentation of organic matter. In this process, acetate is converted to CH_4 and CO_2 by a group of microorganisms called aceticlastic methanogens as shown in **Equation 2.4**.

Two genera of microorganisms, *Methanosarcina* and *Methanosaeta*, use acetate to produce CH_4 [60]. At acetate concentrations above 10^{-3} M, *Methanosarcina* dominates, while *Methanosaeta* dominates at lower concentrations [61]. However, *Methanosaeta* has lower yields and may be more sensitive to pH and changes in acetate concentration compared to *Methanosarcina* [62]. Additionally,

Methanosaeta requires two moles of ATP to activate one mole of acetate at low concentrations, while *Methanosarcina* only requires one mole of ATP at higher acetate concentrations, giving *Methanosarcina* a faster growth rate. However, *Methanosaeta* can operate at lower acetate concentrations with a longer solids retention time. In anaerobic digesters, the two organisms tend to be mutually exclusive, with *Methanosaeta* typically found in high-rate (biofilm) systems [63,64], and *Methanosarcina* found in solid digesters [65].

$$CH_3COOH \rightarrow CH_4 + CO_2 \qquad\qquad \text{Equation 2.4}$$

$$CO_2 + 4\ H_2 \rightarrow CH_4 + 2\ H_2O \qquad\qquad \text{Equation 2.5}$$

Hydrogen-utilizing methanogenesis, on the other hand, is a process in which methane is produced through the reduction of CO_2 with H_2 in **Equation 2.5**. This process occurs in the absence of oxygen and is performed by a group of microorganisms known as hydrogenotrophic methanogens. Some of the well-known genera of hydrogenotrophic methanogens include *Methanobacterium*, *Methanothermobacter*, and *Methanococcus* [66,67]. *Methanobacterium* is one of the most commonly found in various anaerobic environments and is known for its ability to produce methane in environments with high levels of hydrogen gas. *Methanothermobacter* is known for its ability to produce methane at high temperatures, and it has been found in various hot springs and geothermal environments. *Methanococcus* can produce methane in environments with low levels of hydrogen gas, and it has been found in various anaerobic digesters and bioreactors [68].

The mechanism by which these microorganisms produce methane involves the transfer of electrons from hydrogen gas to carbon dioxide, which results in the reduction of carbon dioxide to methane [69]. This process is catalyzed by methanogenic enzymes that are present in the cell membranes of these microorganisms. These enzymes transfer electrons from hydrogen to carbon

dioxide and reduce it to methane, which is then released into the environment.

2.2. Metabolism of methanogenic process

2.2.1. Methanogenesis from formate

The methanogenic archaea have the capability to transform the basic substances, including acetate, H_2 and CO_2, formate, methanol, and methylamines, into CH_4, as demonstrated in **Figure 2.1** [70,71,72].
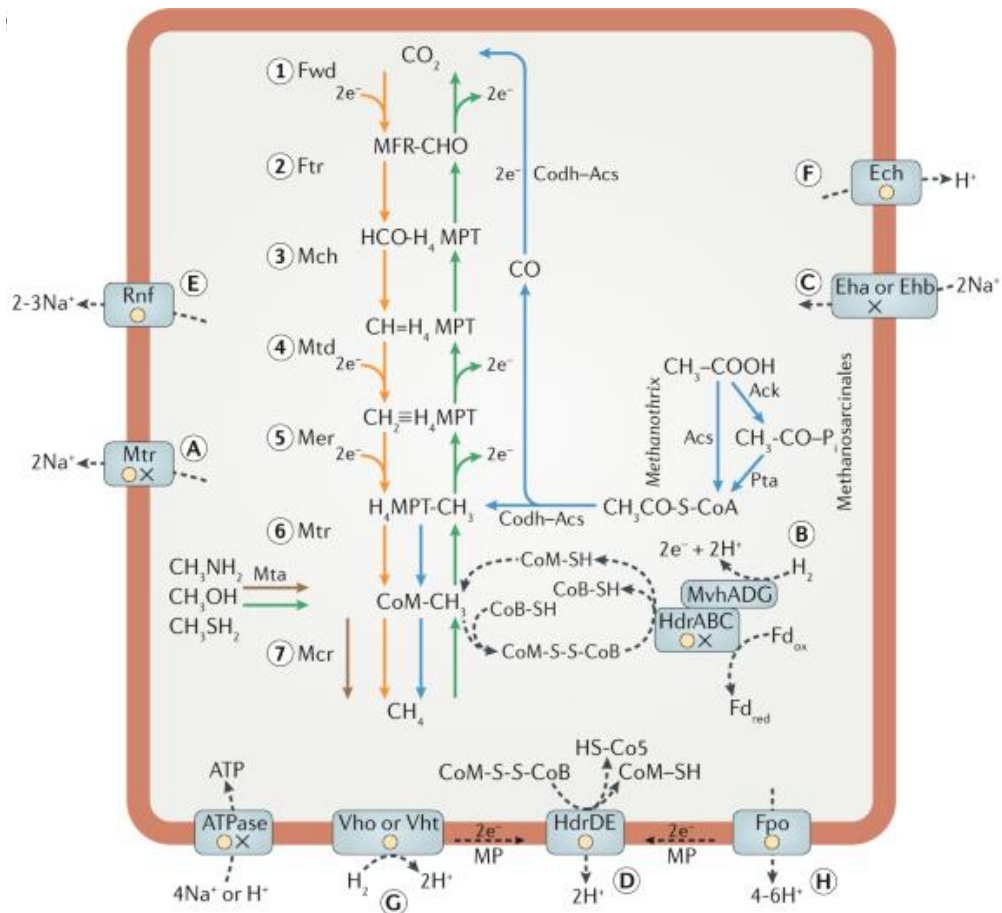
Figure 2.1 Methanogenic and methanotrophic pathways [72].

18

In the process of methanogenesis, both Formate and H_2 serve as equivalent electron donors. The H_2-dependent CO_2 reduction takes place via carrier-bound C_1 intermediates that are gradually reduced to form methane. Many hydrogenotrophic methanogens have the capability to use formate instead of H_2 to produce CH_4 from CO_2. For the conversion of formate, these methanogens use an enzyme called formate dehydrogenase, which consists of two subunits, Fd_{hA} and Fd_{hB} [73]. The activity of this enzyme leads to the production of reduced coenzyme F_{420} [74,75,76].

Moreover, it has been observed that an electron bifurcating enzyme complex can link formate oxidation to heterodisulfide reduction. In this process, hydrogen acts as an electron donor for the reduction of CO_2 to CH_4 (**Orange arrow in Figure 2.1**). The two main hydrogenases used for the oxidation of dihydrogen are the soluble F_{420}-reducing hydrogenase Frh and the soluble Mvh hydrogenase. The Frh reduces the methanogenic cofactor F_{420} to F_{420H2}, which is then re-oxidized during the reduction of carbon dioxide to methane. On the other hand, the Mvh hydrogenase forms a complex with a heterodisulfide reductase (HdrABC) and couples the oxidation of dihydrogen to the reduction of ferredoxin and the heterodisulfide CoM-S-S-CoB in a process called flavin-based electron bifurcation [77].

The reduced ferredoxin is crucial for the first step of methanogenesis, which involves the reduction of carbon dioxide to a cofactor-bound formyl group. The CoM acts as a methyl carrier and forms the heterodisulfide together with CoB in the final step of methanogenesis. Some methanogens use energy-converting hydrogenases, such as Eha, to replenish the cell with reduced ferredoxin, which is also required for the biosynthesis of cell components from CO_2 [78]. Energy conservation during hydrogenotrophic methanogenesis occurs exclusively during a methyl transfer reaction that is part of the core pathway of methanogenesis. The membrane-bound methyltransferase Mtr is responsible for this process and translocates sodium ions across the membrane, leading to the buildup of a sodium motive force that is subsequently used by an ATP synthase. In conclusion, the process of

methanogenesis is an important aspect of the carbon cycle and involves the reduction of carbon dioxide to methane using hydrogen or formate as electron donors. The conversion of formate to CH_4 occurs via formate dehydrogenase, while the energy conservation in this process takes place during a methyl transfer reaction.

2.2.2. Methanogenesis from acetate

The process of converting acetate into methane and carbon dioxide is a complex and multi-step process that requires the activation of acetate to acetyl-CoA (**Bule arrow in Figure 2.1**). The activation process is performed by two groups of microbes: *Methanosarcinaceae* and *Methanotrichaceae*. These microbes take in acetate through an acetate transporter and activate it to acetyl-CoA through the action of acetate kinase and transacetylase in *Methanosarcinaceae* or through the activity of acetyl-CoA synthetase in *Methanotrichaceae* [79,80].

Once acetate has been activated to acetyl-CoA, the molecule is cleaved into a coenzyme-bound methyl moiety and an enzyme-bound carbonyl group. The carbonyl group is oxidized to carbon dioxide while the methyl group is funneled into the central methanogenic pathway and reduced to methane. Energy conservation occurs at the membrane-bound methyltransferase Mtr and through a membrane-bound electron transport chain that utilizes reduced ferredoxin and the heterodisulfide [79].

During aceticlastic methanogenesis, more Na^+/H^+ ions are translocated, but it requires an initial ATP investment for the activation of acetate to acetyl-CoA [81 , 82]. Overall, aceticlastic methanogenesis is an energy-intensive process that is crucial for the production of methane, a valuable source of energy. By understanding the various steps and mechanisms involved in this process, scientists can better understand the microbial communities that play a crucial role in converting acetate into methane and carbon dioxide.

2.3. Acidic failure in methane fermentation and recovery of VFAs

2.3.1. Acid failure phenomenon under high organic loading conditions

In an effort to increase the sources of renewable energy, numerous anaerobic digestion plants converting organic waste to biogas are being built world-wide [83,84]. Most of these biogas plants use chemostat reactors fed with food waste, animal manure and/or municipal solid waste [85]. Organic food waste is an ideal source for biogas recovery as most of the food waste is readily biodegradable. To save space and cost of construction, the biogas recovery systems are often built as high-loaded plants [86]. These high-loaded plants often encounter acidic failure when very high loads of biodegradable material are unexpectedly fed to the reactor. In principle, the acidic failure is caused by the imbalance of reaction rates between fermentative microorganisms (acidogens, fast-grower) and methanogens (slow-grower). The acidogens produce organic acids (volatile fatty acids, lactate, *etc*.) in proportion to its growth whilst the methanogens remove acetate and hydrogen (and formate) which are the end products of acidogenic reactions [12]. During high loading conditions, the acidogens produce high amount of organic acids which are not proportionally removed by the slow-growing methanogens resulting in accumulation of organic acids. In severe cases, accumulation of organic acid and corresponding decrease in pH result in inhibition of methanogen leading to acidic failure of reactor [18,87].

2.3.2. VFAs accumulation and recovery in acid failure

The degradation process of organic material through anaerobic digestion results in the production of VFAs as intermediates. These VFAs have gained widespread attention due to their

versatile applications in various industries, including food, textile, pharmaceutical, leather, and plastic [88]. In addition, hydrogen gas, produced during the acidogenesis step, is a clean and renewable energy source [89,90].The type and concentration of VFAs produced are dependent on various factors, including the substrate composition, operational parameters, microbial population, and process design [91,92,93]. The most common VFAs produced are acetic, propionic, butyric, isovaleric, valeric, and caproic acids [94,95].

Maximizing the accumulation of VFAs in anaerobic digestion requires a multi-faceted approach that balances both production and consumption. To further increase VFA production, a combination of strategies can be used, including adjusting the operational conditions, such as temperature, pH, and hydraulic retention time, to create optimal conditions for VFA-producing microorganisms. Additionally, selecting the appropriate substrate and inoculum can enhance the diversity and activity of the microbial community responsible for producing VFAs.

On the other hand, to achieve optimal production of VFAs from organic waste, the anaerobic digestion process must be optimized to inhibit the production of methane in the final step [96]. Inoculum pretreatment, such as anaerobic sludge stabilization, can reduce the number of methanogens and increase the VFA concentration in the system. Additionally, overloading the system with substrate can also lead to high VFAs concentration that can reduce the number of methanogens. The addition of certain chemicals, such as formic acid, acetic acid, or propionic acid, can also act as methanogen inhibitors and decrease VFA consumption [95]. However, the separation and purification of VFAs is challenging due to their azeotropic mixture with water. To produce VFAs with added value, these mixtures must be converted into chemicals or purified into single components [97].

2.4. Kinetic inhibition of low-pH and high VFAs concentration and its modelling

2.4.1. Decomposition rate and inhibition of high-concentration VFAs

VFA inhibition is one of the influential factors on biological process performance, especially CH_4 fermentation systems where sequential microbial reactions are mediated by acidogens, acetogens and methanogens. In earlier studies conducted between 1970s and 2010s, the VFA inhibition mechanism has been extensively investigated. Kaspar and Wuhrmann (1978) demonstrated that anaerobic oxidation of propionate to acetate was strongly inhibited by high partial pressure of hydrogen [98]. They explained that the inhibition was due to unfavourable thermodynamic symbiotic reactions between acetogens and methanogens at high hydrogen partial pressure. In 1980s, Hill and Holmbert (1988) adopted VFA concentrations as an indicator for anaerobic digestion process stability [99]. The dynamic accumulation of VFAs is supposed to be an early warning of the imbalanced reactions between the acidogens (acetogens) and methanogens, which might result in the acidic failure (system overload). These viewpoints were further strengthened in 1990s. Fukuzaki *et al.* (1990a) and Fukuzaki *et al.* (1990b) showed that the undissociated VFAs (propionic acid and acetic acid) were the inhibitory substances [100,101]. Marchaim and Krause (1993) suggested that the ratio of propionate to acetate could be a relevant process-indicator to predict the system overload [102]. However, Ahring *et al.* (1995) pointed out that the accumulation of VFA was a consequence of the system overload and VFA itself might not be the primary inhibitory substance [103]. This was because unusually high VFA concentration (beyond 50~100 mmol/L) could only inhibit the methanogenic reaction. From this, they deduced that other factors causing methanogenic inhibition would exist. Based on these studies, a VFA inhibition function has been included in IWA ADM1 [12].

The growth inhibition equation in the ADM1 model is a mathematical expression used to describe the effect of inhibitory compounds on the growth and substrate uptake of microorganisms in

AD processes. The equation represents the interplay between the substrate uptake rate and the concentration of inhibitory compounds, taking into account the impact of both on the overall growth rate of the microorganisms. Extensive studies on inhibition and kinetics of substrate uptake and growth can be found in ADM1 [104,105]. Although there are various forms of inhibition, the formula for substrate uptake and inhibition can be uniformly expressed as **Equation 2.6** [12].

$$\left\{ \rho_j = K_m \cdot \frac{S}{K_S + S} \cdot X \cdot I_1 \cdot I_2 \cdots I_n \right.$$

Equation 2.6

Where, ρ_j is kinetic rate of process j (kgCOD $\cdot$m^{-3} $\cdot$d^{-1}), K_m is monod maximum specific uptake rate (kgCOD $\cdot$kgCOD^{-1} $\cdot$d^{-1}), K_S is half saturation value (kgCOD $\cdot$m^{-3}), S is soluble component (kgCOD $\cdot$m^{-3}), X is particulate component (kgCOD $\cdot$m^{-3}), I_n is inhibition function (-).

The exact form of the equation is generally based on the Monod model, which assumes that the growth rate of the microorganisms is proportional to the substrate concentration (S), with inhibition described as a reduction in the maximum growth rate (K_m) or an increase in the half-saturation constant (K_S). This allows for easy replacement or addition of other suppression factors where feasible. The equation consists of the uninhibited Monod-type uptake and the inhibition functions ($I_{1\ldots n} = f(S_{I,1\ldots n})$). The specific parameters used in the equation may be adjusted to fit the specific conditions of the anaerobic digestion system being studied. It is worth noting that the current substrate inhibition equation only pertains to the growth rate of microorganisms. However, it is known that excessively high concentrations of inhibitory compounds can also cause the death of microorganisms to some extent [5]. This effect will be investigated in the subsequent studies.

2.4.2. pH inhibition functions and models on Methanogens

In ADM1, the high concentration of undissociated VFAs (unVFAs) and low pH are assumed to inhibit the microbial substrate conversion rates, which are accompanied with the inhibition of the microbial growth. In other words, the VFA inhibition is assumed to be biostatic in nature. The biostatic inhibitions are those where the microorganisms are not killed in the operational conditions, but its growth rates are inhibited [20]. The lowered reaction rates could be immediately recovered to the previous level when the inhibitory substance concentration is lowered. With respect to biocidal phenomena (irreversible inactivation of microorganisms and biomass decay), Lins *et al.* (2014) reported that very high acetate concentration (150 mM) enhanced methanogens' decay even at a near-neutral pH (pH 7.5) in the thermophilic anaerobic reactors [4]. This was a noticeable experimental finding that VFAs also acted as biocidal reagent. Sun *et al.* (2020) recently showed that low pH simulated by phosphoric acid also led to accelerated methanogens' death (methanogens' inactivation) [5]. In overloaded anaerobic reactors, the low pH is associated with accumulation of unVFAs. Therefore, low pH (high proton concentration) or high unVFA or both are supposedly the biocidal substance. However, the actual biocidal substance and its effect has not been clarified yet due to lack of detailed experimental results.

Regarding pH inhibition during the growth phase, the studies usually utilize the empirical upper and lower inhibition limits in the ADM1 model as depicted in **Equation 2.7** [12]. pH_{UL} and pH_{LL} are the upper and lower limits, respectively, where the methanogenic population is 50% inhibited. For example, acetate-utilising methanogens with a pH_{UL} of 7.5 and a pH_{LL} of 6.5 have an optimum at pH 7.0. The low-pH inhibition function, depicted as **Equation 2.8**, assumes that when $pH > pH_{UL}$, b represents the specific decay rate of methanogens (0.02 d^{-1}), I_{pH} represents the empirical lower-only inhibition switching function, and pH, pH_{UL}, and pH_{LL} represent the pH in the system, the upper level pH where low-pH inhibition begins, and the lower level pH where methanogens are completely

inhibited, respectively. Acetate-utilising methanogens with a pH_{UL} of 7.0 and a pH_{LL} of 6.0 will be completely inhibited below pH 6.0 and not inhibited above pH 7.0. To account for the relationship between pH and system response, an additional inhibition equation was added to the existing ADM1 model. This equation is based on the decay phase of the empirical pH inhibition function, and it was modified by changing the power coefficient from 2 to n (-) [5].

$$I = \frac{1 + 2 \times 10^{0.5(pH_{LL} - pH_{UL})}}{1 + 10^{(pH - pH_{UL})} + 10^{(pH_{LL} - pH)}}$$ Equation 2.7

$$\begin{cases} k_A = \dfrac{b}{I_{pH}} \\ I_{pH} = \exp\left(-3\left(\dfrac{pH - pH_{UL}}{pH_{UL} - pH_{LL}}\right)^2\right) \\ I_{pH} = 1 \quad \text{if } pH \geq pH_{UL} \end{cases}$$ Equation 2.8

Where, k_A is methanogen's specific decay rate (d^{-1}), b = specific decay rate of methanogens without low-pH inhibition (d^{-1}), I_{pH} = empirical lower-only inhibition switching function (-), pH = pH in the system (-), pH_{UL} = upper limit of pH where low-pH inhibition is initiated (-), pH_{LL} = lower limit of pH (-).

Mathematically the biostatic inhibition could be expressed by applying inhibition terms to the specific microbial reaction rate (*e.g.,* a product of switching functions for hydrogen inhibition and ammonia inhibition in Monod-type equation). On the other hand, the biocidal inhibition is correlated with the biomass loss leading to irreversible activity loss. Hence the biocidal inhibitions could be expressed as a stochastic summation of the inactivation probabilities given from the biocidal substances that occur on the microorganism over time [6] (*i.e.,* a summation of the first-order

coefficients for the inherent biomass decay, decay by the inhibitory substance A and decay by the inhibitory substance B…). Using the proposed approach, the VFA (and proton) inhibition could be theoretically applied to biostatic, biocidal or both type of the inhibitions. Nevertheless, unlike these research studies on biostatic inhibition, research on biocidal inhibition is still limited.

2.4.3. Suggested parameters in existing ADM1 model

The ADM1 model is a mathematical representation of the kinetics of the AD process (Matrix is shown in **Tables A2–A3 in Appendix**). It utilizes various kinetic parameters to predict the performance of the process and optimize it for maximum biogas production. The kinetic parameters used in the model mainly include: maximum specific growth rate (μ_{max}), half-saturation constant (K_S), specific decay rate (k_d) and yield of biomass on substrate (Y). These parameters describe the efficiency of substrate utilization, microbial growth, and degradation of organic matter in the anaerobic digestion process (Nomenclature is addressed in **Tables A1 in Appendix**).

Table 2.1 provides recommended kinetic parameter values for mesophilic high-rate, mesophilic solids, and thermophilic solids digesters, along with qualitative variations and sensitivity information. These parameters have been extensively tested for consistency and can provide reliable predictions of system response under various conditions. However, it should be noted that these values are largely based on experience and may not reflect the specific conditions of a given system.

Table 2.1 Suggested parameter values for mesophilic and thermophilic digesters.

Parameter	Mesophilic high-rate (35°C)	Mesophilic solids (35°C)	Thermophilic solids (55°C)
k_{dis} (d^{-1})	0.4	0.5	1.0
k_{hyd_CH} (d^{-1})	0.25	10	10
k_{hyd_PR} (d^{-1})	0.2	10	10
k_{hyd_LI} (d^{-1})	0.1	10	10
$t_{res,X}$ (d)	40	0	0
k_{dec_all} (d^{-1})	0.02	0.02	0.04
$K_{S\_NH3\_all}$ (M)	1×10^{-4}	1×10^{-4}	1×10^{-4}
pH$_{UL\ acet/acid}$	5.5	5.5	5.5
pH$_{LL\ acet/acid}$	4	4	4
k_{m_su} (COD COD^{-1} d^{-1})	30	30	70
K_{S_su} (kgCOD m^{-3})	0.5	0.5	1
Y_{su} (COD COD^{-1})	0.10	0.10	0.10
k_{m_aa} (COD COD^{-1} d^{-1})	50	50	70
K_{S_aa} (kgCOD m^{-3})	0.3	0.3	0.3
Y_{aa} (COD COD^{-1})	0.08	0.08	0.08
k_{m_fa} (COD COD^{-1} d^{-1})	6	6	10
K_{S_fa} (kgCOD m^{-3})	0.4	0.4	0.4
Y_{fa} (COD COD^{-1})	0.06	0.06	0.06
$K_{I,H2\_fa}$ (kgCOD m^{-3})	5×10^{-6}	5×10^{-6}	n/a
k_{m_c4+} (COD COD^{-1} d^{-1})	20	20	30
K_{S_c4+} (kgCOD m^{-3})	0.3	0.2	0.4
Y_{c4+} (COD COD^{-1})	0.06	0.06	0.06
$K_{I,H2\_c4+}$ (kgCOD m^{-3})	1×10^{-5}	1×10^{-5}	3×10^{-5}
k_{m_pro} (COD COD^{-1} d^{-1})	13	13	20
K_{S_pro} (kgCOD m^{-3})	0.3	0.1	0.3
Y_{pro} (COD COD^{-1})	0.04	0.04	0.05
$K_{I,H2\_pro}$ (kgCOD m^{-3})	3.5×10^{-6}	3.5×10^{-6}	1×10^{-5}
k_{m_ac} (COD COD^{-1} d^{-1})	8	8	16
K_{S_ac} (kgCOD m^{-3})	0.15	0.15	0.3
Y_{ac} (COD COD^{-1})	0.05	0.05	0.05
pH$_{UL\_ac}$	7	7	7
pH$_{LL\_ac}$	6	6	6
$K_{I,NH3}$ (M)	0.0018	0.0018	0.011
k_{m_h2} (COD COD^{-1} d^{-1})	35	35	35
K_{S_h2} (kgCOD m^{-3})	2.5×10^{-5}	7×10^{-6}	5×10^{-5}
Y_{h2} (COD COD^{-1})	0.06	0.06	0.06
pH$_{UL\_h2}$	6	6	6
pH$_{LL\_h2}$	5	5	5

CHAPTER 3. METERIALS AND METHODS ON BIOCHEMICAL AND STATISTICAL ANALYSIS

3.1. Introduction

This study aims to address the limited understanding of the effects of high H^+ concentrations on methanogen decay during the decay stage of anaerobic systems by incorporating the impact of low pH in a modified IWA ADM1 model [12,106]. In a series of lab-scale experiments, the effect of pH on methanogens was evaluated under various organic loading rates. Biochemical analysis, including the measurement of VFAs and qPCR analysis, was performed to understand the behavior of acclimated methanogens under different pH conditions. Mathematical calculations were also used to determine the dynamic parameters of the methanogenic biomass. The modified ADM1 model was also compared with the default ADM1 model in terms of its ability to predict process performance and microbial concentrations [107]. Biochemical analysis provides insights into the concentration of specific biochemical compounds, allowing for a better understanding of the underlying biological processes and mechanisms. In addition, the choice and application of appropriate statistical methods can help to account for variability in the data and identify significant differences and trends. The following sections describe the analytical methods utilized in this study. These methods were crucial in understanding the impact of low pH on methanogen decay and evaluating the response of the acclimated methanogens.

3.2. Lab-scale incubation systems of two kinds of methanogenic cultures
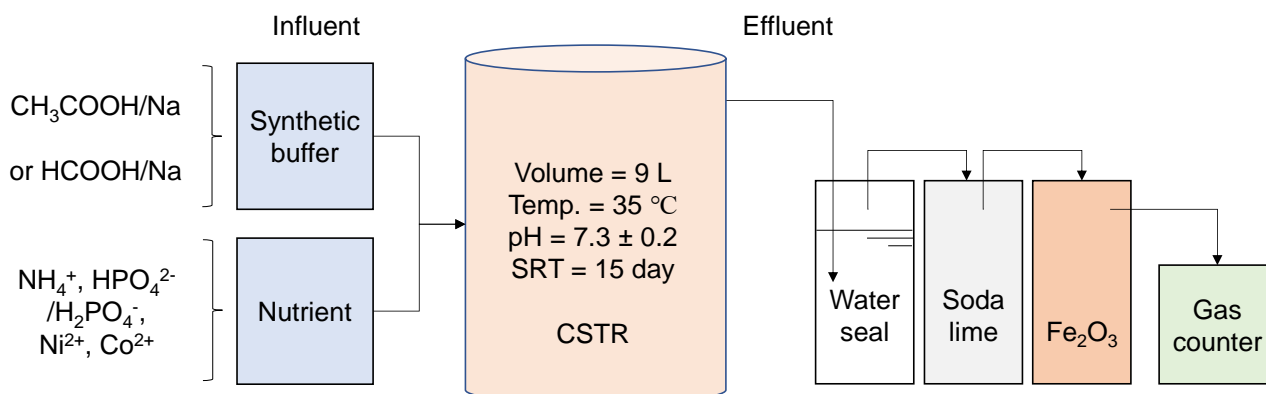
Figure 3.1 Schematic drawing of the methanogen incubation system

Two 10-L jar fermenters (MDL-1000, BEM, Japan) were operated in chemostat mode to cultivate an enriched biomass of acetoclastic and hydrogenotrophic methanogens, respectively. The seed sludge for the reactors was collected from a mesophilic anaerobic digester at the Hiagari municipal wastewater treatment plant in Kitakyushu, Japan. The jar fermenters were operated with a 15-day hydraulic retention time (HRT) and a constant temperature of 35°C, as depicted in **Figure 3.1**. The first reactor (Acetate-fed reactor) was used to enrich acetate-degrading acetoclastic methanogens, which were fed a sole organic carbon source of acetate buffer (CH_3COOH: CH_3COONa = 4:1, mole basis). The second reactor (Formate-fed reactor) was used to enrich formate-degrading hydrogenotrophic methanogens and was fed a formate buffer (formic acid: sodium formate = 2.5 mM: 1 mM).

The synthetic medium consisted of a mixture of carbon sources and inorganic components including ammonium nitrogen (NH_4Cl: NH_4HCO_3 = 1:1 on a mole basis, with 1000 mg-N/L), phosphate (Na_2HPO_4: KH_2PO_4 = 9:1 on a mole basis, with 50 mg-P/L), cobalt (2 mg-Co/L), and nickel (2 mg-Ni/L) in tap water. These ingredients were continuously fed into corresponding jar-

30

fermenters using an electromagnet metering pump (EHN-B11, Iwaki, Japan). The carbon sources were comprised of organic acids and their sodium salts, and the pH of the reactors was automatically maintained around 7.3 ± 0.2 due to the presence of sodium ions and bicarbonate produced during continuous operation. The pH was also monitored by a pH controlling system (EWN-W, Iwaki, Japan) that would inject a small amount of 0.01M NaOH to maintain a neutral pH. However, the pH could be manually adjusted as needed, and sometimes a sharp fluctuation in pH occurred due to the accumulation of high concentrations of acetic or formic acid, resulting in extremely low pH conditions.

The jar fermenters were run for over three months to cultivate methanogen-enriched cultures in steady-state conditions. At steady-state, the acetate-fed jar fermenter produced an average of 0.32 L-CH_4/L/d of biogas, with a sludge particulate concentration of 170 mg-COD/L and a soluble material concentration of 30 mg-COD/L in the effluent. The formate-fed jar fermenter produced a biogas yield of approximately 0.30 L-CH_4/L/d, a sludge concentration of 240 mg-COD/L, and a soluble COD concentration of 20 mg-COD/L in the effluent, as depicted in Chapter 4.

3.3. Laboratory analysis of experimental parameters

3.3.1. Measurement of VFAs concentration and methane production

The sample was centrifuged at 9,187 g for 4 minutes and washed with deionized water, followed by VSS and COD analysis using standard methods [108]. The supernatant was then filtered through a 0.45-μm membrane filter (Advantec 25CS, Tokyo, Japan) to measure the acetate concentration. The acetate concentration was analyzed using an ion-chromatography system (ICS-1000, Thermo Fisher Scientific Inc., Waltham, USA) with an Ion Pac AS11-HC column (Thermo Fisher Scientific Inc.,

Waltham, USA). The filtered sample was mixed with 90% deionized water in a 1 mL vial at a 1: 9 (v: v) ratio. The procedure for VFAs analysis was described by Ngo et al. (2016) [109]. The biogas generated from the jar fermenter was continuously transferred to a soda lime-filled caustic column through a water-sealed vessel. The residual fraction after the removal of CO_2 and H_2S was assumed to be methane and its production rate was recorded with a precise gas-volume counter (MGC-1, Ritter, Bochum, Germany).

After the initial phase washed out high concentrations of suspend solid (SS) continuously, the volatile suspend solid (VSS) analysis was carried out to evaluate the concentration of enriched biomass in the incubation system. The VSS/SS ratio was used to assess the overall operation of the system and the growth of microorganisms. Particulate COD was measured at regular intervals to monitor the COD/VSS ratio for the subsequent simulation process.

3.3.2. Living cell counting by LIVE/DEAD staining

A commercial cell viability kit, the LIVE/DEAD® BacLightTM cell viability kit (L-7012, Molecular Probes, USA), was used to assess the number of viable microorganisms during batch experiments [110]. This experimental method uses reagents that specifically react with living cells to produce green fluorescence. To ensure that the cells were evenly spread on the glass slide, the collected sludge samples were dispersed using ultrasonic waves before microscopic observation.

Before ultrasonication, the sludge sample (5 mL) was centrifuged and washed with deionized water, then diluted tenfold with deionized water. 5 mL of the diluted sample was placed in a 15 mL glass test tube in an ice-water bucket. The ultrasonic waves (20 kHz) were applied to the diluted sample for 45 seconds using an ultrasonic disrupter (UD-200, TOMY, Japan) at level 3 power tension

30 W of the instrument's power consuming [6]. This experimental method was established through a series of preliminary experiments where the ultrasonication time was varied (**Figure 3.2**), which helped to maximize cell viability.
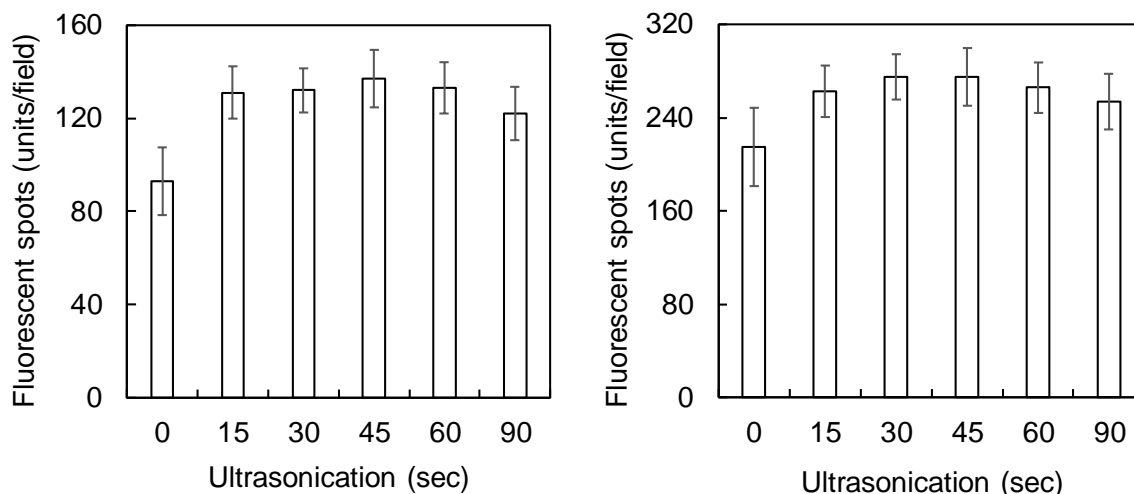
Figure 3.2 Detected number of fluorescent spots against ultrasonication time

(Error bar: 95% confidence interval) (Left: Acetate-fed system, right: Formate-fed system)

After labelling the living microorganisms with the cell staining kit according to the manufacture's protocol, 7.6 µL of the labelled sample was placed on the glass slide with a micropipette, which ensured the sample liquid volume was perfectly spread over the area of the cover slip (22×22 mm = 484 mm^2) without leakage from the edge of the cover slip. For the microscopic observation a fluorescence microscope (ECLIPSE 80i, Nikon, Japan; DS-Fi2, Nikon, Japan) equipped with a bandpass filter cube (GFP-B: excitation wavelength = 460~500 nm; emission wavelength = 515~560 nm) was used. To record the fluorescent cell area per microscopic field at 200 magnification (10×20), a binarised image analysing software having $1,280 \times 960$ pixels was used (Quick Grain, Inotech, Japan). At the magnification the software covered 0.786 mm^2 of the cover slip

area (pixel resolution = 0.8 μm) which allowed to detect the living microorganism in 1.2×10^{-2} μL per photo (per microscopic field). Total 30 photos were taken per glass slide at different places, which corresponded to about 5% of the cover slip area (**Figure 3.3**).
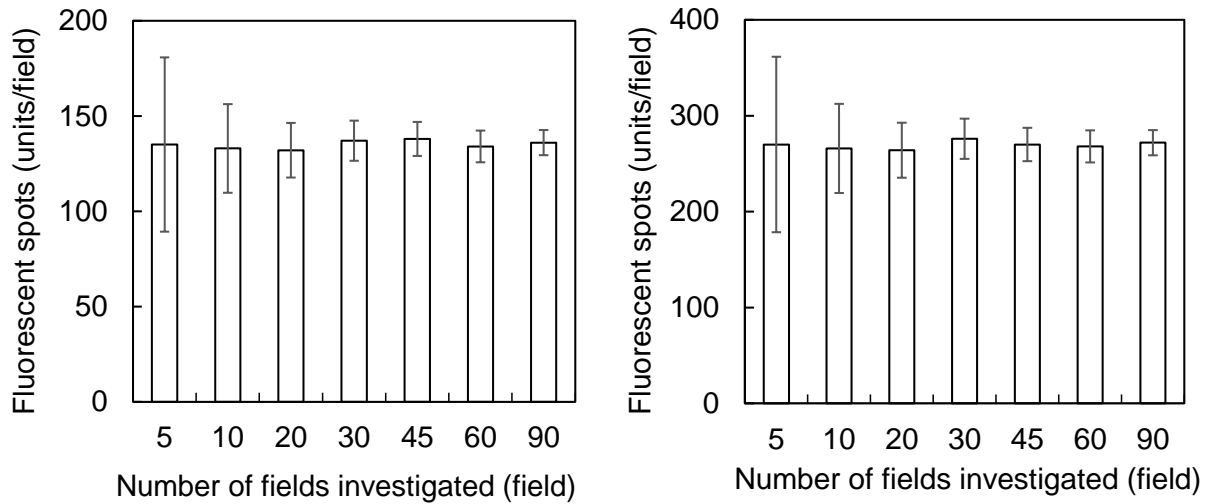
Figure 3.3 Detected number of fluorescent spots against samplings

(Error bar: 95% confidence interval) (Left: Acetate-fed system, right: Formate-fed system)

From the fluorescent cell area per microscopic field (μm^2/field) the concentration of living biomass was estimated. The datasets were statistically analysed using a commercial data analysis software, Igor Pro (WaveMetrics, USA). In addition, assuming that each fluorescent spot was equivalent to a single living cell, conversion factors to calculate the number of living cells from the fluorescent cell area were estimated. The conversion factors were estimated to be 5.9 μm^2-fluorescent cell area /cell$_{-spot}$ for Acetate-fed system and and 5.2 and μm^2-fluorescent cell area /cell$_{-spot}$ for Formate-fed systems respectively (**Figure 3.4**). The estimated values of 5.2~5.9 were noticeably higher than typical microbial cell sizes in electro-microscopic observations mentioned in literature and books (microbial cell diameter ≈ 1.0 μm) [111], and this was likely due to lens flare of the strong

green fluoresce around the stained cells. Therefore the microscopic observation was completed within 0.5~1 day where the intensity of fluorescence was kept constant.
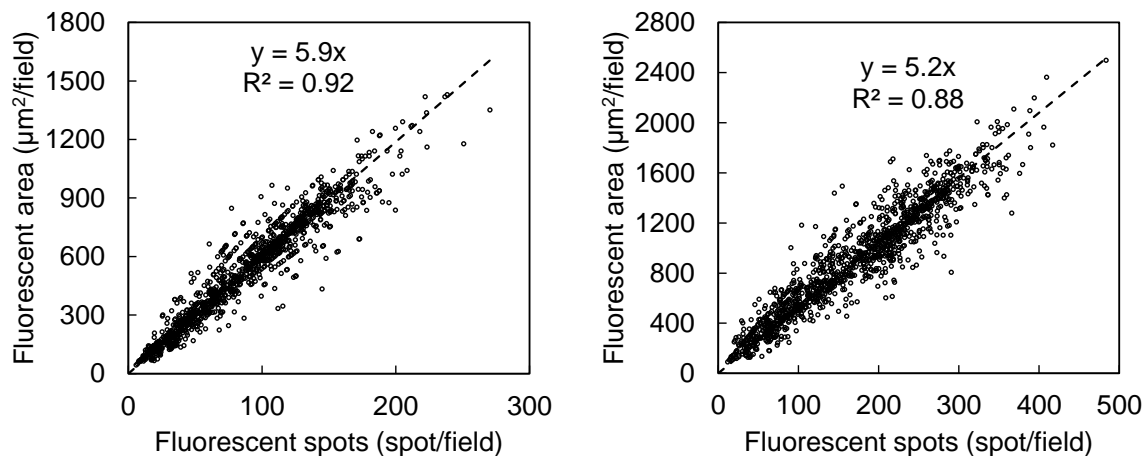
Figure 3.4 Standard curve for fluorescent cell area and fluorescent spots

(Left: Acetate-fed system, right: Formate-fed system)

3.3.3. PMA-qPCR analysis of living archaeal and bacterial biomass

In order to measure fractions of archaea and bacteria in the sludge samples, a PMA-qPCR analysis was conducted where genes of only living microorganisms were amplified and detected [112,113,114]. At the beginning and the end of the batch experiments, 7.5 mL of sludge sample was washed and thickened in phosphate buffer (pH = 7.4) with the above-mentioned high-speed refrigerated centrifuge at $2,297g$ (= 4,000 rpm) for 5 minutes. The thickened sample was diluted with 25-μM propidium monoazide (PMA) to 1 milli litre, and kept for 5 minutes under a dark condition followed by 5-minute radiation of blue LED light in ice water using Illuminator TLB-01 (Gel company, USA). After recovery of the composite DNA with a cell disruption pre-treatment using Tube Mixer (As-one, Japan) for 10 minutes followed by the extraction in 10-mM Tris buffer using PowerWater® DNA isolation kit (Mobio Laboratories, USA), the qPCR reaction was performed in

its 20-µL sample composed of 0.5 µL of composite DNA sample, 10 µL of innuDRY qPCR MasterMix® Probe (Analytik jena, Cermany), 2 µL of primer/probe mix and 7.5 µL of nuclease-free water.

The 16S rRNA gene fragments were amplified on a PCR technique using a universal primer-probe set (Uni340F, Uni806R and Uni516F) (TaKaRa Bio, Japan) and an Archaea-specific primer-probe set (Arch349F, Arch806R and Arch516F) (TaKaRa Bio, Japan) according to the methods in Takai *et al.* (2000) [115]. From the numerical difference between the number of cells detected with the universal primer set and those detected with the Archaea-specific primer set, number of living bacterial cells were calculated. The PCR amplification was performed using TaKaRa Ex Taq polymerase® (TaKaRa Bio, Japan) and a qTOWER^{3}G thermal cycler (Analytik jena, Germany) where the enzymes were activated at 98°C for 2 minutes followed by a sequential treatment composed of 50 cycles of denaturation at 98°C for 10 seconds, annealing at 50°C for 45 seconds, and extension at 72°C for 30 seconds. Together with a blank, these samples were analysed using qPCRsoft 3.4 software (Analytik Jena, Germany) [116].

In qPCR analysis, the number of thermal cycles refers to the number of PCR cycles that are run during the amplification of a specific DNA sequence. The fluorescent signal detected during qPCR is used to monitor the amplification of the DNA sequence in real-time. During qPCR, the DNA sample is first denatured at a high temperature to separate the two strands of DNA. The temperature is then lowered to allow the primers to anneal to the complementary sequence on each strand of the DNA. The temperature is then raised again, and the Taq polymerase enzyme binds to the primers and starts synthesizing new strands of DNA. As the new strands of DNA are synthesized, the fluorescent signal increases in intensity. The number of thermal cycles required to reach a detectable fluorescent signal depends on the starting concentration of the DNA sample and the efficiency of the PCR reaction. Generally, as the number of thermal cycles increases, the amount of amplified DNA also

increases, and the fluorescent signal becomes stronger.
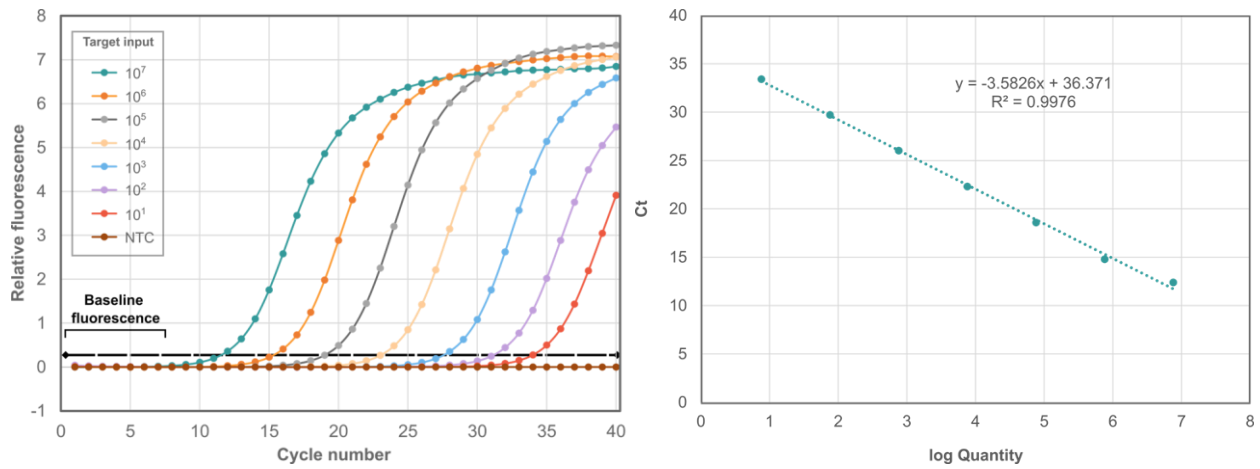
Figure 3.5 The number of thermal cycles versus the fluorescent signals detected [117].

However, there is a limit to the amount of DNA that can be amplified by qPCR, and at some point, the signal reaches a plateau. The point at which the signal reaches a plateau is known as the cycle threshold (Ct). The Ct value is used to determine the starting concentration of the DNA sample. In summary, the number of thermal cycles in qPCR is directly related to the amount of DNA amplified and the strength of the fluorescent signal. As the number of thermal cycles increases, the fluorescent signal becomes stronger until it reaches a plateau, which is used to determine the starting concentration of the DNA sample. An example of a qPCR result is depicted in **Figure 3.5** [117], where the threshold is distinguishable from the background fluorescence. If the Ct value for a sample is high, it indicates that there was little starting material, and conversely, if the Ct value is low, it indicates that there was a large amount of starting material. The reaction efficiency can be calculated using the equation for the linear regression line (y = mx + b): Efficiency = $(10^{(-1/m)} - 1) \times 100$. In this example, m is -3.58, resulting in a reaction efficiency of 90%.

3.4. Methods and tools for statistical analysis

3.4.1. Double exponential function on the decay rates of the cultures

To clarify the influential factors on the cellular decay, the specific decay rates of each experiment were statistically analysed in a double exponential function (**Equation 3.1**) for each of microbial group (methanogenic archaea and acidogenic bacteria) [24]. The fluorescent area of the total living cells at any time ($a_{T(t)}$) was calculated based on the initial concentrations of the living microorganisms ($a_{A(0)}$: methanogen, $a_{B(0)}$: acidogen) and their first-order specific decay rates of k_A and k_B.

$$\begin{cases} a_{A(t)} = a_{A(0)} \cdot \exp\left(-k_A \cdot t\right) \\ a_{B(t)} = a_{B(0)} \cdot \exp\left(-k_B \cdot t\right) \\ a_{T(t)} = a_{A(t)} + a_{B(t)} \end{cases} \qquad \text{Equation 3.1}$$

Where, $a_{T(t)}$: total living cell area (μm^2) at time $= t$, $a_{A(0)}$: initial cell area of living methanogen (μm^2), $a_{B(0)}$: initial cell area of living acidogen (μm^2), k_A: specific decay rate of methanogen (d^{-1}), k_B: specific decay rate of acidogen (d^{-1}), t: time (d)

3.4.2. Modifeid low-pH inhibition function and statistical methods

Covariance is a statistical measurement of the relationship between two or more variables. It indicates the degree to which two variables change together. A positive covariance means that the variables tend to increase or decrease together, while a negative covariance means that one variable tends to increase as the other decreases. Resampling is a statistical method used to generate multiple new datasets from a single original dataset. This is done by randomly selecting samples from the original dataset and using them to create new datasets. The new datasets are then used to estimate

parameters, perform hypothesis tests, and make predictions.

Resampling can be used with covariance to evaluate the variability of the covariance estimate and to assess the stability of the relationship between variables. For example, bootstrapping is a common resampling method that involves creating many new datasets by randomly selecting samples with replacement from the original dataset. The covariance of each new dataset is then calculated, and the results are used to estimate the variability and stability of the covariance estimate. 1,000 sets of pH_{UL}, pH_{LL} and n in **Equation 3.2** were generated from the covariance matrix by a Monte-Carlo simulation equipped with Gibbs-sampler where the data plots were assumed to be scattered in a normal distribution.

$$
\begin{cases}
k_A = \dfrac{b}{I_{pH}} \\[2ex]
I_{pH} = \exp\left(-3\left(\dfrac{pH_{UL} - pH}{pH_{UL} - pH_{LL}} \right)^n \right) \\[2ex]
I_{pH} = 1 \quad \text{if } pH \geq pH_{UL}
\end{cases}
\qquad \text{Equation 3.2}
$$

3.4.3. Igor pro and Rstudio

Igor Pro 8 (WaveMetrics, Portland, USA) is a powerful software designed for statistical analysis and data visualization. It provides an extensive range of tools and features to perform complex data analysis, numerical computations and simulations. Igor Pro has advanced data manipulation capabilities, including filtering, binning, curve fitting and transformations. The software supports a wide range of statistical tests, including regression analysis, t-tests, ANOVA, and chi-square tests. In addition, Igor Pro provides a built-in programming language, known as the Igor Programming Language, which allows users to automate their data analysis workflows. The software

also includes a comprehensive library of macros and functions for performing various statistical and mathematical tasks, reducing the need for manual coding. With its advanced data analysis and visualization tools, Igor Pro is a powerful software solution for users who need to analyze and interpret complex data sets. The procedures for the various analytical techniques employed in this study are outlined in the Appendix.

RStudio is widely used for statistical analysis as an integrated development environment for the programming language R (RStudio, PBC, Boston, USA). It provides a user-friendly interface for coding, data visualization, and analysis. RStudio offers a number of features that make it an ideal tool for the statistical methods. It allows users to manage large amounts of data, run statistical tests, and create professional-quality graphics with ease. Additionally, RStudio integrates seamlessly with other tools and packages, making it a versatile and flexible solution for data analysis. In conclusion, the RStudio is a highly effective and efficient data analysis software that, when combined with Igor Pro, facilitates the easy visualization of statistical analysis results in this study.

3.5. Simulation and modification of Anaerobic Digestion Model No.1

3.5.1. ADM1 equipped with pH inhibition function using GPS-X simulator

The GPS-X simulator is a state-of-the-art tool designed to simulate the waste treatment process. This software helps in the optimization of the process parameters, and is capable of performing virtual experiments and simulating the biodegradation of organic matter. This tool enables the user to evaluate various process parameters, including pH, temperature, and nutrient addition, to optimize the conditions for the best results. The simulator can also be used to design and optimize AD systems and to predict their performance in terms of biogas production and nutrient removal.

The pH value during the anaerobic fermentation process plays a crucial role in the performance of the system, especially with regards to methanogenic activity. As mentioned above, methanogens are the microorganisms responsible for the production of CH_4 in AD, and they have a narrow pH range of 6.5 to 7.5 for optimal growth and activity. The pH of the system affects the stability of the microorganisms and can lead to inhibition or death of the methanogens. A low pH level in the system is often accompanied by the accumulation of VFAs, which are toxic to the methanogens. Additionally, low pH levels can reduce the availability of nutrients for the methanogens, which in turn can affect their growth and activity.

The pH inhibition function on methanogens equipped in ADM1 is an important factor in determining the efficiency of the anaerobic fermentation process. The pH inhibition function determines how the pH level affects the activity of methanogens. In general, methanogens are sensitive to pH changes and their activity decreases as the pH drops below a certain level. This pH inhibition function allows the ADM1 to accurately simulate the impact of pH on methanogenic activity, which is critical for optimizing the AD process. The pH inhibition parameters can be adjusted in the ADM1 to reflect the specific conditions of the AD system, including the type of substrate, the presence of inhibitors, and the pH buffer capacity of the system.

The pH inhibition function in the ADM1 (Equation 2.7 and Equation 2.8) is limited in that it only reflects the inhibition of growth stage, but not the toxicity on the decay stage. The lack of a comprehensive representation of pH effects on both the growth and decay stages can result in inaccurate predictions of biogas production and biomass concentration [5]. To overcome this limitation, it is recommended to incorporate more complex models that consider the interactions between growth and decay stages. Additionally, incorporating real-world data from experiments or actual plant operation can improve the accuracy of the predictions made using the model.

3.5.2. Kinetic parameters and the value ranges of references

The model uses a set of kinetic parameters to describe the behavior of the microorganisms involved in the anaerobic fermentation process (**Table 2.1**). The kinetic parameters used in ADM1 mainly include: Maximum specific growth rate (μ_{max}) - maximum rate at which microorganisms can grow under optimal conditions, Monod saturation constant (K_S) - the concentration of substrate at which the growth rate is half of the maximum growth rate, Inhibition constant (K_I) - the concentration of a substance (such as pH) that inhibits the growth rate of microorganisms, Decay rate (k_d) - refers to the rate at which microorganisms die over time.

The range of values for these parameters can vary greatly depending on the source of organic matter, the operating conditions, and the composition of the inoculum. It is important to note that the values of these parameters can be estimated through experimentation or can be taken from literature references [12]. However, it is recommended to conduct experiments to validate the model and determine the most accurate parameter values for a specific application.

CHAPTER 4. INCUBATION OF TWO KINDS OF METHANOGENIC CULTURALS USING THE SYNTHTIC SUBSTRATE

4.1. Introduction

The anaerobic fermentation system is widely acknowledged as a reliable and economical way to treat waste and produce biogas. This is because these systems are designed and operated with high organic loading rates to minimize construction costs and reduce floor space requirements [86]. However, despite these advantages, the performance of anaerobic processes can be impacted by the buildup of VFAs [118]. This is because the methanogenesis stage is often the limiting factor in the CH_4 fermentation process due to the sensitivity and slow growth rate of methanogenic archaea [119,120]. When high VFA concentrations are produced from the degradation of easily biodegradable organic matter, they are converted into low pH levels, which can be toxic to bacterial communities at high hydrogen ion concentrations. Furthermore, high VFA concentrations can cause instability in the system by acting as potential inhibitors for methanogens when they exceed the inhibition threshold [121]. The low pH inhibition can cause serious stability problems, resulting in catastrophic damage to the process or even its failure.

Organic-rich wastewater treatment often leads to the accumulation of VFAs in the reactor, causing acidic failure during the methanogenesis process. While the effect of pH on hydrolysis and acidogenesis has been extensively researched [122,123], the influence of pH on methanogenesis remains poorly understood and has received less attention on methanogen's decay [5]. pH is a critical factor that affects the stability and CH_4 production in anaerobic fermentation [124,125,126]. Changes in pH can significantly impact various aspects of microbial metabolism, including the biomass growth rate, substrate utilization, and substrate conversion efficiency [127,128]. Moreover, pH determines the concentration of undissociated acids in the reactors, which can penetrate cell membranes and alter

cell structure [129,130]. The environmental pH has a strong effect on CH_4 fermentation performance [131,132].

The aim of this study is to investigate the impact of low pH on the decay of methanogens, using a modified inhibition function of the IWA ADM1 model that has been verified through benchmark dataset [12,106]. Mathematical models are known to be highly effective in the optimization of wastewater treatment plants [133]. The study evaluates the domestication of methanogens through a series of experiments, in which the two kinds of methanogenic cultures are purified and cultured continuously while monitoring CH_4 production and VFAs concentration. This information, along with mathematical calculations, is used to evaluate the response of the domesticated methanogens. The study also examines the effect of pH on the methanogens by gradually increasing the OLR until the target methanogens become dominant and performing laboratory-scale experiments to simulate the effect of pH under different OLRs. Finally, the modified ADM1 model is compared to the default ADM1 to assess its ability to predict process performance and microorganism concentrations, as well as the impact of pH inhibition on the model parameters.

4.2. Cultivation results and Discussion

4.2.1. Cultivation of methanogenic biomass and reactor response

As shown in **Figure 4.1A**, the VSS concentration of the reactor was consistently decreased within the initial 90 days of the continuous operation. The decrease of VSS was due to the wash-out of organic particulates initially present in the inoculum, and the part of which was supposed to the microorganisms that were unable to grow from acetate (*i.e.*, ordinary acidogenic biomass and hydrogenotrophic methanogenic biomass). At day 90, the VSS of the reactor became about 3% of the

inoculum concentration (*ca.* 300 mg/L). As the reactor was continuously operated in a chemostat completely-stirred-tank-reactor (CSTR) mode whilst the operational HRT (= SRT) was fixed at 15-day, the remaining VSS fraction of the inoculum in the reactor at day 90 was calculated to be 0.25% (= exp (-90 day/15 day). During the period, the decrease of VSS concentration was expressed in a semilogarithmic curve, which was also in agreement with the wash-out of the particulates of inoculum in the CSTR. During the 90 days, to continue the enrichment of the acetoclastic methanogen, the influent acetate concentration was increased in a stepwise manner from 5,000 mg-COD/L to 14,000 mg-COD/L. Since the measured VSS after day 90 was as high as 12 times of the calculated particulate concentration from the inoculum (= 3%/0.25%), a growth of acetoclastic methanogen in the reactor was recognised. This increment somewhat compensated the VSS wash-out in the reactor.
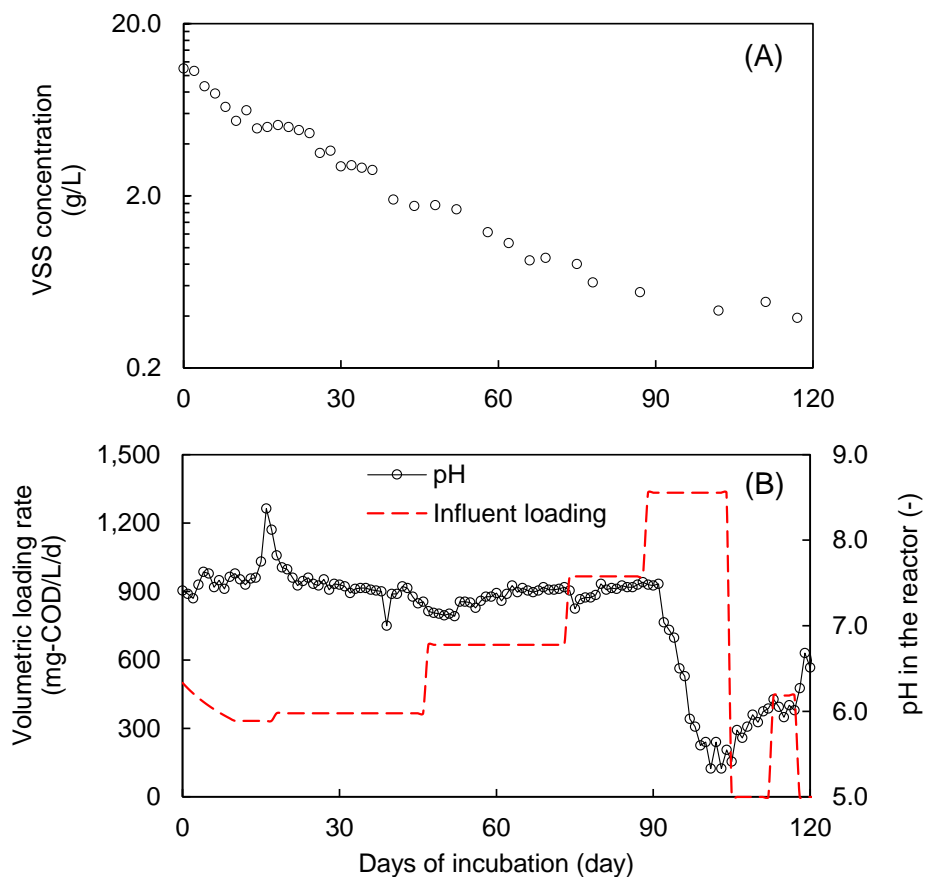
Figure 4.1 VSS concentration of the Acetate-fed reactor (A) and reactor response (B)

45

As shown in **Figure 4.1B**, when the influent acetate concentration was increased to 20,000 mg-COD/L at day 90, a pH-drop was created. This high acetate feeding was intentionally continued in next 14 days until the reactor pH reached pH 5.3 where the methanogen was not killed by the low pH but its growth was only inhibited [5]. Subsequently, the acetate feeding was manipulated by reducing the influent concentration in order to bring back the reactor pH to the original level of pH 7.3. When the acetate feeding was resumed after the discontinuation for 7 days (day 106–112), a new peak of acetate accumulation was additionally created as shown in **Figure 4.2A**. From these operations, together with the accumulated acetate, the volumetric CH_4 production rate was also obtained (**Figure 4.2B**). To investigate the impact of pH range and accumulated acetate concentrations on the reactor performance, the further experimental analysis was conducted as shown in Chapter 6.
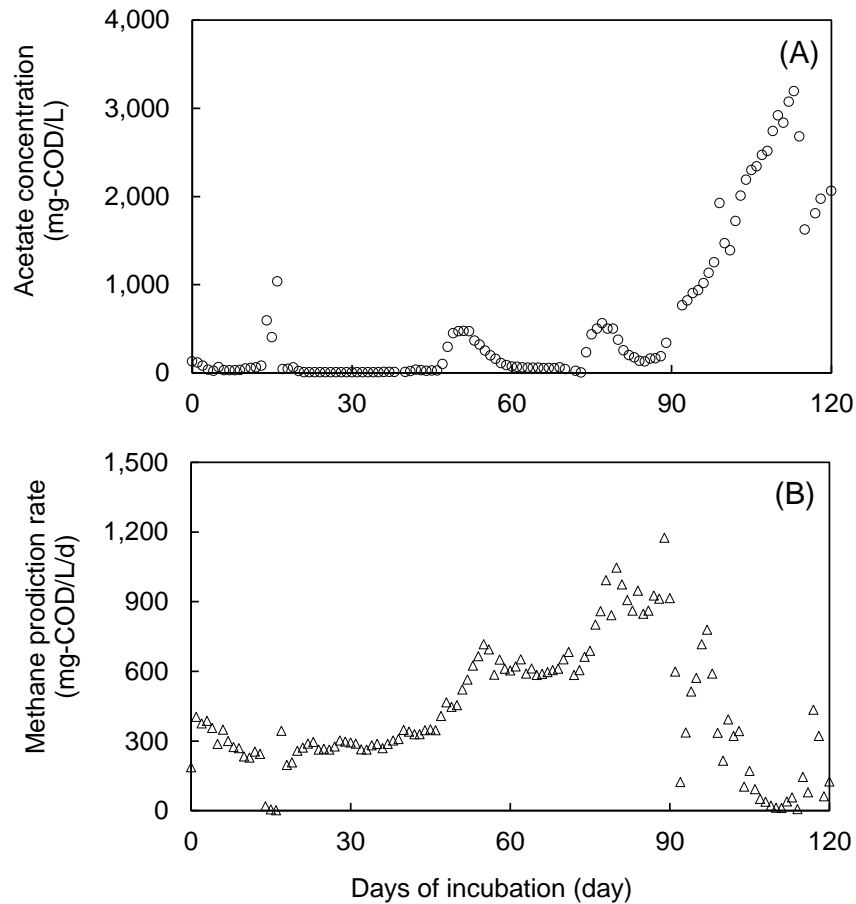
Figure 4.2 Acetate concentration of the reactor (A) and volumetric methane production rate (B)

As shown in **Figure 4.3**, formate-utilizing methanogens have also been continuously domesticated. The VSS concentration of the reactor continued to decrease during 150 days of continuous operation, which followed the same trend as the Acetate-fed system. The reduction in VSS concentration was due to the washing away of the organic particles that were originally present in the inoculum. After several months of cultivation, the VSS concentration stabilized at around 300 mg/L (**Figure 4.3C**). During this period, the VSS concentration decreased in a semi-logarithmic curve, which was consistent with the concentration of the Acetate-fed system. During the 150-day period, to continue the enrichment of formate-utilizing methanogens, the formate loading was gradually increased from 100 mg-COD/L/d to 1,000 mg-COD/L/d (**Figure 4.3D**). Unlike the Acetate-fed

47

system, the pH was strictly controlled in the neutral range with a pH controlling system (EWN-W, Iwaki, Japan).
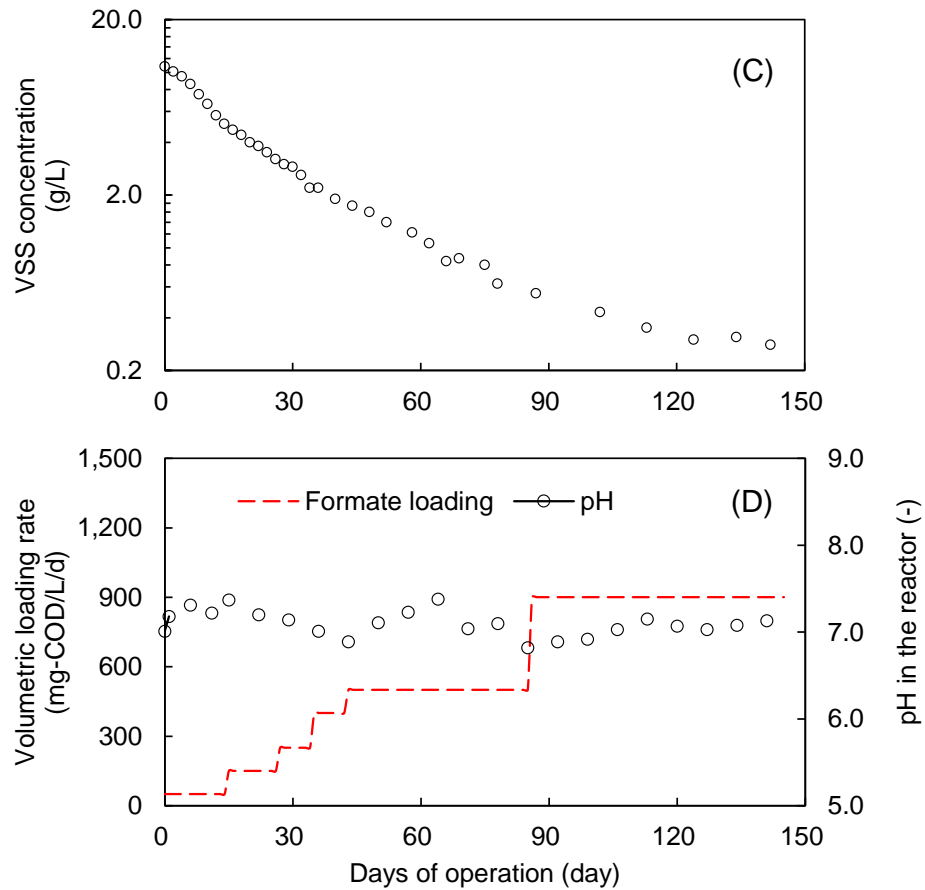
Figure 4.3 VSS concentration of the Formate-fed reactor (C) and reactor response (D)

As shown in **Figure 4.4**, the outlet formate concentration and methane production rate of the formate-fed reactor are also listed. Since the enrichment process did not use a high organic loading of formate and the pH has been maintained in the optimal range around 7.0 ± 0.3, there was no accumulation of formate in the outlet, which remained below 20 mg-COD/L (**Figure 4.4C**). The methane production increased proportionally with the increase in the feed load throughout the cultivation process without any inhibition or decrease (**Figure 4.4D**). The yield of methane gas

exceeded 80% of the OLR of the feed throughout the process, which verifies that most of the feed formate was completely decomposed to produce methane, while the rest was used to generate formate-utilizing methanogens.
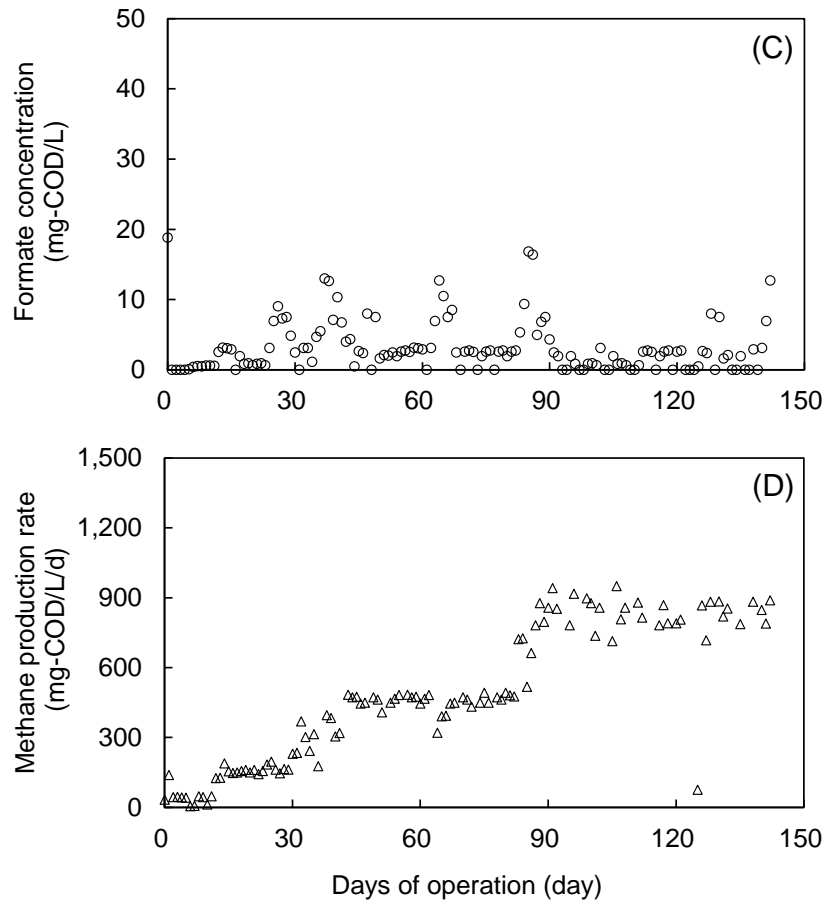
Figure 4.4 Formate concentration of the reactor (C) and volumetric methane production rate (D)

4.2.2. Properties of incubated cultures

Regular measurement of solid concentration, soluble COD concentration and the biogas production in each reactor were performed during the operation. As shown in **Table 4.1**, after stable operation for 90 days the measured solid concentration was 168 ± 20 mg-COD/L for the acetate-fed reactor and 242 ± 30 mg-COD/L for the formate-fed reactor respectively. The effluent soluble COD

49

concentration was observed to be 10–40 mg-COD/L in both reactors whilst the conversion ratio of CH_4 to the influent COD was attained to be $77 \pm 5\%$ for the acetate-fed reactor and $75 \pm 4\%$ for the formate-fed reactor respectively.

Table 4.1 Outflow of chemostat reactors

Influent: 1,000 mg-COD/L	Acetate-fed culture	Formate-fed culture	n
pH (-)	7.0-7.5	7.0-7.5	30
Particulate COD (mg-COD/L)	150-350	200-400	4
Soluble COD (mg-COD/L)	10-50	10-40	10
SS (mg/L)	100-250	150-300	4
VSS (mg/L)	90-230	140-270	4
NH_4 (mg-N/L)	900-1100	900-1100	10
CH_4 per influent COD (mg-COD/g-COD)	720-810	710-780	30

The analysis results of bacteria/archaea ratio in the two reactors before and after cultivation directly demonstrated the enrichment of the methanogens. As shown in **Figure 4.5**, PMA-qPCR experiments quantified the number of archaea and bacteria in the two enriched cultures. Archaea were identified as methanogens in the inoculum sludge, and bacteria were typically various acidogens and other unrelated species. The results of the PMA-qPCR analysis showed that the proportion of methanogenic archaea in the initial sludge was only about 5%, and their numbers were very limited. However, after the enrichment culture, the number of archaea in the acetate-fed system and formate-fed system accounted for 78% and 67%, respectively. At this point, the methanogens in the cultures were already the dominant species and had become the foundation for the subsequent cultures. Batch experiments for various pH tolerances of methanogens are now ready to proceed.
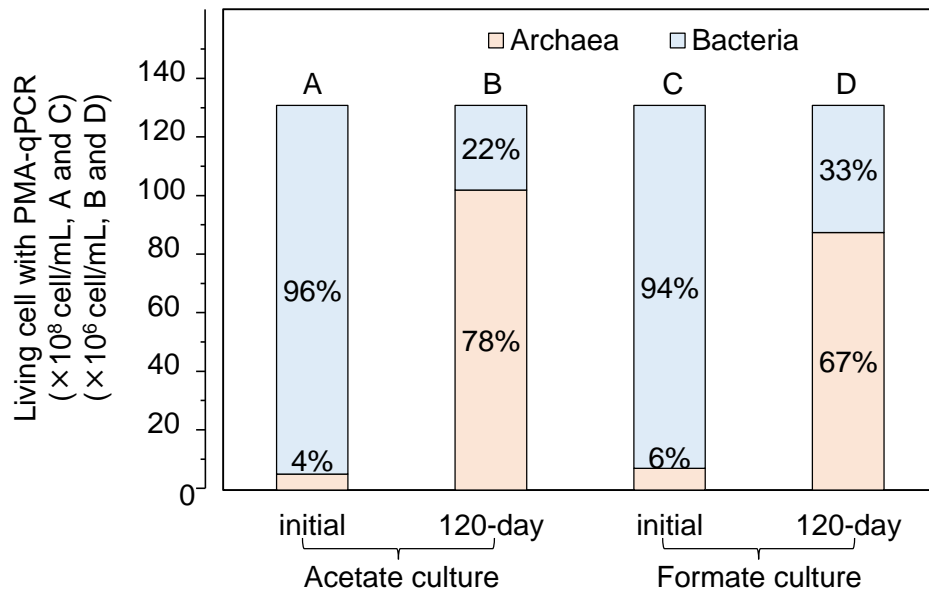
Figure 4.5 Biomass constituents before/after the 120-day incubation

4.3. Conclusions

Based on the experimental data of dynamic dosing of acetate and formate in the anaerobic reactor, the system performance of methane production was obtained during the 120-day cultivation process, and the following conclusions were drawn:

1. Under the condition of a 15-day SRT, it takes more than three months for the domestication and enrichment process to wash out other bacterial species and impurities.

2. The methanogens in municipal digested sludge account for only about 5%, but after cultivation, methanogens occupy a dominant position in the culture, comprising 67-78%.

3. When the pH is at the optimum level, the efficiency of methane production can be stabilized at around 80% under varying OLRs, and the methane production rate will not be suppressed.

CHAPTER 5. ESTIMATION OF LOW PH INHIBITION ON DECAY OF METHAONGENIC BIOMASS

5.1. Introduction

The accumulation of organic acid and corresponding decrease in pH result in inhibition of methanogen leading to acidic failure of reactor [87]. To cope with the acidic failure, the influent feeding is temporarily reduced or discontinued until the concentrations of the accumulated organic acids decrease to an acceptable level. According to Zhang *et al.* (2012), about 40 days were needed to recover the biogas production after digester was operated under acidic conditions (pH 5.4) for two weeks [19]. On the other hand, Capson-Tojo *et al.* (2017) reported that the continued process deterioration due to acidic failure (pH 5.9) over 8 days of operation was recovered after only 2 weeks of operational pause [107]. To achieve maximum biogas yield, it is important to develop reliable operational strategies to prevent digester failure, and to identify the key process reactions for fast process recovery in-case of failure. Therefore, in biogas production engineering, development of process understanding to avoid the risks of acidic failure is one of the key focus areas. Ghofrani-Isfahani *et al.* (2020) developed a supervisory control module for the biogas plants where the reactor pH, volatile fatty acid concentrations and CH_4 gas production rate were monitored to calculate the acceptable influent feeding [134]. To improve digester control strategies, it is therefore important to include the mechanisms that affects the methanogenic activity into the mathematical model.

In this regard, the inhibition of methanogen has been widely studied. Low pH, high concentrations of non-ionised volatile fatty acids and hydrogen sulphide, *etc*. have been identified as inhibitory parameters contributing to the acidic failure [121,135,136,137,138,139]. In all of these studies, the inhibition is accounted by applying an inhibition term to growth rate (reversible inhibition of specific CH_4 production rate) and effect on biomass decay is completely neglected. In fact, only a

few studies are available which distinguish between the inhibition in growth and decay processes. Hao *et al.* (2012) experimentally demonstrated that starvation of the methanogenic culture could increase the kinetic decay rate by as much as 2-3 times [140]. Besides the studies for the anaerobes, Hao *et al.* (2009) also showed that the kinetic decay rates of aerobes in the activated sludge sample were also increased during the starvation conditions [110]. In another study, Liu *et al.* (2018) found that high nitrite concentration inactivated the nitrite oxidising microorganism where the microbial growth was simultaneously inhibited [6]. Based on these experimental studies, it was hypothesised that in addition to growth inhibition, the accelerated decay of methanogenic microorganisms could contribute to the risk of acidic failure and subsequent process recovery under inhibitory conditions. In fact, Ngo *et al.* (2016) experienced that CH_4 production was totally lost after 10 days of the acidic failure where the operation of the lab-scale reactor was halted during the days, and the methanogenic reaction could not be recovered even after the reactor sludge was washed with water to remove the VFAs accumulated in the system [109]. One explanation for the observed behaviour could be that the acidic failure irreversibly inactivated the methanogens of the culture.

In the events of anaerobic reactor overload, the pH and VFA concentrations vary in a wide range depending on the operational conditions [1,2,3]. Depending on the type of inhibition *i.e.*, biostatic or biocidal, the operational approaches for process recovery from the acidic failure could be different. In the case of biostatic inhibition, the operator may be allowed to wait for the process recovery by simply reducing the influent load. Whereas, in the case of biocidal inhibition, the plant operators must eliminate the inhibitory substances as soon as possible to avoid the biomass loss. These two strategies for process recovery are different and require a good understanding of the underlying effects of the inhibitory substances on the microbial growth and decay. However, it seems that biocidal effects of pH and/or VFA concentrations (including target VFA species) and target safe operating concentrations have not been established yet. Perhaps this is because the biocidal

phenomena from the VFA and pH are a relatively new finding in the studies of CH_4 fermentation systems. The product-based inhibition is practically being utilised to develop material-recovery processes (*e.g.*, VFA recovery), which is one of recent hot topics of anaerobic systems [91,121,141]. Therefore, clarification of the biocidal effect about VFAs and pH would help us to develop the new efficient processes as well as help in selecting the right remedial strategies against the acidic failure.

The focus of this experimental study was to elucidate how the decay rate of methanogens was affected during acidic failure (low pH). A set of laboratory scale chemostat reactors were fed with synthetic substrate to enrich methanogenic biomass. The enriched biomass from the continuous reactor was used in batch experiments without external substrate to collect data on the change in active/inactive cells over time (pH inhibition). To avoid the compounding effect of high concentration of volatile fatty acids on biomass decay, the experiments were conducted by reducing the pH with phosphoric acid. To understand the nature of VFA inhibition during acidic failure, several sets of batch experiments were conducted at low pH and high VFA concentration (VFA inhibition). Specifically, the living cells of the methanogen-enriched cultures were measured in the pH-controlled lab-scale batch reactors with addition of either formate, acetate, propionate, butyrate, valerate, or phosphate. Using statistical analysis of the experimental results, the impact of the VFA species and pH on the biomass decay are discussed. The experimental data was further used in an adaptation of IWA ADM1 to simulate the decay rate of target microorganism and explain the process recovery after failure.

5.2. Materials and methods

5.2.1. Batch experiments at low pH conditions using PBS

After over 3-months of continuous operation with the chemostat reactors, 1,200 mL of sludge was harvested from each chemostat reactor for use in first set batch experiments (Set-I). The harvested sludge was centrifuged and washed with deionised water at $9,187g$ of centrifugal force ($= 8,000$ rpm) using a high-speed refrigerated centrifuge (Himac CR22GII, Hitachi, Japan). After mixing phosphate buffer with the sludge pellets, the sludge was evenly transferred to four 300 mL-flasks equipped with a stirring device and a silicone rubber plug having a thin water-sealed tube to release biogas during the incubation. The conditions in each experiment were different with respect to pH and phosphate buffer concentration (flask #1: pH = 7.0 with 0.5 mmol-P/L (15 mg-P/L); flask #2: pH = 7.0 with 50 mmol-P/L (1,500 mg-P/L); flask #3: pH = 5.1 with 0.5 mmol-P/L; flask #4: pH = 5.1 with 50 mmol-P/L). Two different concentration of phosphate buffer were used at each selected pH so that the unintended impact of phosphorus concentration on the biomass decay could be assessed. The air headspace in batch flasks was purged using 0.5 L/min flow rate of dinitrogen gas for 3 minutes. The flasks were placed in a temperature-controlled water bath at 35°C and incubated without addition of external substrates. During the incubation, about 5 mL of the sludge was withdrawn every 24-hour interval for further analysis. The volume loss due to sampling was compensated by adding an equivalent volume of dinitrogen gas in the flask. The batch incubations were run for 6 days where each experiment was duplicated with two flasks in each set.

To collect additional data to study the impact of pH on the biomass decay, another set of batch experiments (Set-II) was performed using the sludge from chemostat reactors. In this set of experiments, the pH of each flask was adjusted to 5.1, 5.5, 6.0, 6.5, 7.0 and 7.5 using 50-mM phosphate buffer with small amount of NaOH or H_3PO_4. Apart from the pH conditioning, the

experimental procedure was identical to the one that used in the previously described batch experiments. The second set of batch experiments was also used to evaluate the recovery of methanogenic reactions after the low-pH inhibition. At the end of the experiment (day 6), the sludges set at pH 5.1 and those set at pH 7.0 were spiked with 3,200 mg-COD/L of the same substrate as those fed to the chemostat reactors. The CH_4 production rates over the flasks for 22 days was monitored to assess system recovery.

5.2.2. Batch experiments under low pH and/or various unVFA concentrations

To elucidate the biocidal effect of unVFA and pH on the methanogens, a set of batch experiments were conducted at different pH and VFA concentrations. The batch tests were conducted several times to cover a wide range of experimental conditions (pH 4.0–7.5, 0.023–53.4 mM unVFA). A volume of 2,000 mL of the methanogen-enriched culture was taken from each jar-fermenter to conduct the batch experiments. The collected cultures were washed using 30 mM of phosphate buffer solution (PBS) with 9,187 g of centrifugal force for 4 minutes at 25 °C (Himac CR22GII, Hitachi, Japan). After re-suspension of the pellets with the inorganic medium, each culture was evenly placed in 300-mL flasks (batch reactors). Next, one of the unVFA of formic acid, acetic acid, propionic acid, butyric acid or valeric acid was added to the batch reactor. The pH of batch reactors was adjusted with either HCl or NaOH solution. To compare the VFA-dosed experiments with controls, a control experiment having the same pH using 30 mM of PBS was carried out. Each batch reactor was plugged with a silicone rubber cap equipped with thin flexible tubes to sample the culture during the incubation period and to release the produced biogas into a water-sealed vessel. Prior to the incubation, the headspace of each batch reactor was purged with dinitrogen gas. A gentle mechanical mixing was achieved in each batch reactor using a small stirring bar. The batch experiments were conducted for

a period of 6 days at controlled temperature of 35°C. The set of experiments were triplicated to collect data that can be used for statistical analysis of the experimental results.

Another batch experiment was performed using the fresh digestate. The results from this test were used to compare the pH inhibition of the methanogen-enriched cultures with the standard mixed microbial population in a full-scale digester. The digestate collected from the full-scale plant was diluted using the PBS to achieve COD concentration of 5,365 mg-COD/L (SS: 4,861 mg/L, VSS: 3,507 mg/L). The diluted digestate was used to setup three additional batch tests at pH 7.0, pH 5.0 and pH 4.0 respectively.

In the VFA-dosed batch experiments, the VFA concentration was expected to deplete with time due to its utilisation by the biomass. To ascertain that the VFA concentration in the batch test remained as close to the initial concentration, additional VFA dosing to the batch reactor was conducted using a computer-controlled syringe pump (SP-2PC, AS ONE, Japan). The VFA injection rate of each pump was optimised every day after the VFA concentrations and pH of the samples were measured. The total volume of the injection until the end of experiment was at most 10% on the basis of the initial culture volume. The VFA concentrations of the vessels were kept almost constant within ±12% of the target values.

5.2.3. Laboratory VFA measurement and the concentration analysis of living biomass

A sample of 5 mL was collected every day from each batch reactor during the 6 days of incubation period. The VFAs of the samples were analysed using an ion chromatography equipped with Ion Pac AS11-HC column (ICS-1000, Thermo Fisher Scientific Inc., USA). To detect the living methanogenic biomass (= archaeal cells) from the samples, Propidium monoazide quantitative

polymerase chain reaction (PMA-qPCR) method was selected [5]. During the incubation period, the total living cell concentration (archaea + bacteria) was precisely monitored using a commercial fluorescent cell staining kit (L-7012, LIVE/DEAD® BacLightTM cell viability kit, Molecular Probes, USA) and a fluorescence microscope at 200 times of magnification (ECLIPSE 80i, Nikon, Japan; DS-Fi2, Nikon, Japan) equipped with a binary image analytical software having 1280 ×960 pixels (Quick Grain, Inotech, Japan). The experimental details are provided in Chapter 3.

5.2.4. Statistical analysis of total living cell and its dynamic simulation

To conduct the regression and the statistical analysis, a commercial software, Igor Pro 8 (WaveMetrics, USA) and open-source software, R and RStudio (RStudio, PBC, USA) were used. Moreover, to check the consistency of the experimental results, the datasets were dynamically simulated using ADM1 with a commercial process simulator, GPS-X ver.8.1 (Hatch Ltd., Canada). In order to check the consistency of the experimental results and investigate the relationship between the pH and decay rate, ADM1 was used to simulate the lab experiments. Steady-state simulation was carried out for each chemostat reactor using the operational conditions of each reactor to estimate concentrations of different solids fractions in reactor effluent. These microbial concentrations were compared with the fractions of methanogens and acidogens detected with PMA-qPCR technique and the living cell concentrations measured by the cell staining method.

Table 5.1 Model parameter list

		Growth					Decay				Remark
		Specific growth rate	Half-saturation Coefficient	Biomass yield	pH upper limit	pH lower limit	Specific decay rate	Production of inert participate	pH upper limit	pH lower limit	
		(d^{-1})	(mg-COD/L)	(-)	(-)	(-)	(d^{-1})	(-)	(-)	(-)	
Disintegration		0.5 ♣									
Hydrolysis	Carbohydrate	10 ♣									
	Protein	10 ♣									
	Lipid	10 ♣									
Acidogenesis	Sugar	3.0 (max) ♣	500 ♣	0.10 ♣	5.5 ♣	4.0 ♣	0.02 ♣	0.08 ♦			
	Amino acid	4.0 (max) ♣	300 ♣	0.08 ♣	5.5 ♣	4.0 ♣	0.02 ♣	0.08 ♦			
	Fatty acid	0.36 (max) ♣	400 ♣	0.06 ♣	5.5 ♣	4.0 ♣	0.02 ♣	0.08 ♦			
			H_2 inhibition $7 \cdot 10^{-6}$ ♣								
Acetogenesis	Valerate /butyrate	1.2 ♣	200 ♣	0.06 ♣	5.5 ♣	4.0 ♣	0.02 ♣	0.08 ♦			
			H_2 inhibition $1 \cdot 10^{-5}$ ♣								
	Propionate	0.52 ♣	100 ♣	0.04 ♣	5.5 ♣	4.0 ♣	0.02 ♣	0.08 ♦			
			H_2 inhibition $3.5 \cdot 10^{-6}$ ♣								
Methanogenesis	Acetate	0.32 ♠	180 ♠	0.05 ♣	7.0 ♣	6.0 ♣	0.02 ♣	0.08 ♦	6.6 ♠	5.9 ♠	μ_{max}: 0.4 ♣ K_S: 150 ♣
	Hydrogen	2.1 ♣	$7 \cdot 10^{-6}$ ♣	0.06 ♣	6.0 ♣	5.0 ♣	0.02 ♣	0.08 ♦	6.6 ♠	5.9 ♠	
	Formate	0.3 ♠	300 ♠	0.06 ♣							

Biomass constituent ♥: total sugar: protein: lipid = 35: 55: 10, ♣: Batstone *et al.* (2002), ♦: Henze *et al.* (2000), ♥: adopted from Jimenez *et al.* (2013) ♠: This study

Table 5.2 Configuration and operating condition of the virtual biogas plant

Configuration	Volume	400 m^3
	Mode	CSTR
Operation	Temperature	35 °C
	HRT	20 days
Influent	Composite carbohydrate	10 kg-COD/ m^3
	Composite protein	10 kg-COD/ m^3
	Composite lipid	12 kg-COD/ m^3
	Composite inert	5 kg-COD/ m^3
	Monosaccharide	Zero $\rightarrow$ 300 kg-COD/ m^3 $\rightarrow$ Zero
	Ammonium N	100 mg-N/L
	Phosphate	35 mg-P/L
	pH	7.0
	Inorganic carbon	500 mg-C/L

A virtual biogas plant was built on a computer to simulate the batch plant responses under acidic conditions (**Table 5.2**). For the above programming and process calculations, a commercial process simulator, GPS-X ver.8.0 (Hydromantis Environmental Software Solutions, Canada) was used. The kinetic and stoichiometric parameters were adapted from the literature [12.142,143] except for those that were measured in this study (**Table 5.1**). The maximum specific growth rates of the methanogens were estimated from the curve fitting of the methanogenic recovery using the pH-neutralised sludge after the low-pH inhibition experiments, whilst the half-saturation coefficients of the substrates for the methanogens were estimated from the effluent soluble COD concentrations of the chemostat reactors.

5.3. Results and discussion

5.3.1. Low-pH inhibition for methanogens on the decay stage

As shown in **Figure 5.1**, **Photo S1** and **Photo S2**, the living biomass estimated from the fluorescent cell area per microscopic field decreased considerably along with time in the flasks set at pH of 5.1. In the initial phase the living cell area was counted to be about 800 μm^2/field (= about 140 fluorescent spots/field) for Acetate-fed system and about 1,400 μm^2/field (= about 270 fluorescent spots/field) for Formate-fed system respectively. After 24 hours, the fluorescent cell area in both the experiments decreased by about 30%. At day 6 the area for Acetate-fed system reached about 200 μm^2/field (= about 40 fluorescent spots/field) whilst the area for Formate-fed system also decreased to 400 μm^2/field (= about 80 fluorescent spots/field), which was about 1/4 of the initial fluorescent cell area. On the other hand, the decrease of fluorescent cell areas of the flasks set at pH of 7.0 was very little indicating that the biomass decay in the systems was very limited.
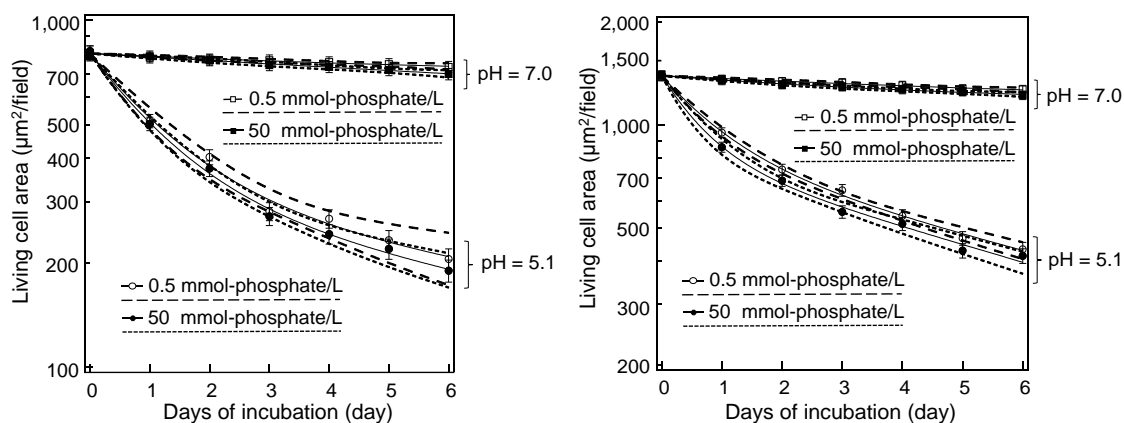
Figure 5.1 Biomass decay under pH = 5.1 and pH = 7.0. (Left: Acetate-fed system, right: Formate-fed system) Plot: experiment, line: regression, bar on the plots: 95%-confidence interval with 30 photos, ---: 95%-confidence interval of the regression for 0.5 mM-P, – –: 95%-confidence interval of the regression for 50 mM-P

Wang *et al.* (2015) suggested that high phosphate concentration (> 1,500 mg-P/L) could inhibit methanogenic activity even at neutral pH [144]. However, in the present study it appeared that the concentration of phosphate (15~1,500 mg-P/L) was not influential on the biomass decay and the decay rate was mainly depended on pH (proton concentration). These experimental results suggested that the low pH enhanced the decay rate of methanogenic biomass.

pH = 5.1, day 0	pH = 5.1, day 3	pH = 5.1, day 6
(1,000 μm²/field)	(400 μm²/field)	(200 μm²/field)
pH = 7.0, day 0	pH = 7.0, day 3	pH = 7.0, day 6
(1,100 μm²/field)	(900 μm²/field)	(700 μm²/field)
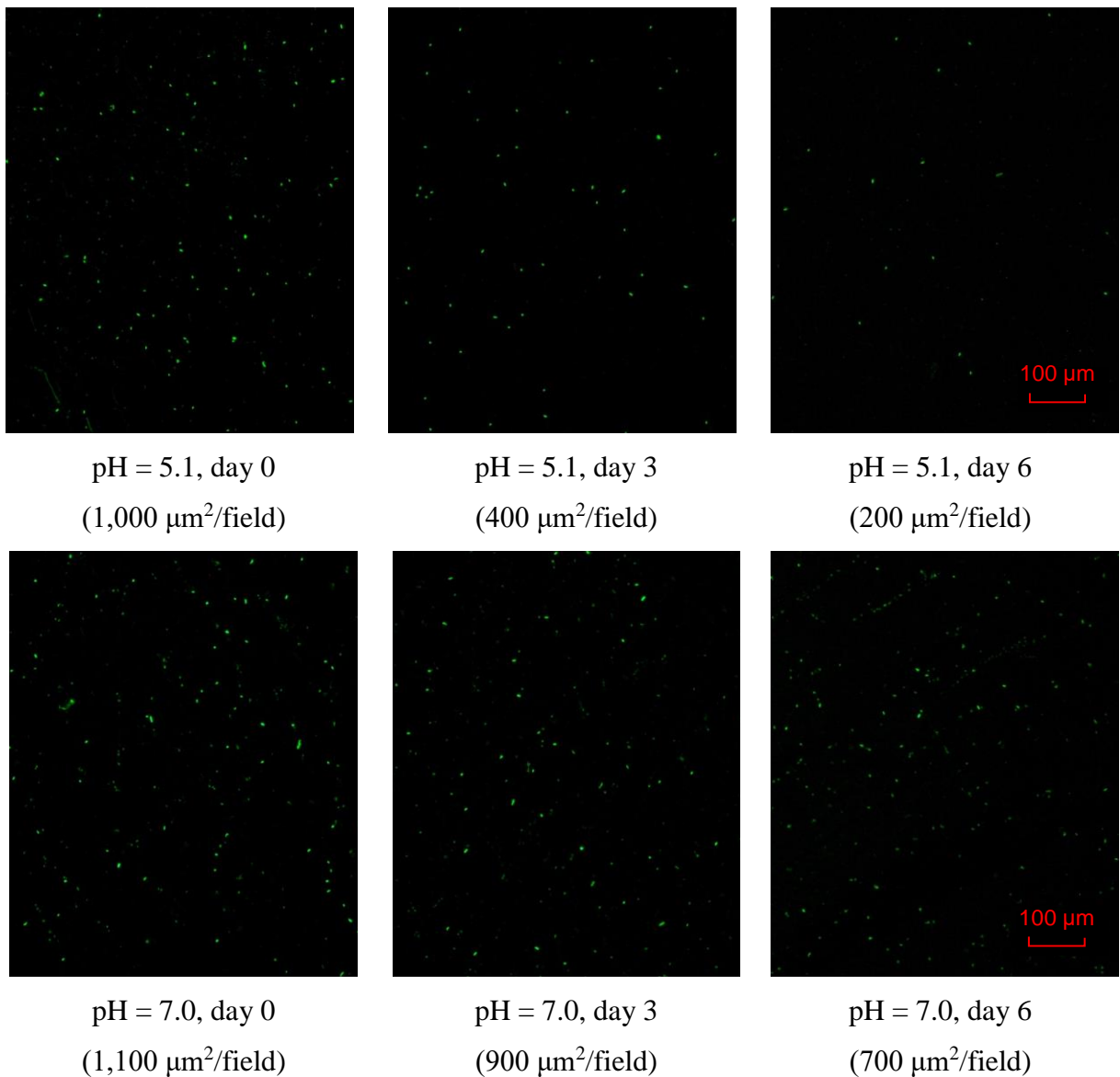
Photo S1 Fluorescent stained living cell (Acetate-fed system)

(200 magnification with 10-time sample dilution)
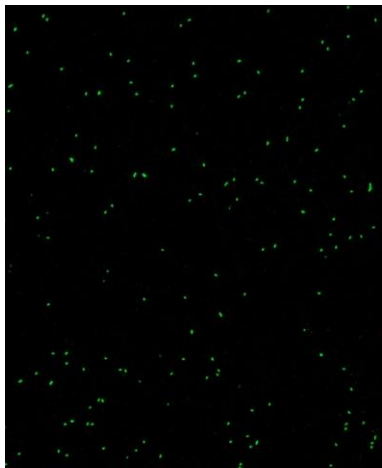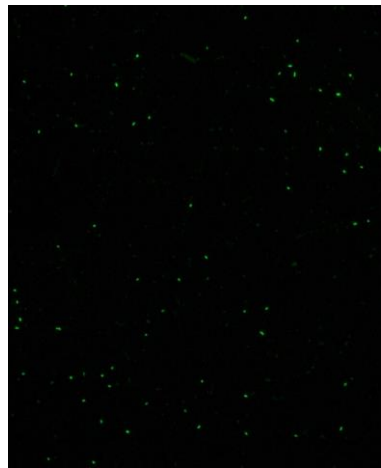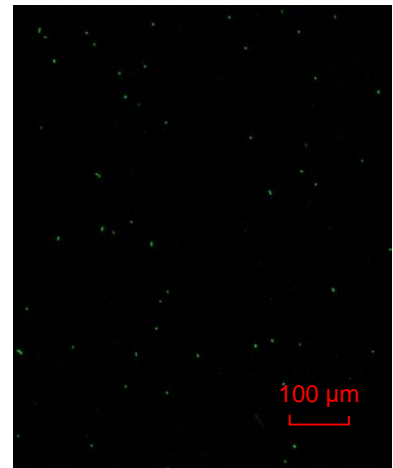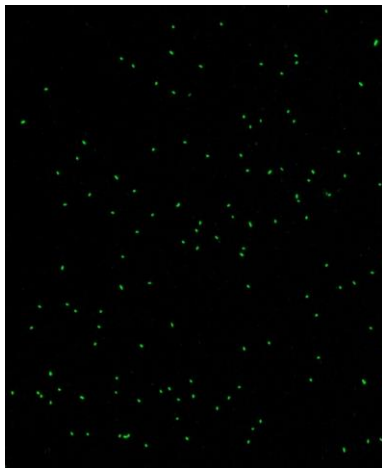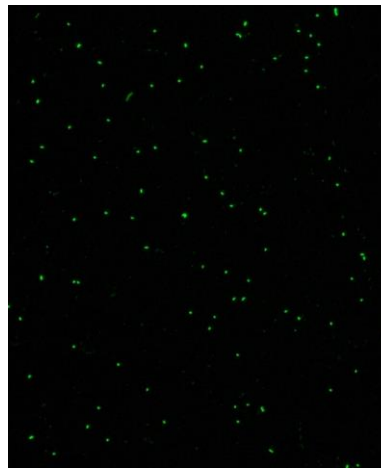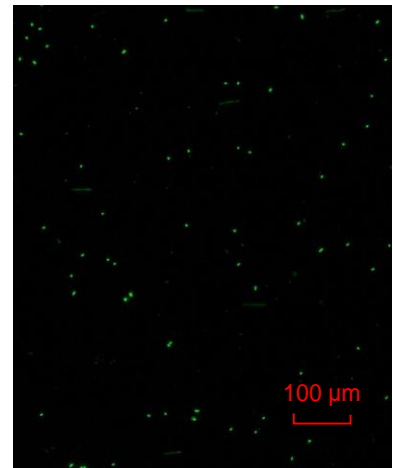
| pH = 5.1, day 0 | pH = 5.1, day 3 | pH = 5.1, day 6 |
| (1,500 μm²/field) | (500 μm²/field) | (300 μm²/field) |

| pH = 7.0, day 0 | pH = 7.0, day 3 | pH = 7.0, day 6 |
| (1,500 μm²/field) | (1,300 μm²/field) | (1,100 μm²/field) |

Photo S2 Fluorescent stained living cell (Formate-fed system)

(200 magnification with 10-time sample dilution)

The results from the Set-II batch experiments with different initial pH values of 5.1, 5.5, 6.0, 6.5, 7.0 and 7.5 were shown on semi-logarithmic plots in **Figure 5.2**. The experimental results from these batch experiments indicated that the decay rate of living biomass correlated to the initial pH condition in the flasks.
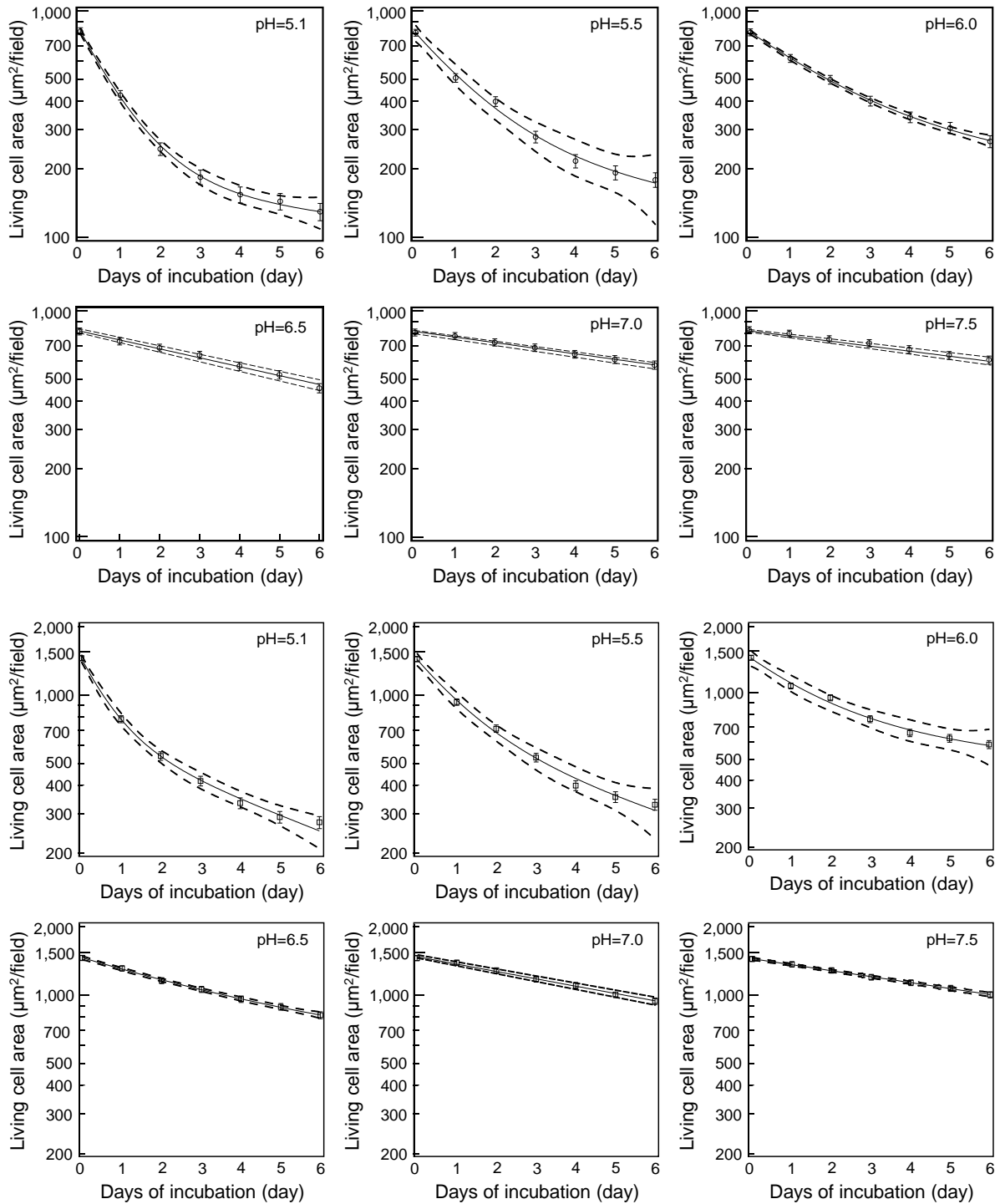
Figure 5.2 Elevation of biomass decay along with lowered pH (P = 50 mM). (Top 6 graphs: Acetate-fed system, bottom 6 graphs: Formate-fed system). Plot: experiment, line: regression, dashed-line: 95%-confidence interval of the regression, bar on the plots: 95%-confidence interval with 30 photos

Higher biomass decay rates were evident at lower pH, indicating that the low pH environments accelerated the biomass decay. This observation was consistent with the conclusion from Set-I batch experiments. Comparing the fluorescent cell area at the initial phase to that at day 6, the fluorescent cell area of Acetate-fed system was dropped by 84 ± 2.6 % for pH = 5.1, $77 \pm 7.5\%$ for pH = 5.5, $64 \pm 2.0\%$ for pH = 6.0, $43 \pm 4.7\%$ for pH 6.5, $28 \pm 2.4\%$ for pH = 7.0, $26 \pm 2.8\%$ for pH = 7.5 respectively. The low-pH driven biomass decay was also recognised in Formate-fed system. At the end of the batch experiment, the fluorescent cell area was decreased by $83 \pm 2.8\%$ for pH = 5.1, $79 \pm 5.4\%$ for pH = 5.5, $63 \pm 7.5\%$ for pH = 6.0, $44 \pm 1.8\%$ for pH 6.5, $34 \pm 3.4\%$ for pH = 7.0, $33 \pm 1.5\%$ for pH = 7.5, respectively.

Considering that the decay rate of a microorganism was generally expressed as a first-order reaction, it was expected that the experiments data of living cell on the semi-logarithmic plot would show a linear trend (constant slope). However, in plots for the datasets at lower pH than 6.0, the data seemed not to be linearly plotted. One possible reason for this observed behaviour could be that the enriched sludge contained two or more microorganisms with different sensitivity to pH. This hypothesis was tested by evaluating a two-microorganism decay model to explain the experimental data in the next section.

5.3.2. Statistical analysis of biomass decay

A double-exponential equation describing the decay of two microorganism was used to explain the non-linearity in experimental data from low pH batch tests. The active biomass concentration at any time ($X_{active(t)}$ = fluorescent cell area) using the double exponential function was described as **Equation 5.1** where $X_{A(0)}$ and $X_{B(0)}$ were the initial concentrations of the microorganisms, and b_A and b_B were the first-order specific decay rates of respective biomass.

65

$$X_{\text{active}(t)} = X_{A(0)} \exp\left(-b_A \cdot t\right) + X_{B(0)} \exp\left(-b_B \cdot t\right)$$

<div align="right">Equation 5.1</div>

As all the three datasets used the same sludge source, a single pair of $X_{A(0)}$ and $X_{B(0)}$ was used to estimate the values of specific decay rates of each biomass type through the regression analysis ($p < 0.05$). The estimated $X_{A(0)}$ and $X_{B(0)}$ for Acetate-fed system were $X_{A(0)} = 577 \pm 39$ μm^2/field and $X_{B(0)} = 215 \pm 39$ μm^2/field for Set-I and $X_{A(0)} = 593 \pm 40$ μm^2/field and $X_{B(0)} = 221 \pm 40$ μm^2/field for Set-II. In both the sets, about 73% of the living biomass was accounted for X_A fraction. For Formate-fed system, X_A fraction was about 53% of the living biomass. These calculation results including the estimated values of b_A and b_B were reported in **Table 5.3** (Acetate-fed system) and **Table 5.4** (Formate-fed system).

Table 5.3 Estimated specific decay rates and initial state variable concentrations of Acetate-fed system

	Specific decay rate b_A (d^{-1})	initial value of $X_{A(0)}$ (μm^2/field)	Specific decay rate b_B (d^{-1})	initial value of $X_{B(0)}$ (μm^2/field)	Regression	Phosphate buffer
pH = 5.1	0.827 ± 0.330	577 ± 38.7	0.090 ± 0.084	214 ± 38.9	D.E.	0.5 mmol/L (Figure 5.1)
	0.806 ± 0.165	ditto	0.080 ± 0.053	ditto	ditto	50 mmol/L (Figure 5.1)
	0.871 ± 0.057	593 ± 39.7	0.080 ± 0.039	220 ± 40.0	ditto	50 mmol/L (Figure 5.2)
pH = 5.5	0.609 ± 0.281	ditto	0.061 ± 0.185	ditto	ditto	ditto
pH = 6.0	0.393 ± 0.095	ditto	0.029 ± 0.078	ditto	ditto	ditto
pH = 6.5	0.091 ± 10^{-5}	425 ± 10^8	0.091 ± 10^{-5}	387 ± 10^8	ditto	ditto
pH = 7.0	0.047 ± 10^{-5}	434 ± 10^8	0.047 ± 10^{-5}	389 ± 10^8	ditto	0.5 mmol/L (Figure 5.1)
	0.056 ± 10^{-8}	433 ± 10^8	0.056 ± 10^{-8}	388 ± 10^8	ditto	50 mmol/L (Figure 5.1)
	0.058 ± 10^{-6}	442 ± 10^8	0.055 ± 10^{-6}	365 ± 10^8	ditto	50 mmol/L (Figure 5.2)
pH = 7.5	0.053 ± 10^{-6}	432 ± 10^8	0.050 ± 10^{-6}	384 ± 10^8	ditto	ditto

	Specific decay rate b_{A+B} (d^{-1})	Initial value of $X_{A+B(0)}$ (μm^2/field)		Regression	Phosphate buffer
pH = 6.5	0.091 ± 0.004	815 ± 2.2		S.E.	50 mmol/L (Figure 5.2)
pH = 7.0	0.012 ± 0.001	812 ± 2.2		ditto	0.5 mmol/L (Figure 5.1)
	0.020 ± 0.001	ditto		ditto	50 mmol/L (Figure 5.1)
	0.057 ± 0.001	815 ± 2.2		ditto	50 mmol/L (Figure 5.2)
pH = 7.5	0.051 ± 0.002	ditto		ditto	ditto

D.E.: fluorescent cell area = $X_{A(0)} \cdot \exp(-b_A \cdot t) + X_{B(0)} \cdot \exp(-b_B \cdot t)$, S.E.: fluorescent cell area = $X_{A+B(0)} \cdot \exp(-b_{A+B} \cdot t)$; ±: 95% confidence interval

Table 5.4 Estimated specific decay rates and initial state variable concentrations of Formate-fed system

	Specific decay rate b_A (d^{-1})	initial value of $X_{A(0)}$ (μm^2/field)	Specific decay rate b_B (d^{-1})	initial value of $X_{B(0)}$ (μm^2/field)	Regression	Phosphate buffer
pH = 5.1	1.138 ± 0.220	757 ± 56.1	0.124 ± 0.016	634 ± 56.3	D.E.	0.5 mmol/L (Figure 5.1)
	1.294 ± 0.281	ditto	0.111 ± 0.023	ditto	ditto	50 mmol/L (Figure 5.1)
	1.082 ± 0.119	775 ± 57.4	0.122 ± 0.028	648 ± 57.6	ditto	50 mmol/L (Figure 5.2)
pH = 5.5	0.609 ± 0.224	ditto	0.073 ± 0.134	ditto	ditto	ditto
pH = 6.0	0.460 ± 0.337	ditto	0.017 ± 0.158	ditto	ditto	ditto
pH = 6.5	0.199 ± 0.147	$784 \pm 1{,}850$	0.023 ± 0.003	$639 \pm 1{,}860$	ditto	ditto
pH = 7.0	0.035 ± 10^{-7}	739 ± 10^8	0.033 ± 10^{-7}	653 ± 10^8	ditto	0.5 mmol/L (Figure 5.1)
	0.041 ± 10^{-8}	744 ± 10^8	0.038 ± 10^{-8}	660 ± 10^8	ditto	50 mmol/L (Figure 5.1)
	0.076 ± 10^{-6}	761 ± 10^8	0.074 ± 10^{-6}	680 ± 10^8	ditto	50 mmol/L (Figure 5.2)
pH = 7.5	0.070 ± 10^{-5}	882 ± 10^8	0.070 ± 10^{-5}	558 ± 10^9	ditto	ditto

	Specific decay rate b_{A+B} (d^{-1})		initial value of $X_{A+B(0)}$ (μm^2/field)		Regression	Phosphate buffer
pH = 6.5	0.100 ± 0.003		1423 ± 4.2		S.E.	50 mmol/L (Figure 5.2)
pH = 7.0	0.016 ± 0.001		1390 ± 4.1		ditto	0.5 mmol/L (Figure 5.1)
	0.020 ± 0.002		ditto		ditto	50 mmol/L (Figure 5.1)
	0.075 ± 0.002		1423 ± 4.2		ditto	50 mmol/L (Figure 5.2)
pH = 7.5	0.070 ± 0.003		ditto		ditto	ditto

D.E.: fluorescent cell area = $X_{A(0)} \cdot \exp(-b_A \cdot t) + X_{B(0)} \cdot \exp(-b_B \cdot t)$, S.E.: fluorescent cell area = $X_{A+B(0)} \cdot \exp(-b_{A+B} \cdot t)$; $\pm$: 95% confidence interval

On the other hand, since the datasets for pH 6.5, 7.0 and 7.5 showed almost a linear decrease on semi-logarithmic plot , the estimated b_A and b_B were almost equal to each other (*e.g.* $b_A = 0.058 \pm 10^{-6}$ d^{-1} and $b_B = 0.055 \pm 10^{-6}$ d^{-1}) for Acetate-fed system at pH =7.0. Moreover, it was not possible to determine a unique set of $X_{A(0)}$ and $X_{B(0)}$ in these experiments as indicated by a large 95% confidence intervals of $X_{A(0)}$ and $X_{B(0)}$ ranging between $-10^8 \sim +10^8$ and $+10^8 \sim -10^8$ in which the estimated values compensated each other. As each biomass type could not be distinguished from each other in this experimental pH range, these data plots were simulated with a single exponential equation having a lumped state variable of $X_{A(0)}$ and $X_{B(0)}$ (= $X_{A+B(0)}$) and a lumped specific decay rate (b_{A+B}) ($p < 0.05$).
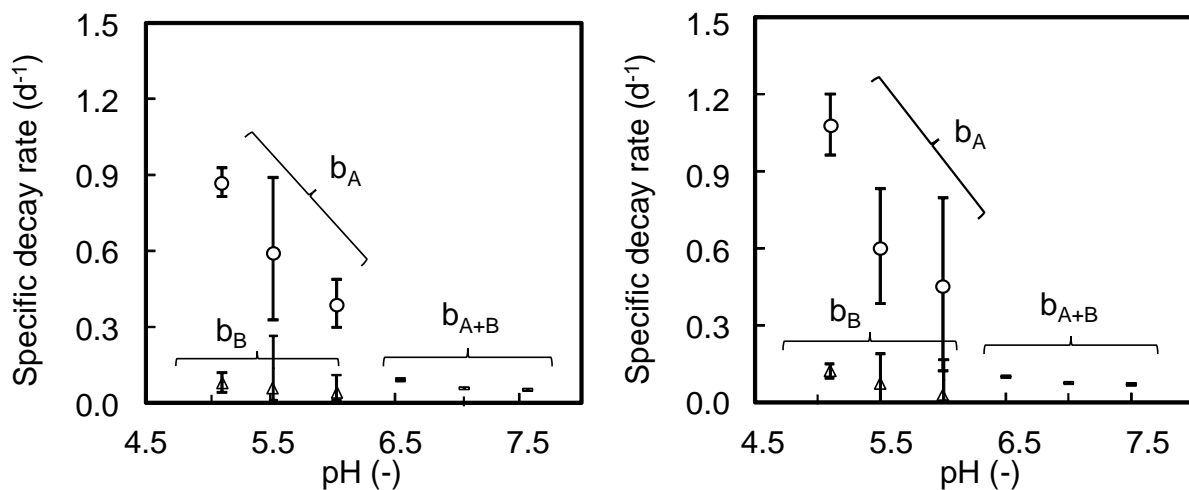
Figure 5.3 Estimated specific decay rates versus. pH value. (Left: Acetate-fed system, right: Formate-fed system), (Plot: regression, bar on the plots: 95%-confidence interval)

As shown in **Figure 5.3**, in both Acetate and Formate-fed systems, it seemed that the pH lower than 6.0 significantly increased the specific decay rates of X_A fraction. In the normal pH range around 7.0, b_{A+B} was around 0.05~0.07 d^{-1} in both the systems. When the experimental pH was decreased to 6.0, the b_A value in both the systems increase to 0.39~0.46 d^{-1}. Similarly for pH of 5.5 and 5.0, the b_A

value increased to 0.62 d^{-1} and 0.87~1.1 d^{-1} respectively. These experiments clearly demonstrated that the biomass decay of methanogenic culture was accelarated in low pH environment. As described in PMA-qPCR analysis section next, the archaeal (methanogenic) biomass was found to be dominant in both the systems. Therefore, the X_A fraction (dominant portion of the fluorescent cell area) in the above analysis affected by low pH was attributed to methanogenic biomass. On the other hand, the pH tolerant X_B fraction (minor portion of the fluorescent cell area) was attributed to acidogen biomass found to be present in PMA-qPCR analysis.

5.3.3. Analysis of biomass constituents under low pH incubation

As shown in **Figure 5.4**, the PMA-qPCR experiment demonstrated that the archaeal biomass was considerably lost when the cultures were exposed to the low pH at 5.1 for 6 days whereas the decrease of bacterial biomass was small. In Acetate-fed system, the archaeal biomass was accounted for about 78% of total living microorganism in the culture, and this fraction decreased to 27% at the end of the batch experiment indicating that significant methanogenic biomass decay took place during the incubation period. For Formate-fed system, the initial archaeal biomass in the culture was estimated to be 67% of total living microorganism, which also decreased to 21% after 6 days. In both the systems, about 75% of the initial living cells were inactivated during 6 days of incubation under pH 5.1 (Acetate-fed system: $140 \cdot 10^6$ cells/mL $\rightarrow$ $35 \cdot 10^6$ cells/mL; Formate-fed system: $240 \cdot 10^6$ cells/mL $\rightarrow$ $70 \cdot 10^6$ cells/mL), and approximately 90% of the cell death was recognised as the archaeal biomass decay (Acetate-fed system: 95% of $105 \cdot 10^6$ cells$_{-decrement}$/mL, Formate-fed system: 86% of $170 \cdot 10^6$ cells$_{-decrement}$/mL).
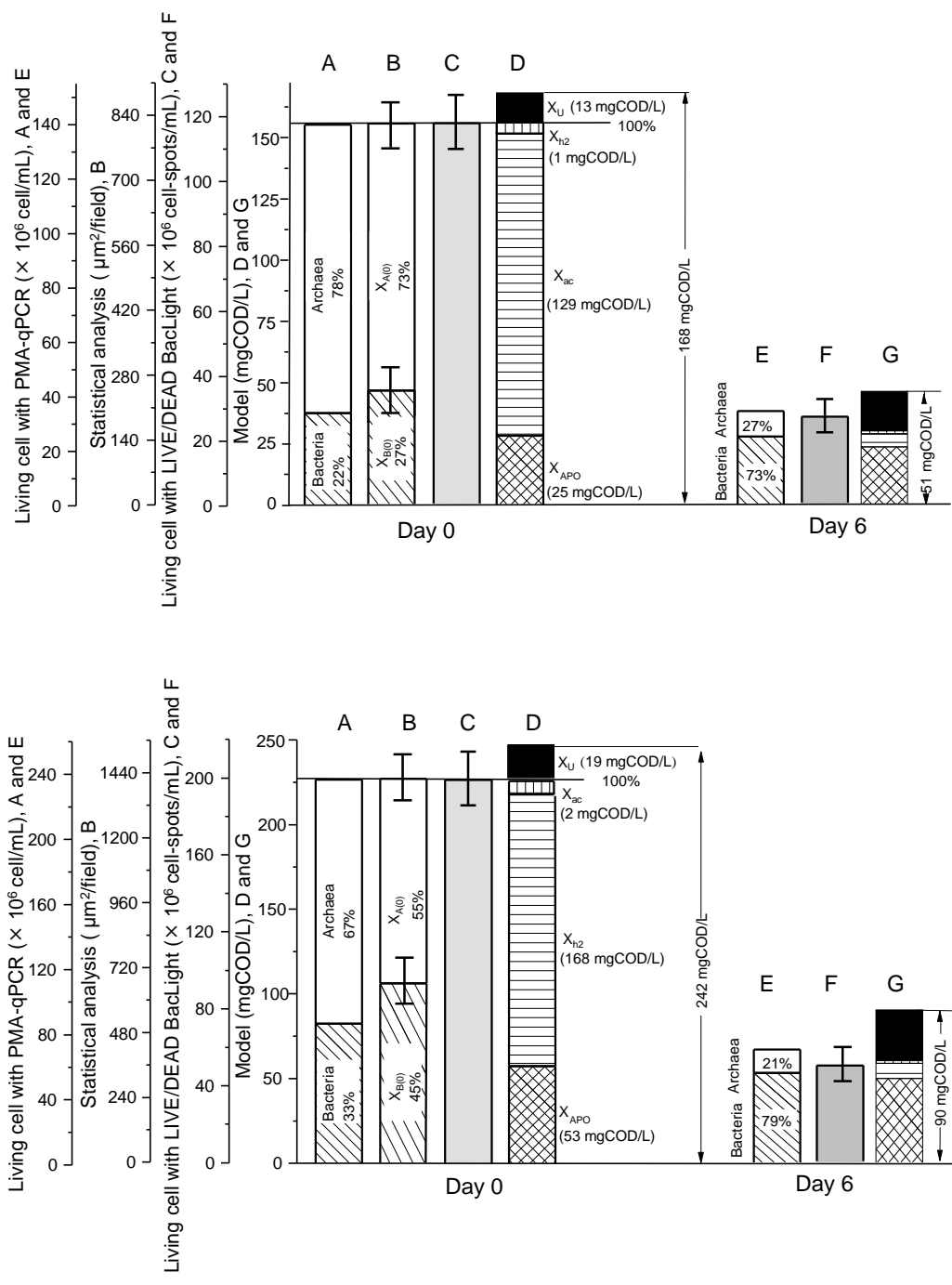
Figure 5.4 Biomass constituents before/after the batch experiments set at pH 5.1

(Upper: Acetate-fed system, lower: Formate-fed system)

71

For Acetate-fed system, $X_{A(0)}$ was accounted for about $73 \pm 4.9\%$ of the fluorescent cell area whilst $X_{B(0)}$ was present in its $27 \pm 4.9\%$. These values were consistent with the archaeal fraction (78%) and bacterial fraction (22%) detected with PMA-qPCR technique respectively. For Formate-fed system, the estimated $X_{A(0)}$ fraction ($55 \pm 8.8\%$) was slightly lower the archaeal fraction detected with the PMA-qPCR technique (67%). Nevertheless these experimental results indicated that archaeal biomass was the dominated microorganism in both the systems, and the species were easily inactivated under low pH environment.

Based on the conversion coefficients of fluorescent cell area per cell spot (μm^2-fluorescent cell area /cell$_{-spot}$), it seemed that about 10^8 of viable cells ($120 \pm 15 \cdot 10^6$ cell$_{-spots}$/mL) were present per 1 mL of the culture collected from the chemostat reactor of Acetate-fed system, which decreased to about $30 \pm 6 \cdot 10^6$ cell$_{-spots}$/mL at day 6 in the experiment set pH at 5.1. Similarly, for Formate-fed system, the number of fluorescent spots in the initial phase ($200 \pm 30 \cdot 10^6$ cell$_{-spots}$/mL) decreased to $60 \pm 11 \cdot 10^6$ cell$_{-spots}$/mL after day 6 in the acidic environment. Although slight mismatch was found between the number of living cells detected by the PMA-qPCR method and the number of living cells detected by the fluorescent cell counting, both visualisation techniques seemed to yield almost comparable results in total living cell number. According to Shibata *et al*., (1987) and Nakamura *et al.* (1989), $1 \cdot 10^6$ active cell/mL was supposed to be almost equivalent to 1 mg/L-order of magnitude for microbial suspended solid [145,146]. Since the sludge concentrations in the chemostat reactors were about 200 mg-COD/L for both systems (168 ± 20 mg-COD/L for Acetate-fed system, 242 ± 30 mg-COD/L for Formate-fed system), these measured living cell concentrations of the 2 cultures ($120 \sim 140 \cdot 10^6$ cells/mL for Acetate-fed system, $180 \sim 240 \cdot 10^6$ cells/mL for Formate-fed system) were quite reasonable. This consistency was maintained at the end of the experiment of 6 days (Acetate-fed system: $30 \sim 40 \cdot 10^6$ cells/mL vs. 51 mg-COD/L; Formate-fed system: $50 \sim 60 \cdot 10^6$ cells/mL vs. 80 mg-COD/L). Recently Ravindran *et al.* (2019) presented that comparative number of *Ascaris* ova were obtained among the measurements of culture, fluorescent cell counting with LIVE/DEAD® BacLight™ kit and cell counting with PMA-qPCR method [147]. These detection consistencies were

also found in the microbial cell counting.

In addition to above experimental techniques, the relative fractions of each microorganism in chemostat reactor was estimated by using ADM1 model. For Acetate-fed system, the concentrations of X_{ac} (acetoclastic methanogenic archaea), X_{h2} (hydrogenotrophic methanogenic archaea) and X_{APO} (total acidogeninc bacteria = $X_{su} + X_{aa} + X_{fa} + X_{c4} + X_{pro}$) were calculated to be 129 mg-COD/L, 1.0 mg-COD/L and 25 mg-COD/L respectively when the simulations were performed using the laboratory operating conditions. The inert fraction (X_U) in the sludge was estimated to be about 8% of total particulate COD. The total particulate COD (168 mg-COD/L) estimated by the model was almost identical to the measured solid concentration in sludge (148~188 mg-COD/L). The estimated archaeal fraction ($X_{ac} + X_{h2}$) of the active biomass (84%) was comparable to that measured with PMA-qPCR analysis (78%). In the simulation of low-pH batch experiments using the estimated specific decay rate of 0.83 d^{-1} for methanogens, the model simulated that 96% of methanogens in the culture was lost under the acidic environment in 6 days whilst only 12% of acidogens were inactivated. This was also consistent with the PMA-qPCR analysis which revealed that the losses of archaea and bacteria were 90% and 25% respectively.

The relative fraction of different microorganism in Formate-fed system also responded in a very similar manner to those of Acetate-fed system. The measured particulate COD of 212~272 mg-COD/L in the chemostat reactor matched well with the model prediction of 242 mg-COD/L. About 92% of the sludge COD was predicted to be the sum of active biomass (X_{h2} = 168 mg-COD/L, X_{ac} = 2 mg-COD/L, X_{APO} = 53 mg-COD/L). From the model, the archaeal fraction and bacterial fraction were calculated to decrease to 8 mg-COD/L and 47 mg-COD/L after 6 days of the low-pH experiment respectively. This also supported the PMA-qPCR analytical results where archaeal biomass: bacterial biomass was detected as 67%: 33% in the initial phase and 21%: 79% at the end of the low-pH experiment.

5.3.4. Fate of methanogens in acidic environments

As shown in **Figure 5.5**, the living methanogen (archaea) cell count in the batch reactors for the enriched cultures were remarkably low after 6-days of acidic incubation. When the incubation of the acetate-fed culture was conducted at pH 4.0, the number of living archaeal cells were reduced by almost 3-order of magnitude from the initial concentration ($99 \cdot 10^6$ copies/mL $\rightarrow$ $0.13 \sim 0.61 \cdot 10^6$ copies/mL) whilst the archaeal cells incubated at a pH of 5.0 was reduced by about 2-order of magnitude ($107 \cdot 10^6$ copies/mL $\rightarrow$ $1.1 \sim 5.1 \cdot 10^6$ copies/mL). In case that the pH was maintained at pH 7.0 without addition of the acidic species, the living archaeal cells were maintained during the period ($99 \sim 107 \cdot 10^6$ copies/mL $\rightarrow$ $78 \sim 91 \cdot 10^6$ copies/mL). With respect to the archaea of the formate-fed culture, comparable experimental results to those of the acetate-fed culture were obtained. During the 6-day incubation set a pH of 4.0, more than 99% of archaeal cells were lost. The biocidal effect decreased as the incubation pH was increased to 5.0 in the batch experiments.

74
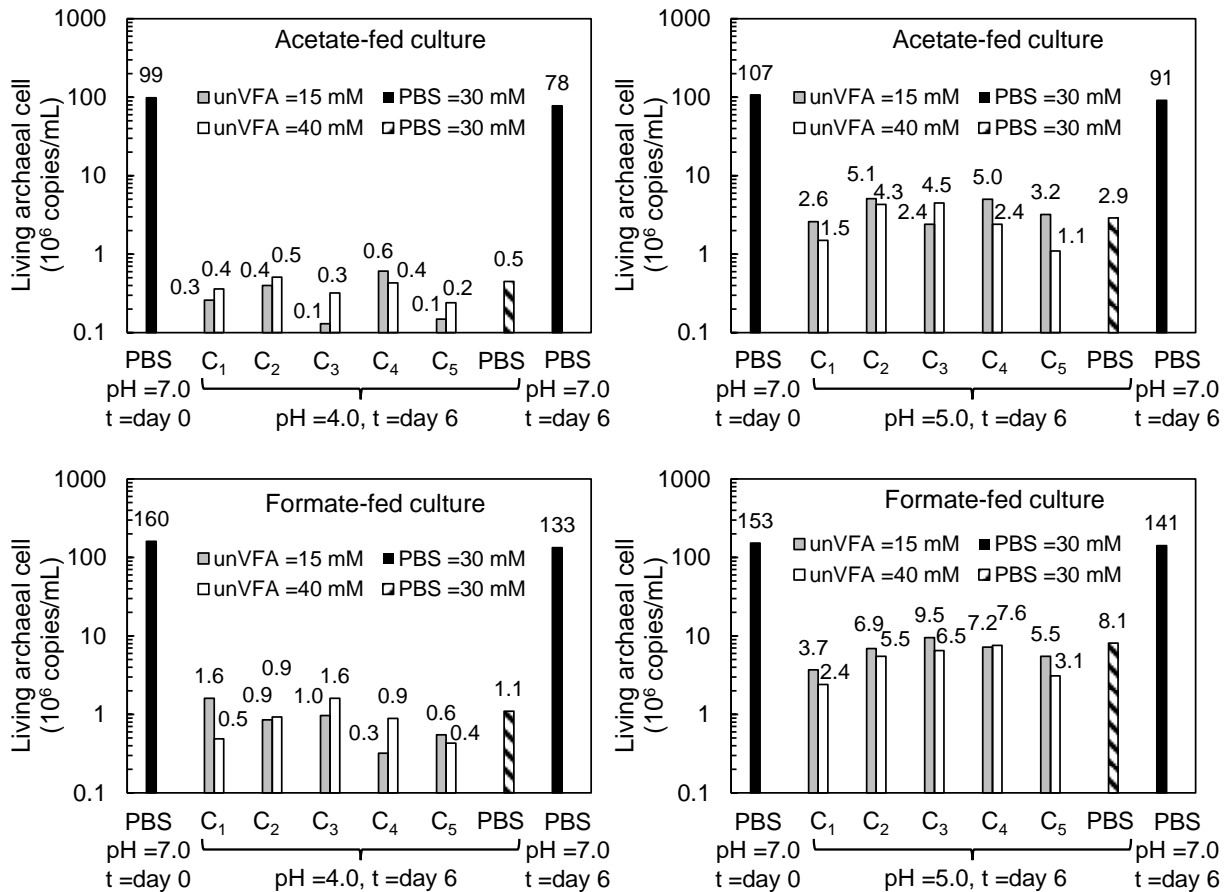
Figure 5.5 PMA-qPCR analysis of methanogen-enriched cultures before/after 6-day acidic incubations. (black: pH =7.0 with 30 mM-PBS, grey: pH =4.0 or 5.0 with 15 mM-unVFA or PBS: 30 mM-PBS, white: pH =4.0 or 5.0 with 40 mM-unVFA, C_1: formic acid, C_2: acetic acid, C_3: propionic acid, C_4: butyric acid, C_5 valeric acid)

For the experiments set pH 5.0 and pH 7.0 using 30 mM-PBS with the acetate-fed culture, the methanogenic activities after 6 days of the incubations were investigated. The pH of the batch reactors was neutralised and the volumetric CH_4 production rates (r_{CH4}) were measured with a precise gas meter (MGC-1, Ritter, Germany) by spiking the batch reactor with 1,000 mg-COD/L of acetate. The r_{CH4} of the experiment incubated at pH 5.0 was below a detectable limit of 3.0 mL over 2-days (r_{CH4} ≤ 15 mL-CH_4/L/d). On the other hand, the control incubation kept pH of 7.0 showed a comparable r_{CH4} to that at day 0 (570 mL-CH_4/L/d at day zero vs. 410 mL-CH_4/L/d at day 6) (graph not shown).

These results from the activity tests validates the data from the living methanogen (archaea) cell count.

Over the examined acidic species (formic acid, acetic acid, propionic acid, butyric acid, valeric acid and phosphoric acid) and the concentrations (unVFA = 15 mM and 40 mM, PBS = 30 mM), the cellular decay (reduction of copy number) seemed to be comparable to each other. These results suggest that high proton concentration is the primary biocidal substance causing enhanced archaeal decay rather than the dissociated or undissociated VFA concentration.

As shown in **Figure 5.6**, the living archaeal cells were also lost during the acidic incubation (30 mM-PBS) of digestate. In the batch experiment set at a pH of 4.0, the number of living archaeal cells were reduced by about 3-order of magnitude within 6 days ($163 \cdot 10^9$ copies/g-initial VSS $\rightarrow 0.4 \cdot 10^9$ copies/g-initial VSS) whilst the living archaea was maintained for 6 days at pH 7.0 ($157 \cdot 10^9$ copies/g-initial VSS at day zero vs. $143 \cdot 10^9$ copies/g-initial VSS at day 6). The archaeal cellular decay was also recognised in the experiment set a pH of 5.0. At day 5~6, the living archaeal cells in pH 5.0 dropped to almost 10% of the initially present in the digestate.
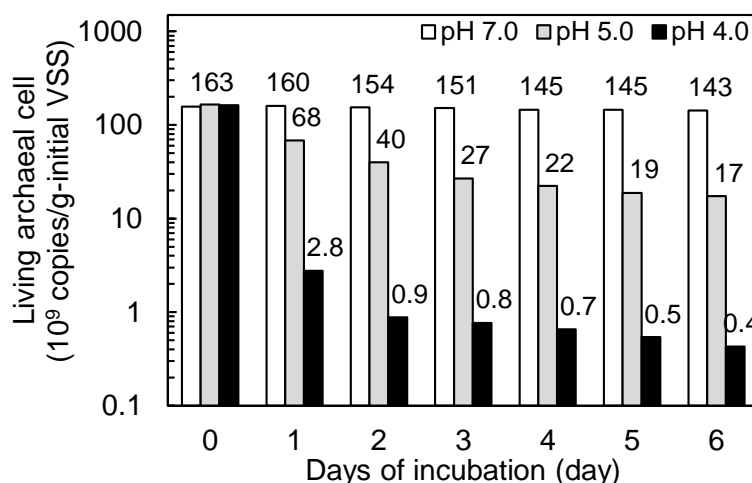

Figure 5.6 PMA-qPCR analysis of digestate exposed to phosphoric acid (30 mM) for 6 days

(white: pH =7.0, grey: pH =5.0, black: pH =4.0)

A set of experiments was conducted in a pH range of 4.0 to 7.5 with a pH increment of 0.5 unit to further refine the pH at which biocidal effect became detrimental. The VFA concentration in these experiments was fixed at 3,000 mg-COD/L using either one of the selected VFA species. As shown in **Figure 5.7**, the living archaeal cells of the acetate-fed culture were all decreased when the incubation pH was set below 6.0 irrespective of the differences in the acidic species used. In the batch experiments set a pH of 5.5, only 5% of initial archaeal cells were live after day 6. In the incubations set a pH of 6.0, the decay was not as pronounced, and the archaeal cells were reduced by only about 50%. When the incubations were carried out in near-neutral pH (pH 6.5–7.5), the biomass was maintained. In fact, the experiments set a pH of 7.0 and 7.5 using acetate showed a slight archaeal growth after 6 days ($110 \cdot 10^6$ copies/mL $\rightarrow 130 \sim 140 \cdot 10^6$ copies/mL). For the formate-fed culture, the archaeal cells were also lost in the incubations conducted below pH 6.0. In the acidic incubations, the degree of cellular decay was found to be comparable to those obtained from the experiments using the acetate-fed culture. The archaeal growth was only observed in the batch reactors where formate was dosed and operated in the moderate pH of 7.0–7.5. Based on these results, it appears that a pH of below 6.0 could lead to significant biocidal effect on the methanogens.
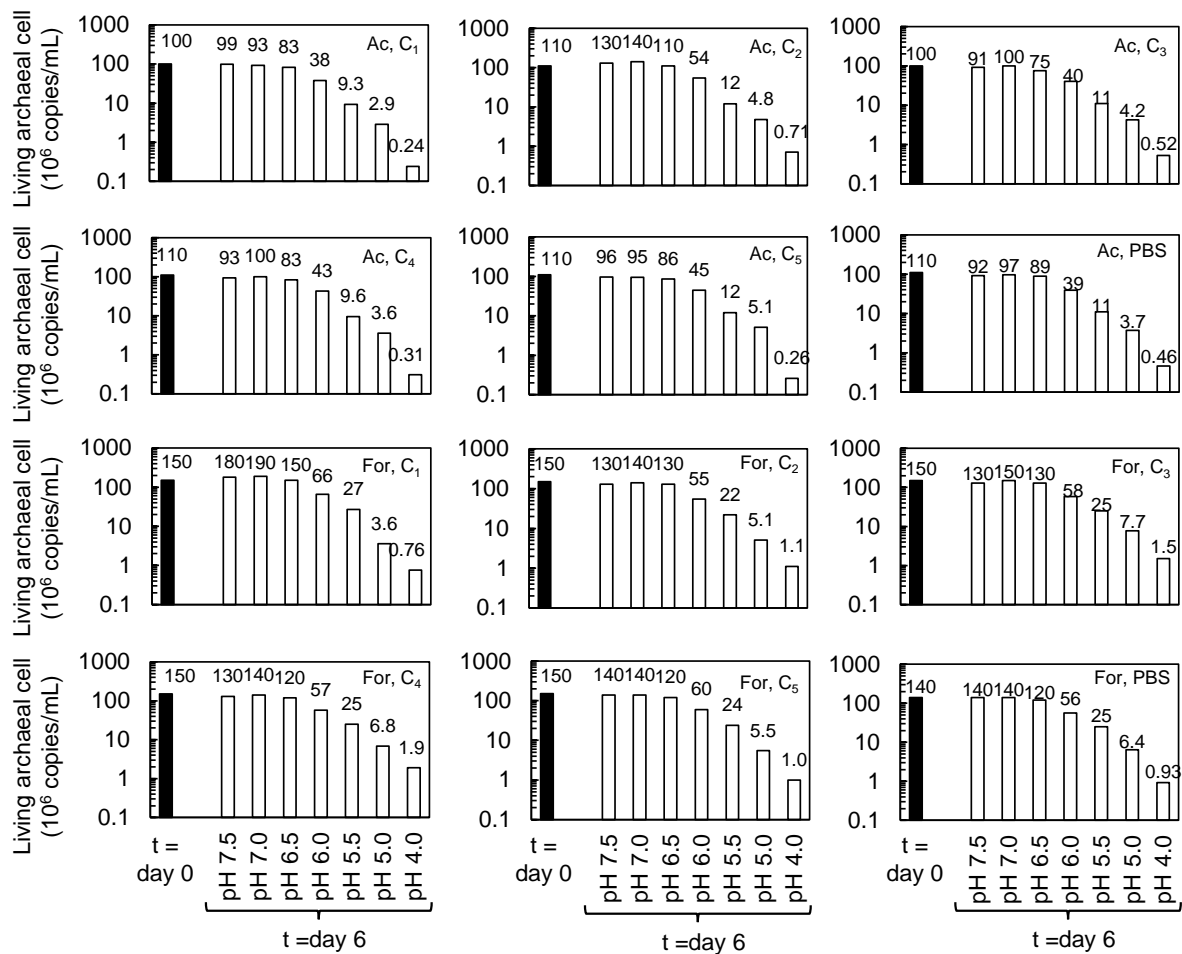
Figure 5.7 PMA-qPCR analysis of methanogen-enriched cultures exposed to various kinds of acidic media for 6 days. (Ac: acetate-fed culture, For: formate-fed culture, C_1: 3 g-COD formate/L, C_2: 3 g-COD acetate /L, C_3: 3 g-COD propionate/L, C_4: 3 g-COD butyrate/L, C_5: 3 g-COD valerate/L, PBS: 30-mM phosphate buffer)

The biocidal effect on acidophilic archaea is limited because the microorganisms have a unique membrane monolayer protecting it against high proton gradient [148]. The methanogenic archaea in the enriched system and the digestate used in this study were weak against the low pH stress leading to biomass decay. Since the sensitivities of the inhibition should depend on microbial species, the research of acidic inhibition on methanogens could be expanded to analyse the fate of each microbial species in the dynamic conditions [149]. In this way the methanogenic species could be listed in the

order of robustness against the low pH stress. At present the exact mechanisms that low pH (high proton concentration) led to the archaeal cellular decay were not clear. Considering the detection principle of the living cells (dead cell = the cell having damaged cellular membrane), it could be speculated that high proton might disrupt the archaeal cell membrane proteins and/or membrane structure leading to the immediate death within a couple of days. On the other hand, Zhang *et al.* (2019) pointed out that the unVFA inhibition for the growth of methanogenic archaea were almost comparable among C_2–C_4 VFA species [150]. According to Lins *et al.* (2014), some thermophilic methanogens (*Methanobacteriales* spp.) were not tolerant against the high acetate, leading to a microbial population shift over the cultivation suggesting that their enzymatic systems were sensitive on the inhibition [4]. Hence, it is likely that thermophilic methanogens are also weak against low pH stress as well as the mesophilic methanogens analysed in this study. In general, the unVFA in the bulk liquid readily diffuse inwards across the cell membrane. However, this requires additional ATP consumption in the cell to discharge the proton outside the cell against the proton motive force [151]. Consequently, the net ATP available for the microbial growth is lowered, leading to a simultaneous decrease of the specific growth rate and/or biomass yield coefficient per unit of substrate. The biocidal phenomena found in this study might be also attributed to the inability of the archaea to generate enough energy (ATP) for cell maintenance at high proton concentration leading to gradual death (maintenance failure). To unravel the dominant mechanism of the cellular decay, monitoring the cellular decay with addition of ATP-uncoupler reagent might be relevant [152]. If the cellular decay is due to the disruption of cell membrane/membrane proteins, the cellular decay rate with addition of the ATP-uncoupler reagent would be comparable to that without addition of the reagent.

5.3.5. Dynamics of living cells in low pH and high unVFA acidic environments

To clarify the influential factors on the cellular decay, the specific decay rates of each experiment were statistically analysed in a double exponential function (**Equation 5.2**) for each of

microbial group (methanogenic archaea and acidogenic bacteria) (Sun *et al.*, 2020). The fluorescent area of the total living cells at any time ($a_{T(t)}$) was calculated based on the initial concentrations of the living microorganisms ($a_{A(0)}$: methanogen, $a_{B(0)}$: acidogen) and their first-order specific decay rates of k_A and k_B.

$$\begin{cases} a_{A(t)} = a_{A(0)} \cdot \exp(-k_A \cdot t) \\ a_{B(t)} = a_{B(0)} \cdot \exp(-k_B \cdot t) \\ a_{T(t)} = a_{A(t)} + a_{B(t)} \end{cases}$$

Equation 5.2

Where, $a_{T(t)}$: total living cell area (μm^2) at time $= t$, $a_{A(0)}$: initial cell area of living methanogen (μm^2), $a_{B(0)}$: initial cell area of living acidogen (μm^2), k_A: specific decay rate of methanogen (d^{-1}), k_B: specific decay rate of acidogen (d^{-1}), t: time (d)

Mathematically, when the specific decay rate of methanogen (k_A) was distinct from that of acidogen (k_B), the experimental data of $a_{T(t)}$ were nonlinearly plotted along with time on a semilogarithmic graph. From the nonlinearity, the pair of k_A and k_B was estimated. By contrast, when the values of k_A and k_B were close to each other, the data were expressed in almost linear plots on the semilogarithmic graph. In this case, the rate coefficients were not statistically distinguishable to each other, and a lumped net specific decay rate (k_{A+B}) was obtained using a single exponential function (**Equation 5.3**) instead.

$$a_{T(t)} = a_{A+B(0)} \cdot \exp(-k_{A+B} \cdot t)$$

Equation 5.3

Where, $a_{T(t)}$: total living cell area (μm^2) at time $= t$, $a_{A+B(0)}$: initial total living cell area (μm^2), k_{A+B}: lumped specific decay rate (d^{-1}) , t: time (d)

Assuming that acidogens were more tolerant against low pH stress than methanogens ($k_A \geq k_B$) [5,153], initial methanogen concentration ($a_{A(0)}$) and the initial acidogen concentration ($a_{B(0)}$) of the methanogen-enriched culture were calculated from **Equation 5.2** and the experimental data. These microbial concentrations are summarised in the supplementary materials together with the estimated specific decay rates and the 95%-confidence intervals (CI_{95}) (**Table 5.5**: the Acetate-fed culture; **Table 5.6**: the Formate-fed culture). From the 65 incubation datasets of the Acetate-fed culture, $a_{A(0)}$: $a_{B(0)}$ was calculated to be 576~654 μm^2/field: 156~230 μm^2/field (*ca.* 2.5~4.2:1; CI_{95} of $a_{A(0)}$:$a_{B(0)}$ = 469–712: 101–338). For the Formate-fed culture, $a_{A(0)}$: $a_{B(0)}$ was also estimated to be 765~984 μm^2/field: 301~521 μm^2/field (*ca.* 1.5~3.3: 1; CI_{95} of $a_{A(0)}$: $a_{B(0)}$ = 612–1072: 220–675) in another set of 65 incubations.

Table 5.5 Estimated Parameters for Acetate-fed culture

Dataset	pH	Species		Concentration	Initial archaea $a_{A(0)}$ (μm²/field)	Initial bacteria $a_{B(0)}$ (μm²/field)	Archaeal specific rate k_A (d⁻¹)	Bacterial specific rate k_B (d⁻¹)	r^2 (-)	Initial a_{A+B} $a_{A+B(0)}$ (μm²/field)	Composite specific rate k_{A+B} (d⁻¹)	r^2 (-)
1A	4.0	C_1	15	mM-unVFA	602±53	201±51	1.61±0.30	0.078±0.056	1.000	803±24	0.63±0.04	0.870
2A		C_1	40	mM-unVFA	602±57	201±54	1.57±0.30	0.083±0.060	1.000	803±24	0.63±0.04	0.880
3A		C_1	3.0	g-COD/L	654±58	156±55	1.58±0.31	0.050±0.070	1.000	795±26	0.74±0.05	0.891
4A		C_2	15	mM-unVFA	602±56	201±54	1.46±0.27	0.066±0.058	1.000	803±24	0.58±0.03	0.868
5A		C_2	40	mM-unVFA	602±52	201±49	1.62±0.30	0.063±0.053	1.000	803±25	0.61±0.04	0.848
6A		C_2	3.0	g-COD/L	624±67	178±63	1.52±0.34	0.050±0.070	1.000	779±28	0.62±0.04	0.869
7A		C_3	15	mM-unVFA	602±55	201±53	1.38±0.24	0.047±0.056	1.000	803±24	0.53±0.03	0.850
8A		C_3	40	mM-unVFA	602±53	201±51	1.46±0.26	0.053±0.054	1.000	803±24	0.56±0.03	0.849
9A		C_3	3.0	g-COD/L	624±59	179±55	1.62±0.35	0.043±0.060	1.000	782±28	0.62±0.04	0.848
10A		C_4	15	mM-unVFA	602±54	201±51	1.57±0.29	0.065±0.055	1.000	803±25	0.60±0.03	0.855
11A		C_4	40	mM-unVFA	602±56	201±53	1.50±0.27	0.070±0.057	1.000	803±24	0.60±0.03	0.869
12A		C_4	3.0	g-COD/L	619±69	185±64	1.57±0.39	0.037±0.070	1.000	778±31	0.58±0.04	0.839
13A		C_5	15	mM-unVFA	591±50	207±48	1.57±0.28	0.074±0.051	1.000	798±23	0.60±0.03	0.861
14A		C_5	40	mM-unVFA	591±49	207±47	1.60±0.27	0.079±0.050	1.000	798±23	0.61±0.03	0.866
15A		C_5	3.0	g-COD/L	613±69	190±65	1.49±0.35	0.040±0.070	1.000	777±29	0.55±0.04	0.845
16A		PBS	30	mM	602±55	201±52	1.56±0.30	0.061±0.057	1.000	803±25	0.60±0.04	0.850
17A		PBS	30	mM	640±71	170±68	1.49±0.34	0.053±0.080	1.000	795±29	0.66±0.05	0.884
18A	5.0	C_1	15	mM-unVFA	576±83	230±84	0.93±0.19	0.037±0.067	1.000	806±20	0.38±0.02	0.888
19A		C_1	40	mM-unVFA	576±69	230±68	1.05±0.19	0.038±0.057	1.000	806±21	0.40±0.02	0.864
20A		C_1	3.0	g-COD/L	654±140	156±142	0.79±0.22	0.025±0.150	1.000	795±24	0.44±0.02	0.949
21A		C_2	15	mM-unVFA	576±105	230±106	0.81±0.19	0.025±0.080	1.000	806±20	0.34±0.02	0.898
22A		C_2	40	mM-unVFA	576±87	230±88	0.92±0.19	0.040±0.070	0.999	806±20	0.38±0.02	0.892
23A		C_2	3.0	g-COD/L	624±159	178±161	0.82±0.27	0.032±0.160	1.000	779±27	0.41±0.03	0.940
24A		C_3	15	mM-unVFA	576±96	230±97	0.86±0.19	0.033±0.075	0.999	806±20	0.36±0.02	0.897
25A		C_3	40	mM-unVFA	576±90	230±91	0.91±0.20	0.039±0.072	1.000	806±21	0.38±0.02	0.893
26A		C_3	3.0	g-COD/L	624±153	179±154	0.82±0.27	0.020±0.150	1.000	782±27	0.40±0.03	0.928
27A		C_4	15	mM-unVFA	576±90	230±90	0.90±0.20	0.029±0.071	1.000	806±21	0.37±0.02	0.884
28A		C_4	40	mM-unVFA	576±87	230±87	0.96±0.21	0.048±0.071	1.000	806±21	0.40±0.02	0.896
29A		C_4	3.0	g-COD/L	619±156	185±157	0.79±0.28	0.001±0.140	0.999	778±29	0.35±0.02	0.910
30A		C_5	15	mM-unVFA	591±92	207±92	0.87±0.19	0.018±0.081	1.000	798±21	0.37±0.02	0.889
31A		C_5	40	mM-unVFA	591±79	207±79	0.95±0.19	0.015±0.071	1.000	798±22	0.39±0.02	0.865
32A		C_5	3.0	g-COD/L	613±159	190±161	0.78±0.28	0.003±0.140	1.000	777±29	0.35±0.02	0.912
33A		PBS	30	mM	576±107	230±108	0.83±0.20	0.034±0.083	0.999	806±20	0.36±0.02	0.904
34A		PBS	30	mM	640±171	170±173	0.76±0.26	0.028±0.170	1.000	795±26	0.41±0.02	0.947

ID	pH	C	conc.	unit			k_A		r^2			r^2
35A	5.5	C_1	3.0	g-COD/L	654±218	156±221	0.65±0.25	0.011±0.22	0.998	795±26	0.37±0.02	0.958
36A		C_2	3.0	g-COD/L	624±287	178±291	0.63±0.31	0.029±0.25	0.999	779±27	0.34±0.02	0.965
37A		C_3	3.0	g-COD/L	624±248	179±252	0.63±0.29	0.011±0.22	1.000	782±27	0.33±0.02	0.953
38A		C_4	3.0	g-COD/L	619±491	185±498	0.51±0.40	0.012±0.37	0.998	778±31	0.28±0.02	0.969
39A		C_5	3.0	g-COD/L	613±288	190±293	0.59±0.32	0.003±0.23	0.999	777±28	0.30±0.02	0.950
40A		PBS	30	mM	640±237	170±240	0.65±0.29	0.003±0.22	0.998	795±28	0.34±0.02	0.947
41A	6.0	C_1	3.0	g-COD/L	654±4.7·10³	156±4.8·10³	0.24±0.96	0.044±2.35	0.993	795±24	0.18±0.01	0.985
42A		C_2	3.0	g-COD/L	624±4.6·10³	178±4.6·10³	0.30±1.13	0.074±2.19	0.998	779±30	0.22±0.02	0.958
43A		C_3	3.0	g-COD/L	624±2.3·10³	179±2.3·10³	0.27±0.74	0.005±1.24	0.976	782±29	0.17±0.01	0.955
44A		C_4	3.0	g-COD/L	619±2.3·10³	185±2.3·10³	0.25±0.76	-0.016±1.21	0.998	778±31	0.15±0.02	0.935
45A		C_5	3.0	g-COD/L	613±1.5·10³	190±1.5·10³	0.27±0.61	-0.030±0.85	0.993	777±30	0.15±0.01	0.962
46A		PBS	30	mM	640±7.3·10³	170±7.4·10³	0.23±1.34	0.054±3.08	0.995	795±27	0.18±0.01	0.985
47A	6.5	C_1	3.0	g-COD/L	654±4.9·10⁴	156±4.9·10⁴	0.07±3.90	-0.015±12.5	0.994	795±29	0.050±0.011	0.937
48A		C_2	3.0	g-COD/L	624±9.1·10³	178±9.1·10³	0.09±1.62	-0.077±3.42	0.997	779±38	0.030±0.014	0.977
49A		C_3	3.0	g-COD/L	624±6.0·10³	179±6.0·10³	0.13±1.19	-0.058±2.42	0.975	782±31	0.060±0.012	0.677
50A		C_4	3.0	g-COD/L	619±2.3·10³	185±2.3·10³	0.15±0.72	-0.105±1.13	0.777	778±33	0.050±0.013	0.951
51A		C_5	3.0	g-COD/L	613±7.5·10³	190±7.5·10³	0.11±1.41	-0.064±2.72	0.962	777±33	0.050±0.013	0.947
52A		PBS	30	mM	640±9.6·10⁵	170±9.6·10⁵	0.06±27.1	0.029±92.3	0.955	795±30	0.050±0.011	0.901
53A	7.0	C_1	3.0	g-COD/L	654±6.9·10⁴	156±6.9·10⁴	0.04±4.99	-0.043±16.3	0.994	795±34	0.020±0.012	0.910
54A		C_2	3.0	g-COD/L	624±5.5·10³	178±5.6·10³	0.02±1.22	-0.178±2.31	0.987	779±42	-0.050±0.013	0.983
55A		C_3	3.0	g-COD/L	624±3.4·10⁴	179±3.4·10⁴	0.04±3.27	-0.061±8.41	0.893	782±31	0.010±0.011	0.593
56A		C_4	3.0	g-COD/L	619±1.2·10⁴	185±1.2·10⁴	0.04±1.89	-0.108±3.98	0.902	778±39	-0.010±0.013	0.952
57A		C_5	3.0	g-COD/L	613±2.9·10⁴	190±2.9·10⁴	0.03±3.21	-0.085±7.35	0.932	777±37	-0.010±0.013	0.948
58A		PBS	30	mM	594±7.5·10⁵	211±7.5·10⁵	0.03±7.20	0.016±19.5	0.993	805±21	0.024±0.007	0.994
59A		PBS	30	mM	640±8.9·10⁶	170±8.9·10⁶	0.03±9.08	0.027±52.4	0.951	795±34	0.020±0.012	0.873
60A	7.5	C_1	3.0	g-COD/L	654±5.9·10⁴	156±5.9·10⁴	0.04±4.46	-0.049±14.5	0.994	795±32	0.010±0.011	0.910
61A		C_2	3.0	g-COD/L	624±1.0·10⁴	178±1.0·10⁴	-0.01±1.72	-0.165±3.68	0.987	779±41	-0.060±0.013	0.983
62A		C_3	3.0	g-COD/L	624±4.0·10⁴	179±4.0·10⁴	0.04±3.64	-0.059±9.46	0.893	782±32	0.010±0.011	0.593
63A		C_4	3.0	g-COD/L	619±1.4·10⁴	185±1.4·10⁴	0.04±2.01	-0.099±4.38	0.902	778±36	-0.010±0.012	0.952
64A		C_5	3.0	g-COD/L	613±1.2·10⁴	190±1.2·10⁴	0.04±1.84	-0.102±3.79	0.932	777±35	-0.010±0.012	0.948
65A		PBS	30	mM	640±8.6·10⁶	170±8.6·10⁶	0.02±49.7	0.024±186	0.951	795±36	0.020±0.013	0.873

Remark: C_1: formate, C_2: acetate, C_3: propionate, C_4: butyrate, C_5: valerate, PBS: phosphate buffer, mM-un: millimolar-based unionised VFA concentration, k_A: specific rate obtained from double exponential function, k_{A+B}: specific rate obtained from single exponential function, ±: half width of 95%-confidence interval from the mean, x: p-value ≤ 0.05, underlined cell: not used for further analysis because of large confidence interval and low r^2.

Table 5.6 Estimated Parameters for Formate-fed culture

Dataset	pH	Species		Concentration	Initial archaea $a_{A(0)}$ (μm²/field)	Initial bacteria $a_{B(0)}$ (μm²/field)	Archaeal specific rate k_A (d⁻¹)	Bacterial specific rate k_B (d⁻¹)	r^2 (-)	Initial a_{A+B} $a_{A+B(0)}$ (μm²/field)	Composite specific rate k_{A+B} (d⁻¹)	r^2 (-)
1F	4.0	C_1	15	mM-unVFA	867±82	405±77	1.58±0.32	0.063±0.042	0.999	1272 ±39	0.46±0.03	0.798
2F		C_1	40	mM-unVFA	867±83	405±79	1.56±0.31	0.066±0.042	0.998	1272 ±38	0.46±0.02	0.808
3F		C_1	3.0	g-COD/L	949±67	327±62	1.71±0.29	0.034±0.040	1.000	1235±41	0.53±0.03	0.787
4F		C_2	15	mM-unVFA	867±84	405±80	1.61±0.34	0.068±0.043	0.999	1272 ±40	0.47±0.03	0.804
5F		C_2	40	mM-unVFA	867±86	405±82	1.50±0.30	0.055±0.043	1.000	1272 ±39	0.43±0.02	0.796
6F		C_2	3.0	g-COD/L	964±70	310±65	1.62±0.28	0.019±0.040	1.000	1232±42	0.52±0.03	0.781
7F		C_3	15	mM-unVFA	867±85	405±80	1.52±0.31	0.055±0.043	0.999	1272 ±39	0.44±0.02	0.791
8F		C_3	40	mM-unVFA	867±85	405±81	1.55±0.32	0.065±0.044	0.999	1272 ±39	0.46±0.03	0.808
9F		C_3	3.0	g-COD/L	984±88	301±81	1.55±0.32	0.007±0.050	1.000	1238±47	0.50±0.03	0.779
10F		C_4	15	mM-unVFA	867±84	405±79	1.56±0.32	0.057±0.043	0.999	1272 ±40	0.44±0.03	0.788
11F		C_4	40	mM-unVFA	867±88	405±84	1.45±0.29	0.054±0.044	0.999	1272 ±39	0.43±0.02	0.800
12F		C_4	3.0	g-COD/L	973±80	311±73	1.63±0.31	0.021±0.050	1.000	1233±44	0.52±0.03	0.788
13F		C_5	15	mM-unVFA	860±85	428±81	1.54±0.31	0.067±0.041	1.000	1288 ±39	0.44±0.02	0.803
14F		C_5	40	mM-unVFA	860±79	428±74	1.65±0.33	0.073±0.039	0.999	1288 ±39	0.46±0.02	0.801
15F		C_5	3.0	g-COD/L	955±73	323±68	1.60±0.28	0.024±0.040	1.000	1222±41	0.49±0.03	0.788
16F		PBS	30	mM	867±83	405±79	1.56±0.32	0.061±0.042	1.000	1272 ±39	0.45±0.03	0.798
17F		PBS	30	mM	960±64	320±58	1.64±0.26	0.023±0.030	1.000	1236±40	0.51±0.03	0.780
18F	5.0	C_1	15	mM-unVFA	765±129	521±129	0.97±0.24	0.038±0.046	0.999	1286 ±32	0.28±0.01	0.827
19F		C_1	40	mM-unVFA	765±117	521±116	1.08±0.25	0.051±0.043	1.000	1286 ±33	0.30±0.01	0.826
20F		C_1	3.0	g-COD/L	949±138	327±138	0.92±0.21	0.005±0.070	0.999	1235±36	0.36±0.02	0.873
21F		C_2	15	mM-unVFA	765±147	521±147	0.93±0.25	0.047±0.052	1.000	1286 ±32	0.28±0.01	0.854
22F		C_2	40	mM-unVFA	765±153	521±154	0.94±0.26	0.051±0.055	1.000	1286 ±33	0.29±0.01	0.860
23F		C_2	3.0	g-COD/L	964±140	310±140	0.92±0.21	0.001±0.080	0.999	1232±37	0.37±0.02	0.875
24F		C_3	15	mM-unVFA	765±125	521±125	0.98±0.24	0.039±0.045	1.000	1286 ±32	0.28±0.01	0.826
25F		C_3	40	mM-unVFA	765±121	521±119	1.08±0.27	0.045±0.045	0.998	1286 ±35	0.29±0.02	0.807
26F		C_3	3.0	g-COD/L	984±176	301±176	0.87±0.24	-0.011±0.100	1.000	1238±43	0.36±0.02	0.874
27F		C_4	15	mM-unVFA	765±133	521±133	0.96±0.24	0.043±0.048	0.999	1286 ±32	0.28±0.01	0.837
28F		C_4	40	mM-unVFA	765±132	521±131	1.04±0.27	0.043±0.048	0.998	1286 ±35	0.29±0.01	0.816
29F		C_4	3.0	g-COD/L	973±138	311±137	0.93±0.21	-0.012±0.080	0.999	1233±40	0.35±0.02	0.851
30F		C_5	15	mM-unVFA	860±157	428±158	0.84±0.21	0.016±0.066	0.999	1288 ±34	0.29±0.01	0.850
31F		C_5	40	mM-unVFA	860±134	428±134	0.93±0.22	0.015±0.058	0.999	1288 ±35	0.30±0.02	0.824
32F		C_5	3.0	g-COD/L	955±150	323±150	0.90±0.22	0.001±0.080	1.000	1222±38	0.35±0.02	0.876
33F		PBS	30	mM	765±134	521±134	1.02±0.27	0.049±0.049	1.000	1286 ±34	0.29±0.01	0.833
34F		PBS	30	mM	960±122	320±122	0.91±0.18	-0.004±0.070	0.999	1236±34	0.35±0.02	0.864

35F	5.5	C_1	3.0	g-COD/L	949±326	327±332	0.59±0.23	-0.001±0.15	0.997	<u>1235±33</u>	<u>0.27±0.01</u>	<u>0.939</u>
36F		C_2	3.0	g-COD/L	964±216	310±220	0.71±0.21	-0.012±0.11	0.999	<u>1232±36</u>	<u>0.31±0.02</u>	<u>0.907</u>
37F		C_3	3.0	g-COD/L	984±309	301±315	0.61±0.25	-0.029±0.16	0.999	<u>1238±41</u>	<u>0.27±0.02</u>	<u>0.916</u>
38F		C_4	3.0	g-COD/L	973±268	311±274	0.61±0.22	-0.038±0.14	0.998	<u>1233±38</u>	<u>0.25±0.02</u>	<u>0.900</u>
39F		C_5	3.0	g-COD/L	955±265	323±270	0.61±0.21	-0.024±0.13	0.999	<u>1222±35</u>	<u>0.26±0.01</u>	<u>0.915</u>
40F		PBS	30	mM	960±274	320±279	0.60±0.20	-0.002±0.13	0.999	<u>1236±31</u>	<u>0.28±0.01</u>	<u>0.939</u>
41F	6.0	C_1	3.0	g-COD/L	949±8.5·103	327±8.5·103	0.17±1.03	-0.010±1.80	0.993	<u>1235±35</u>	<u>0.10±0.01</u>	<u>0.980</u>
42F		C_2	3.0	g-COD/L	964±1.3·103	310±1.3·103	0.32±0.39	-0.028±0.47	0.998	<u>1232±36</u>	<u>0.17±0.01</u>	<u>0.977</u>
43F		C_3	3.0	g-COD/L	984±3.0·103	301±3.0·103	0.26±0.62	-0.010±0.96	0.997	<u>1238±41</u>	<u>0.15±0.01</u>	<u>0.987</u>
44F		C_4	3.0	g-COD/L	973±3.2·103	311±3.2·103	0.24±0.63	-0.020±0.95	0.995	<u>1233±40</u>	<u>0.13±0.01</u>	<u>0.980</u>
45F		C_5	3.0	g-COD/L	955±2.3·103	323±2.3·103	0.25±0.52	-0.025±0.71	1.000	<u>1222±35</u>	<u>0.13±0.01</u>	<u>0.983</u>
46F		PBS	30	mM	960±2.1·103	320±2.2·103	0.30±0.50	0.009±0.68	0.999	<u>1236±33</u>	<u>0.18±0.01</u>	<u>0.989</u>
47F	6.5	C_1	3.0	g-COD/L	<u>949±2.7·107</u>	<u>327±2.7·107</u>	<u>0.00±64.8</u>	<u>0.0077±187</u>	<u>0.558</u>	1235±43	-0.004±0.009	0.948
48F		C_2	3.0	g-COD/L	<u>964±9.1·106</u>	<u>310±9.1·106</u>	<u>0.04±67.5</u>	<u>0.0271±202</u>	<u>0.993</u>	1232±37	0.030±0.008	0.906
49F		C_3	3.0	g-COD/L	<u>984±7.5·103</u>	<u>301±7.6·103</u>	<u>0.11±0.97</u>	<u>-0.079±1.83</u>	<u>0.988</u>	1238±43	0.038±0.010	0.933
50F		C_4	3.0	g-COD/L	<u>973±1.1·104</u>	<u>311±1.1·104</u>	<u>0.10±1.23</u>	<u>-0.061±2.39</u>	<u>1.000</u>	1233±40	0.037±0.009	0.954
51F		C_5	3.0	g-COD/L	<u>955±7.0·103</u>	<u>323±7.0·103</u>	<u>0.10±0.93</u>	<u>-0.082±1.58</u>	<u>0.998</u>	1222±40	0.028±0.009	0.899
52F		PBS	30	mM	<u>960±4.8·103</u>	<u>320±4.8·103</u>	<u>0.13±0.70</u>	<u>-0.069±1.17</u>	<u>0.998</u>	1236±33	0.053±0.008	0.969
53F	7.0	C_1	3.0	g-COD/L	<u>949±3.3·104</u>	<u>327±3.3·104</u>	<u>-0.02±2.34</u>	<u>-0.134±4.80</u>	<u>0.989</u>	1235±45	-0.065±0.008	0.987
54F		C_2	3.0	g-COD/L	<u>964±2.8·104</u>	<u>310±2.8·104</u>	<u>0.03±2.07</u>	<u>-0.084±4.53</u>	<u>0.747</u>	1232±40	-0.010±0.008	0.949
55F		C_3	3.0	g-COD/L	<u>984±3.4·104</u>	<u>301±3.4·104</u>	<u>0.03±2.32</u>	<u>-0.081±5.42</u>	<u>0.934</u>	1238±42	-0.010±0.009	0.949
56F		C_4	3.0	g-COD/L	<u>973±1.1·104</u>	<u>311±1.1·104</u>	<u>0.05±1.22</u>	<u>-0.105±2.35</u>	<u>0.856</u>	1233±43	-0.006±0.009	0.949
57F		C_5	3.0	g-COD/L	<u>955±7.0·103</u>	<u>323±7.1·103</u>	<u>0.06±0.92</u>	<u>-0.120±1.56</u>	<u>0.791</u>	1222±41	-0.011±0.009	0.946
58F		PBS	30	mM	<u>815±2.3·104</u>	<u>462±2.3·104</u>	<u>0.07±2.02</u>	<u>-0.043±2.51</u>	<u>0.994</u>	1267±31	0.022±0.007	0.976
59F		PBS	30	mM	<u>960±2.3·106</u>	<u>320±2.3·106</u>	<u>0.03±32.3</u>	<u>0.0030±89.1</u>	<u>0.983</u>	1236±35	0.014±0.008	0.771
60F	7.5	C_1	3.0	g-COD/L	<u>949±6.2·103</u>	<u>327±6.2·103</u>	<u>0.02±0.85</u>	<u>-0.174±1.37</u>	<u>0.995</u>	1235±43	-0.059±0.008	0.984
61F		C_2	3.0	g-COD/L	<u>964±8.9·106</u>	<u>310±8.9·106</u>	<u>-0.01±20.0</u>	<u>-0.010±63.1</u>	<u>0.951</u>	1232±40	-0.014±0.008	0.950
62F		C_3	3.0	g-COD/L	<u>984±1.2·104</u>	<u>301±1.2·104</u>	<u>0.05±1.26</u>	<u>-0.108±2.56</u>	<u>0.748</u>	1238±43	-0.009±0.009	0.949
63F		C_4	3.0	g-COD/L	<u>973±7.0·103</u>	<u>311±7.1·103</u>	<u>0.07±0.91</u>	<u>-0.116±1.63</u>	<u>0.858</u>	1233±41	-0.003±0.009	0.948
64F		C_5	3.0	g-COD/L	<u>955±3.7·103</u>	<u>323±3.7·103</u>	<u>0.08±0.63</u>	<u>-0.141±0.94</u>	<u>0.796</u>	1222±39	-0.008±0.012	0.945
65F		PBS	30	mM	<u>960±3.8·106</u>	<u>320±3.8·106</u>	<u>0.03±50.0</u>	<u>0.0056±140</u>	<u>0.991</u>	1236±36	0.015±0.008	0.814

Remark: C_1: formate, C_2: acetate, C_3: propionate, C_4: butyrate, C_5: valerate, PBS: phosphate buffer, mM-un: millimolar-based unionised VFA concentration, k_A: specific rate obtained from double exponential function, k_{A+B}: specific rate obtained from single exponential function, ±: half width of 95%-confidence interval from the mean, x: p-value ≤ 0.05, underlined cell: not used for further analysis because of large confidence interval and low r^2.

The ratio of initial concentrations for the methanogen and acidogen was also verified by modelling the chemostat operation of the two jar-fermenters using the ADM1 model. Using the default kinetic parameters in model, the steady-state simulation results showed that the active biomass fraction of acetate-fed culture was composed of 123 mg-COD/L of acetoclastic methanogen, 2 mg-COD/L of hydrogenotrophic methanogen and 30 mg-COD/L of acidogen (methanogen: acidogen ≈ 4 :1). The latter two fractions were the biomass generated from the decayed products of acetoclastic methanogen. For the formate-fed culture, assuming that formate was only decomposed by hydrogenotrophic methanogen, 153 mg-COD/L of hydrogenotrophic methanogen, 15 mg-COD/L of acetoclastic methanogen and 53 mg-COD/L of acidogenic bacteria were calculated as the active biomass (methanogen: acidogen ≈ 3: 1). However, since some other bacterial species are known to uptake formate as well as hydrogenotrophic methanogen [154] and biomass yield from formate is slightly higher than that from hydrogen [155], the calculated fraction of the hydrogenotrophic methanogen might be slightly overestimated. Both ratios of methanogen and bacteria calculated from ADM1 in the steady-state operation of the jar-fermenters were comparable to those estimated from the regression analysis using the first-order decay model.
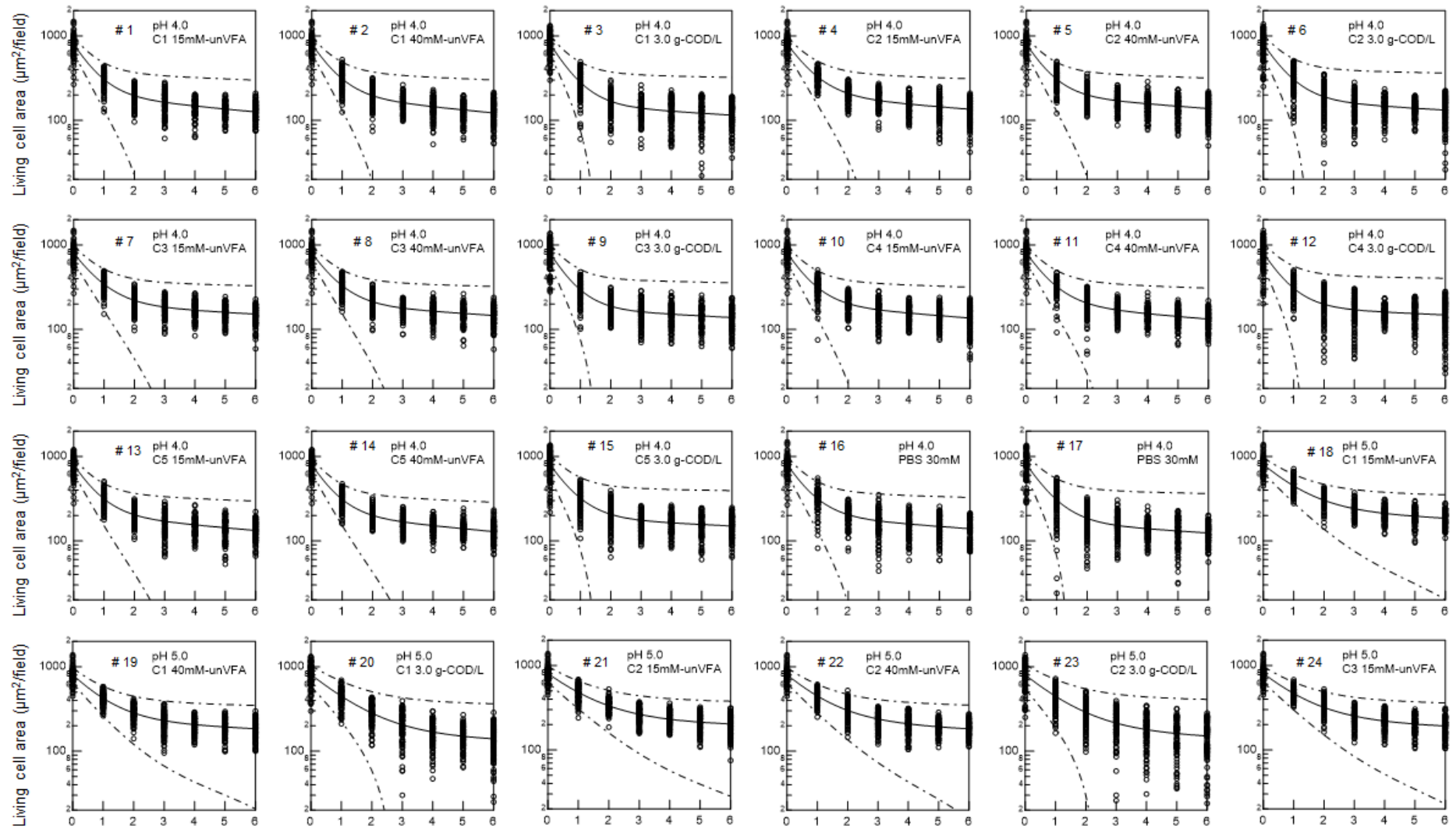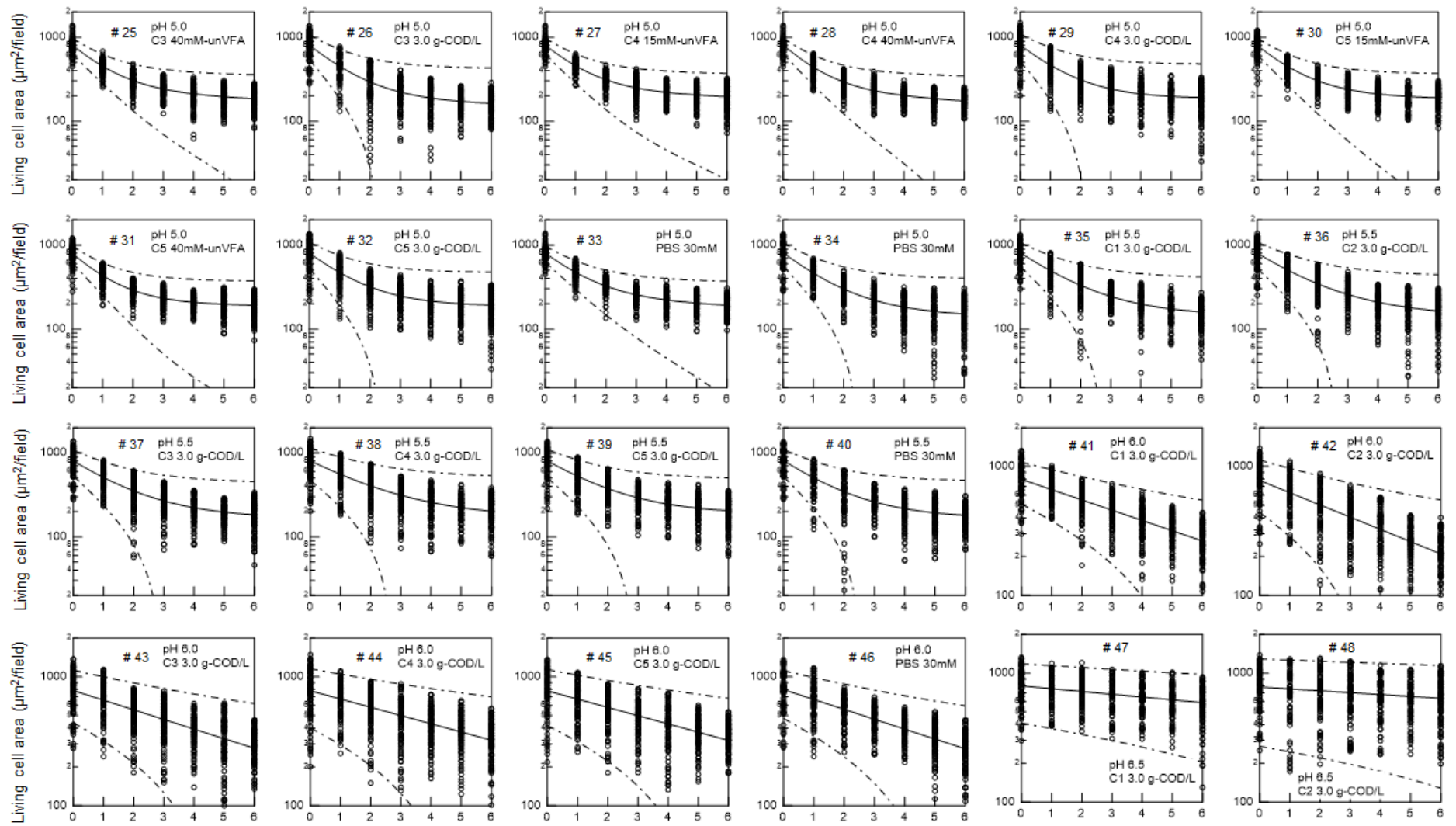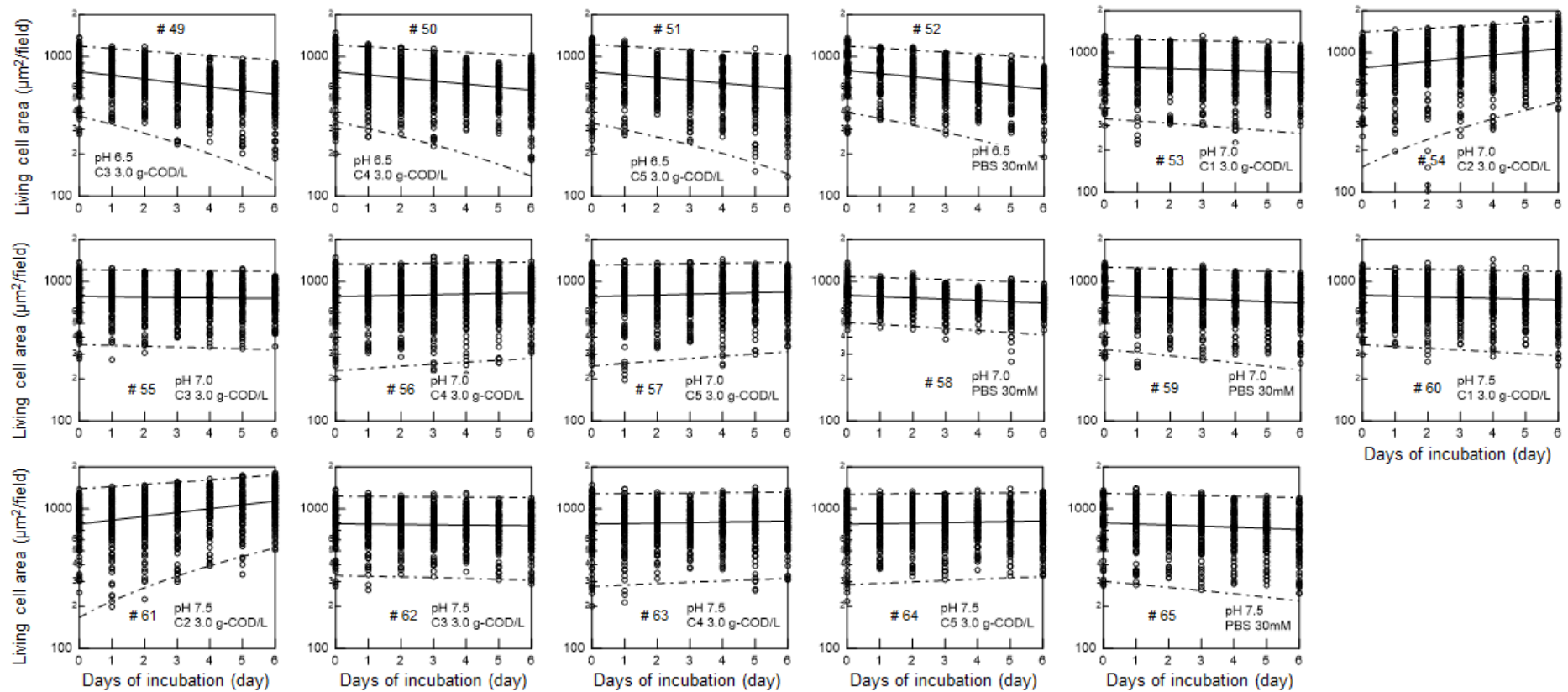
Figure 5.8 Prediction interval of total living cells of Acetate-fed culture. (Dataset #1A~#17A: pH 4.0, dataset #18A~#34A: pH 5.0, dataset #35A~#40A: pH 5.5, dataset #41A~#46A: pH 6.0, dataset #47A~#52A: pH 6.5, dataset #53A~#59A: pH 7.0, dataset #60A~65A: pH 7.5)
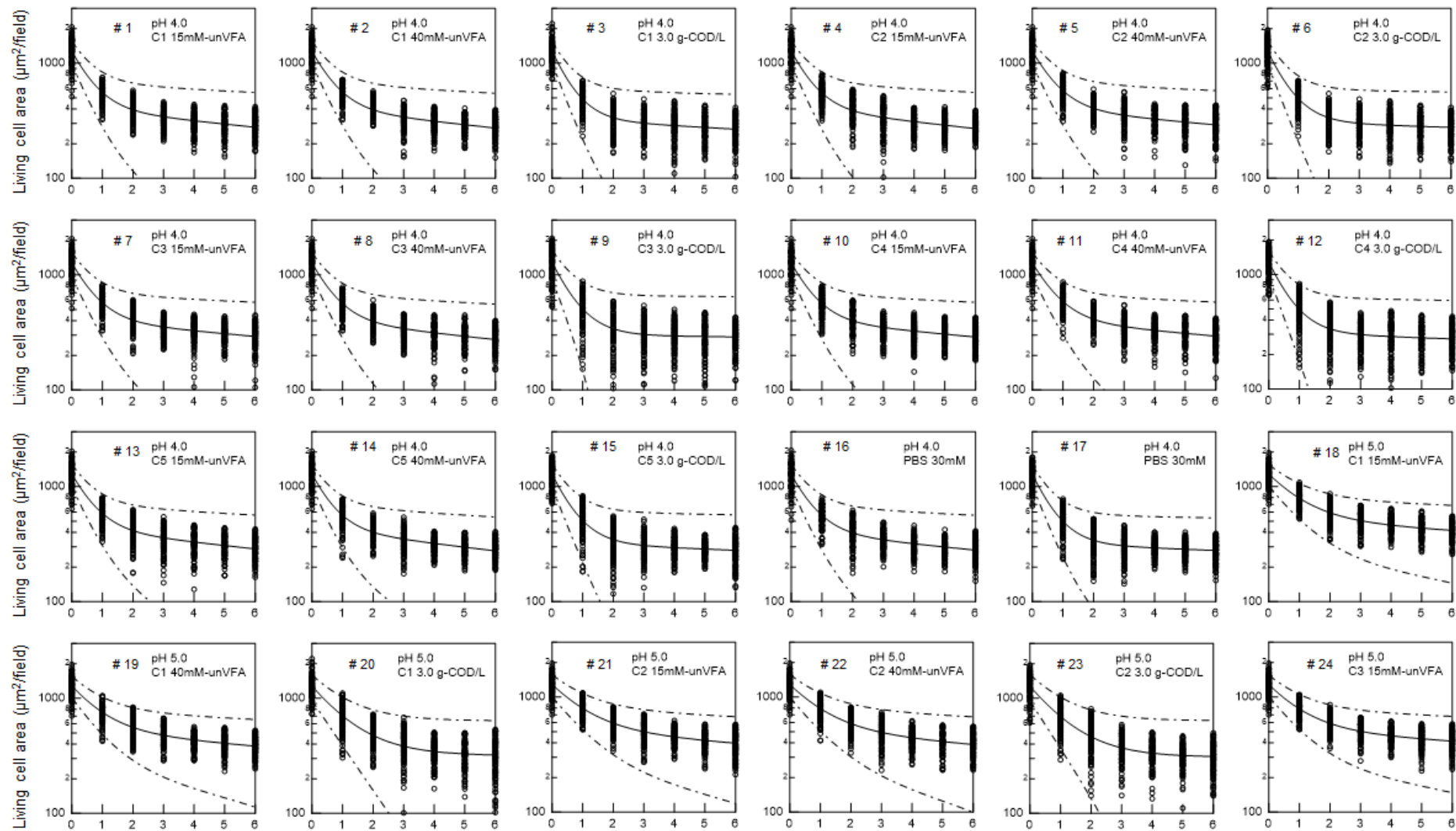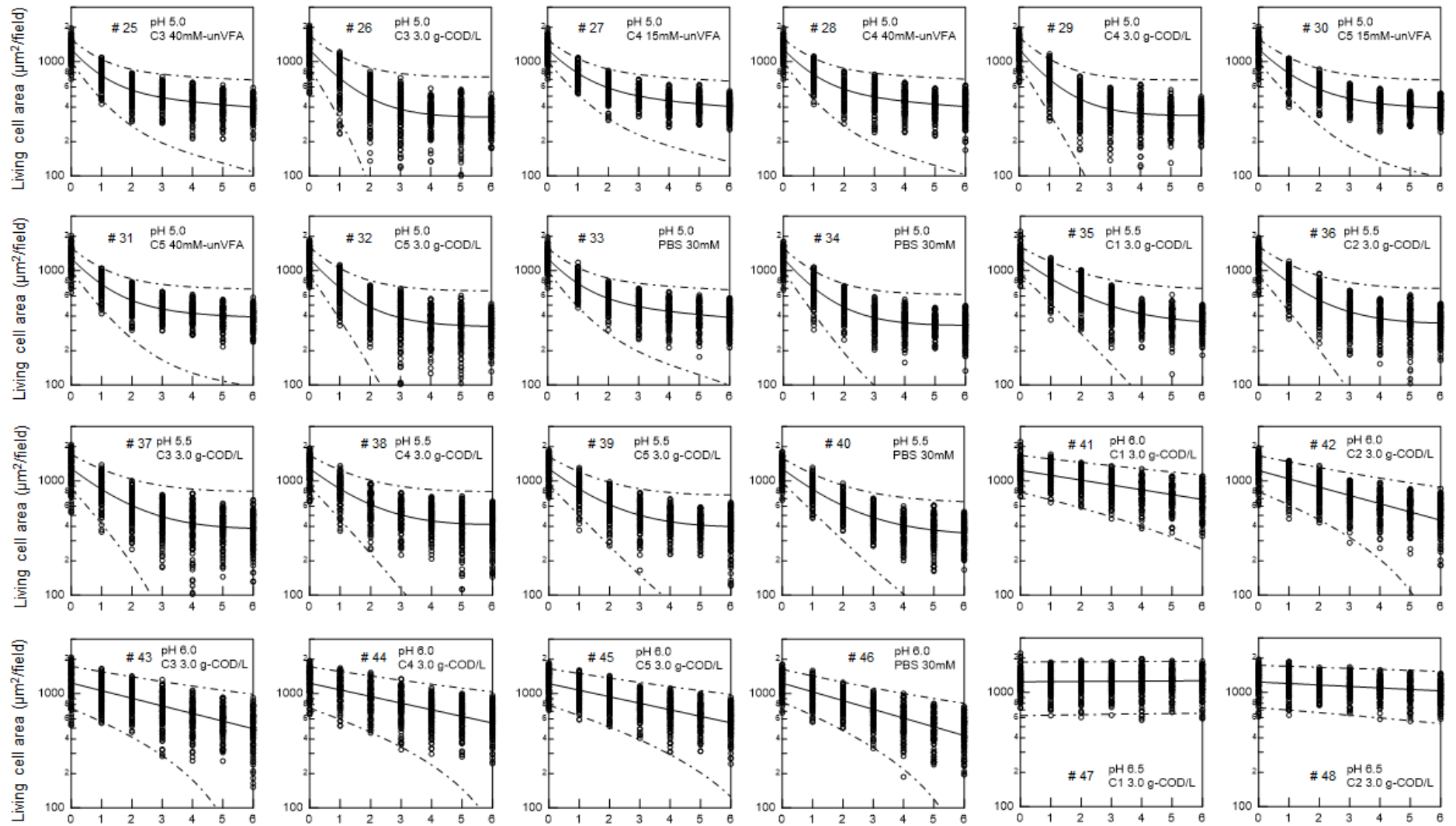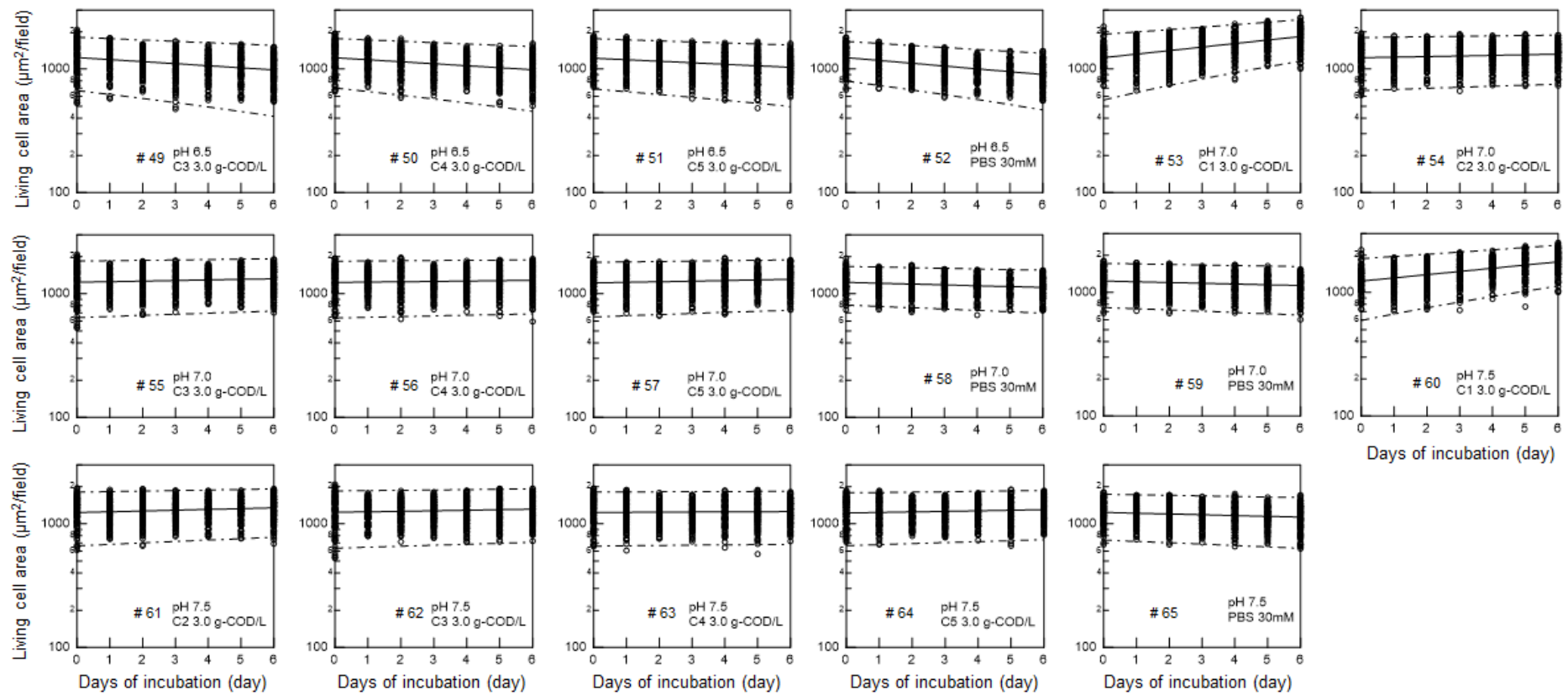
Figure 5.9 Prediction interval of total living cells of Formate-fed culture. (Dataset #1F~#17F: pH 4.0, dataset #18F~#34F: pH 5.0, dataset #35F~#40F: pH 5.5, dataset #41F~#46F: pH 6.0, dataset #47F~#52F: pH 6.5, dataset #53F~#59F: pH 7.0, dataset #60F~#65F: pH 7.5)

With respect to the living cell count during the batch incubations, as shown in **Figure 5.8** (the acetate-fed culture) and **Figure 5.9** (the formate-fed culture), the total living cell area ($a_{T(t)} = a_{A(t)} + a_{B(t)}$) at each sampling time (t) was highly scattered across the mean estimates of $a_{T(t)}$ with 30–200% of analytical error. This resulted in very wide prediction intervals (scatter of data) on each experiment. Nevertheless, the analysis of 90 photos per sample could yield the reasonably narrow CI_{95} on each regression (detection of the population mean). As shown in **Figure 5.10**, using bootstrap method where data were randomly resampled among the 90 photos (= 90 data) to obtain an estimate in the artificial datasets having the pre-determined number of resamples (5–90 photos/dataset), it seemed that at least 45~60 photos per microscopic observation were necessary to reach the narrow confidence intervals with ±5% of the mean.
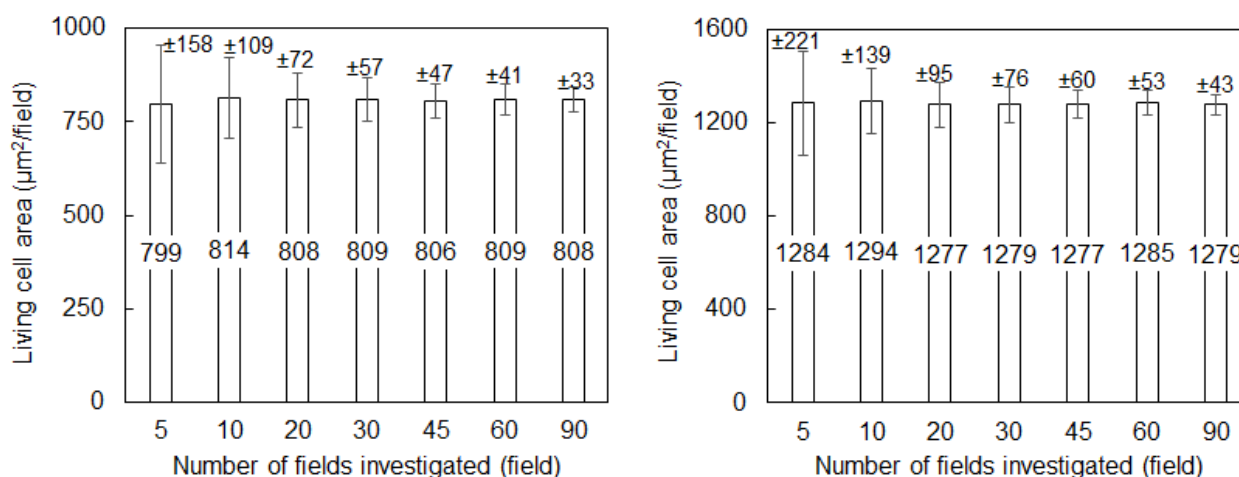
Figure 5.10 Variation of 100-resampled microscopic datasets with Bootstrap method. (Bar: mean of resampled data, error bar: 95%-confidence interval of the mean, Left: Acetate-fed culture, Right: Formate-fed culture)

Using the chi-square test over the estimated specific decay rates of acetate-fed culture (**Tables A4–A6 in Appendix**), the specific decay rates, CI_{95} and p-values are summarised in **Table 5.7**. With respect to the datasets for PBS, the specific decay rate pairs of the experimental pH and the higher pH showed very low p-values ($p < 0.01$) until pH 6.5 vs. pH 7.0. The specific decay rates at pH 7.0 and pH 7.5 were identical to each other (0.020 d^{-1} vs. 0.020 d^{-1}, $p \geq 0.99$) which was also comparable to the default specific decay rate in ADM1. Hence the low-pH inhibition took place at about pH 6.5.

Table 5.7 Specific decay rates and *p*-values for Acetate-fed culture

	Specific decay rate, k_A (CI$_{95}$), (d^{-1})			*p*-value of k_A pair			
Datasets	k_A for PBS / *p*-value vs. higher pH	Minimal k_A for VFA (VFA species and conc.) / *p*-value vs. PBS	Maximal k_A for VFA (VFA species and conc.) / *p*-value vs. PBS	VFA vs. PBS (except Min. k_A & Max, k_A)	within the same VFA species (15–40 mM-unVFA)	within the same unVFA concentration (C$_1$–C$_5$ VFAs)	vs. higher pH
pH 4.0	1.49 d^{-1} (1.15–1.83) / *p* < 0.01 (vs. pH 5.0)	1.38 d^{-1} (1.14–1.62) (15 mM-unC$_3$) / *p* ≥ 0.99	1.62 d^{-1} (1.27–1.97) (40 mM-unC$_2$) / *p* ≥ 0.99	*p* ≥ 0.99	*p* = 0.86–0.99	*p* = 0.88–0.99	*p* < 0.01 [*] (vs. pH 5.0)
pH 5.0	0.76 d^{-1} (0.50–1.02) / *p* < 0.01 (vs. pH 6.0)	0.78 d^{-1} (0.50–1.06) (5.2mM-unC$_5$) / *p* ≥ 0.99	1.05 d^{-1} (0.86–1.24) (40 mM-unC$_1$) / *p* = 0.01	*p* = 0.11–0.99	*p* = 0.28–0.99 [**]	*p* = 0.70–0.99	*p* < 0.01 (vs. pH 6.0)
pH 5.5	0.65 d^{-1} (0.36–0.94) / *p* < 0.01 (vs. pH 6.0)	0.51 d^{-1} (0.11–0.91) (2.6 mM-unC$_4$) / *p* = 0.01	0.65 d^{-1} (0.40–0.90) (2.4 mM-unC$_1$) / *p* ≥ 0.99	*p* = 0.92–0.99	N.A.	N.A.	*p* < 0.01 (vs. pH 6.0)
pH 6.0	0.23 d^{-1} (-1.11–1.57) / *p* < 0.01 (vs. pH 6.0)	0.24 d^{-1} (-0.72–1.20) (0.75 mM-unC$_1$) / *p* ≥ 0.99	0.30 d^{-1} (-0.83–1.43) (2.1 mM-unC$_2$) / *p* = 0.01	*p* = 0.27–0.99	N.A.	N.A.	Nil
	Specific decay rate, k_{A+B} (CI$_{95}$) (d^{-1})			*p*-value of k_{A+B} pair			
Datasets	k_{A+B} for PBS / *p*-value vs. higher pH	Minimal k_{A+B} for VFA (VFA species and conc.) / *p*-value vs. PBS	Maximal k_{A+B} for VFA (VFA species and conc.) / *p*-value vs. PBS	VFA vs. PBS (except Min. k_A & Max, k_A)	within the same VFA species	within the same unVFA concentration (C$_1$–C$_5$ VFAs)	vs. higher pH
pH 6.5	0.050 d^{-1} (0.039–0.061) / *p* < 0.01 (vs. pH 7.0)	0.030 d^{-1} (0.016–0.044) (0.67 mM-unC$_2$) / *p* = 0.06	0.060 d^{-1} (0.048–0.072) (0.48 mM-unC$_3$) / *p* = 0.83	*p* ≥ 0.99	N.A.	N.A.	N.A.
pH 7.0	0.020 d^{-1} (0.008–0.032) / *p* ≥ 0.99 (vs. pH 7.5)	-0.050 d^{-1} (-0.063– -0.037) (0.211 mM-unC$_2$) / *p* < 0.01	0.020 d^{-1} (0.008–0.032) (0.075 mM-unC$_1$) / *p* ≥ 0.99	*p* = 0.01–0.99	N.A.	N.A.	N.A.
pH 7.5	0.020 d^{-1} (0.007–0.033) / Nil	-0.060 d^{-1} (-0.073–0.047) (0.066 mM-unC$_2$) / *p* < 0.01	0.010 d^{-1} (-0.001–0.021) (0.023 mM-unC$_1$ and 0.048 mM-unC$_3$) / *p* = 0.75	*p* = 0.01–0.75	N.A.	N.A.	Nil

N.A.: not available; [*] except k_A pair of 40 mM-unC$_1$ vs.15 mM-unC$_3$ (*p* =0.14); [**] except k_A pair of 40 mM-unC$_1$ vs. 7.2 mM-unC$_1$ (*p* = 0.03).

For the VFA-dosed experiments at pH 4.0, the minimal and maximal specific decay rates among the datasets (1.38 d^{-1}, 1.62 d^{-1}) were close to that measured in PBS (1.49 d^{-1}) with high p-values of $p = 0.94$ and $p \geq 0.99$ respectively. Moreover, the p-values within the same VFA species (among 15–40 mM-unVFA) and within the same unVFA concentrations (among C_1–C_5 VFAs) were both high ($p = 0.86$–0.99, $p = 0.88$–0.99). Considering the narrow CI_{95} over the datasets (about ±20% of the mean), it seemed that the specific decay rates at the pH were dominated by the pH rather than VFA species and concentration.

At pH 5.0, the pair of 40 mM-unC_1 (1.05 d^{-1}) and PBS (0.76 d^{-1}) showed a low p-value ($p < 0.01$). This indicated that that formic acid inhibition was somewhat stronger than phosphate. Except this, all specific decay rates for the VFAs did not show noticeable difference from that for PBS ($p = 0.11$–0.99). The datasets of pH 5.0 were all statistically significant from those at pH 6.0 ($p < 0.01$). In the datasets of pH 5.5, the minimal specific decay rate measured in 2.6 mM-unC_4 (0.51 d^{-1}) only showed a statistical significance with that for PBS (0.65 d^{-1}) ($p < 0.01$). At pH 6.0, the maximal specific decay rate measured in 2.1 mM-unC_2 (0.30 d^{-1}) showed a low p-value ($p < 0.01$) with that measured in PBS (0.23 d^{-1}). However, in overall, the differences of the specific decay rate were highly limited in the same pH.

When the experimental pH was equal to or higher than pH 6.5, the double-exponential function (**Equation 5.2**) yielded very wide CI_{95} (±480–250,000% of the mean) over the datasets. The weak nonlinearities of the data plots resulted in a difficulty to analyse the kinetic parameters. Consequently, the datasets of pH 6.5, pH 7.0 and pH 7.5 were analysed based on k_{A+B} using the single exponential function of **Equation 5.3**. For the VFA-dosed experiments at pH 7.0 and pH 7.5, the minimal specific decay rates were negative, suggesting that the growth of microorganisms took place in the experiments.

With respect to the datasets for the formate-fed culture, as summarised in **Table 5.8** and **Tables A7–A9 in Appendix**, comparable results were obtained to those for the acetate-fed culture. At pH 4.0, no clear difference was found for the specific decay rates irrespective of VFA species and unVFA concentrations. The specific decay rates at pH 5.0 were statistically significant from those for pH 4.0 and pH 6.0 respectively ($p < 0.01$, $p < 0.01$). In the near-neutral pH range, the specific decay rate in PBS (0.053 d^{-1}) at pH 6.5 was statistically significant from that for PBS at 7.0 (0.014 d^{-1}) ($p < 0.01$).

Table 5.8 Specific decay rates and *p*-values for formate-fed culture

	Specific decay rate, k_A (CI$_{95}$), (d^{-1})			*p*-value of k_A pair			
Datasets	k_A for PBS *p*-value vs. higher pH	Minimal k_A for VFA (VFA species and conc.) *p*-value vs. PBS	Maximal k_A for VFA (VFA species and conc.) *p*-value vs. PBS	VFA vs. PBS (except Min. k_A & Max, k_A)	within the same VFA species (15–40 mM-unVFA)	within the same unVFA concentration (C$_1$–C$_5$ VFAs)	vs. higher pH
pH 4.0	1.64 d^{-1} (1.38–1.90) *p* < 0.01 (vs. pH 5.0)	1.45 d^{-1} (1.16–1.74) (40 mM-unC$_4$) *p* = 0.94	1.71 d^{-1} (1.42–2.00) (53 mM-unC$_1$) *p* ≥ 0.99	*p* = 0.94–0.99	*p* = 0.96–0.99	*p* = 0.93–0.99	*p* < 0.01 (vs. pH 5.0)
pH 5.0	0.91 d^{-1} (0.73–1.09) *p* < 0.01 (vs. pH 6.0)	0.84 d^{-1} (0.63–1.05) (15 mM-unC$_5$) *p* = 0.74	1.08 d^{-1} (0.81–1.35) (40 mM-unC$_1$) *p* = 0.48	*p* = 0.43–0.99	*p* = 0.15–0.99	*p* = 0.59–0.99	*p* < 0.01 (vs. pH 6.0)
pH 5.5	0.60 d^{-1} (0.40–0.80) *p* < 0.01 (vs. pH 6.0)	0.59 d^{-1} (0.36–0.82) (2.4 mM-unC$_1$) *p* ≥ 0.99	0.71 d^{-1} (0.50–0.92) (6.0 mM-unC$_2$) *p* = 0.31	*p* = 0.31–0.99	N.A.	N.A.	*p* < 0.01 (vs. pH 6.0)
pH 6.0	0.30 d^{-1} (-0.20–0.80) Nil	0.17 d^{-1} (-0.86–1.20) (0.75 mM-unC$_1$) *p* < 0.01	0.32 d^{-1} (-0.07–0.71) (2.1 mM-unC$_2$) *p* = 0.92	*p* = 0.06–0.34[***]	N.A.	N.A.	Nil
	Specific decay rate, k_{A+B} (CI$_{95}$) (d^{-1})			*p*-value of k_{A+B} pair			
Datasets	k_{A+B} for PBS *p*-value vs. higher pH	Minimal k_{A+B} for VFA (VFA species and conc.) *p*-value vs. PBS	Maximal k_{A+B} for VFA (VFA species and conc.) *p*-value vs. PBS	VFA vs. PBS (except Min. k_A & Max, k_A)	within the same VFA species	within the same unVFA concentration (C$_1$–C$_5$ VFAs)	vs. higher pH
pH 6.5	0.053 d^{-1} (0.045–0.061) *p* < 0.01 (vs. pH 7.0)	-0.004 d^{-1} (-0.013–0,005) (0.24 mM-unC$_1$) *p* < 0.01	0.038 d^{-1} (0.028–0.048) (0.48 mM-unC$_3$) *p* = 0.10	*p* = 0.06–0.34	N.A.	N.A.	N.A.
pH 7.0	0.014 d^{-1} (0.006–0.022) *p* ≥ 0.99 (vs. pH 7.5)	-0.065 d^{-1} (-0.073– -0.057) (0.075 mM-unC$_1$) *p* < 0.01	-0.010 d^{-1} (-0.019– -0.001) (0.15 mM-unC$_3$) *p* < 0.01	*p* < 0.01	N.A.	N.A.	N.A.
pH 7.5	0.015 d^{-1} (0.007–0.023) Nil	-0.05 d^{-1} (-0.042– -0,058) (0.023 mM-unC$_1$) *p* < 0.01	-0.003 d^{-1} (-0.012–0.006) (0.029 mM-unC$_4$) *p* < 0.01	*p* < 0.01	N.A.	N.A.	Nil

N.A.: not available, [***] except k_A pair of 0.91 mM-unC$_4$ vs. PBS (*p* < 0.01).

Over the experiments, the bacterial specific decay rates (k_B) were as low as 1-order of magnitude comparing to the archaeal specific decay rates (k_A). Since the ranges of CI_{95} for k_B were quite wide (about 70–24,000% of the mean), further statistical analysis for k_B was not conducted in this study.

5.3.6. Correlation of archaeal specific decay rates to undissociated species

Next, since the weak-acid species present in the cultures were protonated in a certain extent under the low pH environment, the correlations of the archaeal specific decay rates to the total undissociated concentrations (unVFA + phosphoric acid + carbonic acid) were analysed to investigate whether the undissociated fraction was also the factor leading to the acceleration of archaeal death. As shown in **Figure 5.11**, it appeared that the plots of archaeal specific decay rate (k_A, d^{-1}) vs. the total undissociated concentration (mM) were totally scattered and no clear correlation was found. For instance, at about 25 mM of the total undissociated species, the k_A values highly varied in the range of 0.2 d^{-1} (at pH 6.0) and 1.6 d^{-1} (at pH 4.0) for both cultures. These scattered plots indicated that the sensitivity of the total undissociated concentration on archaeal specific decay rate was very low. Furthermore, comparable k_A values were seen along with the total undissociated concentration when the incubation pH was the same. For the datasets of pH 4.0, the k_A values of both cultures were about 1.6 d^{-1} and consistent irrespective of the total undissociated concentration (25-80 mM) showing very low r^2 on the correlation ($r^2 = 0.027$). Only the datasets of pH 5.5 for the formate-fed culture showed relatively high r^2 ($r^2 = 0.802$). But this high r^2 value was yielded from one outlier out of the six estimates where all estimated k_A had a comparable CI_{95} to each other. As shown in **Figure 5.12** and **Figure 5.13**, the scattered plots and the low dependency of undissociated concentration were also recognised when correlations of k_A values were examined with concentrations of unVFA + phosphoric acid, and with concentrations of only unVFA respectively.
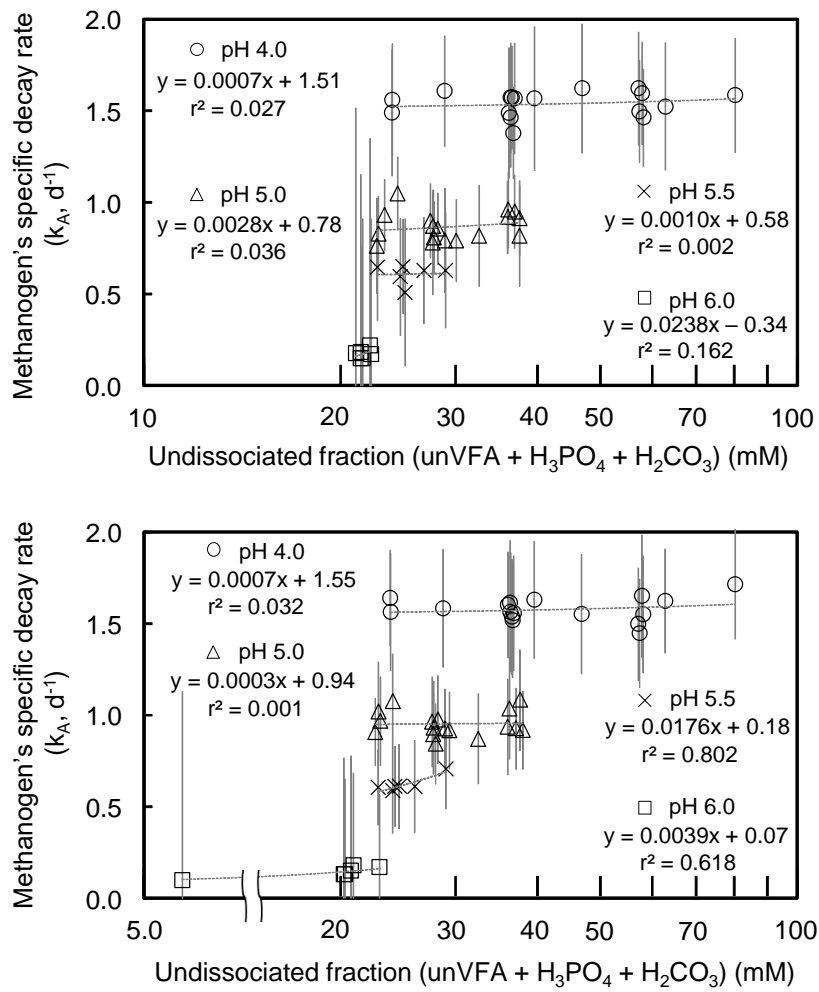
Figure 5.11 Correlation of k_A with undissociated fraction (unVFA + H_3PO_4 + H_2CO_3)

(Upper: Acetate-fed culture, lower: Formate-fed culture, error bar: CI_{95})
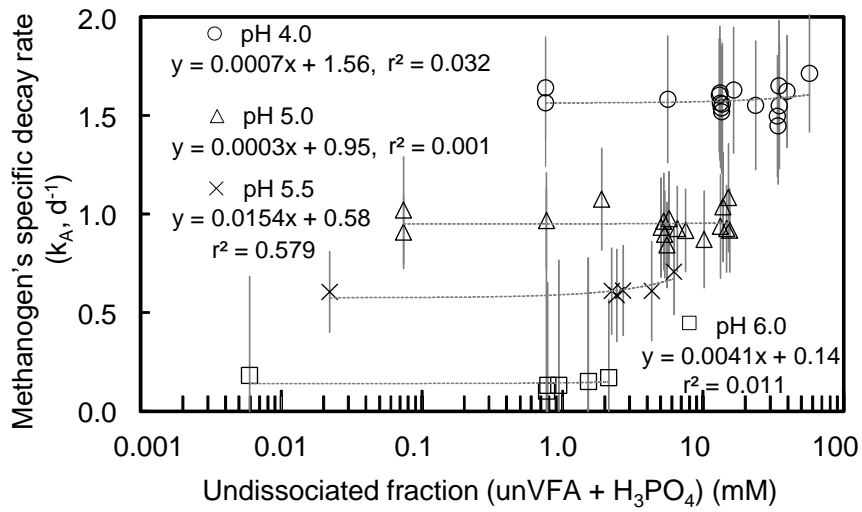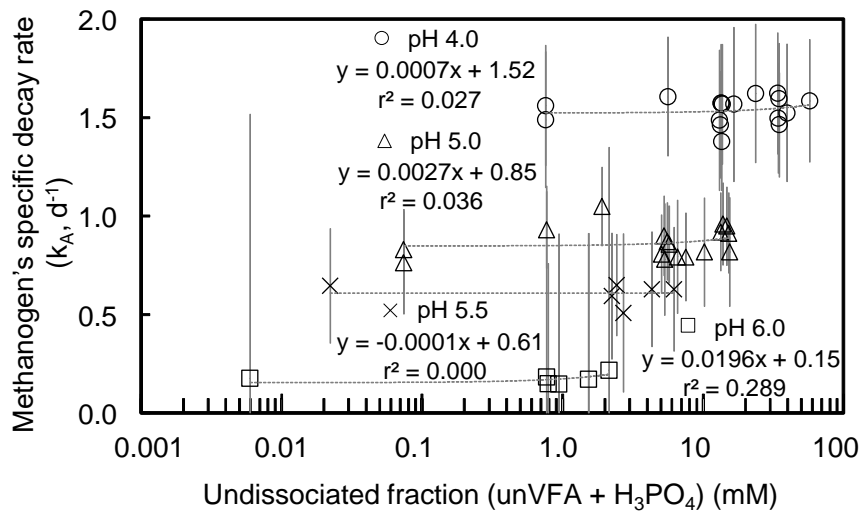
Figure 5.12 Correlation of k_A with undissociated fraction (unVFA + H_3PO_4)

(Upper: Acetate-fed culture, lower: Formate-fed culture, error bar: CI_{95})
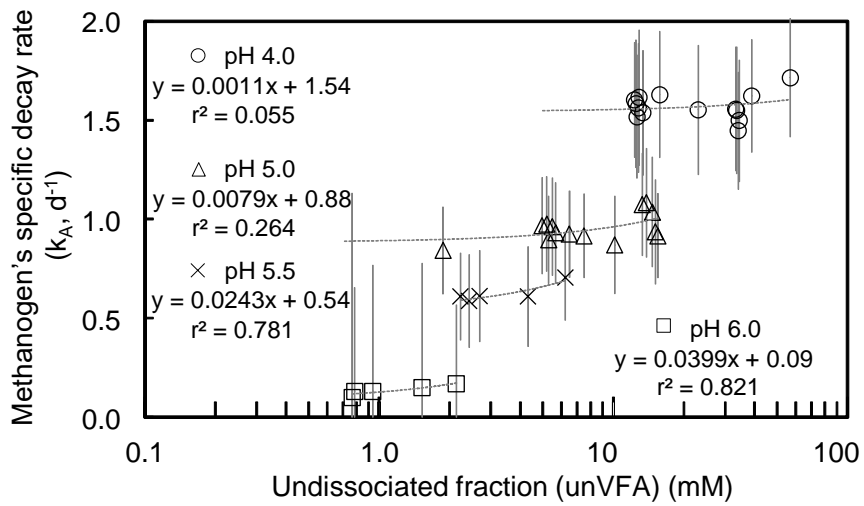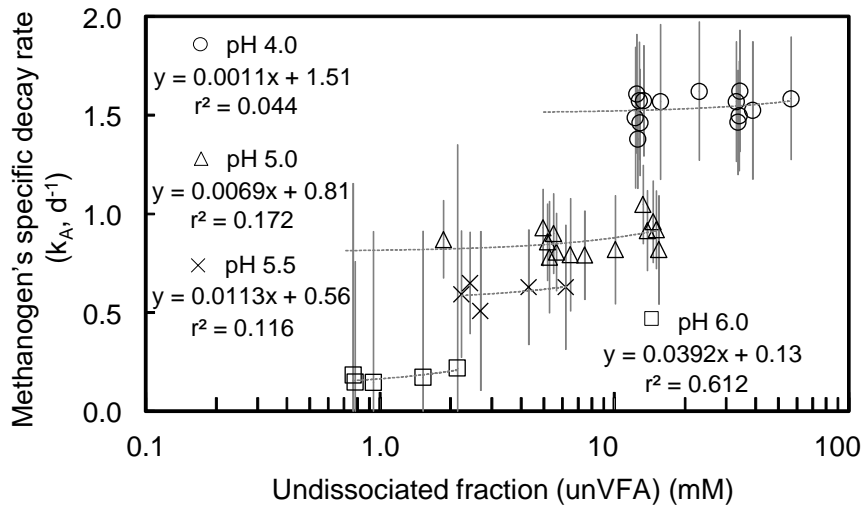
Figure 5.13 Correlation of k_A with undissociated fraction (unVFA)

(Upper: Acetate-fed culture, lower: Formate-fed culture, error bar: CI_{95})

Generally, the protonation due to low pH is supposed to facilitate the passive transport of the undissociated molecules across the cell membrane, and consequently its intra-cellular deprotonation creates the microbial inhibition on growth. In ADM1, the microbial growth inhibition is modelled in such a way that the undissociated fraction is the function of pH and pKa. For the biocidal effect, which has not been modelled in ADM1, the experimental results revealed that low pH (high proton concentration) was a primary factor leading to the acceleration of archaeal death. To map the growth inhibition and the biocidal effect on the model, the apparent microbial specific growth rate (μ_{app}) can be expressed by a formula of $\mu_{max} \cdot \Pi(I_j) - \Sigma(b_k)$ when the substrate concentration is high enough (where μ_{max} is the maximum specific growth rate, I_j is the inhibition switching function ($0 \leq I_j \leq 1$) for the state variable j ($j = 1\ldots j\ldots m$), and b_k is the specific decay rate mediated by the inhibition factor k ($0 \leq b_k$, $k = 1\ldots k\ldots n$)). The state variable j is defined as one of the undissociated species present in the system whilst one of b_k is the elevated stochastic probability of the microbial death which is a function of proton concentration. In this way the effect of undissociated fraction and the effect of pH are mathematically decoupled from each other in the model. Each inhibition effect is placed in either growth process (growth inhibition = reduction of reaction rate = reversible inhibition) or decay process (acceleration of microbial death = reduction of active biomass = irreversible inhibition). Accordingly, the model (ADM1) generally adopted in engineering is still hold its structure whilst the biocidal phenomena for methanogen can be additionally included into the model.

5.3.7. Development of biocidal rate expression

The experimental results from this study were used to develop a pH-dependent methanogen decay model. The experimentally determined k_A values from the first-order decay model at each pH were used to simulate the living methanogen concentrations using ADM1. As shown in **Figure 5.14**, a very high value of specific decay rate of methanogens was required to simulate the dynamics of the 6-day acidic incubation. For the incubation of acetate-fed culture at pH 5.0 with 15 mM of acetic acid (15 mM unVFA-C$_2$), remarkable mismatch was found in the simulated and measured total living cell concentration using the default model for methanogen's specific decay rate of 0.02 d^{-1}. The calculated acetate uptake was almost zero due to the pH inhibition in the methanogen's growth process as described in ADM1. To match the

measured total living cell concentration to simulation, a specific decay rate value of 0.9 d^{-1} was required. A slight increase in acetate concentration at high specific decay rate was created because of acidification of the decayed biomass. The mismatch for living cell concentration was recognised in the datasets until pH 6.0 including those of the formate-fed culture.
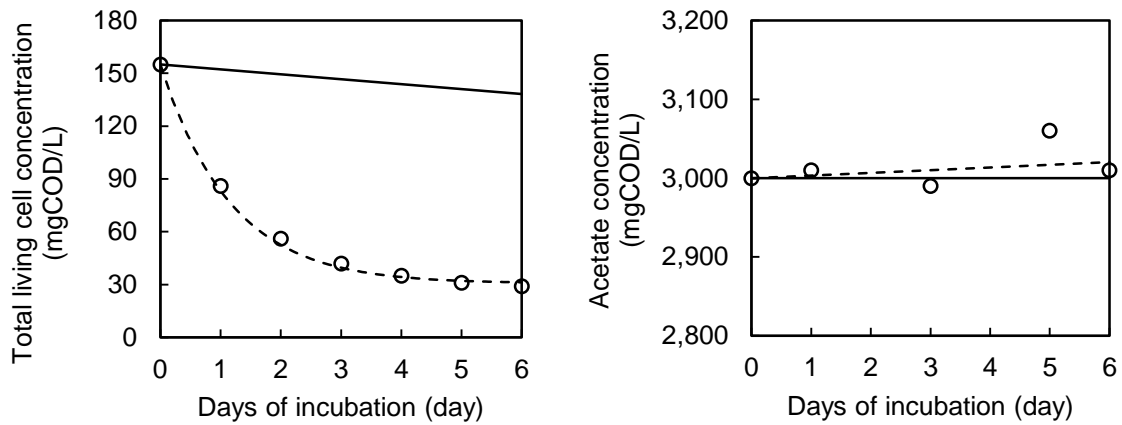

Figure 5.14 Dynamic simulations for living cell concentration and acetate uptake during incubation of acetate-fed culture at pH = 5.0 using 15 mM of acetic acid. (plot: data, line: simulation with methanogen's decay b = 0.02 d^{-1}, dashed-line: simulation with methanogen's decay b = 0.9 d^{-1})

These dynamic simulations are shown in the supplementary materials of **Figure 5.15** (dynamics of VFAs for the acetate-fed culture), **Figure 5.16** (dynamics of VFAs for the formate-fed culture) and **Figure 5.17** and **Figure 5.18** (dynamics of the total living cell concentrations) respectively.

#1A, 15 mM-unC1 pH 4.0

#2A, 40 mM-unC1 pH 4.0

#3A, 3 gCOD/L-C1 pH 4.0

#4A, 15 mM-unC2 pH 4.0

#5A, 40 mM-unC2 pH 4.0

#6A, 3 gCOD/L-C2 pH 4.0

#7A, 15 mM-unC3 pH 4.0

#8A, 40 mM-unC3 pH 4.0

#9A, 3 gCOD/L-C3 pH 4.0

#10A, 15 mM-unC4 pH 4.0

#11A, 40 mM-unC4 pH 4.0

#12A, 3 gCOD/L-C4 pH 4.0

#13A, 15 mM-unC5 pH 4.0

#14A, 40 mM-unC5 pH 4.0

#15A, 3 gCOD/L-C5 pH 4.0

#16A, 30 mM-PBS pH 4.0

#17A, 30 mM-PBS pH 4.0

#18A, 15 mM-unC1 pH 5.0

#19A, 40 mM-unC1 pH 5.0

#20A, 3 gCOD/L-C1 pH 5.0

#21A, 15 mM-unC2 pH 5.0

#22A, 40 mM-unC2 pH 5.0

#23A, 3 gCOD/L-C2 pH 5.0

#24A, 15 mM-unC3 pH 5.0

Axis labels: C1 concentration (g-COD/L), C2 concentration (g-COD/L), C3 concentration (g-COD/L), C4 concentration (g-COD/L), C5 concentration (g-COD/L), VFAs concentration (mg-COD/L), Other VFAs conc. (mg-COD/L), Days of incubation (day)

104

Figure 5.15 VFA concentrations during batch incubations for acetate-fed culture

(Plot: measured, curve: dynamic simulation using ADM1 using calibrated methanogen's specific decay rate in this study, arrow: adjustment of VFA feeding rate, ○: Formate, □: Acetate, △: Propionate, ×: Butyrate, ◇: Valerate)

106
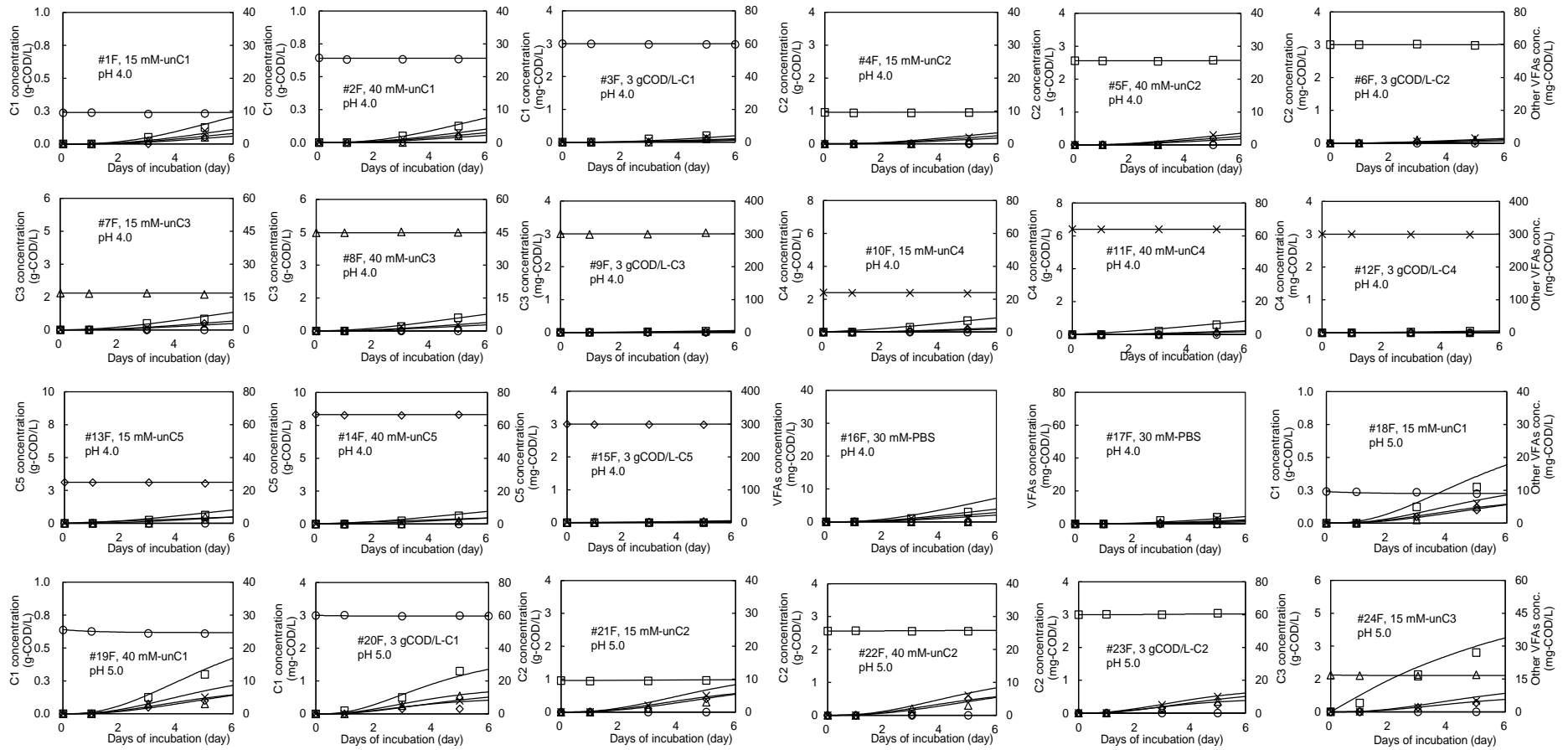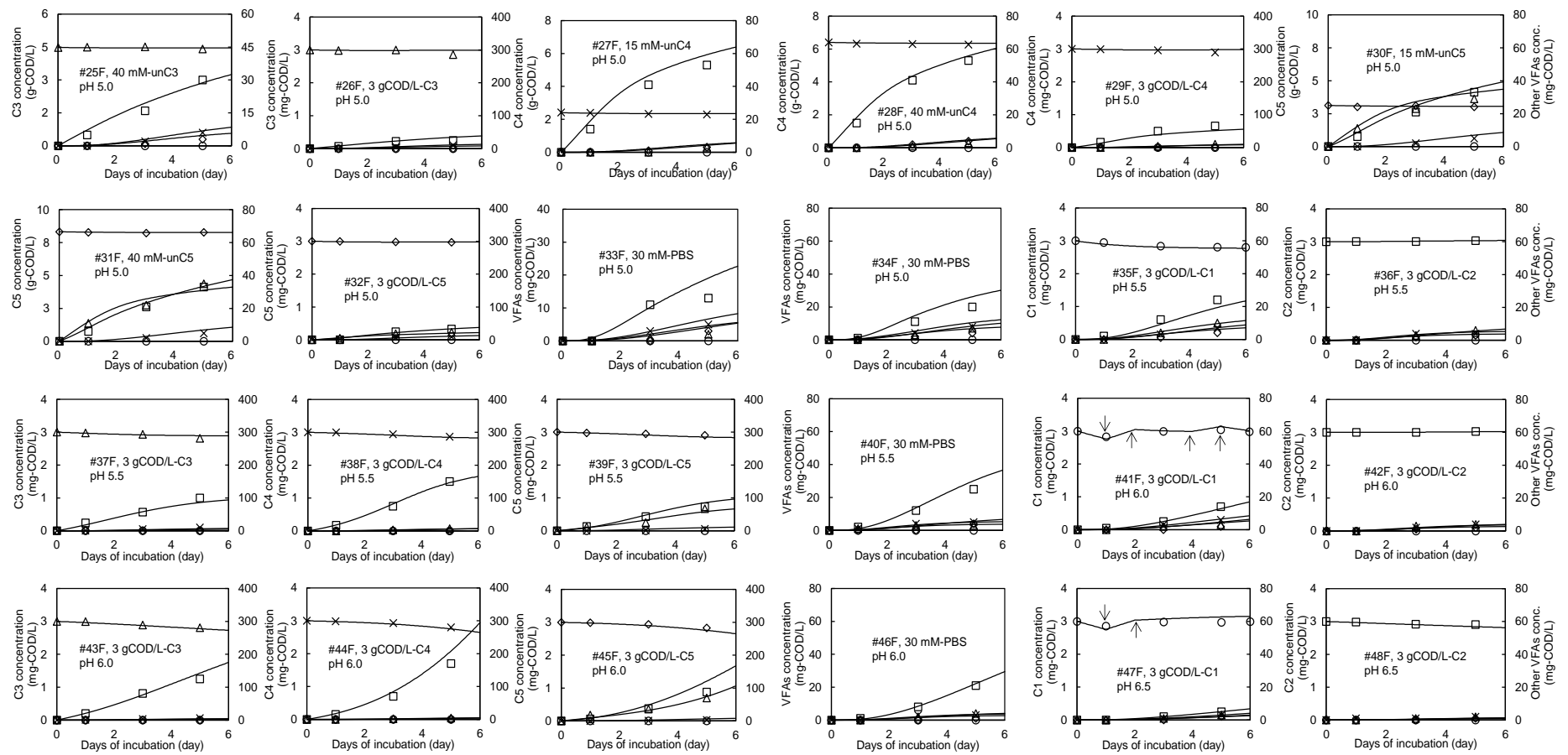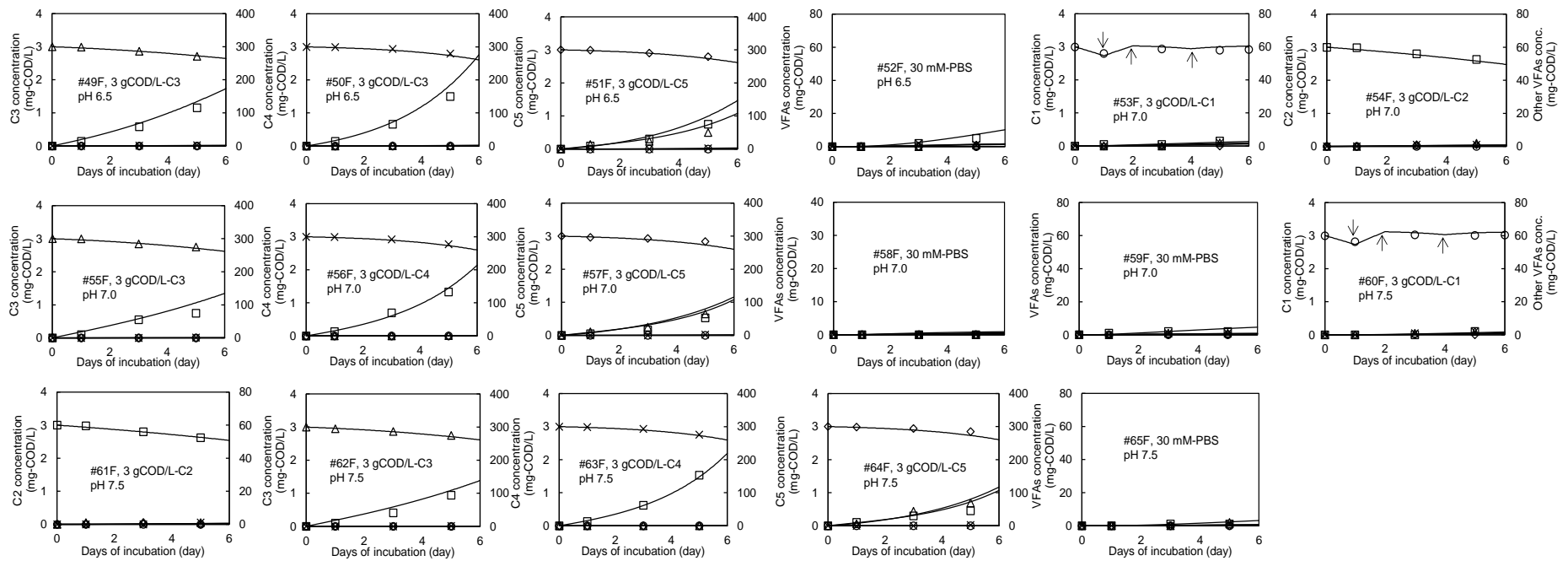
Figure 5.16 VFA concentrations during batch incubations for formate-fed culture

(Plot: measured, curve: dynamic simulation using ADM1 using calibrated methanogen's specific decay rate in this study, arrow: adjustment of VFA feeding rate, ○: Formate, □: Acetate, △: Propionate, ×: Butyrate, ◇: Valerate)
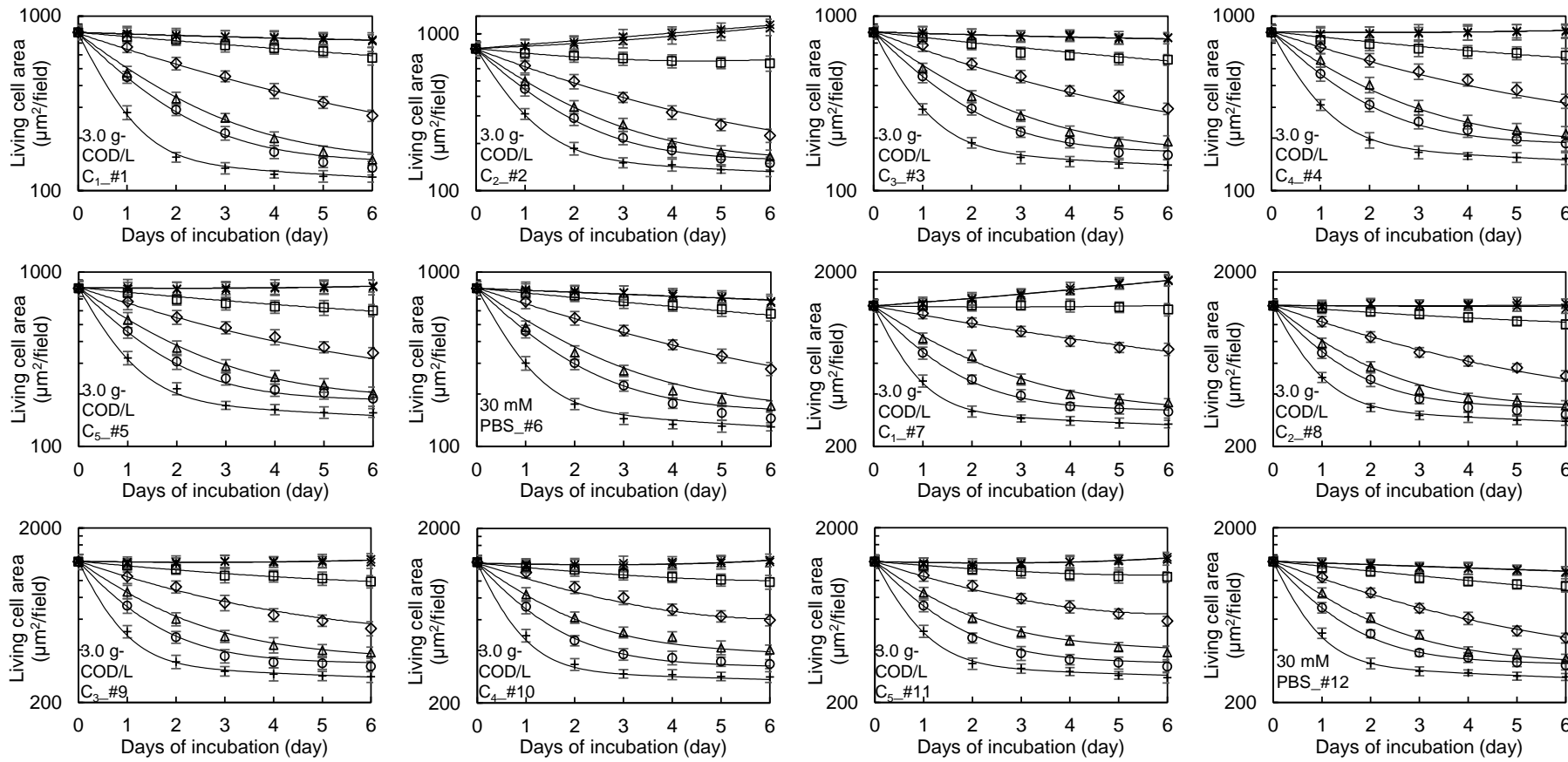
Figure 5.17 Total living cell concentrations during batch incubations

(#1–#6: acetate-fed culture, #7–#12,: formate-fed culture, plot: mean data plot, bar: 95%-confidence interval, curve: simulation using ADM1

with the calibrated methanogen's specific decay rates in this study,

+: pH 4.0, ○: pH 5.0, △: pH 5.5, ◇: pH 6.0, □: pH 6.5, ×: pH 7.0, ✳: pH 7.5)
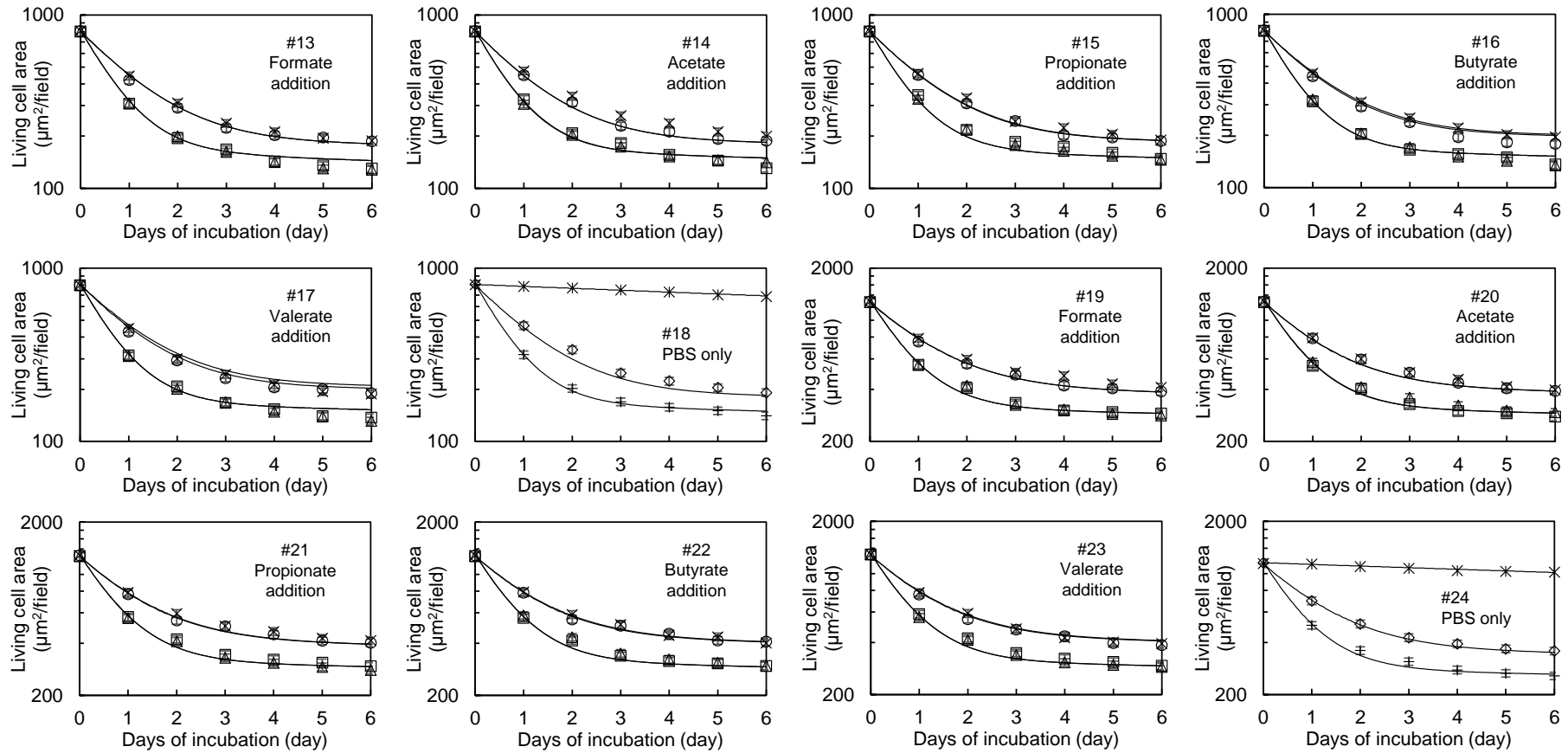
Figure 5.18 Total living cell concentrations during batch incubations

(#13–#18: acetate-fed culture, #19–#24: formate-fed culture, plot: mean data plot, bar: 95%-confidence interval, curve: dynamic simulation

using ADM1 using the calibrated methanogen's specific decay rates in this study,

□: 15 mM-unVFA at pH 4.0, △: 40 mM-unVFA at pH 4.0, ×: 15 mM-unVFA at pH 5.0, ○: 40 mM-unVFA at pH 5.0, ＋: 30 mM-PBS at pH 4.0,

◇: 30 mM-PBS at pH 5.0, ＊: 30 mM-PBS at pH 7)

As shown in **Figure 5.19** (the Acetate-fed culture) and **Figure 5.20** (the Formate-fed culture), when the cultures were incubated in the various pH and acidic species/concentrations, higher cellular decay was recognised in lower pH for both cultures. Overall, even the acidic species and its concentrations were varied, the experimental data (total living cells vs. incubation time) of each acidic incubation were comparably plotted to those conducted in the same pH. Slight microbial growth was recognised in the near-neutral pH of 7.0–7.5 where the VFAs were dosed. Except the experiments, all incubations yielded a reduction of total living cells, and the nonlinearity of data plots was stimulated when the incubation pH was lowered. These results were consistent with those obtained in the aforementioned PMA-qPCR analysis.
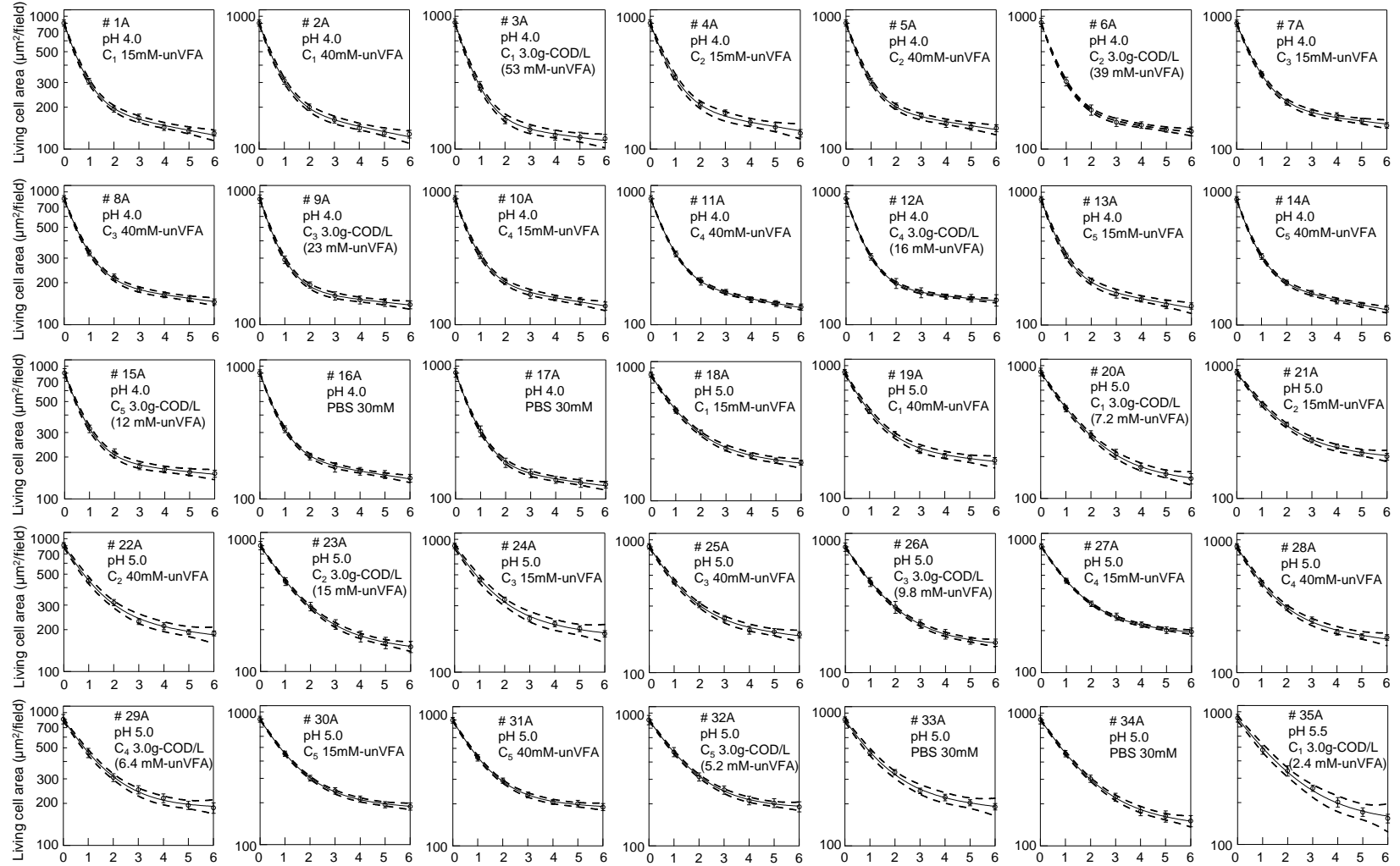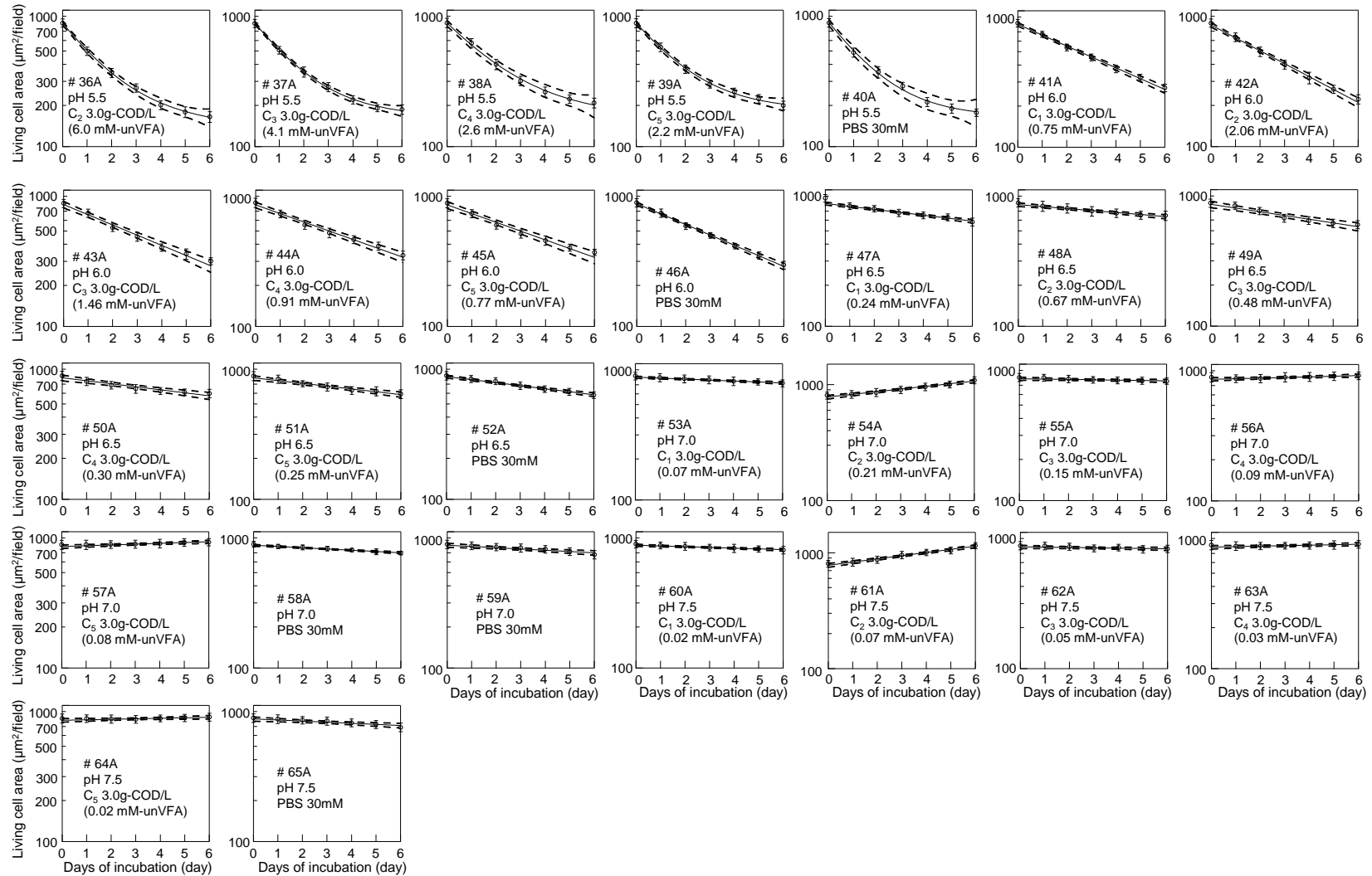
Figure 5.19 Total living cells of Acetate-fed culture in incubations with various pH and acidic species (#: dataset number, plot: the mean of microscopic observation, error bar: CI$_{95}$ of the mean, line: regression curve, dashed-line: CI$_{95}$ of the regression)

1F pH 4.0 C_1 15mM-unVFA

2F pH 4.0 C_1 40mM-unVFA

3F pH 4.0 C_1 3.0g-COD/L (53 mM-unVFA)

4F pH 4.0 C_2 15mM-unVFA

5F pH 4.0 C_2 40mM-unVFA

6F pH 4.0 C_2 3.0g-COD/L (39 mM-unVFA)

7F pH 4.0 C_3 15mM-unVFA

8F pH 4.0 C_3 40mM-unVFA

9F pH 4.0 C_3 3.0g-COD/L (23 mM-unVFA)

10F pH 4.0 C_4 15mM-unVFA

11F pH 4.0 C_4 40mM-unVFA

12F pH 4.0 C_4 3.0g-COD/L (16 mM-unVFA)

13F pH 4.0 C_5 15mM-unVFA

14F pH 4.0 C_5 40mM-unVFA

15F pH 4.0 C_5 3.0g-COD/L (12 mM-unVFA)

16F pH 4.0 PBS 30mM

17F pH 4.0 PBS 30mM

18F pH 5.0 C_1 15mM-unVFA

19F pH 5.0 C_1 40mM-unVFA

20F pH 5.0 C_1 3.0g-COD/L (7.2 mM-unVFA)

21F pH 5.0 C_2 15mM-unVFA

22F pH 5.0 C_2 40mM-unVFA

23F pH 5.0 C_2 3.0g-COD/L (15 mM-unVFA)

24F pH 5.0 C_3 15mM-unVFA

25F pH 5.0 C_3 40mM-unVFA

26F pH 5.0 C_3 3.0g-COD/L (9.8 mM-unVFA)

27F pH 5.0 C_4 15mM-unVFA

28F pH 5.0 C_4 40mM-unVFA

29F pH 5.0 C_4 3.0g-COD/L (6.4 mM-unVFA)

30F pH 5.0 C_5 15mM-unVFA

31F pH 5.0 C_5 40mM-unVFA

32F pH 5.0 C_5 3.0g-COD/L (5.2 mM-unVFA)

33F pH 5.0 PBS 30mM

34F pH 5.0 PBS 30mM

35F pH 5.5 C_1 3.0g-COD/L (2.4 mM-unVFA)

Living cell area (μm^2/field)

Figure 5.20 Total living cells of formate-fed culture in the incubations with various pH and acidic species (#: dataset number, plot: the mean of microscopic observation, error bar: CI$_{95}$ of the mean, line: regression curve, dashed-line: CI$_{95}$ of the regression)

115

The relationship between pH and the experimentally determined values of methanogen specific decay rate (k_A) was expressed using **Equation 5.4** [5]. The proposed equation increases the specific decay rate at low pH conditions. According to the proposed expression, at a pH value equal to the lower limit pH (pH_{LL}), the value of pH inhibition factor I_{pH} becomes 0.05 (I_{pH} = exp (-3)) leading to 20 times increase in the methanogen decay rates. The high level of pH (pH_{UL}) is the threshold pH at which the acceleration of biomass decay is initiated. The power coefficient (n) is to adjust the shape of the curve between the plots. As the switching function (I_{pH}) ranges between zero to one, the specific decay rate changes between b and infinity.

$$
\begin{cases}
k_A = \dfrac{b}{I_{pH}} \\[2ex]
I_{pH} = \exp\left(-3\left(\dfrac{pH_{UL} - pH}{pH_{UL} - pH_{LL}}\right)^n\right) \\[2ex]
I_{pH} = 1 \quad \text{if } pH \geq pH_{UL}
\end{cases}
\qquad \text{Equation 5.4}
$$

Where, k_A = methanogen's specific decay rate (d^{-1}), b = specific decay rate of methanogens without low-pH inhibition (d^{-1}), I_{pH} = empirical lower-only inhibition switching function (-), n = coefficient (-), pH = pH in the system (-), pH_{UL} = upper limit of pH where low-pH inhibition is initiated (-), pH_{LL} = lower limit of pH (-)

Assuming that pH_{UL}, pH_{LL} and n are independent of the acidic species present in solution, the datasets for pH 4.0–6.0 of the acetoclastic and hydrogenotrophic methanogen-enriched cultures were combined separately. Next, **Equation 5.2** was rewritten as **Equation 5.5** by inputting **Equation 5.4**. The value of b was fixed at 0.02 d^{-1} based on the experimental results.

$$\begin{cases} a_{A(t)} = a_{A(0)} \cdot \exp\left(-\dfrac{b}{I_{pH}} \cdot t\right) \\[2mm] a_{B(t)} = a_{B(0)} \cdot \exp\left(-b \cdot t\right) \\[2mm] a_{T(t)} = a_{A(t)} + a_{B(t)} \\[2mm] \end{cases}$$

Equation 5.5

Using **Equation 5.4**, (total living cell area $= f$ (pH, time)), a three-dimensional regression was conducted, and the covariance matrices were obtained in **Table 5.9** accordingly. The calculated value of pH_{UL}, pH_{LL} and n in the biocidal model for acetoclastic methanogen were estimated to be 6.30, 5.74 and 0.25 respectively. For the hydrogenotrophic methanogen, the parameter values were 6.23, 5.73 and 0.24.

Table 5.9 List of three-dimensional regression for pH inhibition between pH 4.0 and pH 6.0

Acetate-fed culture (data plots = 28,980)		Covariance matrix			
$b = 0.02$ d^{-1}			pH_{UL}	pH_{LL}	n
$a_{A(0)} = 628$ μm^2/field	$a_{B(0)} = 176$ μm^2/field	pH_{UL}	$5.11 \cdot 10^{-4}$	$-9.50 \cdot 10^{-5}$	$1.80 \cdot 10^{-4}$
$pH_{UL} = 6.30$ (CI$_{95}$ = 6.28–6.32) $pH_{LL} = 5.74$ (CI$_{95}$ = 5.73–5.74)		pH_{LL}		$4.40 \cdot 10^{-5}$	$-4.25 \cdot 10^{-5}$
$n = 0.25$ (CI$_{95}$ = 0.24–0.26)		n			$6.93 \cdot 10^{-5}$
Formate-fed culture (data plots = 28,980)		Covariance matrix			
$b = 0.02$ d^{-1}			pH_{UL}	pH_{LL}	n
$a_{A(0)} = 912$ μm^2/field	$a_{B(0)} = 365$ μm^2/field	pH_{UL}	$2.72 \cdot 10^{-4}$	$-7.27 \cdot 10^{-5}$	$1.12 \cdot 10^{-4}$
$pH_{UL} = 6.23$ (CI$_{95}$ = 6.22–6.25) $pH_{LL} = 5.73$ (CI$_{95}$ = 5.72–5.74)		pH_{LL}		$4.01 \cdot 10^{-5}$	$-3.70 \cdot 10^{-5}$
$n = 0.24$ (CI$_{95}$ = 0.24–0.25)		n			$5.08 \cdot 10^{-5}$

To visualise the stochastic range of methanogen's specific decay rate at different pH, 1,000 sets of pH_{UL}, pH_{LL} and n were generated from the covariance matrix by a Monte-Carlo simulation equipped with Gibbs-sampler where the data plots were assumed to be scattered in a normal distribution. Subsequently, the produced 1,000 non-linear curves were overlapped with each other to create grey-scale in a graph. As shown in **Figure 5.21**, the grey-scale area of graph appeared in a very narrow range between pH 4.0 and about pH 6.3 (graph A = the Acetate-

fed culture, graph B = the Formate-fed culture). Overall, the grey-scale area became narrow along the pH from 4.0 to 6.0, and became slightly wider at about pH 6.3 (around pH_{UL}). Nevertheless, since the Monte-Carlo simulation yielded the curves similar to each other, the grey-scaled methanogen' specific decay rate was displayed like a single curve along with pH for both cultures. In addition, the parameter values between the acetate-fed culture and the formate-fed culture were highly comparable to each other.
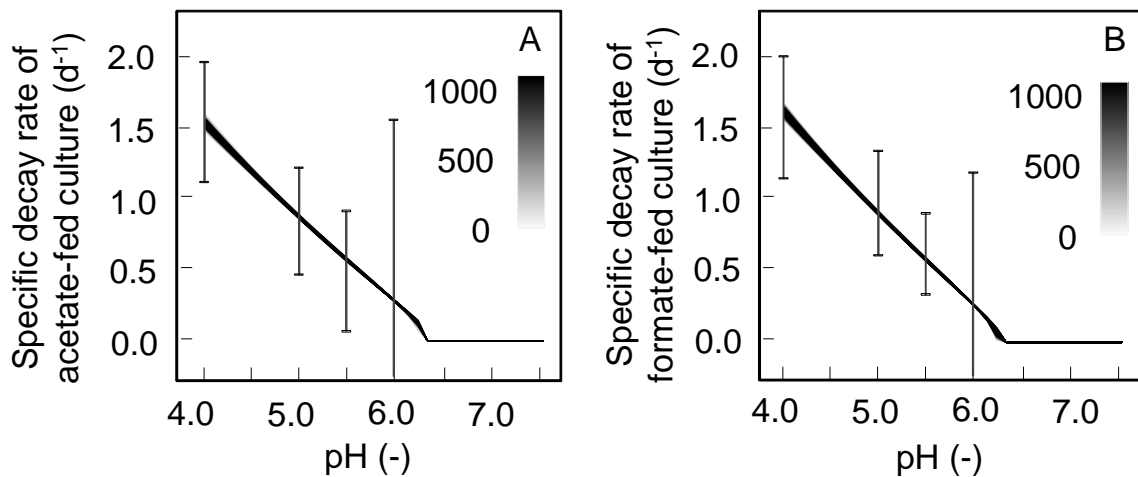
Figure 5.21 Specific decay rates of methanogens along with pH
(Graph A: acetate-fed culture, graph B: formate-fed culture),
(error bar: the range between the highest upper CI_{95} and the lowest lower CI_{95})

The error bars of graph A and graph B (the distance between the highest upper limit of CI_{95} for the maximal k_A and the lowest lower limit of CI_{95} for the minimal k_A) protruded from the grey-scaled methanogen' specific decay rate. The upper curve covering the highest upper limit of CI_{95} below pH 5.5 was intended to allow a conservative calculation for the low pH inhibition (the methanogen-wide specific decay rate plus about 0.4 d^{-1}). This parameter set may be used for plant operation and/or process design, which has a safety margin to avoid the unwanted risks from the acidic failure. For the lower curve covering the lowest lower limit of CI_{95} below pH 5.5, this would yield an optimistic calculation result for the acidic failure (the methanogen-wide specific decay rate minus about 0.4 d^{-1}). Using this parameter set, it is possible to ensure the acidifying process for VFA recovery.

The methanogens' biocidal phenomena found in this study may convince plant operators that immediate pH neutralisation is priority when the reactor pH is decreasing below the

acceptable level. This imperative task has not been pointed out in the previous studies for operation of anaerobic plants. Due to the lack of this awareness, some anaerobic plants are obliged to spend time until recovery from the acidic failure, which could have been avoided if the pH neutralisation had been immediately carried out [134,156]. In case that anaerobic reactor is acidified due to overloading and laid aside for even a week without remedial treatment, about 4 weeks of restart-up period is needed until the full-recovery of methanogenic biomass [5]. The biocidal model developed in this study may provide technical insights for the malfunctioned anaerobic plants in acidic failure and/or to maintain intentional acidification for VFA recovery purpose, which are not equipped with other mathematical models (*e.g.* ADM1). The experimental results of the study showed that the methanogens could be irreversibly inactivated by the low pH induced by the acidogens simultaneously present in the system. However, it should be noted that the set of the estimated biocidal parameter values might not be able to apply to the full-scale plants straightforward. This is because the archaeal species of the cultures were not genetically analysed in this study, which might somewhat differ from those present in full-scale anaerobic reactors. Hence model validation using continuous anaerobic reactors (*e.g.*, at full-scale biogas plant) including analysis of microbial population dynamics is desired in future studies. Nevertheless, the concept of the biocidal model may find significant applicability in developing operational strategies of anaerobic plants and also assessing other inhibitory compounds (*e.g.* H_2S).

5.3.8. Recovery of methanogenic activity after low pH environment

At the end of batch experiment at low pH (Set-II), the recovery of methanogenic activity was examined by increasing the pH of batch reactor and adding respective substrate (Acetate/Formate). As shown the results in **Figure 5.22**, the response of the sludge in the flasks initially set at pH 5.1 ($\times$) was distinct from those kept at pH 7.0 ($\bigcirc$). The addition of substrate to the flasks kept at pH of 7.0 showed quick conversion of external substrate to CH_4 within 1~2 days. As the observed CH_4 production rate was comparable to that from the freshly collected sludge from the chemostat reactor ($\square$), the methanogenic reaction rate under pH 7.0 seemed to be maintained even after 6 days of the incubation without substrate. On the other hand the sludge of the flasks initially set at pH of 5.1 required almost 18~20 days to complete the CH_4 production. This indicated that enhanced decay of methanogen at pH of 5.1 led to significant loss of methanogenic biomass causing a recovery lag.
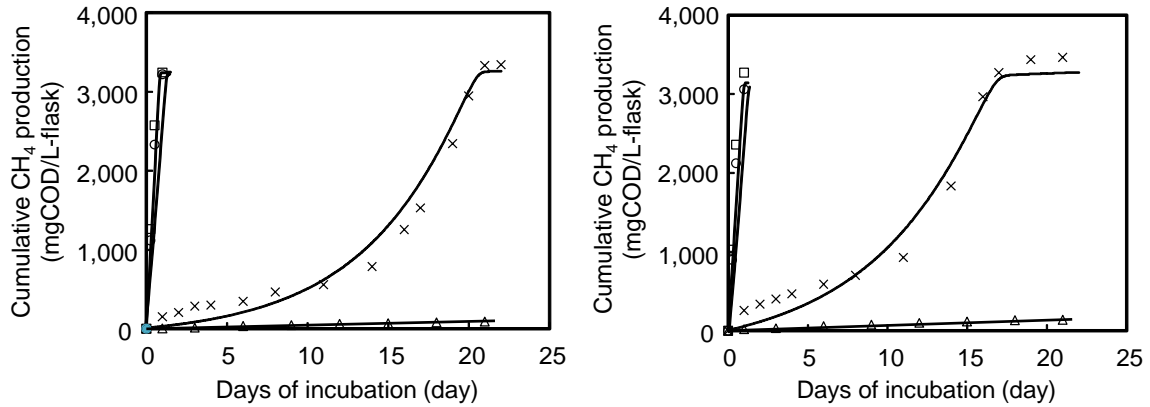
Figure 5.22 Recovery of methanogenic activity after low pH environment set pH at 5.1

(Left: Acetate-fed system, right: Formate-fed system)

□: sludge freshly corrected from the chemostat reactor with substrate

○: sludge with 6-day starvation under pH =7.0 followed by addition of substrate

×: sludge with 6-day starvation under pH = 5.1 followed by addition of substrate

△: sludge freshly corrected from the CSTR reactor without addition of substrate (blank)

Line: simulation with ADM1

Since more methanogenic biomass decay was anticipated when the culture was exposed to lower pH (and longer sludge retention in the acidic environment), the above experimental results could explain the reason of the noticeably delayed recovery from the severe acidic failure (pH = 5.4 for 2 weeks) and the relatively fast recovery from the moderate failure (pH = 5.9 for 8 days) experienced by Zhang *et al.* (2012) and Capson-Tojo *et al.* (2017) respectively which were described in the introduction section [157].

5.3.9. Impact of accelerated methanogen's decay on biogas plant

To highlight the significance of the results in this study, the time periods required for process recovery of a virtual biogas plant with/without the enhanced decay during acidic failure were comparatively discussed using ADM1. The acidic failure was simulated by feeding a high load of monosaccharide to the reactor followed by a sudden pH drop to pH = 5.0. As soon as the pH dropped, the plant operator discontinued the influent feeding for 5 days. After 5 days, the reactor pH in the reactor was adjusted to 7.0 by alkali dosing. To express the acceleration

120

of the methanogen decay, a low-pH inhibition switching function of I_{pH} ($0 < I_{pH} \leq 1$) was developed for the specific decay rates of methanogens. As shown in **Equation 5.6**, the proposed switching function was a modification of the pH inhibition function used in ADM1 for the growth inhibition [12]. In the proposed equation, the value of values of n, pH_{UL} and pH_{LL} were used 0.25, 6.6 and 5.9 respectively. The low level of the pH (pH_{LL}) was such that it resulted in specific decay rate as high as about 20 times (I_{pH} = exp(-3) $\approx$ 0.05).

$$\begin{cases} k_b = \dfrac{b}{I_{pH}} \\ I_{pH} = \exp\left(-3\left(\dfrac{pH_{UL} - pH}{pH_{UL} - pH_{LL}}\right)^n\right) \\ I_{pH} = 1 \text{ if } pH \geq pH_{UL} \end{cases}$$

Equation 5.6

Where, k_b = specific decay rate of methanogens (d^{-1}), b = specific decay rate of methanogens without low-pH inhibition (d^{-1}), I_{pH} = empirical lower-only inhibition switching function (-), pH = pH in the system (-), pH_{UL} = upper level pH where low-pH inhibition is initiated (-), pH_{LL} = lower level pH, n = power coefficient (-).

As shown in **Figure 5.23**, without using the pH inhibition function on decay, the process performance was instantly recovered from the acidic failure when the reactor pH was neutralised. After the pH neutralisation, the plant could produce biogas from the VFAs accumulated in the reactor. This simulation behaviour suggested that a plant operators could achieve normal operation after adjusting the pH in digester, which was quite contrary to the reported observations. On the other hand, in the simulations with the pH inhibition function on decay, the concentration of methanogenic biomass was reduced by 90% during the acidic failure event for 5 days. Consequently, even after neutralisation of the reactor pH, almost no CH_4 gas was produced. The VFAs accumulated in the reactor were not quickly decomposed, and about 18 days of the operation pause was needed until the VFAs concentration reached a reasonable level. Furthermore, as the methanogenic biomass concentration in the reactor was still low, the influent loading needed to be controlled until the VFA concentration reduced to an acceptable level. The simulation results suggested that the full recovery of the methanogenic biomass would require about 30 days. The results of this study suggested that control strategies for

digester operation would need to focus on good pH management in digesters to minimise the risk of losing the methanogenic biomass in the reactor that would require long recovery period.
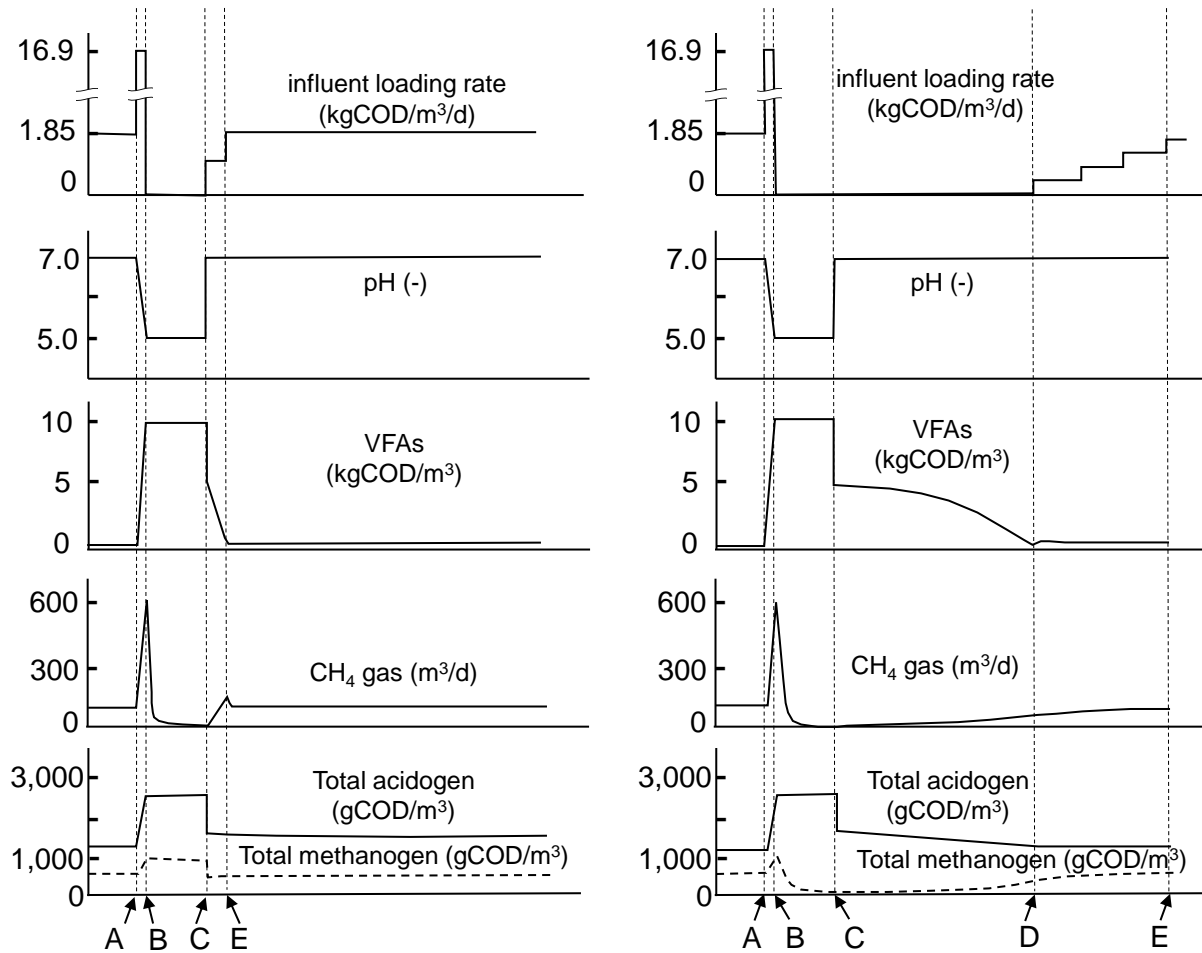
Figure 5.23 Dynamic simulations with/without enhanced methanogen decay in acidic failure. (Left: ADM1 w/o the enhanced decay, right: ADM1 with the enhanced decay) Normal operation: ~A, High load: A~B, Discontinuation of influent feeding: B~C, Adjustment of reactor pH: C, Restart: D, Full recovery of methanogen biomass: E~

5.4. Conclusions

The effect of low-pH inhibition on anaerobic microorganism was investigated using different experimental techniques. In the presence of acidic species (either formic acid, acetic acid, propionic acid, butyric acid, valeric acid or phosphoric acid), its biocidal effect on methanogens was analysed using the set of batch incubation tests. The experimental data was further validated through anaerobic digestion modelling. The key conclusions from this study are listed below:

1) Low pH conditions enhance the decay rate of methanogenic microorganisms causing irreversible inhibition. At pH = 5.1, almost 90% of acetoclastic methanogen and hydrogenotrophic methanogen were lost from the cultures within 6 days of incubation. Whereas, the acidogenic bacteria were found to be more tolerant to the acidic environment.

2) The low-pH inhibition was mainly attributed to the proton concentration in the system. The inhibition response at pH = 5.1 with 50 mmol-P/L of phosphate buffer was comparable to that with 0.5 mmol-P/L, thus ruling out the effect of phosphate buffer on decay rate.

3) Number of living microbial cells measured with the commercial fluorescent kit was comparable to those detected with PMA-qPCR method. The active biomass concentration predicted by ADM1 also correlated well to the measured values from the fluorescent cell staining method and the PMA-qPCR method.

4) Incorporation of the mechanism of irreversible low-pH inhibition on methanogen decay was able to simulate the delay in CH_4 generation for a plant recovering after acidic failure. When the reactor was exposed to low pH at 5.0 for 5 days, more than 30 days were needed until the methanogenic biomass in the reactor was fully recovered.

5) The biomass loss of methanogenic archaea was accelerated in low pH stress. The level of stress was independent of the constituent of acidic species and/or its concentration. The PMA-qPCR analysis detected the biocidal phenomena in the acetoclastic methanogen-enriched culture, the hydrogenotrophic methanogen-enriched culture and the methanogens present in the anaerobic digestate respectively.

6) From the living cell counting method, the irreversible pH inhibition was recognised when the incubation pH was lowered from about pH 6.5. The biocidal effect reached 40-folds when the incubation was conducted at pH 5.0 (methanogen's specific decay rate: 0.02 d^{-1}

at pH 7.0–7.5 → *ca.* 0.86 d^{-1} at pH 5.0).

7) The impacts of undissociated species concentration on the biomass decay were negligibly small comparing to the low pH stress. When the experimental pH was the same, the specific decay rates were comparable to each other. No clear correlation of the specific decay rates with the undissociated species was found until 80 mM of total undissociated species including unVFAs, phosphoric acid and carbonic acid.

8) From the experimental datasets, the low-pH inhibition kinetics were obtained to model the biocidal phenomena in the empirical formula. Moreover, to calculate the potential risks of acidic failure into the design and operation of anaerobic reactors, and to obtain preferable operating conditions for VFA recovery reactors, a parameter set was provided respectively.

CHAPTER 6. MODIFYING ADM1 BY ADDITION OF LAG-PHASE SUB-MODEL TO SIMULATE LONG-TERM PH INCUBATION OF METHANOGENIC SYSTEM

6.1. Introduction

Methane fermentation system has been considered a promising low-cost technology for treating high-strength biodegradable organic wastes [158]. Since the system is often designed and operated at high OLR to minimise its investment cost and footprint [86], intermediate products (e.g., VFAs) are occasionally accumulated in very high OLR operation [118]. In case of significant VFA accumulation, the compounds lead to a pH decrease in the reactor, which results in the inhibition of methanogens [119,120]. When the methanogens are inhibited, the biological removal rate of the accumulated VFAs is also proportionally deteriorated. Eventually, this downward spiral may collapse the system (acidic failure).

Apart from the high VFA concentration of the reactor, low pH is also supposed to be one of the factors to reduce the system stability [107,124,125,126]. The accumulated VFAs from the decomposition of the readily biodegradable organic wastes are the source of proton, which inhibits methanogens [24]. Undissociated acetate (acetic acid) is also considered to undermine the system when its concentration exceeds the threshold of methanogens [121]. This is because the undissociated VFA species are transferred into the microbial cell by molecular diffusion, leading to the pH decrease in the cytoplasm of the cell [129,130]. The lowered pH (high proton) undermines the microbial metabolisms [132]. Consequently, the microbial growth kinetics are reduced [127,128]. To elucidate the inhibition mechanisms in kinetic manner, an approach is modelling the biological responses with/without presence of the inhibitory compounds.

To model the acidic inhibition of methanogens, numerous studies have been carried out using IWA ADM1, which has been quite widely used for modelling anaerobic systems since its release in 2002 [12,122,123,133,155,159,160]. Since most of the studies model the inhibition phenomena using only pH or undissociated VFAs, this simplification often resulted in noticeable inconsistency against the measured operational data of the CH_4 fermentation systems, particularly in the recovery phase from the inhibition [161,162,163,164,165,166,167,168]. One of the backgrounds of the mismatch is that these models totally ignore the phenomenon of lag phase (gradual recovery of microbial activities from the acidic inhibition). On the other hand, until releasing ADM1 to the field of wastewater treatment engineering, Gompertz-curve model was quite widely used to express the lag phase in batch methene fermentation systems

[169, 170, 171, 172]. This model is composed of a stoichiometric term for maximal CH_4 conversion per unit of substrate, and two kinetic terms for activity delay (lag phase) and specific CH_4 production rate. Since the equation is empirical and cannot evaluate each microbial reaction in the reactor unlike ADM1, the Gompertz-curve model is considered outdated. Also, Gompertz-curve model has been discarded in wastewater treatment engineering because this is only applicable for calculation of batch reactors and not continuous reactors that are applied to full-scale CH_4 fermentation systems. Hence improvement of modelling acidic inhibition and its recovery could be anticipated when the lag phase is additionally equipped with ADM1 for continuous reactors.

Based on the above background, a lab-scale continuous experiment was carried out to simulate the dynamic performance where the methanogen was exposed to low pH with accumulation of acetic acid in the reactor, which was the dominant VFA species in acidic failure events of CH_4 fermentation systems. To focus on the acidic inhibition on the methanogen, acetate was the only organic substrate fed to the continuous reactor whilst the influent concentration was dynamically changed, which allowed to reduce the reactor pH when the influent concentration was high. From the dynamic operation, datasets for the concentrations of acetate and VSS, and the volumetric CH_4 production rate were obtained for the base data of the dynamic simulation.

6.2. Dynamic simulation

ADM1 was adopted to simulate the concentrations of acetate, VSS, active methanogen and the volumetric CH_4 production rate [12]. The kinetic parameters and the stoichiometric parameters for acetoclastic methanogen were dynamically calibrated focusing on the above measured parameter values of acetate, VSS and volumetric CH_4 production rate whilst default parameters of ADM1 were used to express the dynamics of the other microorganisms. To program the model and inhibition equations, a commercial process simulator (GPS-X ver.8.1, Hatch. Ltd, Ontario, Canada) was used. For the above-mentioned parameter calibration of the methanogen (growth, decay and inhibition kinetics, and biomass yield coefficient), maximum likelihood method was chosen (**Equation 6.1**). This was because the method could obtain the optimal parameter estimates (parameters to be calibrated) based on the analytical errors over the differently measured parameters of acetate, VSS and volumetric CH_4 production rate, which

were interrelated in the mathematical model. The optimal parameter estimates were the values yielding minimum F of the equation.

$$F = \frac{1}{2}\sum_{j=1}^{m}\left[n_j\left(\ln\left(2\pi\right)+1\right) + n_j\ln\left(\frac{1}{n_j}\sum_{i=1}^{n_j}\frac{\left(z_{i,j}-f_{i,j}\right)^2}{f_{i,j}^{\gamma_j}}\right) + \gamma_j\sum_{i=1}^{n_j}\ln f_{i,j}\right] \qquad \text{Equation 6.1}$$

Where $z_{i,j}$ = the measured value of response j in experiment i, $f_{i,j}$ = the value of response variable j predicted by the process model in experiment i, γ_j = the heteroscedasticity parameter for response j, m = the number of measured response variables, and n_j = the number of experiments for response j.

6.3. Results and discussion

6.3.1. The estimation of methane production rate and effluent VFA concentrations using ADM1 equipped with low-pH inhibition

It appeared that the default set of kinetic parameters equipped with ADM1 model totally failed to simulate the acetate accumulation and the reduction of volumetric CH_4 production rate over the experimental period of 400 days. Specifically, as shown in **Figure 6.1A**, the acetate concentration of the reactor was highly underestimated in all acidification events. For the acidification events of #1 and #2, although the phenomena of acetate accumulation were somewhat reproduced by the model, the calculated acetate concentration during these acidification events were considerably lower than those of the data plots. Moreover, the model could not simulate the acetate accumulation for the acidification events of #3–#6. Similarly, as shown in **Figure 6.1B**, the volumetric CH_4 production rates were also highly overestimated in all acidification events whereas reasonable CH_4 production was calculated when the acetate accumulation was limited. These simulation results indicated that the ADM1's inhibition kinetic parameter values and/or its inhibition sub-model were not satisfactory and should be revised.

127
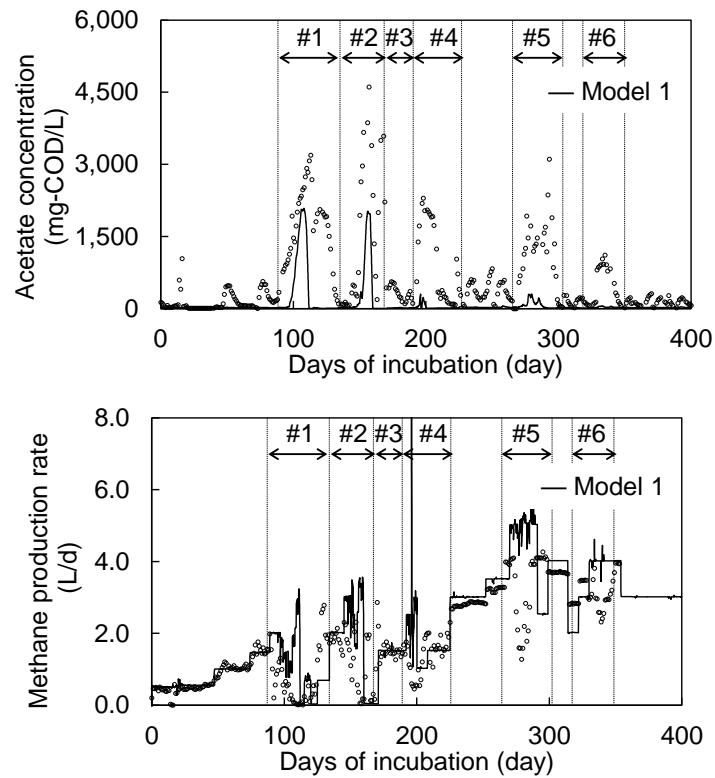
Figure 6.1 Acetate concentration of the reactor (upper: A) and volumetric methane production rate (lower: B)

In ADM1 model, the inhibition phenomena of methanogens on acidification are simplified using an empirical pH sub-model as described in **Equation 6.2**. When the reactor pH is below the threshold of pH lower limit (pH$_{LL}$), methanogenesis is inhibited by 50% or more, leading to the reduction of net specific growth rate of the microorganism ($\cong$ reduction of the microbial acetate uptake rate). The shape of I_{pH} is also determined by another parameter of pH$_{UL}$, which is the pH upper limit where the rate is reduced by 50% in case of high pH. For lower pH, the equation is intended to model overall acidic inhibitions including various kinds of undissociated VFA species. Therefore, when only acetic acid inhibition is focused on, use of undissociated fraction of acetate (unVFA sub-model, **Equation 6.3**) is relevant rather than the pH sub-model. In the equation, I_{ac} is given from the undissociated acetate concentration (acetic acid, S_{ac_un}), the operational pH, the dissociation constant of acetate ($K_{a,\,ac} = 10^{-4.76}$) and the total acetate concentration (S_{ac_total}) of the system (= undissociated acetate + dissociated acetate).

$$\begin{cases} \mu_{\text{net}} = \mu_{\text{max,pH}} \times I_{\text{pH}} \\ I_{\text{pH}} = \dfrac{1 + 2 \times 10^{0.5(\text{pH}_{\text{LL}} - \text{pH}_{\text{UL}})}}{1 + 10^{(\text{pH} - \text{pH}_{\text{UL}})} + 10^{(\text{pH}_{\text{LL}} - \text{pH})}} \end{cases} \qquad \text{Equation 6.2}$$

$$\begin{cases} \mu_{\text{net}} = \mu_{\text{max,ac}} \times I_{\text{ac}} \\ I_{\text{ac}} = \dfrac{K_{\text{I,ac}}}{K_{\text{I,ac}} + S_{\text{ac\_un}}} \\ S_{\text{ac\_un}} = \dfrac{10^{-\text{pH}}}{K_{\text{a,ac}} + 10^{-\text{pH}}} \cdot S_{\text{ac\_total}} \end{cases} \qquad \text{Equation 6.3}$$

As shown in **Figure 6.2A–B**, both simulation qualities of the accumulated acetate and the volumetric CH_4 production rate were significantly improved after the calibration of ADM1's inhibition kinetic parameters (pH sub-model). The retuned pH_{LL} and pH_{UL} were 6.13 ±0.12 of 95%-confidence interval (CI_{95}) and 8.12 with ±1.73 of CI_{95} respectively. Although these were very close to the ADM1's defaults (pH_{LL} = 6.5, pH_{UL} = 8.0), the values of the first decimal place had to be adjusted to meet the data plots. Since this small difference considerably magnified the prediction error between the data plots and the simulation results, the equation was supposed to have too high sensitivity to predict the inhibition phenomena unless the parameter values were precisely calibrated prior to the task. This mathematical nature could be an implicit drawback of the pH sub model.

Moreover, despite the adjustment of inhibition kinetics, the calibrated ADM1 model could not reproduce the small 2nd peak marked in the dash-line box at the acidification event #1 (**Figure 6.1A**). Noticeable simulation mismatch was also found in the data plots at the acidification events #2–6 where the accumulated acetate was being decreased along with the reduced volumetric loading rate (marked in dotted-line boxes in **Figure 6.2A-D**). Accordingly, the recovery of CH_4 production rates after the peak of acetate accumulation were overestimated. In the parameter calibration, the acetoclastic methanogenic biomass yield (Y_{acm}) was 0.06 g-COD/g-COD ±0.04 of CI_{95}, which was consistent with ADM1 default of 0.05 g-COD/g-COD. The specific decay rate of the biomass (b_{acm}) and the maximum specific growth rate ($\mu_{\text{max, acm}}$) were estimated to be 0.038 d^{-1} ±0.015 of CI_{95} and 0.18 d^{-1} ±0.02 of CI_{95} respectively. These estimates were also close to the ADM1 defaults (b_{acm} = 0.02 d^{-1}, $\mu_{\text{max, acm}}$ = 0.4 d^{-1}). The half-saturation coefficient for acetate uptake ($K_{\text{S,ac}}$) was comparable to the ADM1 default (194 mg-

COD/L ±101 of CI$_{95}$ vs. 150 mg-COD/L). This analysis indicated that the ADM1 default parameters for biomass growth and biomass decay were relatively acceptable whereas the pH sub-model required precise parameter calibration to perform simulations in acidic inhibition.

With respect to the modified ADM1 model equipped with unVFA sub-model, as shown in **Figure 6.2C–D**, almost identical simulation curves to those calculated using the calibrated ADM1 model were obtained. The estimates for Y_{acm}, $\mu_{max, acm}$, b_{acm}, $K_{S,ac}$ were 0.06 g-COD/g-COD ±0.04 of CI$_{95}$, 0.17 d^{-1} ±0.01, 0.036 d^{-1} ±0.009 of CI$_{95}$ and 209 mg-COD/L ±83.2 of CI$_{95}$ respectively. The inhibition half-saturation coefficient of acetic acid ($K_{I, ac}$) was 121 mg-COD/L ±24.6 of CI$_{95}$, which resulted in the growth inhibition by 0.1–80% in the continuous operation. As well as the calibrated ADM1 model, the modified ADM1 model failed to reproduce the small 2nd peak at the acidification event #1 and still hold considerable inconsistency against the data plots where the acetate concentration was decreasing after the peak (marked in thin-line boxes). From these simulation mismatches, it seemed that the microbial activity for the acetate uptake was not instantly recovered after reduction of the volumetric loading rate. Since the above-examined models were not equipped with switching functions to express the delay of the activity recovery, addition of a lag-phase sub-model into the ADM1 model was supposed to improve the calculation accuracy.
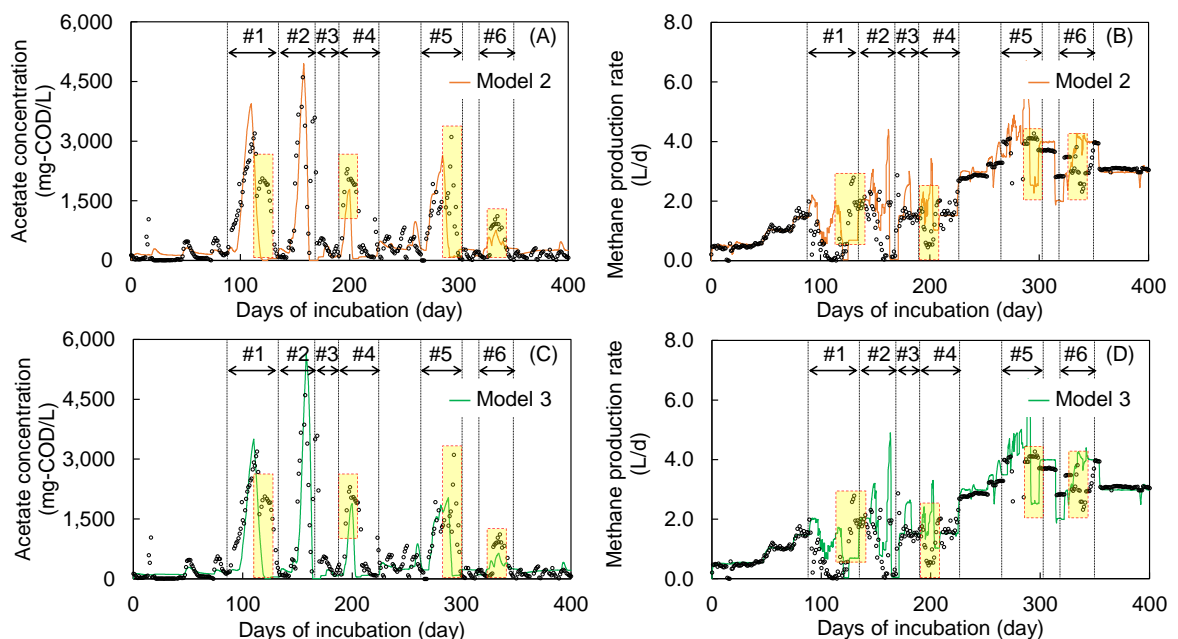

Figure 6.2 Acetate concentration using low-pH sub-model (A), volumetric methane production rate using low-pH sub-model (B), acetate concentration using unVFA sub-model (C), volumetric methane production rate using unVFA sub-model (D)

130

6.3.2. Development of delay function to express lag phase

Assuming that the lag phase is initiated at the time ($t_{lag} = 0$) where the volumetric loading rate is reduced (= the time at which the acetate accumulation peaks), the lag-phase sub-model is defined in **Equation 6.4**. In the equation, the value of η is the remaining relative activity of the microorganism ($0 \leq \eta \leq 100\%$) at $t_{lag} = 0$, which might vary depending on the degree of acidification. The half-saturation coefficient, K_{lag} is to express the specific length of lag phase. During the reduced volumetric loading rate, the value of t_{lag} kept increasing like a time integration meter. Eventually the value of I_{lag} would approach 100% at which the lag phase is terminated. To program the switching function of I_{lag} in ADM1 model, the value of t_{lag} is reset to zero when the next accumulated acetate is peaked.

$$
\begin{cases}
\mu_{lag} = \mu_{max} \times I_{lag} \\
I_{lag} = \eta + (1 - \eta) \dfrac{t_{lag}}{K_{lag} + t_{lag}}
\end{cases}
\qquad\qquad \text{Equation 6.4}
$$

To determine the I_{lag} parameter values of η and K_{lag}, the data plots during each acidification event were extracted in another set of graphs, and the parameters were calibrated in a trial-and-error method with curve-fitting. Specifically, by fixing the K_{lag} value, the η values were correlated with the pH difference (ΔpH) between the ordinary operational pH (pH 7.3) having no inhibition and the lowest pH among those measured in each acidification event (= pH at the peak of acetate accumulation). As shown in **Figure 6.3A**, when the lag-phase sub-model was applied to the ADM1 model having pH sub-model, the η values were linearly expressed along with ΔpH ($r^2 = 0.99$). In the correlation, 40 day of K_{lag} was chosen as a unique value over the datasets, because the value yielded better calculation curves than those using K_{lag} = zero, 10, 20, and 60 day, respectively (**Figure 6.3B–G**). In the graph for η vs. ΔpH, the η value could be extrapolated to 100% (no lag phase) when the ΔpH was small enough (operation under moderately low pH). Similarly, in case of large ΔpH (operation under very low pH), the η value would reach zero leading to the maximal delay of recovery from the inhibition. The ADM1 model equipped with the unVFA sub-model and the lag-phase sub-model also created comparable results to those of **Figure 6.3**.
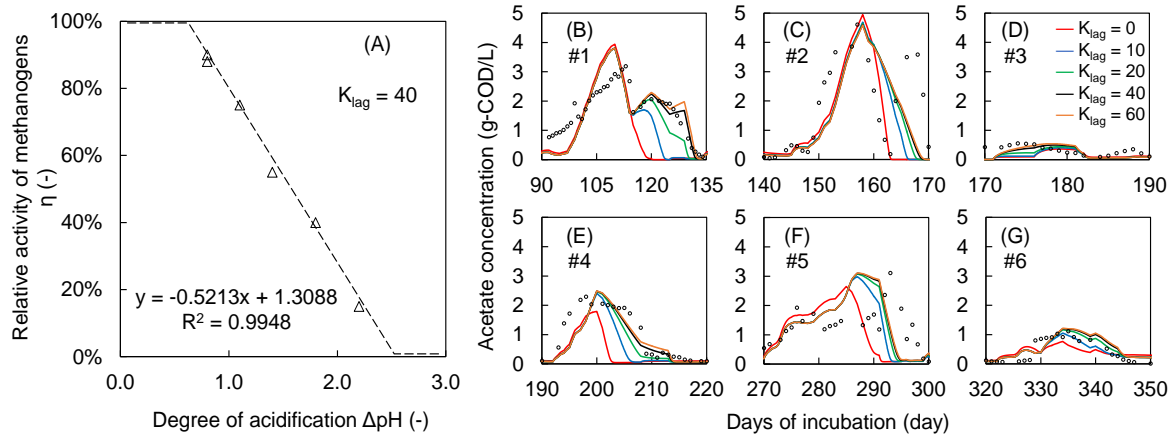
Figure 6.3 Correlation of η with pH difference (A) and curve fitting for K_{lag} parameter (B–G) (Based on the ADM1 model equipped with low-pH sub-model and lag-phase sub-model, #: dataset number)

As shown in **Figure 6.4A–D**, when the net specific growth rate was expressed using the inhibition sub-models and the lag phase sub-model (specific growth rate= $\mu_{\text{max}} \times I_{\text{pH}} \times I_{\text{lag}}$ or $\mu_{\text{max}} \times I_{\text{ac}} \times I_{\text{lag}}$), both ADM1 models successfully simulated the data plots after the peak of acetate accumulation which were not able to be reproduced by the previous models (marked in thin-line boxes). The calculation accuracy of each model was statistically evaluated using Nash-Sutcliffe model efficiency coefficient (NSE) as summarised in **Table 6.1**. The ADM1 model having the default set of kinetic parameters (Model 1) showed the lowest NSE among the models (NSE = -0.04) whilst the calibrated ADM1 model (Model 2) and the modified ADM1 model equipped with only I_{ac} (Model 3) yielded NSE values close to each other, which was about 0.35±10% (NSE =0.38 vs. 0.31). This indicated that the modified ADM1 model had a comparable prediction power to that of the calibrated ADM1 model. Among the ADM1 models examined, the models equipped with lag-phase sub-model showed the highest NSE values of 0.53 and 0.49 for Model 4 and Model 5, respectively. Since very good models were supposed to yield NSE value close to 1 whilst very bad models produced a negative NSE value [173], both ADM1 models equipped with lag-phase sub-model were considered relevant to express the low pH inhibition and/or acetic acid inhibition.
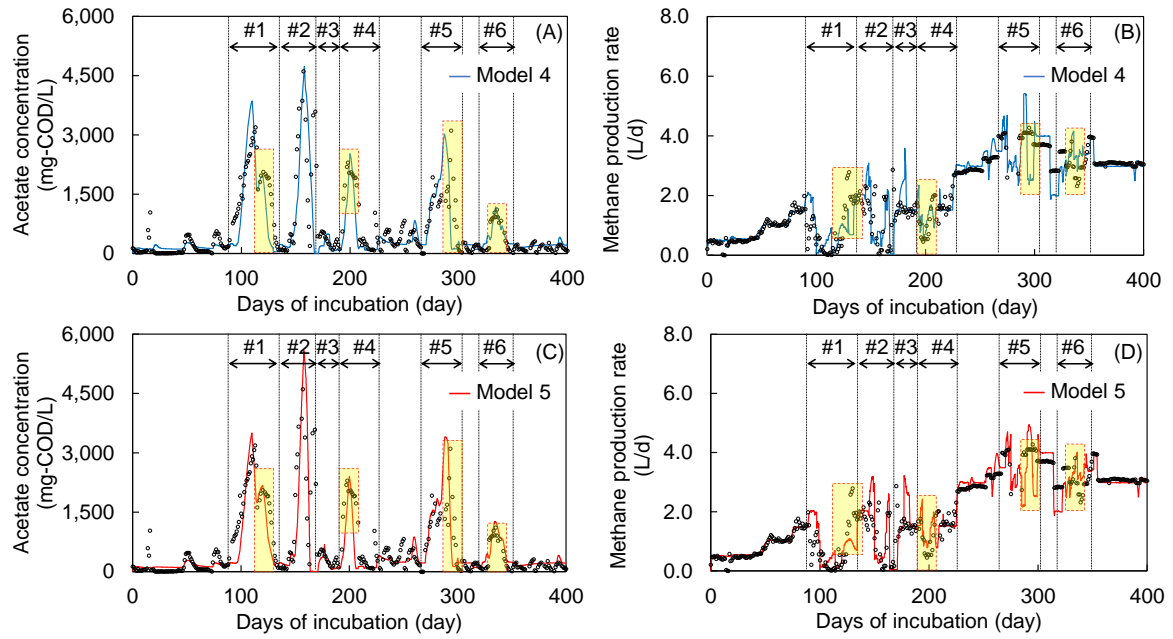
Figure 6.4 Acetate concentration using low-pH sub-model and lag-phase sub-model (A),
volumetric methane production rate using low-pH sub-model and lag-phase sub-model (B),
acetate concentration using acetic acid unVFA sub-model and lag-phase sub-model (C),
volumetric methane production rate using unVFA sub-model and lag-phase sub-model (D)

Table 6.1 Statistical analysis on parameter estimation

		Model 1	Model 2	Model 3	Model 4	Model 5
Biomass yield (Y_{acm}) (g-COD/g-COD)		0.05	0.06±0.04	0.06±0.04	0.06±0.04	0.06±0.04
Specific decay rate (b_{acm}) (d^{-1})		0.03	0.038±0.02	0.036±0.01	0.039±0.01	0.039±0.01
Half-saturation coefficient ($K_{S,ac}$) (mg-COD/L)		150	194±101	209±83.2	111±42.9	178±64.2
Maximum specific growth rate ($\mu_{max,\ acm}$) (d^{-1})		0.41	0.18±0.02	0.17±0.01	0.17±0.01	0.18±0.01
I_{pH} parameters (low-pH sub-model)	pH$_{UL}$	8.0	8.12±1.73	Nil	7.73±0.24	Nil
	pH$_{LL}$	6.5	6.13±0.12	Nil	6.15±0.12	Nil
I_{ac} parameter (unVFA sub-model)	$K_{I,ac}$	Nil	Nil	121±24.6	Nil	123±20.0
I_{lag} parameters (lag-phase sub-model)	η	Nil	Nil	Nil	f(ΔpH)♣	g(ΔpH)♦
	K_{lag}	Nil	Nil	Nil	40	40
Nash-Sutcliffe model efficiency coefficient (NSE)		-0.04	0.38	0.31	0.53	0.49

6.3.3. Active acetoclastic methanogenic biomass

The above inhibition sub-models were validated with the PMA-qPCR analysis. As shown in **Figure 6.5**, the number of living methanogenic cells detected in the reactor (copies/mL) was correlated to the simulation curves of active methanogen (mg-COD/L) obtained from the ADM1 models. During the continuous operation, the calculated active methanogen concentration with ADM1 models ranged between about 100 mg-COD/L and 850 mg-COD/L whilst 25 data plots of DNA copies vs. days of operation were collected. When the factor of DNA copies to the biomass was $0.62 \cdot 10^6$ copy/mg-COD, the highest r^2 value was obtained ($r^2 = 0.81$). In general, 1 mg-COD/L of living microbial cell is supposed to be equivalent to $1 \cdot 10^6$ cell/mL in the order of magnitude [145,174]. Since the calculated methanogen concentrations with Model 1, Model 4 and Model 5 reasonably matched with the plots from the DNA copies, the ADM1 models were thought to be able to calculate the living methanogen concentration as well as its reaction rates. In the acidification event #2, the volumetric CH_4 production rate was strongly inhibited to almost zero after the accumulation of acetate was peaked at day 160. At the initial phase of the acidification event #3 (day 170-190), the calculated methanogen concentration was about 460 mg-COD/L whilst the number of living methanogen was about $250 \cdot 10^6$ copies/mL. This result showed that the set of sub-models was enough to explain the temporary loss of the CH_4 production rate and the microbial acetate uptake rates.
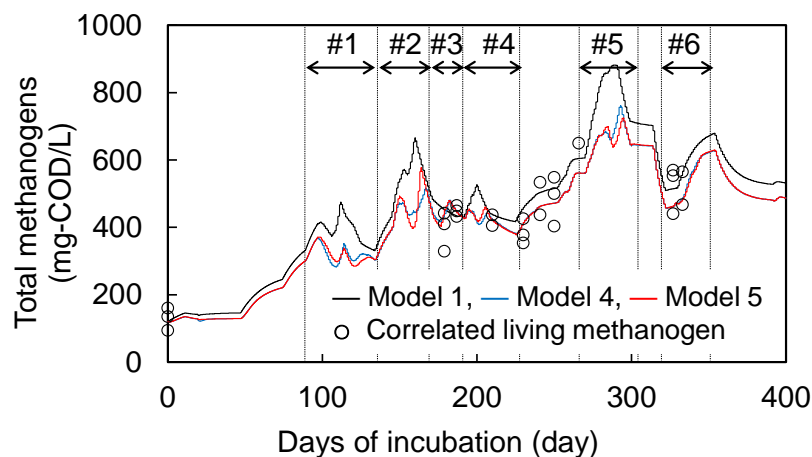
Figure 6.5 Correlation of active methanogen calculated with ADM1 to DNA copies of living archaea (plot: the correlated living methanogen concentration based on PMA-qPCR analysis, line: simulation results using various sub-model)

6.4. Conclusions

Using the experimental data of the continuous operation for 400 days where acetate was dynamically fed to the anaerobic reactor, the methanogenic inhibition term of ADM1 was evaluated, and the following conclusions were obtained.

1) ADM1 could simulate living methanogen concentration using its default parameters and the factor of DNA copies to the biomass ($0.62 \cdot 10^6$ copy/mg-COD). ADM1 also yielded reasonable acetate concentration and CH_4 production as long as the system was not acidified.

2) The default values of acidic inhibition kinetics equipped with ADM1 resulted in unacceptable mismatch against the experimental results. Moreover, since the default values were very close to the calibrated ones (pH_{UL}: 8.0 vs.7.7, pH_{LL}: 6.5 vs. 6.1), this very high sensitivity might lead to technical difficulties to conduct precise evaluation of process performance. To cope with this potential problem, the modified ADM1 model equipped with undissociated acetate inhibition sub-model could be alternatively used to conduct the acidic simulation, which had comparable calculation accuracy to that of the calibrated ADM1 model.

3) To simulate the delay of kinetic recovery from the acidic inhibition, modelling lag phase and its incorporation to ADM1 were necessary. The lag-phase sub-model elaborated in this study was composed of the relative remaining activity of biomass at the maximal acidic inhibition and the empirical delay coefficient. Using the lag-phase sub-model, Nash-Sutcliffe efficiency coefficient for the modified ADM1 showed 0.53, which was improved by 37% compared to the calibrated ADM1 model.

CHAPTER 7. CONCLUSIONS AND RECOMMENDATIONS

7.1. Main findings of the research

The study focused on the effects of low pH on the decay rate of methanogenic microorganisms and their potential VFA inhibition. Results showed that low pH conditions, with a pH below 6.5, significantly enhanced the decay rate of methanogenic microorganisms, leading to irreversible inhibition. Whereas, the acidogenic bacteria were found to be more tolerant to the acidic environment. The biocidal phenomenon was mainly attributed to the proton concentration in the system and was not affected by the presence of phosphate buffer. The impacts of acidic species (C_1–C_5 VFAs) and the VFA concentration (until 40 mM of un-dissociated VFAs) on the biomass decay were negligibly small comparing to the low pH stress.

The active biomass concentration predicted by the default ADM1 model was found to be in good agreement with the measured values obtained from the fluorescent cell staining method and the PMA-qPCR method when the system acidification was slight. However, the model was unable to accurately predict acetate concentration and CH_4 production after the severe acidic failure. To address this issue, a modified ADM1 was used, equipped with a lag-phase sub-model, to better reproduce the deterioration of reactor performance during an acidic failure and the subsequent recovery with lowered OLR. This resulted in a 37% improvement in the Nash-Sutcliffe efficiency coefficient compared to the calibrated ADM1 model. An empirical formula for low-pH inhibition kinetics was also derived from the experimental data, providing a set of parameters for the design and operation of anaerobic reactors.

To calculate the potential risks of acidic failure and obtain preferable operating conditions for VFA recovery reactors, a safety-margin parameters was provided based on **Figure 5.21**. From this, a methanogen-wide specific decay rate against pH was obtained as shown in the thin-line of **Figure 7.1** ($pH_{UL} = 6.25$, $pH_{LL} = 5.74$ and $n = 0.25$).
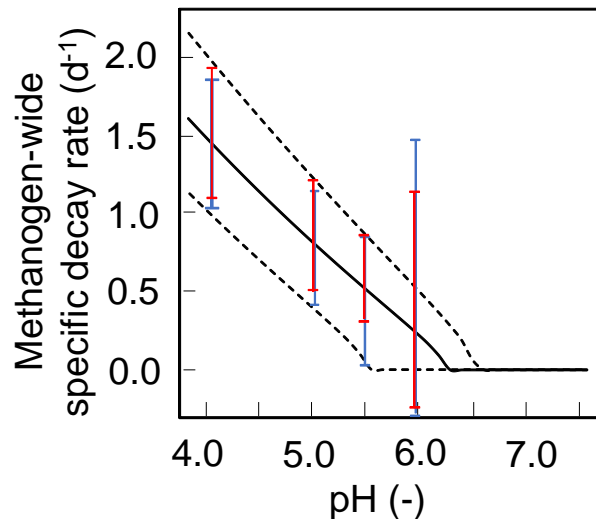
Figure 7.1 Specific decay rates of methanogens along with pH.
(Acetate-fed reactor: blue, Formate-fed reactor: red, error bar: the range between the highest upper CI$_{95}$ and the lowest lower CI$_{95}$, dashed line: regression curves to cover the error bars except for that at pH 6.0)

For application of the biocidal model to practical use, two artificial curves (dashed-lines) were plotted on the graph (upper artificial curve: pH$_{UL}$ = 6.41, pH$_{LL}$ = 5.47 and n = 0.23; lower artificial curve: pH$_{UL}$ = 5.55, pH$_{LL}$ = 5.11 and n = 0.24). The upper curve covering the highest upper limit of CI$_{95}$ below pH 5.5 was intended to allow a conservative calculation for the low pH inhibition (the methanogen-wide specific decay rate plus about 0.4 d^{-1}). This parameter set may be used for plant operation and/or process design, which has a safety margin to avoid the unwanted risks from the acidic failure. For the lower curve covering the lowest lower limit of CI$_{95}$ below pH 5.5, this would yield an optimistic calculation result for the acidic failure (the methanogen-wide specific decay rate minus about 0.4 d^{-1}). Using this parameter set, it is possible to ensure the acidifying process for VFA recovery.

7.2. Hypothesis on the mechanism of pH inhibition

The pH of the environment is an essential parameter that influences the structure and function of the microbial cell [175]. Microorganisms have developed different adaptation strategies to cope with extreme pH conditions, including pH homeostasis and pH tolerance mechanisms [176,177]. However, low pH is a major limiting factor for methanogen's growth

and survival. This section aims to present a hypothesis on the mechanism of low pH inhibition on methanogenic archaea.

Low pH conditions affect the microbial cell in several ways, including disrupting the structure and function of biomolecules [47,178]. The mechanism of low pH inhibition on microorganisms is multifactorial, and several theories have been proposed to explain the inhibitory effects of low pH on microbial growth. One of the most widely accepted theories is the "protonation hypothesis," which suggests that the inhibitory effect of low pH on microorganisms is due to the accumulation of H^+ ions in the environment [179]. The acidic environment can lead to the protonation of amino and carboxyl groups in proteins and nucleic acids, altering their charge and conformation, which can affect their activity and stability. Additionally, the high concentration of H^+ ions in the environment can lead to the collapse of the transmembrane proton motive force (PMF), which is critical for cellular functions such as ATP synthesis, nutrient uptake, and ion exchange [152]. The PMF is generated by the electron transport chain, and the collapse of this gradient can lead to a decrease in energy production, ion imbalance, and ultimately cell death. Another theory proposes that the inhibition of microbial growth at low pH is due to the disruption of membrane function. The cell membrane is critical for maintaining the integrity of the cell and regulating the exchange of nutrients and waste products. Low pH can alter the physical properties of the cell membrane, including its fluidity and permeability, leading to changes in the exchange of ions and metabolites [180]. Additionally, low pH can lead to the denaturation of membrane proteins, which can affect their function and stability.

The mechanism of low pH inhibition on microorganisms also depends on the type of microorganism and its inherent tolerance to acidic conditions [181, 182]. Acidophilic microorganisms, such as acidithiobacillus, have evolved different adaptation mechanisms to cope with low pH conditions, including the production of acid shock proteins and the modification of membrane lipids. In contrast, neutralophilic microorganisms, such as Escherichia coli, have a limited tolerance to acidic conditions and rely on pH homeostasis mechanisms to maintain intracellular pH. Low pH conditions can also lead to the accumulation of toxic byproducts, including organic acids such as lactic acid, acetic acid, and propionic acid, which can further exacerbate the inhibition of microbial growth [121,183]. Organic acids can diffuse through the cell membrane and disrupt intracellular pH homeostasis, leading to further acidification of the cytoplasm. Additionally, organic acids can interact with proteins and nucleic

acids, leading to structural and functional changes.

To conclude, low pH conditions can significantly impact the growth and survival of microorganisms. The inhibitory effects of low pH on microorganisms are multifactorial and depend on several parameters, including the type of microorganism, the pH of the environment, and the exposure time. The proposed protonation hypothesis and the disruption of membrane function theory explain the inhibitory effects of low pH on microorganisms.

7.3. Recommendations for future studies

With the growing interest in anaerobic digestion as a sustainable solution for managing organic waste, several potential areas of future research could further advance the field. First, gaining a complete understanding of the mechanism of pH inhibition on microorganisms and its overall effects is imperative. Next, innovative pre-treatment methods should be implemented to minimize potential toxicity risks in acidic environments. Establishing a set of guidelines for handling potential accidents, while acknowledging that it is not possible to completely eliminate all inhibitory factors in the pre-treatment process, would also be beneficial. To ensure the practicality of the sub-model, real-world data from full-scale wastewater treatment plants should be incorporated, providing a reliable benchmark for refinement. Finally, VFA recovery from anaerobic processes is a hot topic and requires precise control of kinetic parameters to achieve the highest VFA recovery efficiency and prevent CH_4 generation accurately on methanogenesis.

7.3.1. The mechanism of pH inhibition on microorganisms

One critical area of research that requires exploration is the mechanism of pH inhibition on microorganisms and its overall effects. Low pH can disrupt the cell membrane, causing it to lose integrity and leak essential nutrients and ions [175,178]. It can denature proteins by disrupting hydrogen bonds and electrostatic interactions that maintain their structure, leading to a loss of enzymatic activity and other cellular functions necessary for survival [152]. Additionally, low pH can inhibit metabolic pathways, necessary for energy production, leading to a decrease in energy availability and eventual microorganism death [177]. Protons can be added to biomolecules, disrupting their structure and function. Furthermore, low pH can

generate reactive oxygen species, damaging cellular components such as proteins and lipids and causing microorganism death [179-183].

In conclusion, the exact mechanism by which low pH kills microorganisms may depend on the specific organism and the severity and duration of the acidic conditions. However, determining which mechanism or inhibitory mechanism dominates requires further experimental research.

7.3.2. Guidelines for handling potential accidents

Another area of research that needs to be explored is the implementation of innovative pre-treatment methods to minimize potential toxicity risks in acidic environments. While it is not possible to completely eliminate all inhibitory factors in the pre-treatment process, accidents such as overloading of substrate or hydraulic shock can also affect the stability of the process. Therefore, it is essential to have a set of guidelines to handle potential accidents and prevent any significant damage to the digester. These guidelines should include steps to prevent the accumulation of toxic compounds, the management of digester pH, and the recovery of the digester after the accident.

7.3.3. Calibration of the pH inhibition sub-model

Anaerobic digestion is influenced by several parameters such as substrate composition, bacterial diversity, and hydraulic retention time, which can vary from one wastewater treatment plant to another, making it challenging to develop a generalized model to predict the process's performance accurately [12].

One critical component of the anaerobic digestion model is the sub-model for pH inhibition, which can help predict the process's performance under different conditions, allowing operators to make informed decisions regarding the digester's management [5,24]. The pH of the digester plays a crucial role in the process as it affects almost all microorganisms present. Acidic environments promote the growth of acidogenic bacteria while inhibiting the methanogenic archaea, essential for the biogas production. To ensure the practicality and reliability of the sub-model, it is crucial to calibrate it using real-world data from full-scale

wastewater treatment plants [184]. This process involves comparing model predictions with actual data from treatment plants and adjusting the parameters to better match the actual data. Calibration is necessary because the pH inhibition sub-model is sensitive to changes in the process parameters.

By ensuring the practicality and reliability of the sub-model, anaerobic digestion can be further advanced as a sustainable solution for managing organic waste. The calibrated sub-model can accurately predict the process's performance and optimize its efficiency, resulting in higher biogas yields and more sustainable and cost-effective wastewater treatment.

7.3.4. VFA recovery from anaerobic processes

Currently, VFA recovery from anaerobic processes is a hot topic that requires precise control of acidogenesis and methanogenesis kinetics to achieve the highest recovery efficiency. Volatile fatty acids, including acetic acid, propionic acid, butyric acid, iso-butyric acid, valeric acid, iso-valeric acid, and caproic acid, are important intermediate products of anaerobic digestion and have gained increasing interest in a wide range of industrial applications [95]. These VFAs have various applications in different industries such as food and beverage, textiles, bioenergy, cosmetics, perfumes, and rubber and grease production [185]. Furthermore, mixed VFAs can be used as a carbon source to cultivate fungi for animal feed, and specific combinations of VFAs have been used in the synthesis of biodiesel, biopolymers, or to cultivate algae [186]. Therefore, VFA production from AD could be a promising way for resource recovery. However, sustainable and economically feasible production and recovery methods still need to be developed.

pH is one of the critical parameters affecting the VFA concentration and composition since it influences both acidogenic processes and hydrolysis rates [187, 188, 189]. The conversion process in AD from organic wastes to VFA instead of methane can be promoted by controlling pH to enhance the hydrolysis/acidogenesis activity and by inhibiting VFA consumption through methanogens' activity inhibition [95]. Studies have shown that the stepwise pH fermentation strategy (from pH 9 to 11) can enhance the activity of acid-producing bacteria and inhibit the activities of methanogens, resulting in higher production of VFA [190]. Other studies have shown that pH change affects not only VFA concentration and composition but also the microbial community [191]. Furthermore, optimal VFA production occurs under

alkaline pH conditions [192], and pH influences VFA production positively [193]. Recent studies have speculated that intracellular pH affects the metabolic pathways in fermentation and influences VFA composition [194,195]. Lower pH makes the consumption of NADH more favorable, increasing the $NADH/NAD^+$ ratio and causing a shift in the main product(s) [132].

Although many studies have focused on operational pH that influence acidification, the main obstacle to overcome is the uncontrolled metabolic activities and persistence of methanogens in VFA production via bioprocess. Thus, the most important challenges are optimizing the operational parameters for VFA production and selecting feasible recovery pH range in further studies.

REFERENCES

[1]   Li, Y., Yang, G., Li, L., Sun, Y. (2018). Bioaugmentation for overloaded anaerobic digestion recovery with acid-tolerant methanogenic enrichment. Waste management, 79, 744-751.

[2]   Braz, G.H., Fernandez-Gonzalez, N., Lema, J.M., Carballa, M. (2019). Organic overloading affects the microbial interactions during anaerobic digestion in sewage sludge reactors. Chemosphere, 222, 323-332.

[3]   Basak, B., Patil, S.M., Saha, S., Kurade, M.B., Ha, G.S., Govindwar, S.P., Jeon, B.H. (2021). Rapid recovery of methane yield in organic overloaded-failed anaerobic digesters through bioaugmentation with acclimatized microbial consortium. Science of the Total Environment, 764, 144219.

[4]   Lins, P., Reitschuler, C., Illmer, P. (2014). Methanosarcina spp., the key to relieve the start-up of a thermophilic anaerobic digestion suffering from high acetic acid loads. Bioresource technology, 152, 347-354.

[5]   Sun, M., Liu, B., Yanagawa, K., Ha, N.T., Goel, R., Terashima, M., Yasui, H. (2020). Effects of low pH conditions on decay of methanogenic biomass. Water research, 179, 115883.

[6]   Liu, B., Terashima, M., Quan, N.T., Ha, N.T., Van Chieu, L., Goel, R., Yasui, H. (2018). High nitrite concentration accelerates nitrite oxidising organism's death. Water Science and Technology, 77(12), 2812-2822.

[7]   Meynell, P.J. (1976). Methane: Planning a Digester. Sochen Books, Prison Stable Court, Dorset, Clarington.

[8]   Ward, A.J., Hobbs, P.J., Holliman, P.J., Jones, D.L. (2008). Optimisation of the anaerobic digestion of agricultural resources. Bioresour Technol, 99:7928–40.

[9]   IEA Bioenergy Task 37. A perspective on the state of the biogas industry from selected member countries. https://www.ieabioenergy.com/wp-content/uploads/2022/03/IEA_T37_CountryReportSummary_2021.pdf

[10]   American Biogas Council. https://americanbiogascouncil.org/biogas-market-snapshot/

[11]   Hanum, F., Yuan, L.C., Kamahara, H., Aziz, H.A., Atsuta, Y., Yamada, T., Daimon, H. (2019). Treatment of sewage sludge using anaerobic digestion in Malaysia: current state and challenges. Frontiers in Energy Research, 7, 19.

[12]   Batstone, D.J., Keller, J., Angelidaki, I., Kalyuzhnyi, S.V., Pavlostathis, S.G., Rozzi, A.,

Sanders, W.T., Siegrist, H., Vavilin, V.A. (2002). The IWA Anaerobic Digestion Model No 1 (ADM1). Water Sci Technol. 45(10):65-73. PMID: 12188579.

[13] Swetha, T.A., Mohanrasu, K., Sudhakar, M., Raja, R., Ponnuchamy, K., Muthusamy, G., Arun, A. (2022). A comprehensive review on techniques used in conversion of biomass into bioeconomy. Sustainable Energy Technologies and Assessments, 53, 102682.

[14] 野池達也, 佐藤和明, 安井英斉, 李玉友 (2009). メタン発酵. ISBN: 4765534405, 9784765534406, 283頁.

[15] Zieminski, K., Frac, M. (2012). Methane fermentation process as anaerobic digestion of biomass: Transformations, stages and microorganisms. African Journal of Biotechnology, 11(18), 4127-4139.

[16] Ruiz, B., Flotats, X. (2014). Citrus essential oils and their influence on the anaerobic digestion process: An overview. Waste management, 34(11), 2063-2079.

[17] Fagbohungbe, M.O., Herbert, B.M., Hurst, L., Ibeto, C.N., Li, H., Usmani, S.Q., Semple, K.T. (2017). The challenges of anaerobic digestion and the role of biochar in optimizing anaerobic digestion. Waste management, 61, 236-249.

[18] Latif, M.A., Mehta, C.M., Batstone, D.J. (2017). Influence of low pH on continuous anaerobic digestion of waste activated sludge. Water Research, 113, 42-49.

[19] Zhang, Y., Banks, C.J., Heaven, S. (2012). Co-digestion of source segregated domestic food waste to improve process stability. Bioresource technology, 114, 168-178.

[20] Chen, Y., Cheng, J.J., Creamer, K.S. (2008). Inhibition of anaerobic digestion process: a review. Bioresource technology, 99(10), 4044-4064.

[21] Wu, L.J., Kobayashi, T., Kuramochi, H., Li, Y.Y., Xu, K.Q. (2015). Recovery strategies of inhibition for mesophilic anaerobic sludge treating the de-oiled grease trap waste. International Biodeterioration & Biodegradation, 104, 315-323.

[22] Chen, J.L., Ortiz, R., Steele, T.W., Stuckey, D.C. (2014). Toxicants inhibiting anaerobic digestion: a review. Biotechnology advances, 32(8), 1523-1534.

[23] Czatzkowska, M., Harnisz, M., Korzeniewska, E., Koniuszewska, I. (2020). Inhibitors of the methane fermentation process with particular emphasis on the microbiological aspect: A review. Energy Science & Engineering, 8(5), 1880-1897.

[24] Sun, M., Yanagawa, K., Prasitwuttisak, W., Goel, R., Watanabe, R., Harada, H., Liu, B.,

Terashima, M, Yasui, H. (2023). Kinetics for the Methanogen's Death in the Acidic Environments, Journal of Water and Environment Technology, Volume 21, Issue 1, Pages 59-75.

[25] Kwietniewska, E., Tys, J. (2014). Process characteristics, inhibition factors and methane yields of anaerobic digestion process, with particular focus on microalgal biomass fermentation. Renewable and sustainable energy reviews, 34, 491-500.

[26] Silvestre, G., Illa, J., Fernández, B., Bonmatí, A. (2014). Thermophilic anaerobic co-digestion of sewage sludge with grease waste: effect of long chain fatty acids in the methane yield and its dewatering properties. Applied Energy, 117, 87-94.

[27] Hwu, C.S., Lettinga, G. (1997). Acute toxicity of oleate to acetate-utilizing methanogens in mesophilic and thermophilic anaerobic sludges. Enzyme and microbial technology, 21(4), 297-301.

[28] Alves, M.M., Vieira, J.M., Pereira, R.A., Pereira, M.A., Mota, M. (2001). Effects of lipids and oleic acid on biomass development in anaerobic fixed-bed reactors. Part II: Oleic acid toxicity and biodegradability. Water Research, 35(1), 264-270.

[29] Zheng, C.J., Yoo, J.S., Lee, T.G., Cho, H.Y., Kim, Y.H., Kim, W.G. (2005). Fatty acid synthesis is a target for antibacterial activity of unsaturated fatty acids. FEBS letters, 579(23), 5157-5162.

[30] Desbois, A.P., Smith, V.J. (2010). Antibacterial free fatty acids: activities, mechanisms of action and biotechnological potential. Applied microbiology and biotechnology, 85, 1629-1642.

[31] Wu, J.T., Chiang, Y.R., Huang, W.Y., Jane, W.N. (2006). Cytotoxic effects of free fatty acids on phytoplankton algae and cyanobacteria. Aquatic Toxicology, 80(4), 338-345.

[32] Templer, J., Lalman, J.A., Jing, N., Ndegwa, P.M. (2006). Influence of C18 long chain fatty acids on hydrogen metabolism. Biotechnology progress, 22(1), 199-207.

[33] Ma, J., Zhao, Q.B., Laurens, L.L., Jarvis, E.E., Nagle, N.J., Chen, S., Frear, C.S. (2015). Mechanism, kinetics and microbiology of inhibition caused by long-chain fatty acids in anaerobic digestion of algal biomass. Biotechnology for biofuels, 8, 1-12.

[34] Kayhanian, M. (1999). Ammonia inhibition in high-solids biogasification: an overview and practical solutions. Environmental technology, 20(4), 355-365.

[35] Gerardi, M.H. (2006). Wastewater bacteria. John Wiley & Sons.

[36] Wittmann, C., Zeng, A.P., Deckwer, W.D. (1995). Growth inhibition by ammonia and use of a

pH-controlled feeding strategy for the effective cultivation of Mycobacterium chlorophenolicum. Applied microbiology and biotechnology, 44, 519-525.

[37] Sprott, G.D., Shaw, K.M., Jarrell, K.F. (1984). Ammonia/potassium exchange in methanogenic bacteria. Journal of Biological Chemistry, 259(20), 12602-12608.

[38] Koster, I.W., Rinzema, A., De Vegt, A.L., Lettinga, G. (1986). Sulfide inhibition of the methanogenic activity of granular sludge at various pH-levels. Water Research, 20(12), 1561-1567.

[39] Vu, H.P., Nguyen, L.N., Wang, Q., Ngo, H.H., Liu, Q., Zhang, X., Nghiem, L.D. (2021). Hydrogen sulphide management in anaerobic digestion: A critical review on input control, process regulation, and post-treatment. Bioresource Technology, 126634.

[40] Karhadkar, P.P., Audic, J.M., Faup, G.M., Khanna, P. (1987). Sulfide and sulfate inhibition of methanogenesis. Water Research, 21(9), 1061-1066.

[41] Dykstra, C.M., Pavlostathis, S.G. (2021). Hydrogen sulfide affects the performance of a methanogenic bioelectrochemical system used for biogas upgrading. Water Research, 200, 117268.

[42] Okabe, S., Nielsen, P.H., Jones, W.L., Characklis, W.G. (1995). Sulfide product inhibition of Desulfovibrio desulfuricans in batch and continuous cultures. Water research, 29(2), 571-578.

[43] O'Flaherty, V., Mahony, T., O'Kennedy, R., Colleran, E. (1998). Effect of pH on growth kinetics and sulphide toxicity thresholds of a range of methanogenic, syntrophic and sulphate-reducing bacteria. Process Biochemistry, 33(5), 555-569.

[44] Song, Y.C., Kwon, S.J., Woo, J.H. (2004). Mesophilic and thermophilic temperature co-phase anaerobic digestion compared with single-stage mesophilic-and thermophilic digestion of sewage sludge. Water research, 38(7), 1653-1662.

[45] Singh, S.K., Kadi, S., Prashanth, B., Nayak, S.K. (2018). Factors affecting anaerobic digestion of organic waste. Int. J. Eng. Res. Mech. Civ. Eng, 3, 2456-1290.

[46] Mei, R., Narihiro, T., Nobu, M.K., Liu, W.T. (2016). Effects of heat shocks on microbial community structure and microbial activity of a methanogenic enrichment degrading benzoate. Letters in applied microbiology, 63(5), 356-362.

[47] Ye, R., Jin, Q., Bohannan, B., Keller, J.K., McAllister, S.A., Bridgham, S.D. (2012). pH controls over anaerobic carbon mineralization, the efficiency of methane production, and

methanogenic pathways in peatlands across an ombrotrophic–minerotrophic gradient. Soil Biology and Biochemistry, 54, 36-47.

[48] Hagos, K., Zong, J., Li, D., Liu, C., Lu, X. (2017). Anaerobic co-digestion process for biogas production: Progress, challenges and perspectives. Renewable and sustainable energy reviews, 76, 1485-1496.

[49] Ponsá, S., Ferrer, I., Vázquez, F., Font, X. (2008). Optimization of the hydrolytic–acidogenic anaerobic digestion stage (55 C) of sewage sludge: Influence of pH and solid content. Water research, 42(14), 3972-3980.

[50] Amha, Y.M., Anwar, M.Z., Brower, A., Jacobsen, C.S., Stadler, L.B., Webster, T.M., Smith, A.L. (2018). Inhibition of anaerobic digestion processes: applications of molecular tools. Bioresource technology, 247, 999-1014.

[51] Ogejo, J.A., Wen, Z., Ignosh, J., Bendfeldt, E.S., Collins Jr, E.R. (2009). Biomethane technology.

[52] Liu, C.F., Yuan, X.Z., Zeng, G.M., Li, W.W., Li, J. (2008). Prediction of methane yield at optimum pH for anaerobic digestion of organic fraction of municipal solid waste. Bioresource technology, 99(4), 882-888.

[53] Yu, H.Q., Fang, H.H.P. (2002). Acidogenesis of dairy wastewater at various pH levels. Water Science and Technology, 45(10), 201-206.

[54] Vavilin, V.A., Rytov, S.V., Lokshina, L.Y., Rintala, J.A. (1999). Description of hydrolysis and acetoclastic methanogenensis as the rate-limiting steps during anaerobic conversion of solid waste into methane. In Proceedings of the second international symposium on anaerobic digestion of solid wastes, Barcelona, Vol. 2, pp. 1-4.

[55] Gujer, W., Zehnder, A.J. (1983). Conversion processes in anaerobic digestion. Water science and technology, 15(8-9), 127-167.

[56] Sambusiti, C. (2013). Physical, chemical and biological pretreatments to enhance biogas production from lignocellulosic substrates.

[57] Manyi-Loh, C.E., Mamphweli, S.N., Meyer, E.L., Okoh, A.I., Makaka, G., Simon, M. (2013). Microbial anaerobic digestion (bio-digesters) as an approach to the decontamination of animal wastes in pollution control and the generation of renewable energy. International journal of environmental research and public health, 10(9), 4390-4417.

[58] Stronach, S.M., Rudd, T., Lester, J.N., Stronach, S.M., Rudd, T., Lester, J.N. (1986). The biochemistry of anaerobic digestion. Anaerobic digestion processes in industrial wastewater treatment, 1-20.

[59] Anukam, A., Mohammadi, A., Naqvi, M., Granström, K. (2019). A review of the chemistry of anaerobic digestion: Methods of accelerating and optimizing process efficiency. Processes, 7(8), 504.

[60] Madigan, M.T., Martinko, J.M., Parker, J. (2000). Brock biology of microorganisms prentice hall. Inc. Upper Saddle River, New Jersey, 102-112.

[61] Zinder, S.H. (1993). Physiological ecology of methanogens. Methanogenesis: ecology, physiology, biochemistry & genetics, 128-206.

[62] Schmidt, J.E., Ahring, B.K. (1996). Granular sludge formation in upflow anaerobic sludge blanket (UASB) reactors. Biotechnology and bioengineering, 49(3), 229-246.

[63] Harmsen, H.J., Akkermans, A.D., Stams, A.J., De Vos, W.M. (1996). Population dynamics of propionate-oxidizing bacteria under methanogenic and sulfidogenic conditions in anaerobic granular sludge. Applied and Environmental Microbiology, 62(6), 2163-2168.

[64] Sekiguchi, Y., Kamagata, Y., Nakamura, K., Ohashi, A., Harada, H. (1999). Fluorescence in situ hybridization using 16S rRNA-targeted oligonucleotides reveals localization of methanogens and selected uncultured bacteria in mesophilic and thermophilic sludge granules. Applied and environmental microbiology, 65(3), 1280-1288.

[65] Mladenovska, Z., Ahring, B.K. (2000). Growth kinetics of thermophilic Methanosarcina spp. isolated from full-scale biogas plants treating animal manures. FEMS microbiology ecology, 31(3), 225-229.

[66] Garrity, G.M., Stanley, J.T. (2001). Bergey's Manual® of Systematic Bacteriology: Volume One. The Archaea and the Deeply Branching and Phototrophic Bacteria. D. R. Boone, & R. W. Castenholz (Eds.). Springer New York.

[67] Dedysh, S.N., Liesack, W., Khmelenina, V.N., Suzina, N.E., Trotsenko, Y.A., Semrau, J.D., Tiedje, J.M. (2000). Methylocella palustris gen. nov., sp. nov., a new methane-oxidizing acidophilic bacterium from peat bogs, representing a novel subtype of serine-pathway methanotrophs. International Journal of Systematic and Evolutionary Microbiology, 50(3), 955-969.

[68] Janssen, P.H. (2006). Identifying the dominant soil bacterial taxa in libraries of 16S rRNA and

16S rRNA genes. Applied and environmental microbiology, 72(3), 1719-1728.

[69] Thiele, J.H., Zeikus, J.G. (1988). Control of interspecies electron flow during anaerobic digestion: significance of formate transfer versus hydrogen transfer during syntrophic methanogenesis in flocs. Applied and environmental microbiology, 54(1), 20-29.

[70] Nagoya, M., Kouzuma, A., Watanabe, K. (2021). Codh/acs-deficient methanogens are prevalent in anaerobic digesters. Microorganisms, 9(11), 2248.

[71] Walker, C.B., Redding-Johanson, A.M., Baidoo, E.E., Rajeev, L., He, Z., Hendrickson, E.L., Stahl, D.A. (2012). Functional responses of methanogenic archaea to syntrophic growth. The ISME journal, 6(11), 2045-2055.

[72] Evans, P.N., Boyd, J.A., Leu, A.O., Woodcroft, B.J., Parks, D.H., Hugenholtz, P., Tyson, G.W. (2019). An evolving view of methane metabolism in the Archaea. Nature Reviews Microbiology, 17(4), 219-232.

[73] Wood, G.E., Haydock, A.K., Leigh, J.A. (2003). Function and regulation of the formate dehydrogenase genes of the methanogenic archaeon Methanococcus maripaludis. Journal of Bacteriology, 185(8), 2548-2554.

[74] Jones, J.B., Dilworth, G.L., Stadtman, T.C. (1979). Occurrence of selenocysteine in the selenium-dependent formate dehydrogenase of Methanococcus vannielii. Archives of biochemistry and biophysics, 195(2), 255-260.

[75] Schauer, N.L., Ferry, J.G. (1986). Composition of the coenzyme F420-dependent formate dehydrogenase from Methanobacterium formicicum. Journal of bacteriology, 165(2), 405-411.

[76] Schauer, N.L., Ferry, J.G., Honek, J.F., Orme-Johnson, W.H., Walsh, C. (1986). Mechanistic studies of the coenzyme F420-reducing formate dehydrogenase from Methanobacterium formicicum. Biochemistry, 25(22), 7163-7168.

[77] Kaster, A.K., Moll, J., Parey, K., Thauer, R.K. (2011). Coupling of ferredoxin and heterodisulfide reduction via electron bifurcation in hydrogenotrophic methanogenic archaea. Proceedings of the National Academy of Sciences, 108(7), 2981-2986.

[78] Thauer, R.K. (2012). The Wolfe cycle comes full circle. Proceedings of the National Academy of Sciences, 109(38), 15084-15085.

[79] Welte, C., Deppenmeier, U. (2014). Bioenergetics and anaerobic respiratory chains of aceticlastic methanogens. Biochimica et Biophysica Acta (BBA)-Bioenergetics, 1837(7),

1130-1147.

[80] Berger, S., Welte, C., Deppenmeier, U. (2012). Acetate activation in Methanosaeta thermophila: characterization of the key enzymes pyrophosphatase and acetyl-CoA synthetase. Archaea, 2012.

[81] Becher, B., Müller, V. (1994). Delta mu Na+ drives the synthesis of ATP via an delta mu Na (+)-translocating F1F0-ATP synthase in membrane vesicles of the archaeon Methanosarcina mazei Gö1. Journal of bacteriology, 176(9), 2543-2550.

[82] Jasso-Chávez, R., Diaz-Perez, C., Rodríguez-Zavala, J.S., Ferry, J.G. (2017). Functional role of MrpA in the MrpABCDEFG Na^+/H^+ antiporter complex from the archaeon Methanosarcina acetivorans. Journal of bacteriology, 199(2), e00662-16.

[83] Ferella, F., Cucchiella, F., D'Adamo, I., Gallucci, K. (2019). A techno-economic assessment of biogas upgrading in a developed market. Journal of Cleaner Production, 210, 945-957.

[84] Gao, S., Song, W., Guo, M. (2020). The integral role of bioproducts in the growing bioeconomy. Industrial Biotechnology, 16(1), 13-25.

[85] Kaparaju, P., Serrano, M., Angelidaki, I. (2009). Effect of reactor configuration on biogas production from wheat straw hydrolysate. Bioresource technology, 100(24), 6317-6323.

[86] Horváth, I.S., Tabatabaei, M., Karimi, K., Kumar, R. (2016). Recent updates on biogas production-a review. Biofuel research journal, 3(2), 394.

[87] Belostotskiy, D.E., Ziganshina, E.E., Siniagina, M., Boulygina, E.A., Miluykov, V.A., Ziganshin, A.M. (2015). Impact of the substrate loading regime and phosphoric acid supplementation on performance of biogas reactors and microbial community dynamics during anaerobic digestion of chicken wastes. Bioresource Technology, 193, 42-52.

[88] den Boer, E., Łukaszewska, A., Kluczkiewicz, W., Lewandowska, D., King, K., Reijonen, T., Hakalehto, E. (2016). Volatile fatty acids as an added value from biowaste. Waste management, 58, 62-69.

[89] Kim, D.H., Kim, S.H., Jung, K.W., Kim, M.S., Shin, H.S. (2011). Effect of initial pH independent of operational pH on hydrogen fermentation of food waste. Bioresource technology, 102(18), 8646-8652.

[90] Guo, X.M., Trably, E., Latrille, E., Carrère, H., Steyer, J.P. (2010). Hydrogen production from agricultural waste by dark fermentation: a review. International journal of hydrogen

energy, 35(19), 10660-10673.

[91] Wang, K., Yin, J., Shen, D., Li, N. (2014). Anaerobic digestion of food waste for volatile fatty acids (VFAs) production with different types of inoculum: effect of pH. Bioresource technology, 161, 395-401.

[92] Khan, M.A., Ngo, H.H., Guo, W.S., Liu, Y., Nghiem, L.D., Hai, F.I., Wu, Y. (2016). Optimization of process parameters for production of volatile fatty acid, biohydrogen and methane from anaerobic digestion. Bioresource technology, 219, 738-748.

[93] Stein, U.H., Wimmer, B., Ortner, M., Fuchs, W., Bochmann, G. (2017). Maximizing the production of butyric acid from food waste as a precursor for ABE-fermentation. Science of the Total Environment, 598, 993-1000.

[94] Patel, A., Sarkar, O., Rova, U., Christakopoulos, P., Matsakas, L. (2021). Valorization of volatile fatty acids derived from low-cost organic waste for lipogenesis in oleaginous microorganisms-A review. Bioresource Technology, 321, 124457.

[95] Wainaina, S., Lukitawesa, Kumar Awasthi, M., Taherzadeh, M.J. (2019). Bioengineering of anaerobic digestion for volatile fatty acids, hydrogen or methane production: a critical review. Bioengineered, 10(1), 437-458.

[96] Lukitawesa, Patinvoh, R.J., Millati, R., Sárvári-Horváth, I., Taherzadeh, M.J. (2020). Factors influencing volatile fatty acids production from food wastes via anaerobic digestion. Bioengineered, 11(1), 39-52.

[97] Woo, H.C., Kim, Y.H. (2019). Eco-efficient recovery of bio-based volatile C2–6 fatty acids. Biotechnology for biofuels, 12(1), 1-11.

[98] Kaspar, H.F., Wuhrmann, K. (1977). Product inhibition in sludge digestion. Microbial Ecology, 4, 241-248.

[99] Hill, D.T., Holmberg, R.D. (1988). Long chain volatile fatty acid relationships in anaerobic digestion of swine waste. Biological wastes, 23(3), 195-214.

[100] Fukuzaki, S., Nishio, N., Shobayashi, M., Nagai, S. (1990). Inhibition of the fermentation of propionate to methane by hydrogen, acetate, and propionate. Applied and environmental microbiology, 56(3), 719-723.

[101] Fukuzaki, S., Nishio, N., Nagai, S. (1990). Kinetics of the methanogenic fermentation of acetate. Applied and Environmental Microbiology, 56(10), 3158-3163.

[102] Marchaim, U., Krause, C. (1993). Propionic to acetic acid ratios in overloaded anaerobic digestion. Bioresource technology, 43(3), 195-203.

[103] Ahring, B.K., Sandberg, M., Angelidaki, I.J.A.M. (1995). Volatile fatty acids as indicators of process imbalance in anaerobic digestors. Applied microbiology and biotechnology, 43, 559-565.

[104] Pavlostathis, S.G., Giraldo-Gomez, E. (1991). Kinetics of anaerobic treatment. Water science and technology, 24(8), 35-59.

[105] Bastin, G., Dochain, D. (1986). On-line estimation of microbial specific growth rates. Automatica, 22(6), 705-709.

[106] Li, X., Yang, Z., Liu, G., Ma, Z., Wang, W. (2019). Modified anaerobic digestion model No. 1 (ADM1) for modeling anaerobic digestion process at different ammonium concentrations. Water Environment Research, 91(8), 700-714.

[107] Capson-Tojo, G., Astals, S., Robles, Á. (2021). Considering syntrophic acetate oxidation and ionic strength improves the performance of models for food waste anaerobic digestion. Bioresource Technology, 341, 125802.

[108] Rice, E.W., Bridgewater, L., American Public Health Association (Eds.). (2012). Standard methods for the examination of water and wastewater (Vol. 10). Washington, DC: American public health association.

[109] Van Ngo, A., Nguyen, H.T., Van Le, C., Goel, R., Terashima, M., Yasui, H. (2016). A dynamic simulation of methane fermentation process receiving heterogeneous food wastes and modelling acidic failure. Journal of Material Cycles and Waste Management, 18, 239-247.

[110] Hao, X., Wang, Q., Zhang, X., Cao, Y., van Mark Loosdrecht, C. M. (2009). Experimental evaluation of decrease in bacterial activity due to cell death and activity decay in activated sludge. Water Research, 43(14), 3604-3612.

[111] Gannon, J.T., Manilal, V.B., Alexander, M. (1991). Relationship between cell surface properties and transport of bacteria through soil. Applied and environmental microbiology, 57(1), 190-193.

[112] Zacharias, N., Kistemann, T., Schreiber, C. (2015). Application of flow cytometry and PMA-qPCR to distinguish between membrane intact and membrane compromised bacteria cells in an aquatic milieu. International journal of hygiene and environmental health, 218(8), 714-722.

[113] Dorn-In, S., Gareis, M., Schwaiger, K. (2019). Differentiation of live and dead Mycobacterium tuberculosis complex in meat samples using PMA qPCR. Food microbiology, 84, 103275.

[114] Lv, X.C., Li, Y., Qiu, W.W., Wu, X.Q., Xu, B.X., Liang, Y.T., Ni, L. (2016). Development of propidium monoazide combined with real-time quantitative PCR (PMA-qPCR) assays to quantify viable dominant microorganisms responsible for the traditional brewing of Hong Qu glutinous rice wine. Food Control, 66, 69-78.

[115] Takai, K.E.N., Horikoshi, K. (2000). Rapid detection and quantification of members of the archaeal community by quantitative PCR using fluorogenic probes. Applied and environmental microbiology, 66(11), 5066-5072.

[116] Yanagawa, K., Shiraishi, F., Tanigawa, Y., Maeda, T., Mustapha, N.A., Owari, S., Kano, A. (2019). Endolithic microbial habitats hosted in carbonate nodules currently forming within sediment at a high methane flux site in the sea of Japan. Geosciences, 9(11), 463.

[117] Mészáros, É. (2022). qPCR: How SYBR® Green and TaqMan® real-time PCR assays work. https://www.integra-biosciences.com/japan/en/blog/article/qpcr-how-sybrr-green-and-taqmanr-real-time-pcr-assays-work.

[118] Ding, L., Chen, Y., Xu, Y., Hu, B. (2021). Improving treatment capacity and process stability via a two-stage anaerobic digestion of food waste combining solid-state acidogenesis and leachate methanogenesis/recirculation. Journal of Cleaner Production, 279, 123644.

[119] Siegert, I., Banks, C. (2005). The effect of volatile fatty acid additions on the anaerobic digestion of cellulose and glucose in batch reactors. Process Biochemistry, 40(11), 3412-3418.

[120] Amani, T., Nosrati, M., Sreekrishnan, T.R. (2010). Anaerobic digestion from the viewpoint of microbiological, chemical, and operational aspects—a review. Environmental Reviews, 18(NA), 255-278.

[121] Xiao, K., Guo, C., Marquart, Y., Maspolim, Y., Ng, W.J. (2016). Acetic acid effects on methanogens in the second stage of a two-stage anaerobic system. Chemosphere, 144, 1498-1504.

[122] Zhang, B., Zhang, L.L., Zhang, S.C., Shi, H.Z., Cai, W.M. (2005). The influence of pH on hydrolysis and acidogenesis of kitchen wastes in two-phase anaerobic digestion. Environmental technology, 26(3), 329-340.

[123] Shi, E., Li, J., Leu, S.Y., Antwi, P. (2016). Modeling the dynamic volatile fatty acids profiles with pH and hydraulic retention time in an anaerobic baffled reactor during the startup

period. Bioresource technology, 222, 49-58.

[124] Horiuchi, J.I., Shimizu, T., Tada, K., Kanno, T., Kobayashi, M. (2002). Selective production of organic acids in anaerobic acid reactor by pH control. Bioresource technology, 82(3), 209-213.

[125] Zhu, Y., Yang, S.T. (2004). Effect of pH on metabolic pathway shift in fermentation of xylose by Clostridium tyrobutyricum. Journal of Biotechnology, 110(2), 143-157.

[126] Lü, F., He, P.J., Shao, L.M., Lee, D.J. (2008). Stress of pH and acetate on product formation of fermenting polysaccharide-rich organic waste. Biochemical engineering journal, 39(1), 97-104.

[127] Russell, J.B. (1992). Another explanation for the toxicity of fermentation acids at low pH: anion accumulation versus uncoupling. Journal of applied bacteriology, 73(5), 363-370.

[128] Bailey, J.E., Ollis, D.F. (2018). Biochemical engineering fundamentals. McGraw-Hill.

[129] Gottschalk, G. (1986) Bacterial Metabolism. 2nd Edition, Springer-Verlag, New York.

[130] Temudo, M.F., Muyzer, G., Kleerebezem, R., van Loosdrecht, M.C. (2008). Diversity of microbial communities in open mixed culture fermentations: impact of the pH and carbon source. Applied microbiology and biotechnology, 80, 1121-1130.

[131] Zoetemeyer, R.J., Van den Heuvel, J.C., Cohen, A. (1982). pH influence on acidogenic dissimilation of glucose in an anaerobic digestor. Water research, 16(3), 303-311.

[132] Temudo, M.F., Kleerebezem, R., van Loosdrecht, M. (2007). Influence of the pH on (open) mixed culture fermentation of glucose: a chemostat study. Biotechnology and bioengineering, 98(1), 69-79.

[133] Feldman, H., Flores-Alsina, X., Ramin, P., Kjellberg, K., Jeppsson, U., Batstone, D.J., Gernaey, K.V. (2017). Modelling an industrial anaerobic granular reactor using a multi-scale approach. Water research, 126, 488-500.

[134] Ghofrani-Isfahani, P., Valverde-Perez, B., Alvarado-Morales, M., Shahrokhi, M., Vossoughi, M., Angelidaki, I. (2020). Supervisory control of an anaerobic digester subject to drastic substrate changes. Chemical Engineering Journal, 391, 123502.

[135] Van Kessel, J.A.S., Russell, J.B. (1996). The effect of pH on ruminal methanogenesis. FEMS microbiology ecology, 20(4), 205-210.

[136] Horn, M.A., Matthies, C., Küsel, K., Schramm, A., Drake, H.L. (2003). Hydrogenotrophic methanogenesis by moderately acid-tolerant methanogens of a methane-emitting acidic peat. Applied and Environmental Microbiology, 69(1), 74-83.

[137] Kim, I.S., Hwang, M.H., Jang, N.J., Hyun, S.H., Lee, S.T. (2004). Effect of low pH on the activity of hydrogen utilizing methanogen in bio-hydrogen process. International Journal of Hydrogen Energy, 29(11), 1133-1140.

[138] Lv, Z., Hu, M., Harms, H., Richnow, H.H., Liebetrau, J., Nikolausz, M. (2014). Stable isotope composition of biogas allows early warning of complete process failure as a result of ammonia inhibition in anaerobic digesters. Bioresource technology, 167, 251-259.

[139] Zhang, W., Dai, K., Xia, X.Y., Wang, H.J., Chen, Y., Lu, Y.Z., Zeng, R.J. (2018). Free acetic acid as the key factor for the inhibition of hydrogenotrophic methanogenesis in mesophilic mixed culture fermentation. Bioresource technology, 264, 17-23.

[140] Hao, X., Cai, Z., Fu, K., Zhao, D. (2012). Distinguishing activity decay and cell death from bacterial decay for two types of methanogens. water research, 46(4), 1251-1259.

[141] Xiao, K., Zhou, Y., Guo, C., Maspolim, Y., Ng, W.J. (2016). Impact of undissociated volatile fatty acids on acidogenesis in a two-phase anaerobic system. Journal of Environmental Sciences, 42, 196-201.

[142] Henze, M., Gujer, W., Mino, T., Van Loosedrecht, M. (2006). Activated sludge models ASM1, ASM2, ASM2d and ASM3.

[143] Jimenez, J., Vedrenne, F., Denis, C., Mottet, A., Déléris, S., Steyer, J.P., Rivero, J.A.C. (2013). A statistical comparison of protein and carbohydrate characterisation methodology applied on sewage sludge samples. Water research, 47(5), 1751-1762.

[144] Wang, R., Li, Y., Wang, W., Chen, Y., Vanrolleghem, P.A. (2015). Effect of high orthophosphate concentration on mesophilic anaerobic sludge digestion and its modeling. Chemical Engineering Journal, 260, 791-800.

[145] Shibata, M., Nakamura, K., Miyaji, Y. (1987). Biological decomposition of trace organic compounds. Water Science and Technology, 19(3-4), 417-427.

[146] Nakamura, K., Shibata, M., Miyaji, Y. (1989). Substrate affinity of oligotrophic bacteria in biofilm reactors. Water science and technology, 21(8-9), 779-790.

[147] Ravindran, V.B., Shahsavari, E., Soni, S.K., Ball, A.S. (2019). Viability determination of Ascaris ova in raw wastewater: A comparative evaluation of culture-based, BacLight Live/Dead staining and PMA-qPCR methods. Water Science and Technology, 80(5), 817-826.

[148] Siliakus, M.F., van der Oost, J., Kengen, S.W. (2017). Adaptations of archaeal and bacterial

membranes to variations in temperature, pH and pressure. Extremophiles, 21, 651-670.

[149] Roy, C.K., Toya, S., Hoshiko, Y., Sabidi, S., Mustapha, N.A., Miyazaki, T., Maeda, T. (2022). Effect of sodium tungstate on anaerobic digestion of waste sewage sludge: Enhanced methane production via increased acetoclastic methanogens. Journal of Environmental Chemical Engineering, 10(3), 107524.

[150] Zhang, W., Zhang, F., Li, Y.X., Jiang, Y., Zeng, R.J. (2019). No difference in inhibition among free acids of acetate, propionate and butyrate on hydrogenotrophic methanogen of Methanobacterium formicicum. Bioresource technology, 294, 122237.

[151] Hackmann, T.J., Diese, L.E., Firkins, J.L. (2013). Quantifying the responses of mixed rumen microbes to excess carbohydrate. Applied and environmental microbiology, 79(12), 3786-3795.

[152] Rowe, A.R., Rajeev, P., Jain, A., Pirbadian, S., Okamoto, A., Gralnick, J.A, Nealson, K.H. (2018). Tracking electron uptake from a cathode into Shewanella cells: implications for energy acquisition from solid-substrate electron donors. MBio, 9(1), e02203-17.

[153] Jankowska, E., Chwiałkowska, J., Stodolny, M., Oleskowicz-Popiel, P. (2015). Effect of pH and retention time on volatile fatty acids production during mixed culture fermentation. Bioresource Technology, 190, 274-280.

[154] Amao, Y. (2018). Formate dehydrogenase for CO2 utilization and its application. Journal of CO2 Utilization, 26, 623-641.

[155] Sun, H., Yang, Z., Shi, G., Arhin, S.G., Papadakis, V.G., Goula, M.A., Wang, W. (2021). Methane production from acetate, formate and H2/CO2 under high ammonia level: modified ADM1 simulation and microbial characterization. Science of the Total Environment, 783, 147581.

[156] Akuzawa, M., Hori, T., Haruta, S., Ueno, Y., Ishii, M., Igarashi, Y. (2011). Distinctive responses of metabolically active microbiota to acidification in a thermophilic anaerobic digester. Microbial ecology, 61, 595-605.

[157] Capson-Tojo, G., Ruiz, D., Rouez, M., Crest, M., Steyer, J. P., Bernet, N., Escudié, R. (2017). Accumulation of propionic acid during consecutive batch anaerobic digestion of commercial food waste. Bioresource technology, 245, 724-733.

[158] Khedim, Z., Benyahia, B., Cherki, B., Sari, T., Harmand, J. (2018). Effect of control parameters on biogas production during the anaerobic digestion of protein-rich substrates. Applied Mathematical Modelling, 61, 351-376.

[159] Cheng, Q., Chen, Z., Deng, F., Liao, Y., Xiao, B., Li, J. (2016). Kinetic evaluation on the degradation process of anaerobic digestion fed with piggery wastewater at different OLRs. Biochemical engineering journal, 113, 123-132.

[160] Bayu, A.I., Lestary, R.A., Dewayanto, N., Mellyanawaty, M., Wicaksono, A., Kartika, R.W.A., Budhijanto, W. (2022). Kinetic study of thermophilic anaerobic digestion of sugarcane vinasse in a single-stage continuous stirred tank reactor. Results in Engineering, 14, 100432.

[161] Menzel, K., Zeng, A.P., Biebl, H., Deckwer, W.D. (1996). Kinetic, dynamic, and pathway studies of glycerol metabolism by Klebsiella pneumoniae in anaerobic continuous culture: I. The phenomena and characterization of oscillation and hysteresis. Biotechnology and bioengineering, 52(5), 549-560.

[162] Aoyagi, T., Inaba, T., Aizawa, H., Mayumi, D., Sakata, S., Charfi, A., Hori, T. (2020). Unexpected diversity of acetate degraders in anaerobic membrane bioreactor treating organic solid waste revealed by high-sensitivity stable isotope probing. Water Research, 176, 115750.

[163] Baquerizo, G., Fiat, J., Buffiere, P., Girault, R., Gillot, S. (2021). Modelling the dynamic long-term performance of a full-scale digester treating sludge from an urban WRRF using an extended version of ADM1. Chemical Engineering Journal, 423, 128870.

[164] Cai, G., Zhu, G., Zhou, M., Lv, N., Wang, R., Li, C., Pan, X. (2021). Syntrophic butyrate-oxidizing methanogenesis promoted by anthraquinone-2-sulfonate and cysteine: Distinct tendencies towards the enrichment of methanogens and syntrophic fatty-acid oxidizing bacteria. Bioresource Technology, 332, 125074.

[165] Lopez-Gutierrez, I., Montiel-Corona, V., Calderon-Soto, L.F., Palomo-Briones, R., Mendez-Acosta, H.O., Razo-Flores, E., Alatriste-Mondragon, F. (2021). Evaluation of the continuous methane production from an enzymatic agave bagasse hydrolysate in suspended (CSTR) and granular biomass systems (UASB). Fuel, 304, 121406.

[166] Gao, J., Feng, E., Zhang, W. (2022). Modeling and parameter identification of microbial batch fermentation under environmental disturbances. Applied Mathematical Modelling, 108, 205-219.

[167] Insel, G., Ozyildiz, G., Okutman-Tas, D., Guven, D., Zengin, G.E., Pala-Ozkok, I., Cokgor, E. (2022). A comprehensive evaluation of process kinetics: A plant-wide approach for nutrient removal and biogas production. Water Research, 217, 118410.

[168] Wang, X., Yang, H. (2022). Nitrogen removal performance of anammox immobilized fillers in

response to seasonal temperature variations and different operating modes: Substrate utilization and microbial community analysis. Science of The Total Environment, 829, 154574.

[169] Gompertz, B. (1825). XXIV. On the nature of the function expressive of the law of human mortality, and on a new mode of determining the value of life contingencies. In a letter to Francis Baily, Esq. FRS &c. Philosophical transactions of the Royal Society of London, (115), 513-583.

[170] Zwietering, M.H., Jongenburger, I., Rombouts, F.M., Van't Riet, K.J.A.E.M. (1990). Modeling of the bacterial growth curve. Applied and environmental microbiology, 56(6), 1875-1881.

[171] Lay, J.J., Li, Y.Y., Noike, T., Endo, J., Ishimoto, S. (1997). Analysis of environmental factors affecting methane production from high-solids organic waste. Water science and technology, 36(6-7), 493-500.

[172] Rahmani, A.M., Tyagi, V.K., Ahmed, B., Kazmi, A.A., Ojha, C.S.P., Singh, R. (2022). Critical insights into anaerobic co-digestion of wheat straw with food waste and cattle manure: Synergistic effects on biogas yield and kinetic modeling. Environmental Research, 212, 113382.

[173] Pérez, I.A., García, M.Á., Sánchez, M.L., Pardo, N. (2022). Trend analysis and outlier distribution of CO2 and CH4: A case study at a rural site in northern Spain. Science of The Total Environment, 819, 153129.

[174] Nakamura, K., Shibata, M., Miyaji, Y. (1989). Substrate affinity of oligotrophic bacteria in biofilm reactors. Water science and technology, 21(8-9), 779-790.

[175] Jin, Q., Kirk, M.F. (2018). pH as a primary control in environmental microbiology: 1. thermodynamic perspective. Frontiers in Environmental Science, 6, 21.

[176] Ratzke, C., Gore, J. (2018). Modifying and reacting to the environmental pH can drive bacterial interactions. PLoS biology, 16(3), e2004248.

[177] Lund, P.A., De Biase, D., Liran, O., Scheler, O., Mira, N.P., Cetecioglu, Z., O'Byrne, C. (2020). Understanding how microorganisms respond to acid pH is central to their control and successful exploitation. Frontiers in microbiology, 11, 556140.

[178] Bortolotti, A., Vazquez, D.B., Almada, J.C., Inda, M.E., Drusin, S.I., Villalba, J.M., Cybulski, L.E. (2020). A transmembrane histidine kinase functions as a pH sensor. Biomolecules, 10(8), 1183.

[179] Zhou, X., Zeitz, J.O., Meile, L., Kreuzer, M., Schwarm, A. (2015). Influence of pH and the

degree of protonation on the inhibitory effect of fatty acids in the ruminal methanogen Methanobrevibacter ruminantium strain M1. Journal of applied microbiology, 119(6), 1482-1493.

[180] Marquart, K.A., Haller, B.R., Paper, J.M., Flynn, T.M., Boyanov, M.I., Shodunke, G., Kirk, M.F. (2019). Influence of pH on the balance between methanogenesis and iron reduction. Geobiology, 17(2), 185-198.

[181] Stams, A.J.M., Elferink, S.O., Westermann, P. (2003). Metabolic interactions between methanogenic consortia and anaerobic respiring bacteria. Biomethanation I, 31-56.

[182] Hanaki, K., Hirunmasuwan, S., Matsuo, T. (1994). Protection of methanogenic bacteria from low pH and toxic materials by immobilization using polyvinyl alcohol. Water research, 28(4), 877-885.

[183] Zhou, X., Zeitz, J.O., Meile, L., Kreuzer, M., Schwarm, A. (2015). 4 Influence of pH on the inhibitory effect of fatty acids on the rumen methanogen Methanobrevibacter ruminantium. Investigating the mode of action of fatty acids against rumen methanogens, 46.

[184] Sun, M., Zhang, X., Liu, B., Goel, R., Terashima, M., Yasui, H.. Upgrading ADM1 by Addition of Lag-phase Sub-model to Simulate Acidic Inhibition of Methanogenic Reactor. Journal of Water and Environment Technology, Vol.22, No.2, 2023.

[185] Baumann, I., Westermann, P. (2016). Microbial production of short chain fatty acids from lignocellulosic biomass: current processes and market. BioMed research international, 2016.

[186] Bhatia, S.K., Gurav, R., Choi, T.R., Jung, H.R., Yang, S.Y., Song, H.S., Yang, Y.H. (2019). Poly (3-hydroxybutyrate-co-3-hydroxyhexanoate) production from engineered Ralstonia eutropha using synthetic and anaerobically digested food waste derived volatile fatty acids. International journal of biological macromolecules, 133, 1-10.

[187] Begum, S., Anupoju, G.R., Sridhar, S., Bhargava, S.K., Jegatheesan, V., Eshtiaghi, N. (2018). Evaluation of single and two stage anaerobic digestion of landfill leachate: Effect of pH and initial organic loading rate on volatile fatty acid (VFA) and biogas production. Bioresource technology, 251, 364-373.

[188] Begum, S., Anupoju, G.R., Sridhar, S., Bhargava, S.K., Jegatheesan, V., Eshtiaghi, N. (2018). Evaluation of single and two stage anaerobic digestion of landfill leachate: Effect of pH and initial organic loading rate on volatile fatty acid (VFA) and biogas production. Bioresource technology, 251, 364-373.

[189] Zhao, J., Wang, D., Liu, Y., Ngo, H.H., Guo, W., Yang, Q., Li, X. (2018). Novel stepwise pH control strategy to improve short chain fatty acid production from sludge anaerobic fermentation. Bioresource technology, 249, 431-438.

[190] Zhao, Y., Xu, C., Ai, S., Wang, H., Gao, Y., Yan, L., Wang, W. (2019). Biological pretreatment enhances the activity of functional microorganisms and the ability of methanogenesis during anaerobic digestion. Bioresource technology, 290, 121660.

[191] Jiang, J., Zhang, Y., Li, K., Wang, Q., Gong, C., Li, M. (2013). Volatile fatty acids production from food waste: effects of pH, temperature, and organic loading rate. Bioresource technology, 143, 525-530.

[192] Hussain, A., Filiatrault, M., Guiot, S. R. (2017). Acidogenic digestion of food waste in a thermophilic leach bed reactor: effect of pH and leachate recirculation rate on hydrolysis and volatile fatty acid production. Bioresource technology, 245, 1-9.

[193] Eryildiz, B., Taherzadeh, M.J. (2020). Effect of pH, substrate loading, oxygen, and methanogens inhibitors on volatile fatty acid (VFA) production from citrus waste by anaerobic digestion. Bioresource technology, 302, 122800.

[194] Mohd-Zaki, Z., Bastidas-Oyanedel, J.R., Lu, Y., Hoelzle, R., Pratt, S., Slater, F.R., Batstone, D.J. (2016). Influence of pH regulation mode in glucose fermentation on product selection and process stability. Microorganisms, 4(1), 2.

[195] Zhou, M., Zhou, J., Tan, M., Du, J., Yan, B., Wong, J.W., Zhang, Y. (2017). Enhanced carboxylic acids production by decreasing hydrogen partial pressure during acidogenic fermentation of glucose. Bioresource technology, 245, 44-51.

APPENDIX

1. List of terminology and matrix in the ADM1

Table A1 Nomenclature and units used in the ADM1

Symbol	Description	Units
C_i	carbon content of component i	kmoleC·kgCOD^{-1}
i	component index (see appendix)	
I	inhibition function (various, see Table A2)	
j	process index (see appendix)	
$k_{A/B,i}$	acid-base rate constant for component i	M^{-1}·d^{-1}
k_{dec}	first order decay rate for biomass death	d^{-1}
$k_L a$	gas–liquid transfer coefficient	d^{-1}
k_m	specific Monod maximum uptake rate	kgCOD·m^{-3}_S·kgCOD·m^{-3}_X·d^{-1}
K_a	acid-base equilibrium constant	M (kmole·m^{-3})
K_H	Henry's law coefficient	M.bar^{-1}
K_I	inhibition constant	nominally kgCOD·m^{-3}
K_S	Monod half saturation constant	kgCOD·m^{-3}
N_i	nitrogen content of component I	kmoleN·kg COD^{-1}
p_{gas}	pressure of gas	bar
pH	$-\log_{10}[S_{H+}]$	
pK_a	$-\log_{10}[K_a]$	
q	flow	m^3
S_i	soluble component i (dynamic or algebraic variable)	nominally kgCOD·m^{-3}
S_I	inhibitory component	nominally kgCOD·m^{-3}
t	time	d
T	temperature	K
V	volume	m^3
X_i	particulate component i	kgCOD·m^{-3}
$Y_{substrate}$	yield of biomass on substrate	kgCOD_X·kgCOD_S
$v_{i,j}$	rate coefficients for component i on process j	nominally kgCOD·m^{-3}
$f_{product,substrate}$	yield (catabolism only) of product on substrate	kgCOD·kgCOD^{-1}
ρ_j	rate for process j	kgCOD.m^{-3}

161

Table A2: Biochemical rate coefficients ($v_{i,j}$) and kinetic rate equations (ρ_j) for soluble components (i = 1–12; j = 1–19).

j	Component → / Process ↓	1 S_{su} Monosaccharides (kgCOD·m⁻³)	2 S_{aa} Amino acids (kgCOD·m⁻³)	3 S_{fa} Long chain fatty acids (kgCOD·m⁻³)	4 S_{va} Total valerate (kgCOD·m⁻³)	5 S_{bu} Total butyrate (kgCOD·m⁻³)	6 S_{pro} Total propionate (kgCOD·m⁻³)	7 S_{ac} Total acetate (kgCOD·m⁻³)	8 S_{h2} Hydrogen gas (kgCOD·m⁻³)	9 S_{ch4} Methane gas (kgCOD·m⁻³)	10 S_{ic} Inorganic carbon (kmoleC·m⁻³)	11 S_{IN} Inorganic nitrogen (kmoleN·m⁻³)	12 S_I Soluble inerts (kgCOD·m⁻³)	Rate (ρ_j, kg COD·m⁻³·d⁻¹)
1	Disintegration												$f_{sI,xc}$	$k_{dis} X_c$
2	Hydrolysis carbohydrates	1												$k_{hyd,ch} X_{ch}$
3	Hydrolysis of proteins		1											$k_{hyd,pr} X_{pr}$
4	Hydrolysis of lipids	$1-f_{fa,li}$		$1-f_{fa,li}$										$k_{hyd,li} X_{li}$
5	Uptake of sugars	−1				$(1-Y_{su})f_{bu,su}$	$(1-Y_{su})f_{pro,su}$	$(1-Y_{su})f_{ac,su}$	$(1-Y_{su})f_{h2,su}$		$-\sum\limits_{i=9,11-24} C_i v_{i,5}$	$-(Y_{su})N_{bac}$		$k_{m,su}\dfrac{S_{su}}{K_S+S}X_{su} I_1$
6	Uptake of amino acids		−1		$(1-Y_{aa})f_{va,aa}$	$(1-Y_{aa})f_{bu,aa}$	$(1-Y_{aa})f_{pro,aa}$	$(1-Y_{aa})f_{ac,aa}$	$(1-Y_{aa})f_{h2,aa}$		$-\sum\limits_{i=1-9,11-24} C_i v_{i,6}$	$N_{aa}-(Y_{aa})N_{bac}$		$k_{m,aa}\dfrac{S_{aa}}{K_S+S_{aa}}X_{aa} I_1$
7	Uptake of LCFA			−1				$(1-Y_{fa})0.7$	$(1-Y_{fa})0.3$			$-(Y_{fa})N_{bac}$		$k_{m,fa}\dfrac{S_{fa}}{K_S+S_{fa}}X_{fa} I_2$
8	Uptake of valerate				−1		$(1-Y_{c4})0.54$	$(1-Y_{c4})0.31$	$(1-Y_{c4})0.15$			$-(Y_{c4})N_{bac}$		$k_{m,c4}\dfrac{S_{va}}{K_S+S_{va}}X_{c4}\dfrac{1}{1+S_{bu}/S_{va}} I_2$
9	Uptake of butyrate					−1		$(1-Y_{c4})0.8$	$(1-Y_{c4})0.2$			$-(Y_{c4})N_{bac}$		$k_{m,c4}\dfrac{S_{bu}}{K_S+S_{bu}}X_{c4}\dfrac{1}{1+S_{va}/S_{bu}} I_2$
10	Uptake of propionate						−1	$(1-Y_{pro})0.57$	$(1-Y_{pro})0.43$		$-\sum\limits_{i=1-9,11-24} C_i v_{i,10}$	$-(Y_{pro})N_{bac}$		$k_{m,pr}\dfrac{S_{pro}}{K_S+S_{pro}}X_{pro} I_2$
11	Uptake of acetate							−1		$(1-Y_{ac})$	$-\sum\limits_{i=1-9,11-24} C_i v_{i,11}$	$-(Y_{ac})N_{bac}$		$k_{m,ac}\dfrac{S_{ac}}{K_S+S_{ac}}X_{ac} I_3$
12	Uptake of hydrogen								−1	$(1-Y_{h2})$	$-\sum\limits_{i=1-9,11-24} C_i v_{i,12}$	$-(Y_{h2})N_{bac}$		$k_{m,h2}\dfrac{S_{h2}}{K_S+S_{h2}}X_{h2} I_1$
13	Decay of X_{su}													$k_{dec,Xsu} X_{su}$
14	Decay of X_{aa}													$k_{dec,Xaa} X_{aa}$
15	Decay of X_{fa}													$k_{dec,Xfa} X_{fa}$
16	Decay of X_{c4}													$k_{dec,Xc4} X_{c4}$
17	Decay of X_{pro}													$k_{dec,Xpro} X_{pro}$
18	Decay of X_{ac}													$k_{dec,Xac} X_{ac}$
19	Decay of X_{h2}													$k_{dec,Xh2} X_{h2}$

Inhibition factors:
$$I_1 = I_{pH} I_{IN,lim}$$
$$I_2 = I_{pH} I_{IN,lim} I_{h2}$$
$$I_3 = I_{pH} I_{IN,lim} I_{NH3,xac}$$

Table A3: Biochemical rate coefficients ($v_{i,j}$) and kinetic rate equations (ρ_j) for particulate components (i = 13–24; j = 1–19).

j	Process ↓ / Component →	13 X_c Composites (kgCOD·m⁻³)	14 X_{ch} Carbohydrates (kgCOD·m⁻³)	15 X_{pr} Proteins (kgCOD·m⁻³)	16 X_{li} Lipids (kgCOD·m⁻³)	17 X_{su} Sugar degraders (kgCOD·m⁻³)	18 X_{aa} Amino acid degraders (kgCOD·m⁻³)	19 X_{fa} LCFA degraders (kgCOD·m⁻³)	20 X_{c4} Valerate and butyrate degraders (kgCOD·m⁻³)	21 X_{pro} Propionate degraders (kgCOD·m⁻³)	22 X_{ac} Acetate degraders (kgCOD·m⁻³)	23 X_{h2} Hydrogen degraders (kgCOD·m⁻³)	24 X_I Particulate inerts (kgCOD·m⁻³)	Rate (ρ_j, kg COD·m⁻³·d⁻¹)
1	Disintegration	-1	$f_{ch,xc}$	$f_{pr,xc}$	$f_{li,xc}$								$f_{xI,xc}$	$k_{dis}X_c$
2	Hydrolysis carbohydrates		-1											$k_{hyd,ch}X_{ch}$
3	Hydrolysis of proteins			-1										$k_{hyd,pr}X_{pr}$
4	Hydrolysis of lipids				-1									$k_{hyd,li}X_{li}$
5	Uptake of sugars					Y_{su}								$k_{m,su}\dfrac{S_{su}}{K_S+S_{su}}X_{su}I_1$
6	Uptake of amino acids						Y_{aa}							$k_{m,aa}\dfrac{S_{aa}}{K_S+S_{aa}}X_{aa}I_1$
7	Uptake of LCFA							Y_{fa}						$k_{m,fa}\dfrac{S_{fa}}{K_S+S_{fa}}X_{fa}I_2$
8	Uptake of valerate								Y_{c4}					$k_{m,c4}\dfrac{S_{va}}{K_S+S_{va}}X_{c4}\dfrac{1}{1+S_{bu}/S_{va}}I_2$
9	Uptake of butyrate								Y_{c4}					$k_{m,c4}\dfrac{S_{bu}}{K_S+S_{bu}}X_{c4}\dfrac{1}{1+S_{va}/S_{bu}}I_2$
10	Uptake of propionate									Y_{pro}				$k_{m,pr}\dfrac{S_{pro}}{K_S+S_{pro}}X_{pro}I_2$
11	Uptake of acetate										Y_{ac}			$k_{m,ac}\dfrac{S_{ac}}{K_S+S_{ac}}X_{ac}I_3$
12	Uptake of hydrogen											Y_{h2}		$k_{m,h2}\dfrac{S_{h2}}{K_S+S_{h2}}X_{h2}I_1$
13	Decay of X_{su}	1				-1								$k_{dec,Xsu}X_{su}$
14	Decay of X_{aa}	1					-1							$k_{dec,Xaa}X_{aa}$
15	Decay of X_{fa}	1						-1						$k_{dec,Xfa}X_{fa}$
16	Decay of X_{c4}	1							-1					$k_{dec,Xc4}X_{c4}$
17	Decay of X_{pro}	1								-1				$k_{dec,Xpro}X_{pro}$
18	Decay of X_{ac}	1									-1			$k_{dec,Xac}X_{ac}$
19	Decay of X_{h2}	1										-1		$k_{dec,Xh2}X_{h2}$

Inhibition factors:
$$I_1 = I_{pH,Iin}$$
$$I_2 = I_{pH,Iin}\cdot I_{h2}$$
$$I_3 = I_{pH,Iin}\cdot I_{NH3,Xac}$$

2. The layout of batch experiments in GPS-X simulator

2.1. Low-pH inhibition with PBS (pH + phosphate) (Chapter 5)
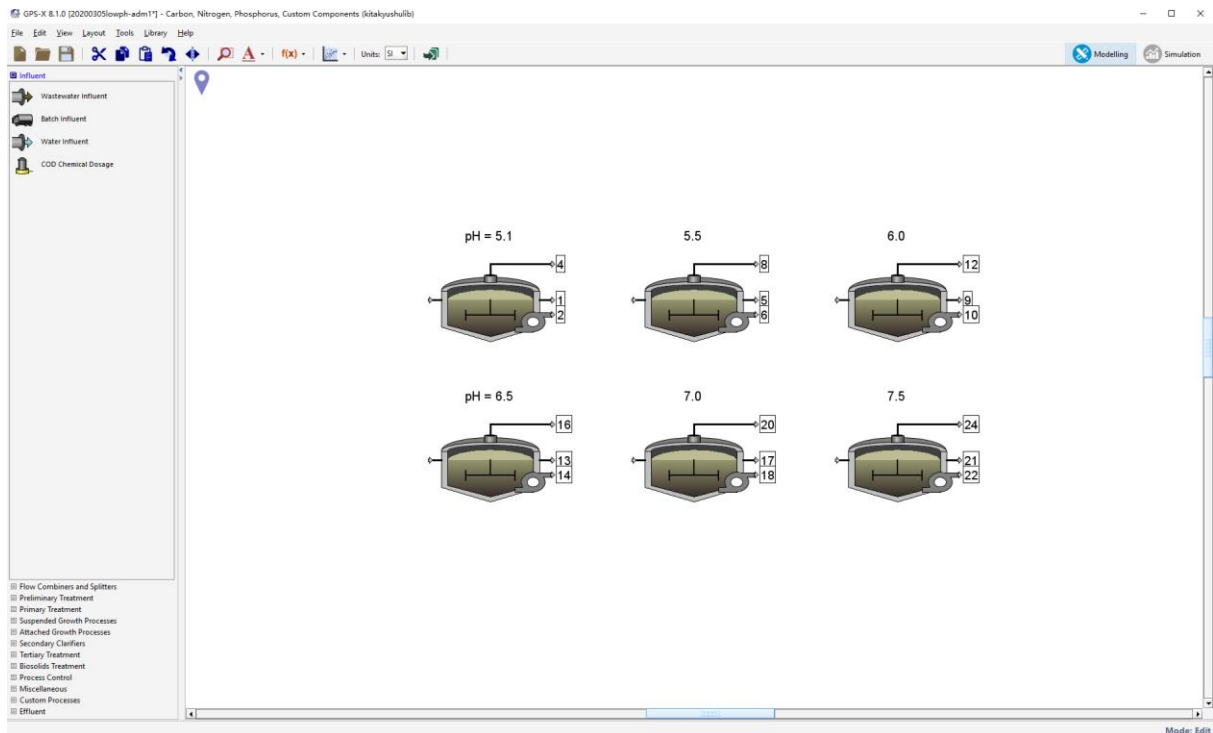
2.2. Recovery of methanogenic activity after acidic failure
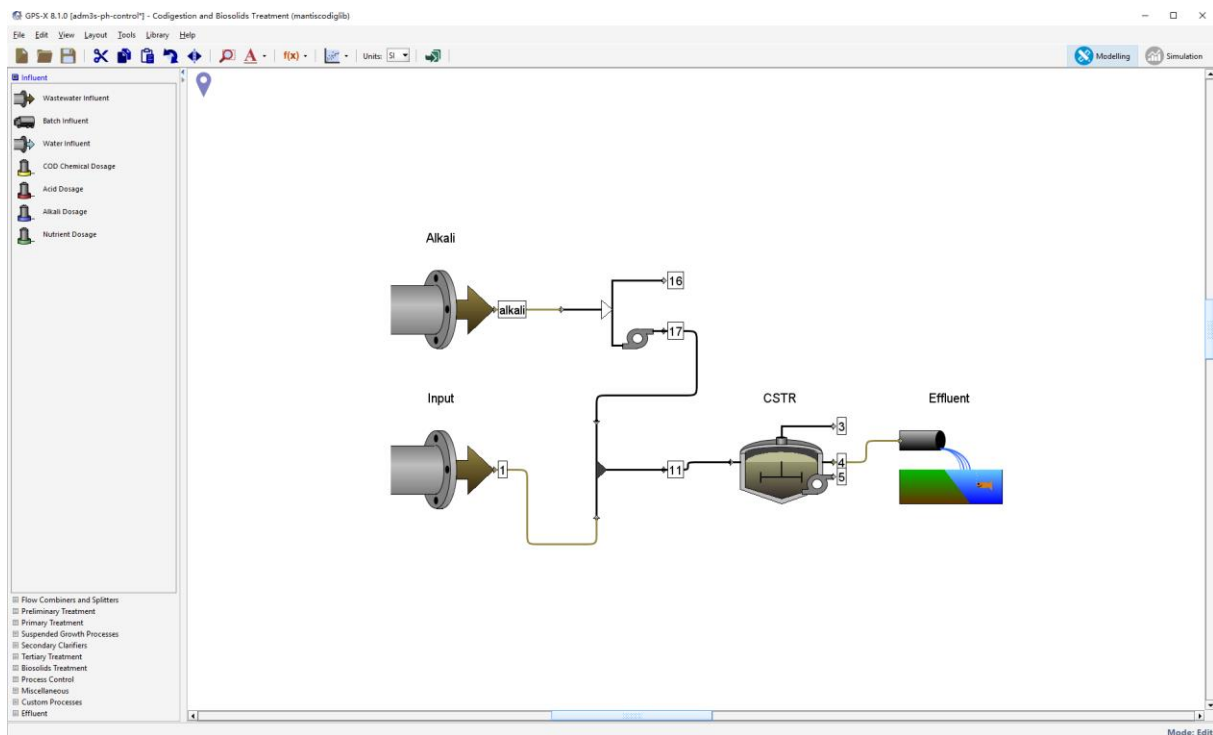
2.3. Low-pH inhibition with additional VFA dosing (pH + unVFA)
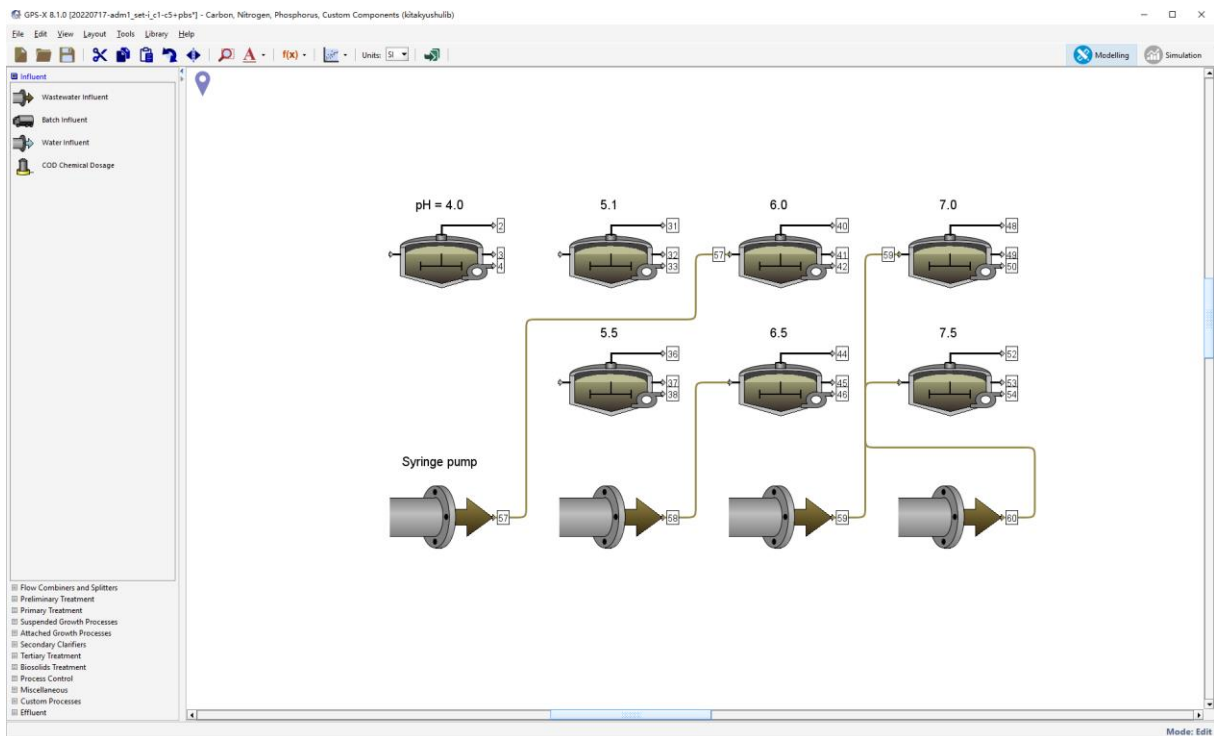
2.4. Methanogen enrichment process with a synthetic acetate/formate buffer (Chapter 6)
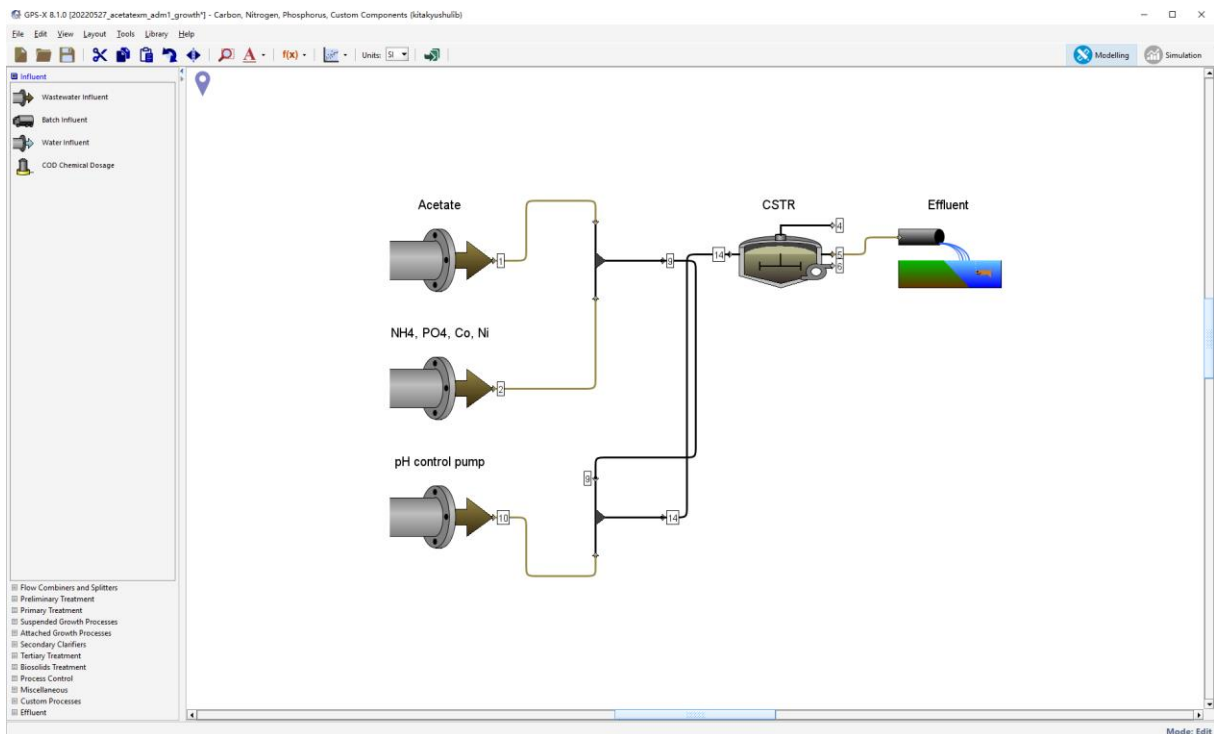
3. Overview of Curve Fitting and Global Fitting in Igor pro

3.1. Curve Fitting

Igor Pro is a scientific data analysis software that offers a wide range of data analysis and graphing capabilities. One of the key features of Igor Pro is the curve fitting feature that allows users to fit mathematical models to their data. The curve fitting process involves defining the mathematical model, estimating the parameters of the model, and evaluating the fit.

The first step in curve fitting involves selecting an appropriate mathematical model that can describe the data being analyzed. Igor Pro offers a range of mathematical models to choose from, such as linear, polynomial, exponential, and logarithmic models. Additionally, you have the option to create custom models using Igor's built-in programming language. After selecting the model, the next step is to establish the data set that will be used for curve fitting. Igor Pro allows for importing data in various formats, such as text files, spreadsheets, and databases. Once the data is imported, you can visualize it using Igor's graphing tools to determine the suitability of the selected model. The following step involves estimating the parameters of the model. Igor Pro provides several methods for parameter estimation, including non-linear least squares, maximum likelihood, and Bayesian estimation. Custom estimation methods can also be defined using Igor's built-in programming language. Finally, the fit of the model to the data must be evaluated. Igor Pro provides several tools for evaluating the fit, such as residual plots, R-squared statistics, and confidence intervals. Additionally, Igor's graphing capabilities can be used to compare the model fit to the data.

In this section, dataset of **Figure 5.1** is taken as an example to introduce the operation steps of curve fitting in detail. First, open the 'New Table' from the 'Windows' menu on the taskbar, name it, and click 'OK' to create the table for importing data. Then, import the corresponding data into the table and rename each column of data. To visualize the imported data, open the 'New Graph' from the 'Windows' menu, select the corresponding X-axis and Y-axis data, and click 'OK' to generate a graph. The color, format, and other options of the graph can be edited by double-clicking on the graph.

Next, select the 'Curve Fitting' icon in the 'Analysis' menu for mathematical analysis. The first step required is to select the corresponding mathematical model in the 'Function and Data' column or create a new model suitable for the data using the 'New Fit Function' option. The data range and weight can be set in the 'Data Options' pane. Finally, give initial estimates for

each parameter in the model in the 'Coefficients' section, and click 'OK' to simulate the data with the set model. The simulation results will appear on the graph created earlier, and the value of each parameter will be displayed in the output pane as shown in **Figure A1**. Of course, the simulated lines can also be edited and modified by double-clicking on them. The above is the basic operation process of the 'Curve Fitting' function in Igor Pro 8.04.
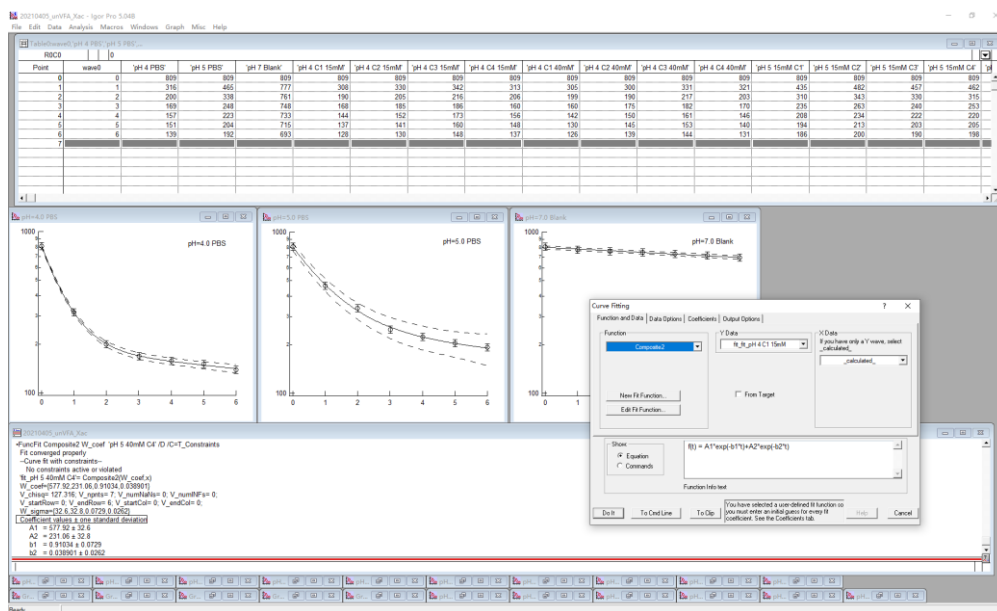
Figure A1 Curve fitting function of Igor pro.

3.2. Global Fit

Another important function of Igor Pro is its global fit tool, which allows users to fit a function to multiple data sets simultaneously. The steps of data import are the same as the curve fitting function mentioned above. To access the global fit tool, go to the 'Analysis' menu and select 'Global fit'. You will be prompted to select the dataset to fit under 'Data sets and Functions'. After selecting a dataset in 'Add data sets', you can choose a fit function from the list of available functions or create a custom function using the formula language in Igor Pro. The global fit tool supports a wide range of fitting functions, including linear, polynomial, exponential, and sinusoidal. The choice of fitting function should depend on the type of data and the type of curve desired. If the available functions do not meet your needs, you can create custom fitting functions using the Igor Pro formula language.

After selecting the fitting function, the fitting parameter '# Coefs' can be adjusted to obtain

the best fit for the data. In the fitting settings 'Coefs-K0', you can flexibly choose to associate some parameters with 'Link Selection' or 'Unlink Selection' according to the relationship between parameters between different data groups. Link correlation means that the selected parameter has the same value in the two sets of data, such as the initial concentration of microorganisms, etc. Moving on to the 'coefficient control' column, you can adjust the initial value of the fitting parameter or set a given value range and choose whether to fix 'Hold' or release during the fitting process. Finally, click 'fit' to obtain the global fit result, as shown in **Figure A2**.
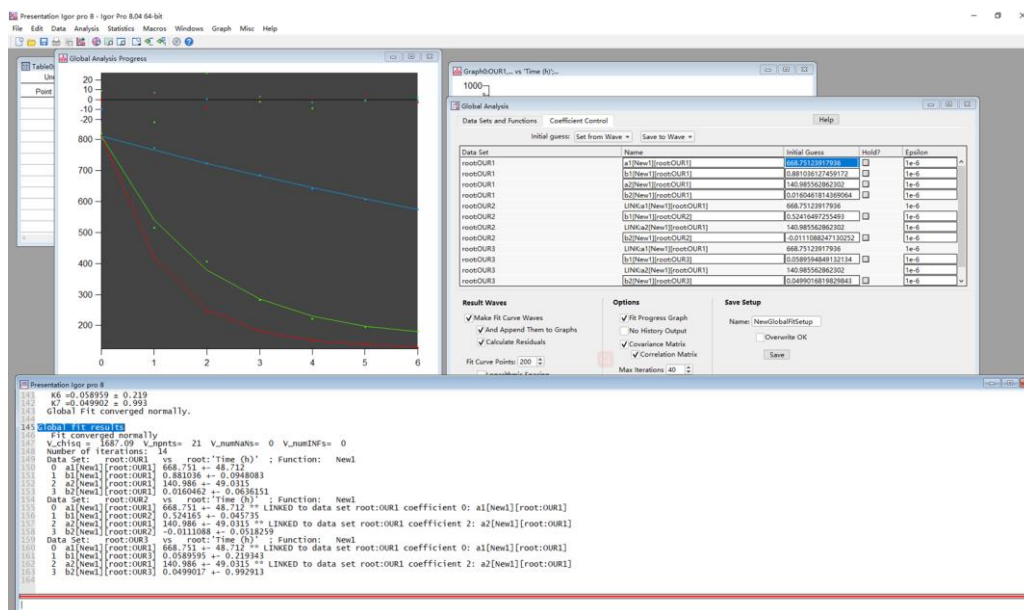
Figure A2 Global fit function of Igor pro.

The Global Fit tool provides information about the quality of the fit, such as the R-squared value and the standard deviation of the fit. It also creates a new graph window showing the raw data and the fitted function. You can use the graph window to adjust the appearance of the graph, such as axis labels and line colors. Additionally, you can save the fitting function as a macro for later use. Igor Pro's statistical tools, including the Global Fit tool, are powerful tools that allow for fitting a function to multiple data sets simultaneously. For more information on Igor Pro's statistical tools and other features, refer to the Igor Pro user manual.

4. RStudio Panes

RStudio is an integrated development environment (IDE) that is designed to enhance productivity in daily data science work. The interface is divided into four key regions or 'panes': the Source pane, the Console pane, the Environment pane, and the Output Pane. The Source pane allows users to edit and save R or Python scripts, or author computational documents. The Console pane is used to write short interactive R commands. The Environment pane displays temporary R objects that are created during the R session, while the Output pane displays the plots, tables, or HTML outputs of executed code, along with files saved to disk.
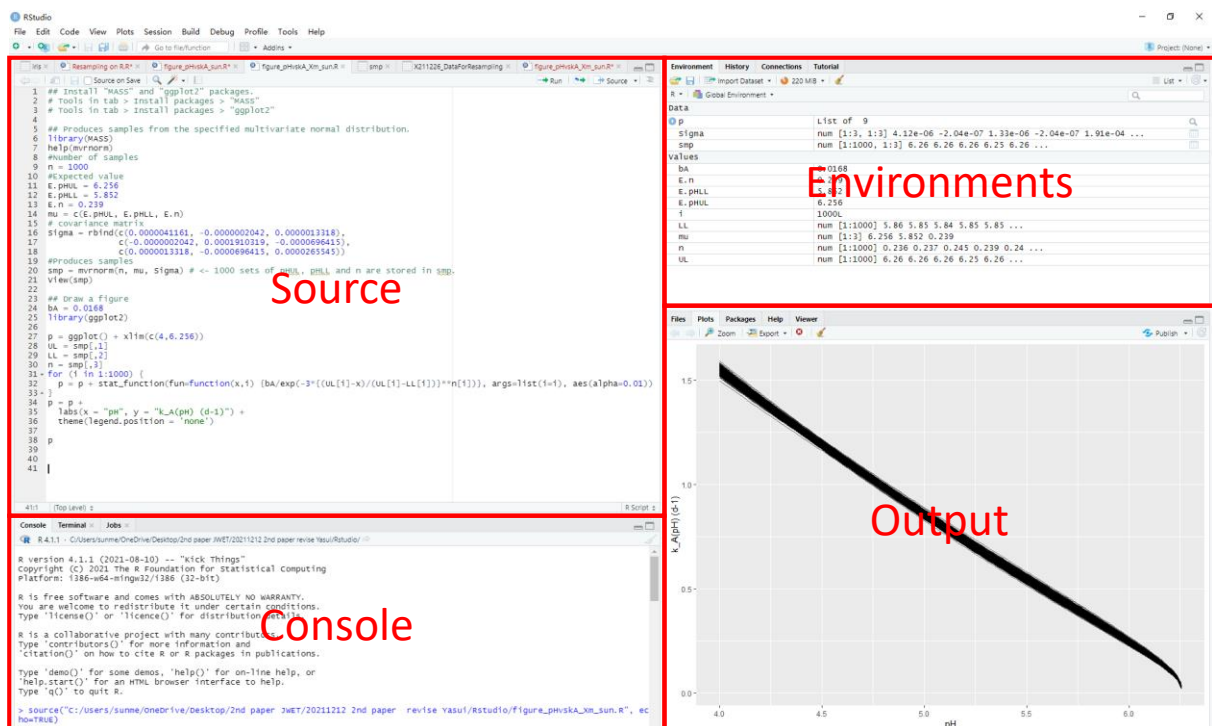
Figure A3 The interface of RStudio.

To visualise the stochastic range of methanogen's specific decay rate at different pH by RStudio, 1,000 sets of pH_{UL}, pH_{LL} and n were generated from the covariance matrix by a Monte-Carlo simulation equipped with Gibbs-sampler where the data plots were assumed to be scattered in a normal distribution. Subsequently, the produced 1,000 non-linear curves were overlapped with each other to create grey-scale in **Figure A**3. The compilation steps to create the Figure 5.21 were demonstrated in **Script A1** and **Script A2**.

Script A1 is the compilation step of Figure 5.21A

```
## Install "MASS" and "ggplot2" packages.
# Tools in tab > Install packages > "MASS"
# Tools in tab > Install packages > "ggplot2"


## Produces samples from the specified multivariate normal distribution.
library(MASS)
help(mvrnorm)
#Number of samples
n = 1000
#Expected value
E.pHUL = 6.2889
E.pHLL = 5.6374
E.n = 0.2595
mu = c(E.pHUL, E.pHLL, E.n)
# covariance matrix
Sigma = rbind(c(0.000479280605232908, -0.000121071463600712, 0.000177592793917508),
        c(-0.000121071463600712, 0.0000591479279761281, -0.000053390103587502),
        c(0.000177592793917508, -0.000053390103587502, 0.000072089316384443))
#Produces samples
smp = mvrnorm(n, mu, Sigma) # <- 1000 sets of pHUL, pHLL and n are stored in smp.
View(smp)

## Draw a figure
bA = 0.0227
library(ggplot2)

p = ggplot() + xlim(c(4,6.288))
UL = smp[,1]
LL = smp[,2]
n = smp[,3]
for (i in 1:1000) {
 p  =  p  +  stat_function(fun=function(x,i)  {bA/exp(-3*{(UL[i]-x)/(UL[i]-LL[i])}**n[i])},
args=list(i=i), aes(alpha=0.01))
}
p = p +
 labs(x = "pH", y = "k_A(pH) (d-1)") +
 theme(legend.position = 'none')

p
```

Script A2 is the compilation step of Figure 5.21B

```
## Install "MASS" and "ggplot2" packages.
# Tools in tab > Install packages > "MASS"
# Tools in tab > Install packages > "ggplot2"


## Produces samples from the specified multivariate normal distribution.
library(MASS)
help(mvrnorm)
#Number of samples
n = 1000
#Expected value
E.pHUL = 6.256
E.pHLL = 5.852
E.n = 0.239
mu = c(E.pHUL, E.pHLL, E.n)
# covariance matrix
Sigma = rbind(c(0.0000041161, -0.0000002042, 0.0000013318),
        c(-0.0000002042, 0.0001910319, -0.0000696415),
        c(0.0000013318, -0.0000696415, 0.0000265545))
#Produces samples
smp = mvrnorm(n, mu, Sigma) # <- 1000 sets of pHUL, pHLL and n are stored in smp.
View(smp)

## Draw a figure
bA = 0.0168
library(ggplot2)

p = ggplot() + xlim(c(4,6.256))
UL = smp[,1]
LL = smp[,2]
n = smp[,3]
for (i in 1:1000) {
 p = p + stat_function(fun=function(x,i) {bA/exp(-3*{(UL[i]-x)/(UL[i]-LL[i])}**n[i])},
args=list(i=i), aes(alpha=0.01))
}
p = p +
 labs(x = "pH", y = "k_A(pH) (d-1)") +
 theme(legend.position = 'none')

p
```

Table A4 Chi-square test for Acetate-fed culture (datasets of pH 4.0 and pH 5.0)

Species	Conc.	k_A (d⁻¹)	1	2	3	4	5	6	7	8	9	10	11	12	13	14	15	16	17	18	19	20	21	22	23	24	25	26	27	28	29	30	31	32	33	34
Dataset			A	A	A	A	A	A	A	A	A	A	A	A	A	A	A	A	A	A	A	A	A	A	A	A	A	A	A	A	A	A	A	A	A	A
pH			pH 4.0																	pH 5.0																
Species			C₁	C₁	C₁	C₂	C₂	C₂	C₃	C₃	C₃	C₄	C₄	C₄	C₅	C₅	C₅	PBS	PBS	C₁	C₁	C₁	C₂	C₂	C₂	C₃	C₃	C₃	C₄	C₄	C₄	C₅	C₅	C₅	PBS	PBS
Conc.			15 mM-un	40 mM-un	3 g-COD/L	15 mM-un	40 mM-un	3 g-COD/L	15 mM-un	40 mM-un	3 g-COD/L	15 mM-un	40 mM-un	3 g-COD/L	15 mM-un	40 mM-un	3 g-COD/L	30 mM	30 mM	15 mM-un	40 mM-un	3 g-COD/L	15 mM-un	40 mM-un	3 g-COD/L	15 mM-un	40 mM-un	3 g-COD/L	15 mM-un	40 mM-un	3 g-COD/L	15 mM-un	40 mM-un	3 g-COD/L	30 mM	30 mM
		k_A (d⁻¹)	1.61 ±0.30	1.57 ±0.30	1.58 ±0.31	1.46 ±0.27	1.62 ±0.30	1.52 ±0.34	1.38 ±0.24	1.46 ±0.26	1.62 ±0.35	1.57 ±0.29	1.50 ±0.27	1.57 ±0.39	1.57 ±0.28	1.60 ±0.27	1.49 ±0.35	1.56 ±0.30	1.49 ±0.34	0.93 ±0.19	1.05 ±0.19	0.79 ±0.22	0.81 ±0.19	0.92 ±0.19	0.82 ±0.27	0.86 ±0.19	0.91 ±0.20	0.82 ±0.27	0.90 ±0.20	0.96 ±0.21	0.99 ±0.28	0.75 ±0.19	0.85 ±0.19	0.99 ±0.19	0.73 ±0.20	0.76 ±0.26
C₁	15 mM-un	1.61 ±0.30		0.99	0.99	0.99	0.99	0.88	0.99	0.99	0.99	0.99	0.99	0.99	0.99	0.99	0.99	0.99	0.99	2.E-06	2.E-03	1.E-12	9.E-12	7.E-07	4.E-11	2.E-09	5.E-07	3.E-11	1.E-07	1.E-05	1.E-12	9.E-09	6.E-06	2.E-13	1.E-10	2.E-14
C₁	40 mM-un	1.57 ±0.30			0.99	0.99	0.99	0.99	0.94	0.99	0.99	0.99	0.99	0.99	0.99	0.99	0.99	0.99	0.99	5.E-06	4.E-03	8.E-12	5.E-11	3.E-06	2.E-10	1.E-08	2.E-06	2.E-10	5.E-07	4.E-05	8.E-12	4.E-08	2.E-05	1.E-12	6.E-10	1.E-13
C₁	3 g-COD/L	1.58 ±0.31				0.99	0.99	0.99	0.93	0.99	0.99	0.99	0.99	0.99	0.99	0.99	0.99	0.99	0.99	4.E-06	3.E-03	4.E-12	3.E-11	2.E-06	1.E-10	6.E-09	1.E-06	9.E-11	3.E-07	3.E-05	4.E-12	3.E-08	1.E-05	7.E-13	4.E-10	6.E-14
C₂	15 mM-un	1.46 ±0.27					0.98	0.99	0.99	0.99	0.98	0.99	0.99	0.99	0.99	0.99	0.99	0.99	0.99	1.E-04	0.003	8.E-10	4.E-09	7.E-05	1.E-08	5.E-07	5.E-05	1.E-08	2.E-05	8.E-04	8.E-10	2.E-06	4.E-04	1.E-10	4.E-08	2.E-11
C₂	40 mM-un	1.62 ±0.30						0.99	0.86	0.98	0.99	0.99	0.99	0.99	0.99	0.99	0.99	0.99	0.99	1.E-06	1.E-03	9.E-13	6.E-12	5.E-07	2.E-11	2.E-09	3.E-07	2.E-11	9.E-08	1.E-05	9.E-13	6.E-09	4.E-06	1.E-13	8.E-11	1.E-14
C₂	3 g-COD/L	1.52 ±0.34							0.98	0.99	0.99	0.99	0.99	0.99	0.99	0.99	0.99	0.99	0.99	2.E-05	0.001	6.E-11	4.E-10	1.E-05	1.E-09	6.E-08	8.E-06	1.E-09	3.E-06	2.E-04	6.E-11	2.E-07	8.E-05	1.E-11	4.E-09	1.E-12
C₃	15 mM-un	1.38 ±0.24								0.99	0.86	0.93	0.99	0.94	0.93	0.90	0.99	0.95	0.99	2.E-03	0.14	3.E-08	2.E-07	9.E-04	5.E-07	1.E-05	7.E-04	4.E-07	3.E-04	7.E-03	3.E-08	4.E-05	4.E-05	7.E-04	1.E-06	9.E-10
C₃	40 mM-un	1.46 ±0.26									0.98	0.99	0.99	0.99	0.99	0.99	0.99	0.99	0.99	1.E-04	0.003	8.E-10	4.E-09	7.E-05	1.E-08	5.E-07	5.E-05	1.E-08	2.E-05	8.E-04	8.E-10	2.E-06	4.E-04	1.E-10	4.E-08	2.E-11
C₃	3 g-COD/L	1.62 ±0.35										0.99	0.99	0.99	0.99	0.99	0.99	0.99	0.99	1.E-06	1.E-03	9.E-13	6.E-12	5.E-07	2.E-11	2.E-09	3.E-07	2.E-11	9.E-08	1.E-05	9.E-13	6.E-09	4.E-06	1.E-13	8.E-11	1.E-14

	C_4	15 mM-un	1.57 ±0.29								0.99	0.99	0.99	0.99	0.99	0.99	0.99	5.E-06	3.E-03	6.E-12	4.E-11	2.E-06	2.E-10	9.E-09	2.E-06 1.E-10 5.E-07 4.E-05 6.E-12 3.E-08 2.E-05 1.E-12 5.E-10 9.E-14
	C_4	40 mM-un	1.50 ±0.27									0.99	0.99	0.99	0.99	0.99	0.99	5.E-05	0.02	2.E-10	1.E-09	2.E-05	3.E-09	1.E-07	2.E-05 3.E-09 6.E-06 3.E-04 2.E-10 5.E-07 2.E-04 3.E-11 1.E-08 3.E-12
	C_4	3 g-COD/L	1.57 ±0.39										0.99	0.99	0.99	0.99	0.99	5.E-06	4.E-03	8.E-12	5.E-11	3.E-06	2.E-10	1.E-08	2.E-06 2.E-10 5.E-07 4.E-05 8.E-12 4.E-08 2.E-05 1.E-12 6.E-10 1.E-13
	C_5	15 mM-un	1.57 ±0.28											0.99	0.99	0.99	0.99	5.E-06	3.E-03	6.E-12	4.E-11	2.E-06	2.E-10	9.E-09	2.E-06 1.E-10 5.E-07 4.E-05 6.E-12 3.E-08 2.E-05 1.E-12 5.E-10 9.E-14
	C_5	40 mM-un	1.60 ±0.27												0.99	0.99	0.99	2.E-06	2.E-03	2.E-12	1.E-11	1.E-06	6.E-11	4.E-09	7.E-07 5.E-11 2.E-07 2.E-05 2.E-12 2.E-08 1.E-06 9.E-13 4.E-10 3.E-14
	C_5	3 g-COD/L	1.49 ±0.35													0.99	0.99	6.E-05	0.02	2.E-10	1.E-09	3.E-05	5.E-09	2.E-07	2.E-05 4.E-09 8.E-06 4.E-04 2.E-10 7.E-07 2.E-04 5.E-11 1.E-08 5.E-12
	PBS	30 mM	1.56 ±0.30														0.99	7.E-06	5.E-03	1.E-11	7.E-11	3.E-06	3.E-10	2.E-08	3.E-06 2.E-10 8.E-07 6.E-05 1.E-11 6.E-08 3.E-05 2.E-12 9.E-10 2.E-13
	PBS	30 mM	1.49 ±0.34															5.E-05	0.02	2.E-10	1.E-09	3.E-05	4.E-09	2.E-07	2.E-05 3.E-09 7.E-06 4.E-04 2.E-10 6.E-07 2.E-04 4.E-11 1.E-08 4.E-12
pH 5.0	C_1	15 mM-un	0.93 ±0.19	x x x x x x x x x x x x x x x x x												0.88	0.56	0.70	0.99	0.80	0.97	0.99	0.79 0.99 0.99 0.56 0.99 0.99 0.42 0.87 0.26
	C_1	40 mM-un	1.05 ±0.19	x x x x x x x x x x x x x x x x												0.03	0.06	0.83	0.10	0.32	0.80	0.09	0.69 0.97 0.03 0.44 0.95 0.02 0.14 0.01
	C_1	3 g-COD/L	0.79 ±0.22	x x x x x x x x x x x x x x x x x											x	0.99	0.64	0.99	0.97	0.68	0.99	0.79	0.33 0.99 0.99 0.41 0.99 0.99 0.99
	C_2	15 mM-un	0.81 ±0.19	x x x x x x x x x x x x x x x x x												0.78	0.99	0.99	0.80	0.99	0.99	0.47 0.99 0.99 0.55 0.99 0.99 0.99
	C_2	40 mM-un	0.92 ±0.19	x x x x x x x x x x x x x x x x x													0.86	0.99	0.99	0.85	0.99	0.99	0.64 0.99 0.99 0.50 0.99 0.33
	C_2	3 g-COD/L	0.82 ±0.27	x x x x x x x x x x x x x x x x x													0.99	0.88	0.99	0.94	0.48	0.99	0.99 0.67 0.99 0.99 0.98

			x1	x2	x3	x4	x5	x6	x7	x8	x9	x10	x11	x12	x13	x14	x15	x16	x17												
C_3	15 mM-un	0.86 ±0.19	x	x	x	x	x	x	x	x	x	x	x	x	x	x	x	x	x		0.99	0.99	0.99	0.88	0.97	0.99	0.92	0.93	0.99	0.83
C_3	40 mM-un	0.91 ±0.20	x	x	x	x	x	x	x	x	x	x	x	x	x	x	x	x	x			0.87	0.99	0.99	0.68	0.99	0.99	0.54	0.93	0.36
C_3	3 g-COD/L	0.82 ±0.27	x	x	x	x	x	x	x	x	x	x	x	x	x	x	x	x	x				0.93	0.56	0.99	0.99	0.65	0.99	0.99	0.98
C_4	15 mM-un	0.90 ±0.20	x	x	x	x	x	x	x	x	x	x	x	x	x	x	x	x	x					0.99	0.79	0.99	0.99	0.66	0.97	0.48
C_4	40 mM-un	0.96 ±0.21	x	x	x	x	x	x	x	x	x	x	x	x	x	x	x	x	x						0.33	0.94	0.99	0.22	0.68	0.11
C_4	3 g-COD/L	0.79 ±0.28	x	x	x	x	x	x	x	x	x	x	x	x	x	x	x	x	x	x						0.94	0.41	0.99	0.99	0.99
C_5	15 mM-un	0.87 ±0.19	x	x	x	x	x	x	x	x	x	x	x	x	x	x	x	x	x								0.96	0.87	0.99	0.73
C_5	40 mM-un	0.95 ±0.19	x	x	x	x	x	x	x	x	x	x	x	x	x	x	x	x	x									0.28	0.76	0.15
C_5	3 g-COD/L	0.78 ±0.28	x	x	x	x	x	x	x	x	x	x	x	x	x	x	x	x	x	x									0.99	0.99
PBS	30 mM	0.83 ±0.20	x	x	x	x	x	x	x	x	x	x	x	x	x	x	x	x	x											0.96
PBS	30 mM	0.76 ±0.26	x	x	x	x	x	x	x	x	x	x	x	x	x	x	x	x	x	x										

Remark: C_1: formate, C_2: acetate, C_3: propionate, C_4: butyrate, C_5: valerate, PBS: phosphate buffer, mM-un: millimolar-based unionised VFA concentration, k_A: specific rate obtained from double exponential function, k_{A+B}: specific rate obtained from single exponential function, ±: half width of 95%-confidence interval from the mean, x: p-value ≤ 0.05, greyed-out cell: not used for further analysis because of large confidence interval and low r^2.

Table A5 Chi-square test for Acetate-fed culture (datasets of pH 5.0–6.0)

Dataset			18A	19A	20A	21A	22A	23A	24A	25A	26A	27A	28A	29A	30A	31A	32A	33A	34A	35A	36A	37A	38A	39A	40A	41A	42A	43A	44A	45A	46A
pH			pH 5.0																	pH 5.5						pH 6.0					
	Species		C_1	C_1	C_1	C_2	C_2	C_2	C_3	C_3	C_3	C_4	C_4	C_4	C_5	C_5	C_5	PBS	PBS	C_1	C_2	C_3	C_4	C_5	PBS	C_1	C_2	C_3	C_4	C_5	PBS
	Conc.		15 mM-un	40 mM-un	3 g-COD/L	15 mM-un	40 mM-un	3 g-COD/L	15 mM-un	40 mM-un	3 g-COD/L	15 mM-un	40 mM-un	3 g-COD/L	15 mM-un	40 mM-un	3 g-COD/L	30 mM	30 mM	3 g-COD/L	3 g-COD/L	3 g-COD/L	3 g-COD/L	3 g-COD/L	30 mM	3 g-COD/L	3 g-COD/L	3 g-COD/L	3 g-COD/L	3 g-COD/L	30 mM
		k_A (d^{-1})	0.93 ±0.19	1.05 ±0.19	0.79 ±0.22	0.81 ±0.19	0.92 ±0.19	0.82 ±0.27	0.86 ±0.19	0.91 ±0.20	0.82 ±0.27	0.90 ±0.20	0.96 ±0.21	0.79 ±0.28	0.87 ±0.19	0.95 ±0.19	0.78 ±0.28	0.83 ±0.20	0.76 ±0.26	0.65 ±0.25	0.63 ±0.31	0.63 ±0.29	0.51 ±0.40	0.59 ±0.32	0.65 ±0.29	0.24 ±0.96	0.30 ±1.13	0.27 ±0.74	0.25 ±0.76	0.27 ±0.61	0.23 ±1.34
pH 5.0 C_1	15 mM-un	0.93 ±0.19		0.88	0.56	0.70	0.99	0.80	0.97	0.99	0.79	0.99	0.99	0.56	0.99	0.99	0.42	0.87	0.26	1.E-04	1.E-05	1.E-05	2.E-16	6.E-08	9.E-05	0.E+00	0.E+00	0.E+00	0.E+00	0.E+00	0.E+00
C_1	40 mM-un	1.05 ±0.19			0.03	0.06	0.83	0.10	0.32	0.80	0.09	0.69	0.97	0.03	0.44	0.95	0.02	0.14	0.01	5.E-08	2.E-09	2.E-09	0.E+00	2.E-12	3.E-08	0.E+00	0.E+00	0.E+00	0.E+00	0.E+00	0.E+00
C_1	3 g-COD/L	0.79 ±0.22			x	0.99	0.64	0.99	0.97	0.68	0.99	0.79	0.33	0.99	0.94	0.41	0.99	0.99	0.99	0.16	0.05	0.05	3.E-09	2.E-03	0.13	0.E+00	0.E+00	0.E+00	0.E+00	0.E+00	0.E+00
C_2	15 mM-un	0.81 ±0.19					0.78	0.99	0.99	0.80	0.99	0.89	0.47	0.99	0.98	0.55	0.99	0.99	0.99	0.09	0.02	0.02	5.E-10	9.E-04	0.07	0.E+00	0.E+00	0.E+00	0.E+00	0.E+00	0.E+00
C_2	40 mM-un	0.92 ±0.19						0.86	0.98	0.99	0.85	0.99	0.99	0.64	0.99	0.99	0.50	0.91	0.33	3.E-04	2.E-05	2.E-05	8.E-16	1.E-07	2.E-04	0.E+00	0.E+00	0.E+00	0.E+00	0.E+00	0.E+00
C_2	3 g-COD/L	0.82 ±0.27							0.99	0.88	0.99	0.94	0.58	0.99	0.99	0.67	0.99	0.99	0.98	0.06	0.01	0.01	1.E-10	4.E-04	0.04	0.E+00	0.E+00	0.E+00	0.E+00	0.E+00	0.E+00
C_3	15 mM-un	0.86 ±0.19								0.99	0.99	0.99	0.88	0.97	0.99	0.92	0.93	0.99	0.83	9.E-03	2.E-03	1.E-03	1.E-12	2.E-05	7.E-03	0.E+00	0.E+00	0.E+00	0.E+00	0.E+00	0.E+00
C_3	40 mM-un	0.91 ±0.20									0.87	0.99	0.99	0.68	0.99	0.99	0.54	0.93	0.36	3.E-04	3.E-05	3.E-05	1.E-15	2.E-07	2.E-04	0.E+00	0.E+00	0.E+00	0.E+00	0.E+00	0.E+00
C_3	3 g-COD/L	0.82 ±0.27										0.93	0.56	0.99	0.99	0.65	0.99	0.99	0.98	0.06	0.01	0.01	2.E-10	4.E-04	0.05	0.E+00	0.E+00	0.E+00	0.E+00	0.E+00	0.E+00
C_4	15 mM-un	0.90 ±0.20											0.99	0.79	0.99	0.99	0.66	0.97	0.48	9.E-04	9.E-05	8.E-05	8.E-15	7.E-07	6.E-04	0.E+00	0.E+00	0.E+00	0.E+00	0.E+00	0.E+00

		Mean ±SD																			
	C_4	40 mM-un	0.96 ±0.21							0.33	0.94	0.99	0.22	0.68	0.11	2.E-05	1.E-06	1.E-06	0.E+00	5.E-09	1.E-05	0.E+00 0.E+00 0.E+00 0.E+00 0.E+00 0.E+00
	C_4	3 g-COD/L	0.79 ±0.28	x					0.94	0.41	0.99	0.99	0.99	0.16	0.05	0.05	3.E-09	2.E-03		0.13	0.E+00 0.E+00 0.E+00 0.E+00 0.E+00 0.E+00
	C_5	15 mM-un	0.87 ±0.19							0.96	0.87	0.99	0.73	4.E-03	6.E-04	6.E-04	3.E-13	8.E-06	3.E-03	0.E+00 0.E+00 0.E+00 0.E+00 0.E+00 0.E+00
	C_5	40 mM-un	0.95 ±0.19								0.28	0.76	0.15	4.E-05	3.E-06	3.E-06	0.E+00	1.E-08	2.E-05	0.E+00 0.E+00 0.E+00 0.E+00 0.E+00 0.E+00
	C_5	3 g-COD/L	0.78 ±0.28	x								0.99	0.99	0.26	0.09	0.09	1.E-08	6.E-03	0.22	0.E+00 0.E+00 0.E+00 0.E+00 0.E+00 0.E+00
	PBS	30 mM	0.83 ±0.20										0.96	0.04	7.E-03	7.E-03	4.E-11	2.E-04	0.03	0.E+00 0.E+00 0.E+00 0.E+00 0.E+00 0.E+00
	PBS	30 mM	0.76 ±0.26	x										0.42	0.18	0.17	9.E-08	2.E-02	0.36	0.E+00 0.E+00 0.E+00 0.E+00 0.E+00 0.E+00
pH 5.5	C_1	3 g-COD/L	0.65 ±0.25	x x	x	x x	x x	x x	x			0.99	0.99	0.01	0.90	0.99	0.E+00 0.E+00 0.E+00 0.E+00 0.E+00 0.E+00
	C_2	3 g-COD/L	0.63 ±0.31	x x x x x x x x x x x x	x						0.99	0.04	0.98	0.99	0.E+00 0.E+00 0.E+00 0.E+00 0.E+00 0.E+00
	C_3	3 g-COD/L	0.63 ±0.29	x x x x x x x x x x x x	x							0.04	0.98	0.99	0.E+00 0.E+00 0.E+00 0.E+00 0.E+00 0.E+00
	C_4	3 g-COD/L	0.51 ±0.40	x x x x x x x x x x x x x x x	x x x					0.30	0.01	0.E+00 0.E+00 0.E+00 0.E+00 0.E+00 0.E+00
	C_5	3 g-COD/L	0.59 ±0.32	x x x x x x x x x x x x x x x								0.92	0.E+00 0.E+00 0.E+00 0.E+00 0.E+00 0.E+00
	PBS	30 mM	0.65 ±0.29	x x x x x x x x x x x	x				x		0.E+00 0.E+00 0.E+00 0.E+00 0.E+00 0.E+00

pH																															
pH 6.0	C_1	3 g-COD/L	0.24 ±0.96	x	x	x	x	x	x	x	x	x	x	x	x	x	x	x	x	x	x	x	x	x		**0.03**	0.71	0.99	0.68	0.99
	C_2	3 g-COD/L	0.30 ±1.13	x	x	x	x	x	x	x	x	x	x	x	x	x	x	x	x	x	x	x	x	x	x		0.75	0.12	0.78	**0.01**
	C_3	3 g-COD/L	0.27 ±0.74	x	x	x	x	x	x	x	x	x	x	x	x	x	x	x	x	x	x	x	x				0.94	0.99	0.29
	C_4	3 g-COD/L	0.25 ±0.76	x	x	x	x	x	x	x	x	x	x	x	x	x	x	x	x	x	x	x	x					0.92	0.93
	C_5	3 g-COD/L	0.27 ±0.61	x	x	x	x	x	x	x	x	x	x	x	x	x	x	x	x	x	x	x	x						0.27
	PBS	30 mM	0.23 ±1.34	x	x	x	x	x	x	x	x	x	x	x	x	x	x	x	x	x	x	x	x	x						

Remark: C_1: formate, C_2: acetate, C_3: propionate, C_4: butyrate, C_5: valerate, PBS: phosphate buffer, mM-un: millimolar-based unionised VFA concentration, k_A: specific rate obtained from double exponential function, k_{A+B}: specific rate obtained from single exponential function, ±: half width of 95%-confidence interval from the mean, x: p-value ≤ 0.05, greyed-out cell: not used for further analysis because of large confidence interval and low r^2.

Table A6 Chi-square test for Acetate-fed culture (datasets of pH 6.5–7.5)

pH	Species	Conc.	k_A (d^{-1})	k_{A+B} (d^{-1})	47A	48A	49A	50A	51A	52A	53A	54A	55A	56A	57A	58A	59A	60A	61A	62A	63A	64A	65A
pH	Species	Conc.			pH 6.5						pH 7.0							pH 7.5					
					C1	C2	C3	C4	C5	PBS	C1	C2	C3	C4	C5	PBS	PBS	C1	C2	C3	C4	C5	PBS
					3 g-COD/L	3 g-COD/L	3 g-COD/L	3 g-COD/L	3 g-COD/L	30 mM	3 g-COD/L	3 g-COD/L	3 g-COD/L	3 g-COD/L	3 g-COD/L	30 mM	30 mM	3 g-COD/L	3 g-COD/L	3 g-COD/L	3 g-COD/L	3 g-COD/L	30 mM
			k_A (d^{-1})		0.07 ±3.90	0.09 ±1.62	0.13 ±1.19	0.15 ±0.72	0.11 ±1.41	0.06 ±27.1	0.04 ±4.99	0.02 ±1.22	0.04 ±3.27	0.04 ±1.89	0.03 ±3.21	0.03 ±7.20	0.03 ±9.08	0.04 ±4.46	-0.01 ±1.72	0.04 ±3.64	0.04 ±2.01	0.04 ±1.84	0.02 ±49.7
				k_{A+B} (d^{-1})	0.050 ±0.011	0.030 ±0.014	0.060 ±0.012	0.050 ±0.013	0.050 ±0.013	0.050 ±0.011	0.020 ±0.012	-0.050 ±0.013	0.010 ±0.011	-0.010 ±0.013	-0.010 ±0.013	0.024 ±0.007	0.020 ±0.012	0.010 ±0.011	-0.060 ±0.013	0.010 ±0.011	-0.010 ±0.012	-0.010 ±0.012	0.020 ±0.013
pH 6.5	C1	3 g-COD/L	0.07 ±3.90	0.050 ±0.011		0.06	0.83	0.99	0.99	0.99	1.E-04	0.E+00	4.E-09	0.E+00	0.E+00	2.E-03	1.E-04	4.E-09	0.E+00	4.E-09	0.E+00	0.E+00	1.E-04
	C2	3 g-COD/L	0.09 ±1.62	0.030 ±0.014			2.E-04	0.06	0.06	0.06	0.79	0.E+00	0.04	4.E-10	4.E-10	0.98	0.79	0.04	0.E+00	0.04	4.E-10	4.E-10	0.79
	C3	3 g-COD/L	0.13 ±1.19	0.060 ±0.012			x	0.83	0.83	0.83	1.E-08	0.E+00	2.E-14	0.E+00	0.E+00	9.E-07	1.E-08	2.E-14	0.E+00	2.E-14	0.E+00	0.E+00	1.E-08
	C4	3 g-COD/L	0.15 ±0.72	0.050 ±0.013					0.99	0.99	1.E-04	0.E+00	4.E-09	0.E+00	0.E+00	2.E-03	1.E-04	4.E-09	0.E+00	4.E-09	0.E+00	0.E+00	1.E-04
	C5	3 g-COD/L	0.11 ±1.41	0.050 ±0.013						0.99	1.E-04	0.E+00	4.E-09	0.E+00	0.E+00	2.E-03	1.E-04	4.E-09	0.E+00	4.E-09	0.E+00	0.E+00	1.E-04
	PBS	30 mM	0.06 ±27.1	0.050 ±0.011							1.E-04	0.E+00	4.E-09	0.E+00	0.E+00	2.E-03	1.E-04	4.E-09	0.E+00	4.E-09	0.E+00	0.E+00	1.E-04
pH 7.0	C1	3 g-COD/L	0.04 ±4.99	0.020 ±0.012	x		x	x	x	x		0.E+00	0.75	1.E-05	1.E-05	0.99	0.99	0.75	0.E+00	0.75	1.E-05	1.E-05	0.99
	C2	3 g-COD/L	0.02 ±1.22	-0.050 ±0.013	x	x	x	x	x	x	x		0.E+00	1.E-12	1.E-12	0.E+00	0.E+00	0.E+00	0.57	0.E+00	1.E-12	1.E-12	0.E+00
	C3	3 g-COD/L	0.04 ±3.27	0.010 ±0.011	x		x	x	x	x		x		0.02	0.02	0.36	0.75	0.99	0.E+00	0.99	0.02	0.02	0.75
	C4	3 g-COD/L	0.04 ±1.89	-0.010 ±0.013	x	x	x	x	x	x	x	x	x		0.99	3.E-07	1.E-05	0.02	0.E+00	0.02	0.99	0.99	1.E-05
	C5	3 g-COD/L	0.03 ±3.21	-0.010 ±0.013	x	x	x	x	x	x	x	x	x	x		3.E-07	1.E-05	0.02	0.E+00	0.02	0.99	0.99	1.E-05
	PBS	30 mM	0.03 ±7.20	0.024 ±0.007	x		x	x	x	x	x			x	x		0.99	0.36	0.E+00	0.36	3.E-07	3.E-07	0.99
	PBS	30 mM	0.03 ±9.08	0.020 ±0.012	x		x	x	x	x	x		x		x			0.75	0.E+00	0.75	1.E-05	1.E-05	0.99

178

pH			k_A	k_{A+B}																					
pH 7.5	C₁	3 g-COD/L	0.04 ±4.46	0.010 ±0.011	x	x	x	x	x	x		x		x	x						0.E+00	0.99	0.02	0.02	0.75
	C₂	3 g-COD/L	-0.01 ±1.72	-0.060 ±0.013	x	x	x	x	x	x	x		x	x	x	x	x		x		0.E+00	0.E+00	0.E+00	0.E+00
	C₃	3 g-COD/L	0.04 ±3.64	0.010 ±0.011	x	x	x	x	x	x		x		x	x				x			0.02	0.02	0.75
	C₄	3 g-COD/L	0.04 ±2.01	-0.010 ±0.012	x	x	x	x	x	x	x	x	x			x	x	x	x	x				0.99	1.E-05
	C₅	3 g-COD/L	0.04 ±1.84	-0.010 ±0.012	x	x	x	x	x	x	x	x	x			x	x	x	x	x					1.E-05
	PBS	30 mM	0.02 ±49.7	0.020 ±0.013	x		x	x	x	x		x		x	x				x				x	x	

Remark: C₁: formate, C₂: acetate, C₃: propionate, C₄: butyrate, C₅: valerate, PBS: phosphate buffer, mM-un: millimolar-based unionised VFA concentration, k_A: specific rate obtained from double exponential function, k_{A+B}: specific rate obtained from single exponential function, ±: half width of 95%-confidence interval from the mean, x: p-value ≤ 0.05, greyed-out cell: not used for further analysis because of large confidence interval and low r^2.

Table A7 Chi-square test for Formate-fed culture (datasets of pH 4.0 and pH 5.0)

Dataset			1F	2F	3F	4F	5F	6F	7F	8F	9F	10F	11F	12F	13F	14F	15F	16F	17F	18F	19F	20F	21F	22F	23F	24F	25F	26F	27F	28F	29F	30F	31F	32F	33F	34F
pH			pH 4.0																	pH 5.0																
	Species		C_1	C_1	C_1	C_2	C_2	C_2	C_3	C_3	C_3	C_4	C_4	C_4	C_5	C_5	C_5	PBS	PBS	C_1	C_1	C_1	C_2	C_2	C_2	C_3	C_3	C_3	C_4	C_4	C_4	C_5	C_5	C_5	PBS	PBS
	Conc.		15 mM-un	40 mM-un	3 g-COD/L	15 mM-un	40 mM-un	3 g-COD/L	15 mM-un	40 mM-un	3 g-COD/L	15 mM-un	40 mM-un	3 g-COD/L	15 mM-un	40 mM-un	3 g-COD/L	30 mM M	30 mM M	15 mM-un	40 mM-un	3 g-COD/L	15 mM-un	40 mM-un	3 g-COD/L	15 mM-un	40 mM-un	3 g-COD/L	15 mM-un	40 mM-un	3 g-COD/L	15 mM-un	40 mM-un	3 g-COD/L	30 mM M	30 mM M
		k_A (d^{-1})	1.58 ±0.32	1.56 ±0.31	1.71 ±0.29	1.61 ±0.34	1.50 ±0.30	1.62 ±0.28	1.52 ±0.31	1.52 ±0.32	1.55 ±0.32	1.56 ±0.32	1.45 ±0.29	1.63 ±0.31	1.54 ±0.31	1.55 ±0.33	1.60 ±0.28	1.56 ±0.32	1.64 ±0.26	0.97 ±0.24	1.08 ±0.25	0.92 ±0.21	0.93 ±0.25	0.94 ±0.26	0.92 ±0.21	0.98 ±0.24	1.08 ±0.27	0.87 ±0.24	0.96 ±0.24	1.04 ±0.27	0.93 ±0.21	0.84 ±0.21	0.93 ±0.22	0.90 ±0.22	1.02 ±0.27	0.91 ±0.18
pH 4.0 — C_1 — 15 mM-un — 1.58 ±0.32				0.99	0.99	0.99	0.99	0.99	0.99	0.99	0.99	0.99	0.98	0.99	0.99	0.99	0.99	0.99	0.99	4.E-06	3.E-03	7.E-08	3.E-07	4.E-07	9.E-08	9.E-06	4.E-03	6.E-10	3.E-06	4.E-04	2.E-07	3.E-11	2.E-07	1.E-08	1.E-04	3.E-08
C_1 — 40 mM-un — 1.56 ±0.31					0.98	0.99	0.99	0.99	0.99	0.99	0.99	0.99	0.99	0.99	0.99	0.99	0.99	0.99	0.99	1.E-05	5.E-03	2.E-07	7.E-07	1.E-06	2.E-07	2.E-05	6.E-03	2.E-09	7.E-06	7.E-04	4.E-07	8.E-11	4.E-07	3.E-08	3.E-04	8.E-08
C_1 — 3 g-COD/L — 1.71 ±0.29						0.99	0.92	0.99	0.95	0.98	0.98	0.98	0.80	0.99	0.97	0.99	0.99	0.98	0.99	5.E-08	1.E-04	5.E-10	2.E-09	4.E-09	6.E-10	1.E-07	1.E-04	3.E-12	4.E-08	1.E-05	1.E-09	8.E-14	1.E-09	6.E-11	3.E-06	2.E-10
C_2 — 15 mM-un — 1.61 ±0.34							0.99	0.99	0.99	0.99	0.99	0.99	0.97	0.99	0.99	0.99	0.99	0.99	0.99	2.E-06	1.E-03	2.E-08	9.E-08	1.E-07	3.E-08	3.E-06	2.E-03	2.E-10	1.E-06	2.E-04	5.E-08	7.E-12	5.E-08	3.E-09	6.E-05	9.E-09
C_2 — 40 mM-un — 1.50 ±0.30								0.99	0.99	0.99	0.99	0.99	0.99	0.99	0.99	0.98	0.99	0.99	0.99	7.E-05	0.02	2.E-06	6.E-06	9.E-06	2.E-06	1.E-04	0.02	2.E-08	5.E-05	3.E-03	4.E-06	1.E-09	4.E-06	3.E-07	2.E-03	8.E-07
C_2 — 3 g-COD/L — 1.62 ±0.28									0.99	0.99	0.99	0.99	0.96	0.99	0.99	0.99	0.99	0.99	0.99	1.E-06	1.E-03	2.E-08	7.E-08	1.E-07	2.E-08	2.E-06	1.E-03	1.E-10	9.E-07	1.E-04	4.E-08	5.E-12	4.E-08	2.E-09	5.E-05	7.E-09
C_3 — 15 mM-un — 1.52 ±0.31										0.99	0.99	0.99	0.99	0.99	0.99	0.99	0.99	0.99	4.E-05	0.01	9.E-07	3.E-06	5.E-06	1.E-06	7.E-05	0.02	1.E-08	3.E-05	2.E-03	2.E-06	6.E-10	2.E-06	1.E-07	1.E-03	4.E-07
C_3 — 40 mM-un — 1.55 ±0.32											0.99	0.99	0.99	0.99	0.99	0.99	0.99	0.99	1.E-05	6.E-03	2.E-07	1.E-06	1.E-06	3.E-07	2.E-05	8.E-03	3.E-09	1.E-05	9.E-04	6.E-07	1.E-10	6.E-07	4.E-08	4.E-04	1.E-07
C_3 — 3 g-COD/L — 1.55 ±0.32												0.99	0.99	0.99	0.99	0.99	0.99	0.99	1.E-05	6.E-03	2.E-07	1.E-06	1.E-06	3.E-07	2.E-05	8.E-03	3.E-09	1.E-05	9.E-04	6.E-07	1.E-10	6.E-07	4.E-08	4.E-04	1.E-07

			(left values)							(right values)																
	C_4	15 mM-un	1.56 ±0.32							0.99	0.99	0.99	0.99	0.99	0.99	0.99	9.E-06	4.E-03	2.E-07	6.E-07	9.E-07	2.E-07	2.E-05	6.E-03	2.E-09	7.E-06	6.E-04	4.E-07	7.E-11	4.E-07	2.E-08	3.E-04	7.E-08
	C_4	40 mM-un	1.45 ±0.29							0.96	0.99	0.93	0.98	0.99	0.94	4.E-04	0.05	1.E-05	4.E-05	5.E-05	1.E-05	6.E-04	0.06	2.E-07	3.E-04	0.01	2.E-05	1.E-08	2.E-05	2.E-06	6.E-03	6.E-06
	C_4	3 g-COD/L	1.63 ±0.31							0.99	0.99	0.99	0.99	0.99	1.E-06	9.E-04	1.E-08	6.E-08	9.E-08	2.E-08	2.E-06	1.E-03	1.E-10	8.E-07	1.E-04	3.E-08	4.E-12	3.E-08	2.E-09	4.E-05	6.E-09
	C_5	15 mM-un	1.54 ±0.31							0.99	0.99	0.99	0.99	2.E-05	8.E-03	4.E-07	2.E-06	2.E-06	5.E-07	4.E-05	0.01	5.E-09	2.E-05	1.E-03	9.E-07	2.E-10	9.E-07	7.E-08	6.E-04	2.E-07
	C_5	40 mM-un	1.65 ±0.33							0.99	0.99	0.99	4.E-07	5.E-04	5.E-09	2.E-08	4.E-08	7.E-09	9.E-07	7.E-04	4.E-11	4.E-07	3.E-07	6.E-05	1.E-08	1.E-12	1.E-08	7.E-10	2.E-05	2.E-09
	C_5	3 g-COD/L	1.60 ±0.28							0.99	0.99	3.E-06	2.E-03	4.E-08	2.E-07	2.E-07	5.E-08	5.E-06	2.E-03	3.E-10	2.E-06	2.E-04	9.E-08	1.E-11	9.E-08	5.E-09	9.E-05	2.E-08
	PBS	30 mM	1.56 ±0.32							0.99	9.E-06	4.E-03	2.E-07	6.E-07	9.E-07	2.E-07	2.E-05	6.E-03	2.E-09	7.E-06	6.E-04	4.E-07	7.E-11	4.E-07	2.E-08	3.E-04	7.E-08
	PBS	30 mM	1.64 ±0.26								7.E-07	7.E-04	9.E-09	4.E-08	6.E-08	1.E-08	1.E-06	1.E-03	1.E-11	6.E-07	5.E-05	8.E-05	2.E-08	2.E-12	2.E-08	1.E-09	3.E-05	4.E-09
pH 5.0	C_1	15 mM-un	0.97 ±0.24	x	x	x	x	x	x	x	x	x	x	x	x	x	x	x	x	x	0.90	0.99	0.99	0.99	0.99	0.99	0.87	0.99	0.99	0.98	0.99	0.99	0.69	0.99	0.97	0.99	0.99
	C_1	40 mM-un	1.08 ±0.25	x	x	x	x	x	x	x	x	x	x	x	x	x	x	x	x	x	0.56	0.69	0.73	0.58	0.94	0.99	0.18	0.89	0.99	0.64	0.07	0.64	0.38	0.99	0.48
	C_1	3 g-COD/L	0.92 ±0.21	x	x	x	x	x	x	x	x	x	x	x	x	x	x	x	x	x	0.99	0.99	0.99	0.99	0.50	0.99	0.99	0.82	0.99	0.95	0.99	0.99	0.89	0.99
	C_2	15 mM-un	0.93 ±0.25	x	x	x	x	x	x	x	x	x	x	x	x	x	x	x	x	x	0.99	0.99	0.99	0.64	0.99	0.99	0.99	0.99	0.99	0.99	0.95	0.99
	C_2	40 mM-un	0.94 ±0.26	x	x	x	x	x	x	x	x	x	x	x	x	x	x	x	x	x	0.99	0.99	0.68	0.99	0.99	0.99	0.92	0.99	0.88	0.99	0.99	0.96	0.99
	C_2	3 g-COD/L	0.92 ±0.21	x	x	x	x	x	x	x	x	x	x	x	x	x	x	x	x	x	0.99	0.52	0.99	0.99	0.83	0.99	0.95	0.99	0.99	0.90	0.99

VFA	Conc.	k_A	1	2	3	4	5	6	7	8	9	10	11	12	13	14	15	16	17	18	19	20	21	22	23	24	25	26	27
C_3	15 mM-un	0.98 ±0.24	x	x	x	x	x	x	x	x	x	x	x	x	x	x	x	x	x	0.91	0.84	0.99	0.99	0.99	0.61	0.99	0.96	0.99	0.98
C_3	40 mM-un	1.08 ±0.27	x	x	x	x	x	x	x	x	x	x	x		x	x	x	x	x		0.15	0.85	0.99	0.59	0.05	0.59	0.33	0.99	0.43
C_3	3 g-COD/L	0.87 ±0.24	x	x	x	x	x	x	x	x	x	x	x	x	x	x	x	x	x			0.91	0.42	0.99	0.99	0.99	0.99	0.54	0.99
C_4	15 mM-un	0.96 ±0.24	x	x	x	x	x	x	x	x	x	x	x	x	x	x	x	x	x				0.98	0.99	0.72	0.99	0.98	0.99	0.99
C_4	40 mM-un	1.04 ±0.27	x	x	x	x	x	x	x	x	x	x	x	x	x	x	x	x	x					0.87	0.20	0.87	0.66	0.99	0.76
C_4	3 g-COD/L	0.93 ±0.21	x	x	x	x	x	x	x	x	x	x	x	x	x	x	x	x	x						0.93	0.99	0.99	0.93	0.99
C_5	15 mM-un	0.84 ±0.21	x	x	x	x	x	x	x	x	x	x	x	x	x	x	x	x	x		x					0.93	0.99	0.29	0.97
C_5	40 mM-un	0.93 ±0.22	x	x	x	x	x	x	x	x	x	x	x	x	x	x	x	x	x								0.99	0.93	0.99
C_5	3 g-COD/L	0.90 ±0.22	x	x	x	x	x	x	x	x	x	x	x	x	x	x	x	x	x									0.77	0.99
PBS	30 mM	1.02 ±0.27	x	x	x	x	x	x	x	x	x	x	x	x	x	x	x	x	x										0.85
PBS	30 mM	0.91 ±0.18	x	x	x	x	x	x	x	x	x	x	x	x	x	x	x	x	x										

Remark: C_1: formate, C_2: acetate, C_3: propionate, C_4: butyrate, C_5: valerate, PBS: phosphate buffer, mM-un: millimolar-based unionised VFA concentration, k_A: specific rate obtained from double exponential function, k_{A+B}: specific rate obtained from single exponential function, ±: half width of 95%-confidence interval from the mean, x: p-value ≤ 0.05, greyed-out cell: not used for further analysis because of large confidence interval and low r^2.

Table A8 Chi-square test for Formate-fed culture (datasets of pH 5.0–6.0)

	Dataset			18F	19F	20F	21F	22F	23F	24F	25F	26F	27F	28F	29F	30F	31F	32F	33F	34F	35F	36F	37F	38F	39F	40F	41F	42F	43F	44F	45F	46F
pH				pH 5.0																	pH 5.5						pH 6.0					
	Species			C_1	C_1	C_1	C_2	C_2	C_2	C_3	C_3	C_3	C_4	C_4	C_4	C_5	C_5	C_5	PBS	PBS	C_1	C_2	C_3	C_4	C_5	PBS	C_1	C_2	C_3	C_4	C_5	PBS
		Conc.		15 mM-un	40 mM-un	3 g-COD/L	15 mM-un	40 mM-un	3 g-COD/L	15 mM-un	40 mM-un	3 g-COD/L	15 mM-un	40 mM-un	3 g-COD/L	15 mM-un	40 mM-un	3 g-COD/L	30 mM	30 mM	3 g-COD/L	3 g-COD/L	3 g-COD/L	3 g-COD/L	3 g-COD/L	30 mM	3 g-COD/L	3 g-COD/L	3 g-COD/L	3 g-COD/L	3 g-COD/L	30 mM
			k_A (d⁻¹)	0.97 ±0.24	1.08 ±0.25	0.92 ±0.21	0.93 ±0.25	0.94 ±0.26	0.92 ±0.21	0.98 ±0.24	1.08 ±0.27	0.87 ±0.24	0.96 ±0.24	1.04 ±0.27	0.93 ±0.21	0.84 ±0.21	0.93 ±0.22	0.90 ±0.22	1.02 ±0.27	0.91 ±0.18	0.59 ±0.23	0.71 ±0.21	0.61 ±0.25	0.61 ±0.22	0.61 ±0.21	0.60 ±0.20	0.17 ±1.03	0.32 ±0.39	0.26 ±0.62	0.24 ±0.63	0.25 ±0.52	0.30 ±0.50
pH 5.0	C_1	15 mM-un	0.97 ±0.24		0.90	0.99	0.99	0.99	0.99	0.99	0.87	0.89	0.99	0.98	0.99	0.69	0.99	0.97	0.99	0.99	2.E-11	9.E-04	2.E-09	2.E-09	2.E-09	6.E-10	0.E+00	0.E+00	0.E+00	0.E+00	0.E+00	0.E+00
	C_1	40 mM-un	1.08 ±0.25			0.56	0.69	0.73	0.58	0.94	0.99	0.18	0.89	0.99	0.64	0.07	0.64	0.38	0.99	0.48	2.E-16	1.E-06	5.E-14	7.E-14	5.E-14	1.E-14	0.E+00	0.E+00	0.E+00	0.E+00	0.E+00	0.E+00
	C_1	3 g-COD/L	0.92 ±0.21				0.99	0.99	0.99	0.99	0.50	0.99	0.99	0.82	0.99	0.95	0.99	0.99	0.89	0.99	3.E-09	0.01	2.E-07	2.E-07	2.E-07	7.E-08	0.E+00	0.E+00	0.E+00	0.E+00	0.E+00	0.E+00
	C_2	15 mM-un	0.93 ±0.25					0.99	0.99	0.99	0.64	0.98	0.99	0.90	0.99	0.90	0.99	0.99	0.95	0.99	6.E-10	0.01	4.E-08	5.E-08	4.E-08	2.E-08	0.E+00	0.E+00	0.E+00	0.E+00	0.E+00	0.E+00
	C_2	40 mM-un	0.94 ±0.26						0.99	0.99	0.68	0.97	0.99	0.92	0.99	0.88	0.99	0.99	0.96	0.99	4.E-10	5.E-03	3.E-08	4.E-08	3.E-08	1.E-08	0.E+00	0.E+00	0.E+00	0.E+00	0.E+00	0.E+00
	C_2	3 g-COD/L	0.92 ±0.21							0.99	0.52	0.99	0.99	0.83	0.99	0.95	0.99	0.99	0.90	0.99	2.E-09	0.01	1.E-07	2.E-07	1.E-07	5.E-08	0.E+00	0.E+00	0.E+00	0.E+00	0.E+00	0.E+00
	C_3	15 mM-un	0.98 ±0.24								0.91	0.84	0.99	0.99	0.99	0.61	0.99	0.96	0.99	0.98	7.E-12	5.E-04	7.E-10	9.E-10	7.E-10	2.E-10	0.E+00	0.E+00	0.E+00	0.E+00	0.E+00	0.E+00
	C_3	40 mM-un	1.08 ±0.27									0.15	0.85	0.99	0.59	0.05	0.59	0.33	0.99	0.43	1.E-16	6.E-07	2.E-14	3.E-14	2.E-14	6.E-15	0.E+00	0.E+00	0.E+00	0.E+00	0.E+00	0.E+00
	C_3	3 g-COD/L	0.87 ±0.24										0.91	0.42	0.99	0.99	0.99	0.99	0.54	0.99	3.E-07	0.10	1.E-05	1.E-05	1.E-05	4.E-06	0.E+00	0.E+00	0.E+00	0.E+00	0.E+00	0.E+00
	C_4	15 mM-un	0.96 ±0.24											0.98	0.99	0.72	0.99	0.98	0.99	0.99	3.E-11	1.E-03	2.E-09	3.E-09	3.E-09	9.E-10	0.E+00	0.E+00	0.E+00	0.E+00	0.E+00	0.E+00

	C_4	40 mM-un	1.04 ±0.27														0.87	0.20	0.87	0.66	0.99	0.76	1.E-14	1.E-05	2.E-12	3.E-12	3.E-12	7.E-13	0.E+00	0.E+00	0.E+00	0.E+00	0.E+00	0.E+00
	C_4	3 g-COD/L	0.93 ±0.21															0.93	0.99	0.99	0.93	0.99	1.E-09	0.01	7.E-08	9.E-08	8.E-08	3.E-08	0.E+00	0.E+00	0.E+00	0.E+00	0.E+00	0.E+00
	C_5	15 mM-un	0.84 ±0.21	x															0.93	0.99	0.29	0.97	4.E-06	0.25	9.E-05	1.E-04	9.E-05	4.E-05	0.E+00	0.E+00	0.E+00	0.E+00	0.E+00	0.E+00
	C_5	40 mM-un	0.93 ±0.22																	0.99	0.93	0.99	1.E-09	0.01	7.E-08	9.E-08	8.E-08	3.E-08	0.E+00	0.E+00	0.E+00	0.E+00	0.E+00	0.E+00
	C_5	3 g-COD/L	0.90 ±0.22																		0.77	0.99	2.E-08	0.03	1.E-06	1.E-06	1.E-06	4.E-07	0.E+00	0.E+00	0.E+00	0.E+00	0.E+00	0.E+00
	PBS	30 mM	1.02 ±0.27																			0.85	7.E-14	4.E-05	1.E-11	2.E-11	1.E-11	3.E-12	0.E+00	0.E+00	0.E+00	0.E+00	0.E+00	0.E+00
	PBS	30 mM	0.91 ±0.18																				7.E-09	0.02	3.E-07	5.E-07	4.E-07	1.E-07	0.E+00	0.E+00	0.E+00	0.E+00	0.E+00	0.E+00
pH 5.5	C_1	3 g-COD/L	0.59 ±0.23	x	x	x	x	x	x	x	x	x	x	x	x	x	x	x	x	0.12	0.99	0.99	0.99	0.99					0.E+00	0.E+00	0.E+00	0.E+00	0.E+00	0.E+00
	C_2	3 g-COD/L	0.71 ±0.21	x	x	x	x	x	x		x	x	x		x	x	x	x		0.39	0.41	0.39	0.31					0.E+00	0.E+00	0.E+00	0.E+00	0.E+00	0.E+00
	C_3	3 g-COD/L	0.61 ±0.25	x	x	x	x	x	x	x	x	x	x	x	x	x	x				0.99	0.99	0.99					0.E+00	0.E+00	0.E+00	0.E+00	0.E+00	0.E+00
	C_4	3 g-COD/L	0.61 ±0.22	x	x	x	x	x	x	x	x	x	x	x	x	x	x					0.99	0.99					0.E+00	0.E+00	0.E+00	0.E+00	0.E+00	0.E+00
	C_5	3 g-COD/L	0.61 ±0.21	x	x	x	x	x	x	x	x	x	x	x	x	x	x						0.99					0.E+00	0.E+00	0.E+00	0.E+00	0.E+00	0.E+00
	PBS	30 mM	0.60 ±0.20	x	x	x	x	x	x	x	x	x	x	x	x	x	x											0.E+00	0.E+00	0.E+00	0.E+00	0.E+00	0.E+00

pH																															
pH 6.0	C_1	3 g-COD/L	0.17 ±1.03	x	x	x	x	x	x	x	x	x	x	x	x	x	x	x	x	x	x	x	x	x			0.E+00	1.E-14	7.E-09	1.E-11	0.E+00
	C_2	3 g-COD/L	0.32 ±0.39	x	x	x	x	x	x	x	x	x	x	x	x	x	x	x	x	x	x	x	x	x	x		0.01	8.E-06	6.E-04	0.92
	C_3	3 g-COD/L	0.26 ±0.62	x	x	x	x	x	x	x	x	x	x	x	x	x	x	x	x	x	x	x	x	x	x	x		0.78	0.99	0.34
	C_4	3 g-COD/L	0.24 ±0.63	x	x	x	x	x	x	x	x	x	x	x	x	x	x	x	x	x	x	x	x	x	x	x			0.99	4.E-03
	C_5	3 g-COD/L	0.25 ±0.52	x	x	x	x	x	x	x	x	x	x	x	x	x	x	x	x	x	x	x	x	x	x	x				0.06
	PBS	30 mM	0.30 ±0.50	x	x	x	x	x	x	x	x	x	x	x	x	x	x	x	x	x	x	x	x	x	x				x	

Remark: C_1: formate, C_2: acetate, C_3: propionate, C_4: butyrate, C_5: valerate, PBS: phosphate buffer, mM-un: millimolar-based unionised VFA concentration, k_A: specific rate obtained from double exponential function, k_{A+B}: specific rate obtained from single exponential function, ±: half width of 95%-confidence interval from the mean, x: p-value ≤ 0.05, greyed-out cell: not used for further analysis because of large confidence interval and low r^2.

Table A9 Chi-square test for Formate-fed culture (datasets of pH 6.5–7.5)

Dataset	47F	48F	49F	50F	51F	52F	53F	54F	55F	56F	57F	58F	59F	60F	61F	62F	63F	64F	65F
pH	pH 6.5						pH 7.0							pH 7.5					
Species	C$_1$	C$_2$	C$_3$	C$_4$	C$_5$	PBS	C$_1$	C$_2$	C$_3$	C$_4$	C$_5$	PBS	PBS	C$_1$	C$_2$	C$_3$	C$_4$	C$_5$	PBS
Conc.	3 g-COD/L	3 g-COD/L	3 g-COD/L	3 g-COD/L	3 g-COD/L	30 mM	3 g-COD/L	3 g-COD/L	3 g-COD/L	3 g-COD/L	3 g-COD/L	30 mM	30 mM	3 g-COD/L	3 g-COD/L	3 g-COD/L	3 g-COD/L	3 g-COD/L	30 mM
k_A (d^{-1})	0.00 ±64.8	0.04 ±67.5	0.11 ±0.97	0.10 ±1.23	0.10 ±0.93	0.13 ±0.70	-0.02 ±2.34	0.03 ±2.07	0.03 ±2.32	0.05 ±1.22	0.06 ±0.92	0.07 ±2.02	0.03 ±32.3	0.02 ±0.85	-0.01 ±20.0	0.05 ±1.26	0.07 ±0.91	0.08 ±0.63	0.03 ±50.0
k_{A+B} (d^{-1})	-0.004 ±0.009	0.030 ±0.008	0.038 ± 0.01	0.037 ±0.009	0.028 ±0.009	0.053 ±0.008	-0.065 ±0.008	-0.010 ±0.008	-0.010 ±0.009	-0.006 ±0.009	-0.011 ±0.009	0.022 ±0.007	0.014 ±0.008	-0.05 ±0.008	-0.014 ±0.008	-0.009 ±0.009	-0.003 ±0.009	-0.008 ±0.012	0.015 ±0.008
pH 6.5, C$_1$, 3 g-COD/L, 0.00 ±64.8, -0.004 ±0.009		1.E-11	0.E+00	0.E+00	3.E-10	0.E+00	0.E+00	0.91	0.91	0.99	0.82	1.E-06	5.E-03	0.E+00	0.41	0.95	0.99	0.98	2.E-03
pH 6.5, C$_2$, 3 g-COD/L, 0.04 ±67.5, 0.030 ±0.008	x		0.79	0.87	0.99	3.E-04	0.E+00	1.E-16	1.E-16	3.E-13	0.E+00	0.78	0.04	0.E+00	0.E+00	6.E-16	7.E-11	5.E-15	0.07
pH 6.5, C$_3$, 3 g-COD/L, 0.11 ±0.97, 0.038 ± 0.01	x			0.99	0.55	0.10	0.E+00	0.E+00	0.E+00	0.E+00	0.E+00	0.05	5.E-05	0.E+00	0.E+00	0.E+00	0.E+00	0.E+00	1.E-04
pH 6.5, C$_4$, 3 g-COD/L, 0.10 ±1.23, 0.037 ±0.009	x				0.67	0.06	0.E+00	0.E+00	0.E+00	0.E+00	0.E+00	0.08	1.E-04	0.E+00	0.E+00	0.E+00	2.E-16	0.E+00	4.E-04
pH 6.5, C$_5$, 3 g-COD/L, 0.10 ±0.93, 0.028 ±0.009	x					4.E-05	0.E+00	3.E-15	3.E-15	9.E-12	4.E-16	0.94	0.12	0.E+00	0.E+00	3.E-14	2.E-09	2.E-13	0.18
pH 6.5, PBS, 30 mM, 0.13 ±0.70, 0.053 ±0.008	x	x			x		0.E+00	0.E+00	0.E+00	0.E+00	0.E+00	2.E-08	4.E-14	0.E+00	0.E+00	0.E+00	0.E+00	0.E+00	2.E-13
pH 7.0, C$_1$, 3 g-COD/L, -0.02 ±2.34, -0.065 ±0.008	x	x	x	x	x	x		0.E+00	0.E+00	0.E+00	0.E+00	0.E+00	0.E+00	0.83	0.E+00	0.E+00	0.E+00	0.E+00	0.E+00
pH 7.0, C$_2$, 3 g-COD/L, 0.03 ±2.07, -0.010 ±0.008							x		0.99	0.98	0.99	1.E-10	1.E-05	0.E+00	0.99	0.99	0.82	0.99	3.E-06
pH 7.0, C$_3$, 3 g-COD/L, 0.03 ±2.32, -0.010 ±0.009							x			0.98	0.99	1.E-10	1.E-05	0.E+00	0.98	0.99	0.82	0.99	3.E-06
pH 7.0, C$_4$, 3 g-COD/L, 0.05 ±1.22, -0.006 ±0.009							x				0.96	8.E-08	9.E-04	0.E+00	0.69	0.99	0.99	0.99	3.E-04
pH 7.0, C$_5$, 3 g-COD/L, 0.06 ±0.92, -0.011 ±0.009							x					2.E-11	3.E-06	0.E+00	0.99	0.99	0.70	0.99	8.E-07
pH 7.0, PBS, 30 mM, 0.07 ±2.02, 0.022 ±0.007	x		x			x	x	x	x	x	x		0.75	0.E+00	6.E-14	7.E-10	5.E-06	3.E-09	0.85
pH 7.0, PBS, 30 mM, 0.03 ±32.3, 0.014 ±0.008	x	x	x	x		x	x	x	x	x	x			0.E+00	3.E-08	3.E-05	0.01	1.E-04	0.99

pH		Conc.	k_A	k_{A+B}																		
pH 7.5	C₁	3 g-COD/L	0.02 ±0.85	-0.05 ±0.008	x	x	x	x	x	x		x	x	x	x	x	x		0.E+00	0.E+00	0.E+00	0.E+00	0.E+00
	C₂	3 g-COD/L	-0.01 ±20.0	-0.014 ±0.008		x	x	x	x	x	x			x	x	x		0.96	0.29	0.90	8.E-09
	C₃	3 g-COD/L	0.05 ±1.26	-0.009 ±0.009		x	x	x	x	x	x			x	x	x			0.90	0.99	1.E-05
	C₄	3 g-COD/L	0.07 ±0.91	-0.003 ±0.009		x	x	x	x	x	x			x	x	x				0.96	6.E-03
	C₅	3 g-COD/L	0.08 ±0.63	-0.008 ±0.012		x	x	x	x	x	x			x	x	x					4.E-05
	PBS	30 mM	0.03 ±50.0	0.015 ±0.008	x		x	x		x	x	x	x	x	x		x	x	x	x	x	

Remark: C₁: formate, C₂: acetate, C₃: propionate, C₄: butyrate, C₅: valerate, PBS: phosphate buffer, mM-un: millimolar-based unionised VFA concentration, k_A: specific rate obtained from double exponential function, k_{A+B}: specific rate obtained from single exponential function, ±: half width of 95%-confidence interval from the mean, x: *p*-value ≤ 0.05, greyed-out cell: not used for further analysis because of large confidence interval and low r^2.

LIST OF PUBLICATIONS

1. <u>Meng Sun,</u> Bing Liu, Katsunori Yanagawa, Nguyen Thi Ha, Rajeev Goel, Mitsuharu Terashima*, Hidenari Yasui. **Effects of low pH conditions on decay of methanogenic biomass**. *Water Research*, Vol.179, 2020, 115883. doi.org/10.1016/j.watres.2020.115883

2. <u>Meng Sun,</u> Katsunori Yanagawa, Wipoo Prasitwuttisak, Rajeev Goel, Ryuichi Watanabe, Hidenori Harada, Bing Liu, Mitsuharu Terashima*, Hidenari Yasui. **Kinetics for the methanogen's death in the acidic environments**. *Journal of Water and Environment Technology*, Vol.21, No.1, 59-75, 2023. doi.org/10.2965/jwet.22-113.

3. <u>Meng Sun,</u> Xi Zhang, Bing Liu, Rajeev Goel, Mitsuharu Terashima, Hidenari Yasui*. **Upgrading ADM1 by Addition of Lag-phase Sub-model to Simulate Acidic Inhibition of Methanogenic Reactor**. *Journal of Water and Environment Technology*, Vol.22, No.2, 2023.

PARTICIPATION TO INTERNATIONAL CONFERENCES

1. <u>Meng Sun</u>, Bing Liu, Katsunori Yanagawa, Mitsuharu Terashima, Hidenari Yasui. **A Kinetic Model for Low pH Poisoning on Methanogenic Microorganism**. IWA World Water Congress & Exhibition 2018, p.101, Session 8-209, September 16th-21st, 2018, Tokyo, Japan.

2. <u>Meng Sun</u>, Bing Liu, Katsunori Yanagawa, Rajeev Goel, Mitsuharu Terashima, Hidenari Yasui. **Dynamic Behaviors of Methanogenic Biomass for Anaerobic Fermentation under Various Acidic VFAs conditions**. The 3R International Scientific Conference on Material Cycles and Waste Management, p.13, Session C-5-1, March 16th-18th, 2020, Tsukuba, Japan.

3. <u>Meng Sun</u>, Bing Liu, Rajeev Goel, Mitsuharu Terashima, Hidenari Yasui. **Kinetic Simulations of Accelerated Decay Rate for Methanogenic Biomass under Various Acidic VFAs Conditions**. The Water and Environment Technology Conference Online2020 (WET2020-online), p.31, Session 1E-6, November 7th-8th, 2020, Japan.

4. <u>Meng Sun</u>, Xi Zhang, Bing Liu, Rajeev Goel, Mitsuharu Terashima, Hidenari Yasui. **Benchmark of Chemostat Methane Production from Acetate and Its Dynamic Modelling**. The Water and Environment Technology Conference Online2022 (WET2022-online), p.58, Session 4A-2-b, July 9th-10th, 2022, Japan.